FAULT ROCK EVOLUTION AND FLUID FLOW
IN SEDIMENTARY BASINS

Susan Johanna Hippler

Abstract

Structural studies have been undertaken in two extensional fault regimes associated with post-Caledonian basin-forming events in northern Scotland. A combination of detailed mapping and microstructural analysis has revealed the deformation processes and mechanisms involved in fault rock evolution and fluid flow associated with extensional faulting in upper crustal conditions.

Intrabasinal fault rock evolution has been investigated in the Orcadian Basin, NE Scotland, which developed in Old Red Sandstone (ORS) times, soon after cessation of the Caledonian Orogeny. High pore fluid pressures developed in lower Middle ORS lacustrine facies sediments as a result of overpressuring due to rapid subsidence in the early stages of basin evolution. This facilitated gravity-driven movement of sediments in the hangingwalls of tilted half-grabens, resulting in the development of bedding parallel detachment horizons. These horizons contain shear sense indicators showing displacement to the W-WNW, whilst normal faults which detach onto these horizons show NW-SE extension directions. Microstructures indicate that displacement within the bedding parallel detachment horizons was accommodated by independent particulate flow processes in weakly lithified sediments.

The Scapa Fault System was active in upper Middle ORS to Upper ORS times during deposition of the fluvial Scapa Sandstone. Microstructures in the Scapa Sandstone in the hangingwall of the North Scapa Fault indicate that this early faulting led to extreme grain size reduction by a combination of grain boundary and transgranular fracture processes. The cataclasis, together with subsequent precipitation of illite cement up to one metre from the fault plane resulted in the sealing of the fault early in the diagenetic history of the sediment.

Subsequent uplift of the Orcadian Basin, most probably during Carboniferous times, resulted in a range of inversion geometries. In the lower Middle ORS lacustrine facies rocks, thrusts exploited the bedding parallel detachment horizons, and folds and reverse faults developed as a result of buttressing against the earlier normal faults. The presence of vein arrays associated with these later reverse faults suggests the existence of high pore fluid pressures. Bitumen in these veins indicates the mobility of hydrocarbons at the time of deformation.

The North Scapa Fault was reactivated in a sinistral, oblique-slip sense during the inversion event. Fracture arrays and narrow cataclastic zones outside the previously developed sealed domain provided pathways for the migration of mature hydrocarbons. The East Scapa Fault reactivated in a reverse sense, and also contains fault rocks which record the presence of hydrocarbons at this time.

Permo-Carboniferous dykes on Orkney are deformed during later dextral movements on the Great Glen fault system, which further reactivated the East Scapa Fault in a (dextral) transtensional sense. The development of fault rocks along the East Scapa Fault at this time is complex and heterogeneous, and is dependent on fault geometry and kinematics.

Basin-margin faults exposed on the NW Scottish Mainland are most probably related to extension during evolution of the Minch Basin to the west of Scotland. The steeply-dipping extensional faults cut through Caledonian thrust sheets in Sango Bay, Durness. The resulting cataclastic deformation in a quartzite with an originally mylonitic microstructure has allowed assessment of the influence of initial microstructure on the cataclastic grain size reduction processes. The evolution of the fault rocks in terms of clast size, and clast/matrix ratios is not a simple function of displacement magnitude on the faults.

Detalied microstructural investigation in the quartzite thrust sheet reveals a range of cataclastic fault rocks, from clast dominated microbreccias to matrix dominated ultracataclasites. The recrystallised grain size and the sub-grain size in the original mylonite appear to control the development of the fine-grained matrix in the microbreccias and cataclasites by locating fracture along grain and sub-grain boundaries. Further grain size reduction generating the ultracataclasites and the finer-grained matrix zones in the microbreccias is dominated by transgranular fracturing.

The host rock clasts present in the fault zones in the quartzite show a significant increase in dislocation density indicating that a component of low temperature crystal plasticity is associated with the faulting. In addition, the fault rocks show evidence of partial cementation by the growth of quartz and carbonate cements. This emphasises the importance of fluids during healing of the fault zone.

Acknowledgements

The people of Durness are thanked for their many years of kind hospitality and drams at the right times. Dottie, Robbie, and John provided smiles, conversation and memories which will draw me back to the Highlands for years to come.

The Otley crew showed me how to enjoy life, and brought me back to reality. Sue, Linda, and Ron are gratefully thanked for an endless list of things for which I hope to repay them some day.

The writing of this thesis would not have been possible without Niels-Henrik Schmidt, who made life during the last part of my stay in England (Jægerspris!) worthwhile.

Many sincere thanks to Gretchen and David Mills for positive thinking and patience over the past few years, and to Mrs. Elsie Nelson for the many letters which I gratefully appreciated over the past three years. I'm sure they would understand that this thesis is dedicated to my Mother and Father, for many years of encouragement and support, and for the time I could not spend with them while experiencing a life which they so unselfishly made possible. I don't know how to say thanks enough.

Contents

Chapter 1: Introduction

Chapter 2: A Review of Basin Evolution and Extensional Faulting

Chapter 3: A Review of Fault Rock Evolution

Chapter 4: A Review of Fluid Flow and Faulting in Basins

Chapter 5: The Orcadian Basin

Chapter 6: The Durness Extensional Fault Array

Chapter 7. Discussion and Conclusions

List of Figures
(mp = map pocket)

Chapter 6

List of Tables

Abbreviations used in this thesis

BIF	Brittle Intergranular Fracture
DMT	Diffusive Mass Transfer
ESF	East Scapa Fault
ESS	East Scapa Sandstone
FW	Footwall
HW	Hangingwall
LTDF	Low Temperature Ductile Fracture
LORS	Lower Old Red Sandstone
MORS	Middle Old Red Sandstone
NSF	North Scapa Fault
NSS	North Scapa Sandstone
ORS	Old Red Sandstone
PPL	Plane polarized light
SEM	Scanning electron microscope
ST	Sensitive tint plate
TEM	Transmission electron microscope
UORS	Upper Old Red Sandstone
XP	Crossed polarized light
XRD	X-ray diffraction

Chapter 1. Introduction

1.1 Introduction and Aims

Microstructural studies of localised displacement zones have provided detailed information about the faulting processes and kinematics operating at deeper levels in the crust during orogeny (e.g., Schmid, 1982; White et al., 1982; Law et al., 1984, 1986; Knipe and Law, 1987; Knipe, 1989b). In contrast, it is only relatively recently that similar interest has concentrated on the products of brittle faulting, for example, the deformation mechanisms involved in the formation of cataclasites (House and Gray, 1982; Blenkinsop and Rutter, 1986; Tullis, 1986; Wang, 1986; Knipe, 1989b; Lloyd and Knipe; submitted). These studies are natural precursors to the application of microstructural analysis of fault zones in terms of the evolution of sedimentary basins. The geometrical aspects of basin defining structures have already received considerable attention (McKenzie, 1978; Wernicke, 1981; Wernicke and Burchfiel, 1982; Coward, 1986). It is the aim of this thesis to integrate detailed microstructural analysis of the processes involved in fault zone evolution with larger scale aspects of basin formation, including the significance of fluid migration, especially the effects of faulting on hydrocarbon potential.

In order to fulfill this aim, detailed field mapping of structures within extensional basin regimes, and microstructural analysis of the fault rocks collected from the fault zones mapped has been undertaken. The study of cataclastic fault rocks has been significantly influenced by the fracture mechanics approach recently applied to the understanding of failure modes and conditions in rocks (Rudnicki, 1980; see review edited by Atkinson, 1987; Lloyd and Knipe, submitted). Therefore, the fracture mechanics approach has been used during the microstructural analysis of the cataclastic fault rocks collected from the extensional fault zones studied in this thesis.

Two field areas were chosen: 1. The intra-basinal faults exposed on Orkney, NE Scotland, active during evolution of the Orcadian Basin during Old Red Sandstone (Devonian) times (Anderton et al., 1979; Enfield and Coward, 1987), and; 2. The basin margin fault array exposed onshore near Durness, NW Scotland. This fault array represents the onshore equivalent of post-Caledonian extensional faulting which is observed in offshore seismic data (see Smythe et al., 1982; Enfield and Coward, 1987) (fig. 1.1).

The aims of this study are: 1. To identify the processes and conditions of fault zone evolution from detailed microstructural analysis of fault rocks collected from the well-defined basin structures; 2. To assess the larger (field scale) processes of fault reactivation during subsequent deformation events from consideration of the nature of pre-existing fault zones (macroscopic structures and fault rock development); 3. To identify fluid pathways associated with faulting events and fault geometries, and; 4. To integrate the fault rock analysis with the evolution of the fault array in context of the basin history.

1.2 Introduction to study areas

1.2.1 The Orcadian Basin

The deep seismic reflection data from the Moine and Outer Isles Seismic Traverse (MOIST), shot north of the Scottish mainland by the British Institutions Reflection Profiling Syndicate (BIRPS), shows a series of easterly-dipping faults to the west of the Orkney Islands which are thought to represent half-grabens on which the West Orkney Basin formed (see Smythe et al., 1982; Brewer and Smythe, 1984, 1986; Blundell et al., 1985; Cheadle at al., 1987; and Kirton and Hitchon, 1987) (fig. 1.2). Coward and Enfield (1987; see also Enfield and Coward, 1987) studied commercial data from the West Orkney Basin, and suggested that initial extension in the West Orkney Basin occurred during Devonian times on the low-angle reactivated Caledonian thrust faults seen on the MOIST profile.

The Orcadian Basin sediments now exposed in Caithness and Orkney represent the onshore continuation of the West Orkney Basin (Enfield and Coward, 1987). The exposures on Orkney provide beautiful examples of the range of intrabasinal fault geometries and inversion-related structures which can be mapped in detail in context of the large-scale basin evolution models derived by the workers listed above. In addition, the well-exposed North Scapa, East Scapa, and North Coast fault zones on the Mainland have allowed thorough examination and collection of the fault rocks derived from faulting related to basin evolution and inversion events.
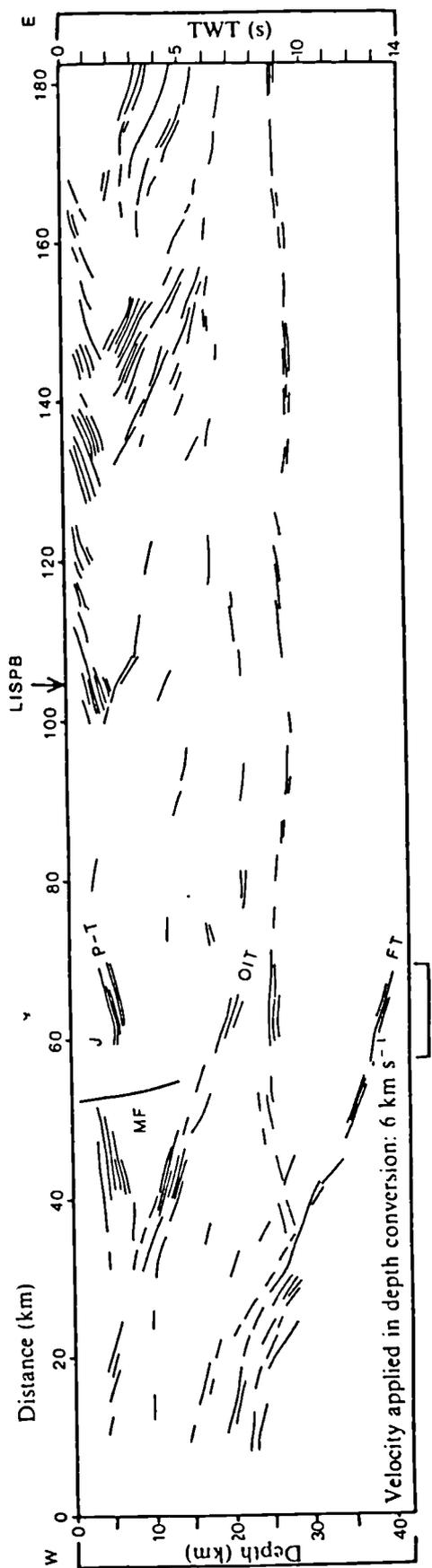
Figure 1.2. Line drawing of MOIST profile (from Smythe et al., 1982). Based on migrated sections but also using data from unmigrated stacks. Vertical depth scale assumes a constant velocity of 6 km s-1; no vertical exaggeration. Intersection of LISPB line near Cape Wrath shown. MF, Minch Fault (drawn from other data); J, Jurassic; P-T, Permo-Triassic; OIT, Outer Isles Thrust; FT, Flannan Thrust.

1.2.2 The Durness extensional fault array

The NE-SW/NW-SE trending extensional fault array in NW Sutherland forms the margin of a series of basins located to the north of the Scottish mainland (see Smythe et al., 1982; Enfield and Coward, 1987; Kirton and Hitchen, 1987). This part of the study focuses upon the fault rocks developed from Cambrian quartz mylonites during the evolution of the extensional fault array exposed near Durness, NW Scotland, (fig. 1.1). These mylonites provide an opportunity to study the development of a range of cataclastic fault rocks associated with varied extensional fault displacements and to assess the influence of the initial mylonite microstructure on the fracture processes.

1.3 Methods used in this study

A combination of methods were used in this study to investigate the faulting processes operating during basin evolution. Field mapping of the extensional fault geometries at scales of 1:5000 and 1:1000 was undertaken in the Orkney and Durness study areas, respectively. These maps are presented in the back pocket of this thesis. The more complex fault geometries showing the relationship between early basin structures and their interaction and relationship to structures formed during basin inversion on Orkney were mapped at a 1:500 scale.

The North Scapa and East Scapa Faults are well-exposed in along-strike coastal sections on Orkney, and hence allowed detailed fault zone analysis. This involved assessment of fault movement indicators, fracture orientations and spacing, fault rock character, and evidence for fluid movement during faulting. A major part of this thesis involved extensive analysis of deformation in porous sandstone in the hangingwall of the North Scapa Fault. This included X-ray diffraction of clay separates from the sandstone, to identify the relationship between diagenesis and fault movements and fluid flow events near the fault. In addition, carbon microelemental analysis (by gas chromatography) of specimens collected from each fault zone domain was undertaken in order to identify major hydrocarbon migration pathways in relationship to fracture arrays developed during faulting. Optical and transmission electron microscopy of the sandstone was used in order to assess the evolution of the cataclastic grain size reduction, and the morphology and distribution of diagenetic clay phases within each fault zone domain mapped in the field.

The analysis of fracture orientation and spacing, together with characterisation of the development of cataclastic fault rock types within a quartz mylonite thrust sheet offset by extensional faults in Durness allowed assessment of the clast size and shape, matrix content, and clast/matrix proportions in different cataclastic fault rocks. Optical and transmission electron microscopy of the original quartzite microstructure, and the range of cataclastic fault rocks identified in the field was utilized in order to identify the detailed microstructural changes which occurred in the mylonite during grain size reduction in the fault zone, and to assess the deformation mechanisms which operated during the extensional faulting.

1.5 Layout of thesis

Chapter 2 will review models of sedimentary basin evolution and extensional fault geometries, and discuss basin inversion. Chapter 3 is a review of the deformation mechanisms which operate in fault zones, and a discussion of previous work on experimental and natural cataclastic deformation. Chapter 4 outlines the important relationship between fluid flow and faulting in conjunction with ideas of fault seals in sedimentary basins. Chapter 5 presents field observations and microstructural data (optical and TEM) from the Orcadian Basin. The data is presented in three sections, each of which contains a discussion of the results and interpretations, and a list of the specific conclusions. X-ray diffraction and carbon microelemental analyses data from the North Scapa Sandstone are also included in Chapter 5. The chapter ends with a synthesis of the important points from the conclusions, and presents a deformation history for the faults in the Orkney area, including assessment of the fault rock development within the area. Chapter 6 presents field and microstructural data from the the Durness study area. The evolution of the cataclastic fault rocks are discussed in terms of both the microstructural and field scale mechanisms of faulting. Chapter 7 lists the conclusions of this thesis, and includes an outline of directions for future work.

Chapter 2. A Review of Basin Evolution and Extensional
Fault Geometries

2.1 Introduction

The first section of this chapter (2.2) discusses basin evolution models. Section 2.3 reviews the published work on the geometry of normal fault systems in extensional regimes. Section 2.4 discusses the recent approaches to the understanding of fault growth and displacement. Section 2.5 reviews published work on the interaction and development of structures related to the inversion of sedimentary basins.

2.2   Models of basin evolution

McKenzie's (1978) stretching model emphasized the link between extension in the lithosphere and basin development. The model gained popularity for its ease in which extension in the continental lithosphere could be calculated directly from back-stripped sediment thicknesses and data from seismic refraction studies. The extension factor, ß, is related directly to a phase of initial subsidence, which represents the competing mechanisms of crustal stretching, which causes subsidence, and thinning of the mantle lithosphere which causes uplift. After stretching, in McKenzie's model heat is lost by vertical conduction (lateral heat flow is ignored), and subsidence continues due to thermal contraction. This is called the thermal phase. The sum of the initial and thermal subsidence was termed the tectonic subsidence by Roydon and Keen (1980).

As a result of observations seen on seismic refraction data showing different styles of extensional faulting in the upper crust, coupled with changing ideas about how the upper crust responds to thinning and subsidence of the lower lithosphere, several other models have been proposed. It should be emphasized that McKenzie's (1978) model assumes homogeneous thinning of the lithosphere: both the crust and lithosphere extend by bulk pure shear over the entire width of the basin (fig. 2.1a). Also, instananeous stretching is assumed to occur. This implies that the thermal anomaly was produced entirely by vertical advection, with no heat loss due to diffusion during extension, which is valid provided the period of stretching is short compared to the relevent thermal time constant (Jarvis and McKenzie, 1980). Therefore, if stretching occurs over a period comparable to the diffusion time scale, some of the heat diffuses away before stretching is completed, and the resultant thermal anomaly is thus reduced.
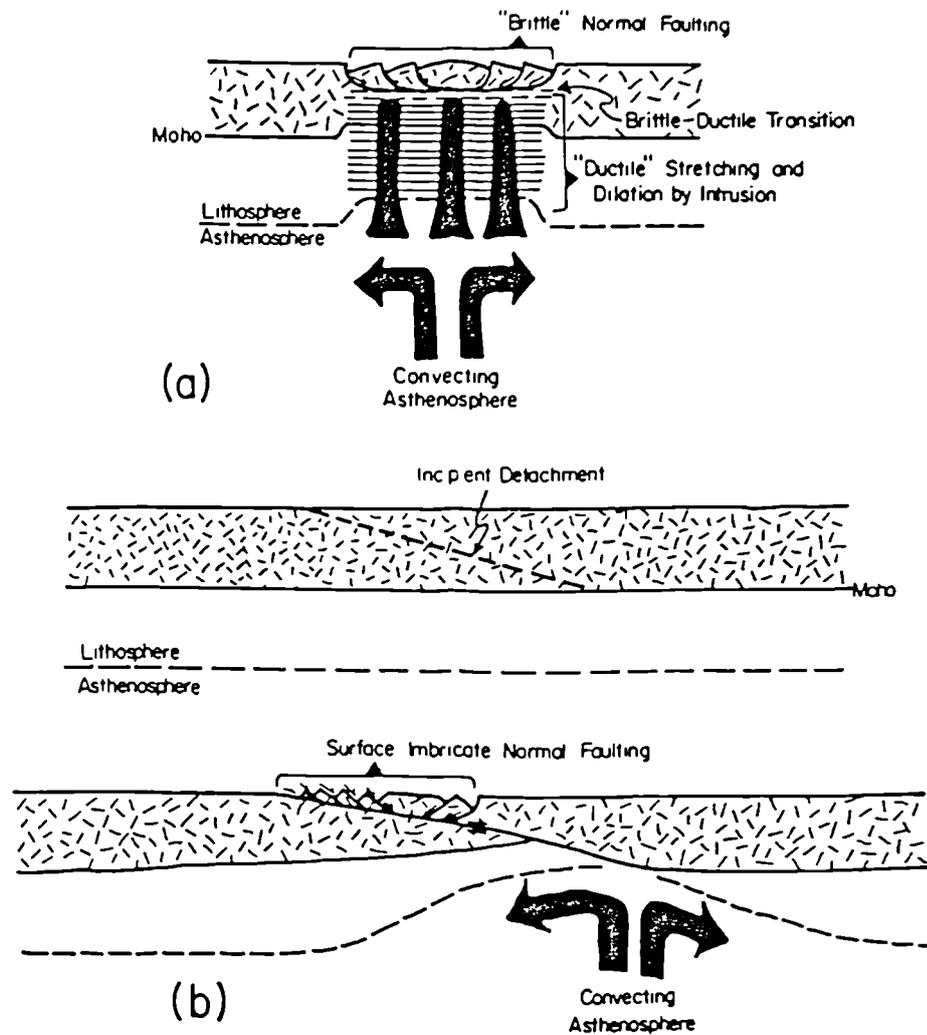
Figure 2.1. End-member models of strain geometry in rifts. a) "Pure-shear" model, in which crust and mantle lithosphere are attenuated uniformly along any given vertical reference line. b) "Simple-shear" model, in which relative extension of crust and mantle lithosphere along any given vertical line is nonuniform (from Wernicke, 1985).

In basins showing very slow extension, no thermal anomaly is produced. Jarvis and McKenzie (1978) investigated the effects of finite rates of extension on the heat flux and subsidence histories of sedimentary basins to provide tighter constraints on McKenzie's (1978) model. They found that for most basins, the duration of extension is likely to be short enough to warrent the use of the instantaneous stretching model in calculation of the subsidence history, and that for large extensions (ß >3), heat flow is more sensitive to the history of the extension, and care should be taken that the extension is sufficiently rapid before using the heat flow to establish ß. McKenzie's (1978) model has been confirmed in several basins (Christie and Sclater, 1980; Sclater and Christie, 1980; Le Pichon and Sibouet, 1981; Le Pichon et al., 1982).

Royden and Keen (1980) tried to apply the uniform stretching model to well data from the Nova Scotia and Labrador shelves, and found that the initial subsidence is considerably overestimated. They noted that to reduce the initial subsidence the mantle lithosphere must be thinned more than the crust, which Royden and Keen (op.cit.) accomplished by stretching the crust and the mantle lithosphere by different amounts, resulting in a non-uniform stretching model. The thermal subsidence is not significantly affected by differential stretching unless there is a great difference in the stretching factors. The ultimate amount of tectonic subsidence is still controlled by the amount of crustal thinning.

Other studies which attempted to apply McKenzie's (1978) model to certain basins also found discrepancies in the amount of stretching in the upper crust with that of the lower crust, and discrepancies between the extension estimated from well data and that obtained from variations in crustal thickness as shown by seismic refraction methods (Wood and Barton, 1983; Barton and Wood, 1984). Models were then developed which explained anomolous subsidence values in different areas of a particular basin (heterogeneous stretching). For example, Wernicke (1981, 1985) modelled lithospheric extension by accommodating slip along a fault or "detachment" of very low dip (<30°) that offsets the Moho and penetrates the entire lithosphere (fig. 2.1b). He suggested this model from observations in the Basin and Range Province where he noted there was often a discrepancy between the negligable thinning observed locally in upper crustal levels and the substantial estimates of crustal thinning obtained from seismic data.

In Wernicke's (1981, 1985) model, the large-scale gently dipping shear zone transfers extension from the upper part of the crust in one region to the lower crust and lithosphere elsewhere. Hence, the zone of upwelled asthenosphere does not lie beneath the main zone of upper crustal extension. Wernicke (1985) envisages three main zones in his extensional shear zone model: the zone where the upper crust has thinned and there are abundant faults above the detachment zone, the discrepant zone where the lower crust has thinned while there is negligible thinning in the upper crust, and the zone where the shear zone extends through the lithospheric mantle.

Coward (1986) suggests that heterogeneous lithospheric stretching combined with the simple shear model can explain many of the anomalies between the various stretching estimates made using different structural, stratigraphic and geophysical techniques. He calls attention to discrepancies between β values obtained by different techniques in the Witch Ground Graben (Christie and Sclater, 1980), Inner Moray Firth (Barr, 1985), and West Orkney Basin (Enfield and Coward, 1987). Coward (op. cit.) observed that in some basins, extension was transferred to the east and that the location of the thermal phase did not coincide with the location of the initial phase of subsidence, and that there was no evidence for a thermal sag basin at the same location as the location of the initial subsidence phase. White (1989), however, demonstrates that the factors which critically distinguish between pure shear and simple shear in basins are not those which Coward (1986) lists. White (op.cit.) shows that although the initial subsidence is distributed asymetrically in Wernicke's model, it is not laterally displaced from the thermal subsidence or crustal thinning. White (1989) indicates that observations of the spatial coincidence of subsidence and symmetric crustal thinning appear to be common to both mechanisms, and that only observations of the geometry of the initial and thermal subsidence (usually the best constrained observations) can distinguish between the two models.

2.2.1   Summary of basin evolution models

We can view the McKenzie (1978) and Wernicke (1981, 1985) models as two possible end members of basin evolution models, all of which have been derived from an interaction of variables in a thermo-mechanical basin system. The basin models can be linked to basin morphologies, which can be inferred to affect sedimentation patterns (Leeder and Gawthorpe, 1987; Ord et al., 1988; Collier 1988). It is obvious that much can be gained by studying

the origin and processes involved during evolution of a particular basin from study of the basin morphology, for example, the geometry of the extensional fault system in the basin. In addition, temporal changes in structural style as infered from seismic studies (Badley et al., 1984) and in the field (Spencer and Chase, 1989), have been used to reflect the activity of large-scale lithospheric cooling processes and to syn- and post-rift stages of basin development, therefore reflecting the timing of development of structures on the basin-wide scale. The next section discusses the geometrical aspects of extensional fault arrays.

2.3 Extensional Fault Geometries

2.3.1 Planar Faults

The simple basin morphology composed of purely dip-slip extensional faults can be described in terms of basin and blocks defined by grabens and half-grabens. Graben morphology may be symmetrical, reflecting basins bounded on two sides by faults of equal displacement, or asymmetrical, possessing boundary faults with different magnitudes of displacement. Half-graben basins are bounded by a fault on one side only, and are an end member of the asymmetrical basin pattern.

Seismic cross-sections from extensional basins commonly show the occurrence of relatively steeply-dipping planar normal faults. These faults occur as sub-parallel sets, bounding blocks that have rotated in a domino fashion (fig. 2.2). The rotating domino model describes large normal faults which are approximately planar and rotate as they move. The model allows an easy estimate of ß, the amount of extension, from the initial (Θ_0) and final (Θ_1) fault dips, using the relation:

$$\text{ß}\sin\Theta_1 = \sin\Theta_0$$

One of the main problems which has been identified with the domino model is that there is a space problem at the base of the rotating blocks. It has been suggested that this can be accommodated by a listric bounding fault (Barr, 1987), by an array of antithetic normal faults dipping in opposed directions to the major normal fault (Eyidogan and Jackson, 1985), or by internal deformation of the rotating block adjacent to a non-rotating footwall (Barr, 1987; Jackson et. al., 1988).
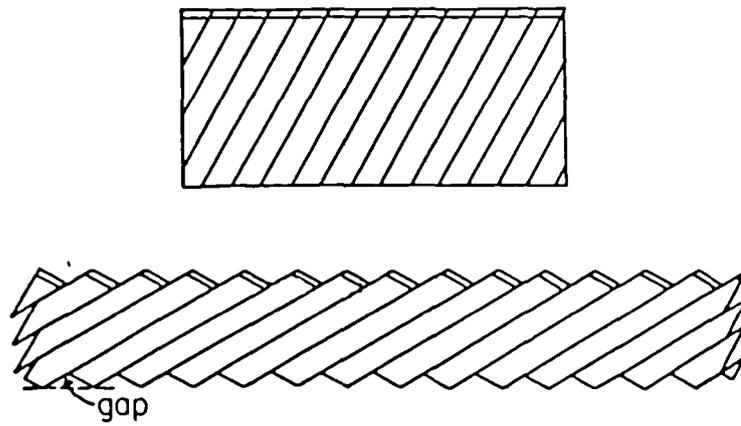
Figure 2.2. Model of the extension and attenuation of a rock mass by planar normal faulting in the "domino" fashion (from Wernicke and Burchfiel, 1982).

Jackson and White (1989) have suggested the existence of a space problem is a common misconception which can be explained if the seismic-aseismic transition (which they describe as a temperature horizon), is seen as neither compositional nor fixed to the rotating blocks. They propose that rotation of the blocks produces a perturbation to the initial temperature profile which decays with a time constant dependant on the thermal diffusivity and spacing of the faults. Whether the aseismic/seismic transition is perturbed (raised) depends primarily on the extensional strain rate (see also England and Jackson, 1987). Jackson and White (1989) also point out that although the lower crust is assumed to deform by flow, there is no need for a subhorizontal 'detachment' or 'decollement' zone of discrete slip at the base of the tilted blocks.

Other problems exist with the domino model in its simplest form. Differential rotation about the horizontal axis between a tilted extended terrain and its stable· margin or a horst block is a difficulty with planar faults (see Wernicke and Burchfiel, 1982). Jackson and White (1989) note that the domino model requires all the faults to be active across the basin at the same time, with the same dip and the same tilt to the fault bounded blocks, when in fact it is shown in several studies that the timing, tilting, and extension varies across a basin (see Barton and Wood, 1984; Gans, 1987). Problems with the domino model can be resolved if the faults are not perfectly planar and internal block deformation occurs by faulting or folding (Jackson and White, 1989).

An alternative to the planar, rotating faults in the domino model are shallow-dipping (0-20°), non-rotational faults as described by Wernicke and Burchfiel (1982). They suggest that to achieve the large extension values seen in basins such as the Basin and Range, shallow dipping fault planes are necessary. Wernicke (1981) originally suggested that extension in the crust can occur on large, planar, non-rotational normal faults that dip at very low-angles (0-20°) through the entire upper seismogenic crust. Recent work on active normal faults suggests that nearly all faults dip in the range of 30-60° and cut through the upper seismogenic layer (Jackson and White, 1989). Jackson and White (op.cit.) also state that there are no known examples of large earthquakes on subhorizontal normal faults on the continents.

Jackson (1987) discussed the reasons for the observation that earthquakes do not occur on very shallowly dipping faults. He proposed that very low-angle normal faults move aseismically (i.e. by creep), that they are

spatially separated from high-angle normal faults, or that the data which suggests that the low-angle faults and earthquakes do not exist was collected in too short of a time period ($\leq$30 years). Jackson and McKenzie (1983) have also shown that studying normal fault systems in active extensional terranes can also provide constraints on fault kinematics. This can help determine the intensity and distribution of the internal deformation of fault blocks and the timing of development and interaction of certain structures.

Gross and Hillmeyer (1982) found that the rotation of blocks above a detachment surface could be accommodated by the successive development of new normal faults at steeper angles as pre-existing faults were rotated to lower angles. This agrees well with observations by Proffett (1977), who documented the rotation of higher-angle faults to low-angle orientations upon the nucleation of new high-angle faults when the earlier generated planar faults became mechanically inefficient, and therefore lock after rotation of the fault to a dip of about 30°.

2.3.2 Listric faults

Listric faults diminish in dip with depth onto a low-angle or horizontal decollement surface (Bally et al., 1981; Gibbs, 1984a). Listric extensional faults have been described by many authors in the the North Sea (Gibbs, 1983, 1984a, 1984b) and the Basin and Range Province (Anderson, 1971; Proffett, 1977; Wernicke and Burchfiel, 1982). The geometry of listric faults is summarized by Bally et. al. (1981) and Shelton (1984).

Gibbs (1984a) has described ramp and flat extensional structural styles associated with listric faults, and detachment geometries similar to those seen in thrust systems (Butler, 1984). Gibbs (op.cit.) suggests that folding is a consequence of listric faulting, and 'reverse drag' or rollover occurs. Rollover anticlines are characteristic, but not definitive evidence of listric fault geometries (Barnett et al., 1987). Gibbs (op.cit.) shows that vertical extension on the rollover on the hangingwall must occur, and describes the development of antithetic or counter faults which result from the rollover geometry (fig. 2.3). He also describes ramp and flat geometries in extensional systems with a floor and roof fault forming a duplex geometry, again similar to structures found in regions of contraction (fig 2.4). These zones are similar to the chaos zones proposed by Wernicke and Burchfiel (1982). It is the fact that all listric extensional fault systems require geometrically neccessary hangingwall structures which makes the study of hangingwall deformation in extensional fault arrays important.

a

Shallow Counter Fan

b

Antithetic Fault
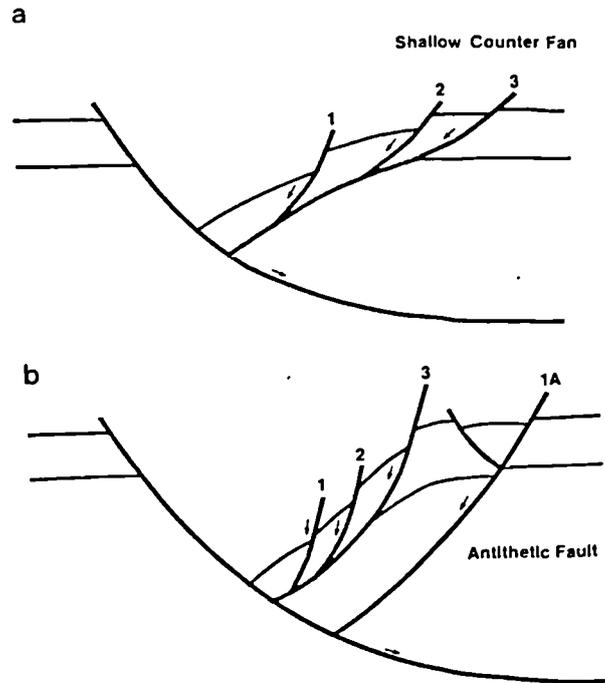
Figure 2.3. Geometry for faulting due to rollover above a listric normal fault. a) Roll-over thinned and extended on low-angle faults detaching on bedding surfaces. b) Roll-over thinned by shallow and deep counter faults (from Gibbs, 1984).

a

Flat

Ramp

Flat

b

Listric Fan

Horse

Extensional Duplex

c

Listric Fan   Central High Hanging Wall
Counter Fan   Shortcut Fault
Floor Fault
Roof Fault
Extensional Duplex
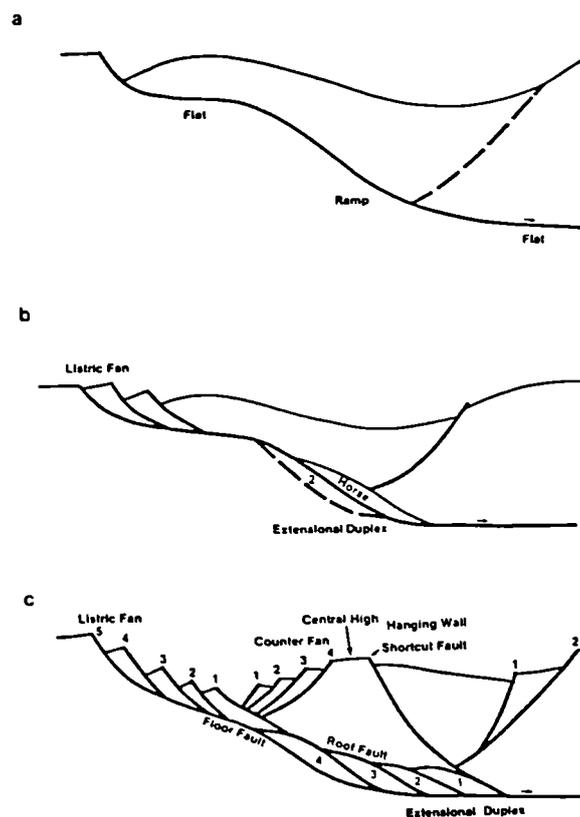
Figure 2.4. Geometry above listric faults with flat and ramp profiles. a) Listric fault with necessary hangingwall anticline and syncline. Antithetic fault developing on hangingwall as a result of ramp. b) Listric fault with listric fan developed on trailing edge of hangingwall. Migration of the footwall fault on the ramp has formed a duplex zone with and extensional horse. c) Fully developed system with a listric fan and counter fan on an extensional duplex formed by migrating footwall faults. Central high developed above the ramp as a result of the formation of a short cut fault on the hangingwall (from Gibbs, 1984).

The geometries of hangingwall structures are also of great consequence to area balance techniques, as the balancing techniques are based on various assumptions of the internal strain history of the hangingwall block in two dimensions (Gibbs, 1983; White et al., 1986; Williams and Vann, 1987; Wheeler, 1987). Moreover, it is the geometry of high-level structures developed above listric fault detachments which are so often significant in hydrocarbon · exploration.

Estimating the geometry and detachment levels of listric normal faults is dependent on the assumptions in the balancing techniques. Gibbs (1983) suggests that the curvature and depth to detachment on the listric fault can be derived from calculating bed length and excess area balance in cross section as well as graphically from the rollover associated with the listric fault geometry. Wheeler (1987) discussed the problems involved in using the 'modified Chevron' and slip line models of Williams and Vann (1987). Wheeler (1987) derived amended versions of the models in which area is locally conserved whilst heave is allowed to vary, and also lists the limitations of the models.

2.3.3 Analogue models of extensional fault systems

McClay and Ellis (1987a, 1987b) and Ellis and McClay (1988) have described analogue model experiments carried out with homogeneous sand, and more recently, sand/clay constructions designed to examine the detailed geometric and kinematic evolution of both planar and listric fault systems. In the initial homogeneous sand experiments, four different extensional models were investigated, resulting in a variety of listric and planar faults. However, in all the experiments, once the major fault has developed, second-order fault nucleation occurred in the hangingwall fault block. The fault generation sequences described by McClay and Ellis (1987a) do not conform to the footwall nucleation models proposed by Gibbs (1984). The experiments outlined by Ellis and McClay (1988), concentrating on listric extensional fault systems, confirmed the hangingwall nucleation model as seen in the earlier experiments (McClay and Ellis, 1987a, 1987b). In addition, the experiments showed that the location of graben development during extension was controlled by the geometry of the underlying detachment. This was also confirmed in models constructed of different materials, which produce similar structures, confirming that the geometry of the detachment was the fundamental control on the evolution of the hangingwall structures.

2.3.4 Transfer faults

The problems regarding differential tilt and rotation of blocks in planar domino style fault systems resulting in variable displacements and space problems can often be resolved with transfer fault zones, often found at high angles to basin margins. Therefore, blocks or 'compartments' of distinct structural geometry can be offset or linked by transfer zones or faults analogous to lateral ramps in thrust tectonics (Butler, 1984; Gibbs, 1984a, 1987). Gibbs (1987) points out that transfer faults act as lateral and side-wall ramps, and in the case of staircase arrays, the faults can detach at intermediate detachment levels in the crust. Transfer faults will develop the 'flower' type geometry in cross-section, as described for strike-slip flower structures (Harding and Lowell, 1979).

Jackson and White (1989) have also discussed important factors influencing the scale of normal faulting, the size of rotating blocks, and continuity along strike of large normal faults. The linking (transfer) fault systems associated with the normal fault systems are of importance to their model. They suggest that there is an apparent similarity in size between the maximum fault segment length and the thickness of the upper seismogenic crust. They point out that it is not suprising that blocks (and faults) break up along strike as a result of the overall rotation and tilting which occurs. Jackson and White (op.cit.) suggest an alternative: that there is a maximum size over which such rotations can be coherent, the size being limited by the strength of the outer elastic layer. Interestingly, they point out that if this suggestion is correct, it is perhaps reasonable that the maximum width of a block should be similar to its maximum length. It should be pointed out that many studies have found that original anisotropies in basement structures exerted an important influence on later extension, and the orientation of the associated normal fault system which developed (i.e., Enfield and Coward, 1987; Laubach and Marshak, 1987).

2.4 Fault growth and displacement

Many of the problems regarding fault geometries discussed above relate to how displacement is accommodated on faults, both singularly, and within fault systems. A recent approach to understanding the formation and growth of faults in terms of their geometries and related displacements has been through the work of Watterson (1986), Barnett et al., (1987), and Walsh and Watterson (1987, 1988). Their work initiated with the assumption of an ideal single fault: one which does not intersect its contemporary surface and on which displacement is not transferred onto a splay or other structure.

The displacement gradient on a fault is a measure of the rate at which displacement changes along the fault plane in a specified direction (Walsh and Watterson, 1988). For an ideal single fault surface, displacement decreases to zero in all directions from a point of maximum displacement. In the simplest cases, the fault surface appears as an ellipse bounded by the zero displacement contour or tip-line loop (fig. 2.5). As outlined by Walsh and Watterson (1988), the parameters used to calculate displacement gradients are defined as follows. The fault width (W) is defined as the maximum dimension of the surface in a direction normal to the slip direction and the fault length is the maximum dimension parallel to the slip direction. The radius (R) of a fault is half of either the width or the length; in the work of Walsh and Watterson (1988), the term radius refers to half of the width in most cases because of the nature of their data. Displacement (D) refers to the displacement accumulated throughout the active life of the fault, and slip (u) refers to the slip occurring during a single seismic event or cycle.

Although their approach is simplified, their conclusions on the usual range of gradients can be used either for testing the geometric compatibility of a fault interpretation or for extrapolating a fault into an area for which no data is available. The characteristic displacement gradient of a fault is given by the ratio D/R, but as these values are less than one, for convenience, they refer to the reciprocal of the displacement gradient (R/D). They find that the relationship between D and R for a variety of faults is non-linear, and that R/D values range from 5 to 1000 (Walsh and Watterson, 1988).
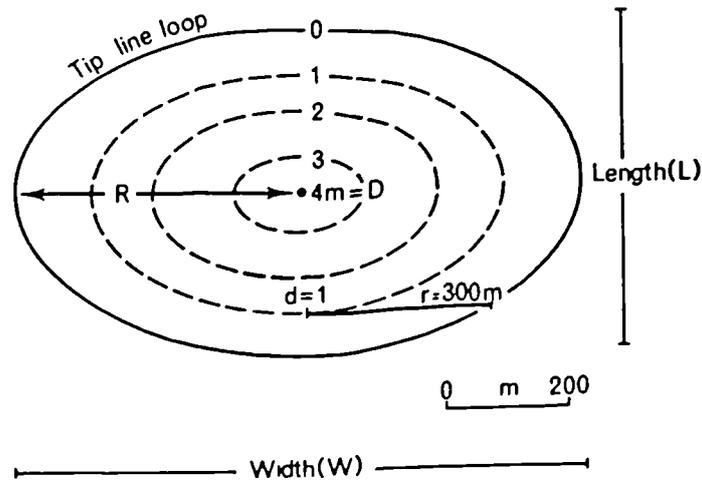
Figure 2.5. Schematic diagram of contoured displacements on a fault surface with maximum displacement (D) at the centre of the fault and with the tip-line loop corresponding to the zero displacement contour. Radius (R) is half the width. Displacement (d) is the maximum displacement along a chord of half-width (r) (from Walsh and Watterson, 1988).
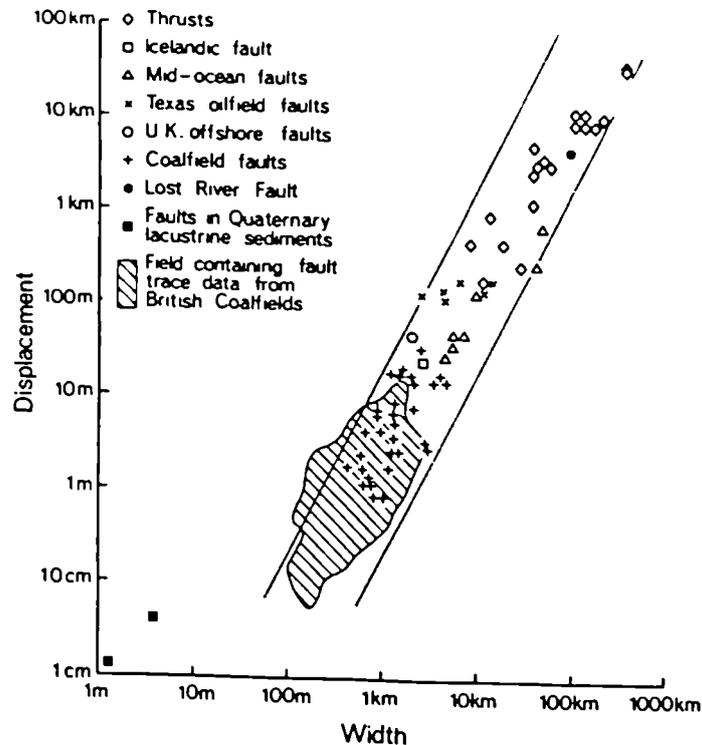
Figure 2.6. Logarithmic plot of width against maximum displacement for faults. Continuous lines have a slope of 2, as appropriate to the fault growth model (from Walsh and Watterson, 1988).

However, Watterson (1986) demonstrated that a systematic relationship exists between the widths and maximum displacements on single faults. This relationship was interpreted in terms of a fault growth model, such that:

$$D = W^2/P,$$

where D = maximum displacement on the fault;

W = maximum dimension of the fault surface in the direction normal
    to the slip direction; and,

P = variable related to rock properties (Walsh and Watterson, 1988).

The systematic relationship can be seen from the data in fig. 2.6. Walsh and Watterson (op.cit.) suggest that the trend of the data on the log-log plot is a reliable indication that the data represent a growth sequence, i.e., that the larger faults have grown in a series of stages represented by the smaller faults. However, the slope of the line on the graph shows that the relationship between displacement and width is non-linear: an increase in D corresponds to a much smaller proportional increase in W. They then make an important point: this relationship contrasts with the linear relationship between the width of a fault and the amount of slip during a single seismic event (Scholz, 1982). Walsh and Watterson's (1988) data shows that the width of a fault increases by a constant amount, as opposed to a constant proportion, with each successive event. Growth models in which width increases by a constant proportion with each slip show a linear relationship between D and W which is not consistent with the data shown in fig. 2.6 (Walsh and Watterson, 1988). They point out that the unexpected feature of the arithmetic fault growth model defined by their data is that the slip increment is independent of the size of the fault.

2.5 Review of structural studies on basin inversion

Complex deformation styles in basins are not only created by subsidence, but can also result from reversal of fault displacements during basin inversion. Basin inversion can markedly influence basin structure and sedimentation patterns. It was Harding (1983) who formally suggested the terms positive inversion for an area which has changed from subsidence to uplift, and negative inversion for an area which has changed from uplift to subsidence. The better known examples of basin inversion and fault reactivation have been described from commercial seismic data (Ziegler, 1983; Harding, 1983).

Gillcrist et al. (1987) emphasized that there are other mechanisms which can cause inversion than just compression and uplift of sedimentary basins resulting in the reversal of movement on normal faults. These mechanisms are: 1. Uplift due to flexure: uplift generated by the flexural bending of a lithospheric plate as a result of localized loading by sedimentation (Beaumont, 1978), or by the accummulation of a thrust mass; 2. Uplift along low-angle strike-slip faults: changes in strike of a strike-slip fault, or offsets in the faults may cause the development of basin or uplift zones; 3. Isostatic uplift of sedimentary basins due to heterogeneous thinning of the crust and lithospheric mantle; 4. Slight changes in plate vectors resulting in strike-slip belts which bound sedimentary basins or act as compartmental faults to heterogeneous extension in the basin which become zones of transpression and uplift; 5. Major stress reversals in the crust: basins with major changes in stress magnitudes such that directions of extension reverse to become directions of compression, and; 6. Variations in basin opening rate. This mechanism can create tectonic inversion on a local scale during regional extension through changes in basin development causing reversals in displacement sense along a transfer zone and earlier normal faults within the transfer zone.

Gillcrist et al. (op. cit.) recorded observations of the detailed interaction of early basin structures with the later inversion related structures. The important conclusions made in the study were that: 1. A steeply dipping normal fault generally acts as a buttress to compressive movements. 2. Normal faults which developed between rotated blocks may invert by back-rotation. 3. The variably rotated and hence variably dipping normal faults resulted in different structures during later thrusting. Gently dipping faults in the basement inverted into a major thrust stack. Steeper faults are better preserved and show tight folds and back-thrusts in the sediments in the half-grabens. The footwalls to the normal faults often collapsed during thrusting, producing triangular shaped 'floating' horses of basement (short-cut contractional faults). 4. Steeper dipping normal faults are seen to deform by oblique slip movements, acting as tram-lines in controlling the later regional movement direction. 5. Areas of earlier extensional tectonics may be stronger than adjacent unstretched lithosphere due to the fact that the strength of the lithosphere beneath a basin increases with time.

Welbon (1988) assessed the role of early intrabasinal faults on later thrust fault evolution in Mesozoic and Cenozoic rocks in the Arve valley region of the External French Alps. He found that the intrabasinal faults exerted a major influence on the distribution of mechanical heterogeneities, including those arising from variations of stratigraphic thickness and type across faults, fault-related unconformities and the presence of the fault itself. He observed many of the same relationships between the orientation of the earlier intrabasinal faults and the deformational structures resulting from the uplift, as also described by Gillcrist et al. (1987). Welbon (op.cit.) divided the differences in structures into two categories: those pre-existing faults dipping in the oppposite direction to the advancing thrusts, and those dipping in the same direction. He concluded that: 1. Pre-existing faults dipping in the opposite direction to thrusts are generally cut through (with buttressing possibly occurring at this stage), and can be overturned during this process. The fault can be reactivated if the overturning is of sufficient magnitude, forming a thrust which may have a more complicated profile than a simple reactivated fault. 2. Pre-existing faults dipping in the same direction as the thrusts may: a. be reactivated, cause a ramping of the thrust ahead of the pre-existing faults so that it joins the older fault at a change in angle of the ramp; b. be cut through by a thrust; or, c. cause pinning of the thrust at the footwall of the fault followed by buttressing above the thrust.

McClay et. al. (1987) presented data from their model studies of inversion structures in sand box and clay analogue systems. Models which were first extended were then subjected to contraction. Initially planar, listric, listric ramp-flat and uniform extension geometries were investigated. Only partial reactivation of earlier formed extensional faults occurred. Both in the high-angle planar and ramp-flat geometries, short-cut contractional faults were common. Their models showed asymmetrical uplifts on both old extensional faults and on new contractional faults.

Chapter 3. A Review of Fault Rock Evolution

3.1 Introduction

The study of fault behaviour in both experiment and nature has rewarded geologists with advances in the understanding of the mechanics of faulting, and their relationship to earthquake generation and frictional stability in the earth's crust. In addition, the study of fault rocks preserved in exhumed fault zones has provided information about fault activity at different depths in the crust. Sibson (1983) suggested that the maximum depth of seismicity is limited by a transition in deformation mechanism from localized brittle fracture to homogeneous plastic flow. Therefore, it has been widely assumed that rocks in fault zones behave in a frictional manner in the shallower parts of fault zones where earthquakes are located, and that at greater depths fault zones become wider and deformation in them occurs by mechanisms involving crystal plasticity, such as either dislocation or diffusion creep. The observations of the fault rock products, inferred faulting mechanisms, and the frictional and seismic behaviour of faults have been combined to produce crustal fault zone models, such as those proposed by Sibson (1977, 1986, 1989) and Scholz (1989) (fig. 3.1).

This thesis focuses upon fault rock evolution and identification of the deformation mechanisms accompanying shallow level faulting (<10 km) associated with sedimentary basin development [i.e., faulting at relatively low temperatures (<250°C) and pressures (<3 Kb)]. Section 3.2 presents a review of the range of deformation mechanisms which can operate in fault zones at shallow levels in the crust in the context of the fault zone models described above.

In this study, an emphasis has been placed upon identifying specific fracture processes from microstructures in cataclastic fault rocks adjacent to normal faults. Therefore, a more detailed discussion of the fracture mechanics approach now successfully applied to rocks (see review edited by Atkinson, 1987; Lloyd and Knipe, submitted), is presented in section 3.3. Section 3.4 briefly reviews the important aspects of experimental work on microcracking. Section 3.5 reviews recent work on cataclastic fault rocks in both experiment and nature.
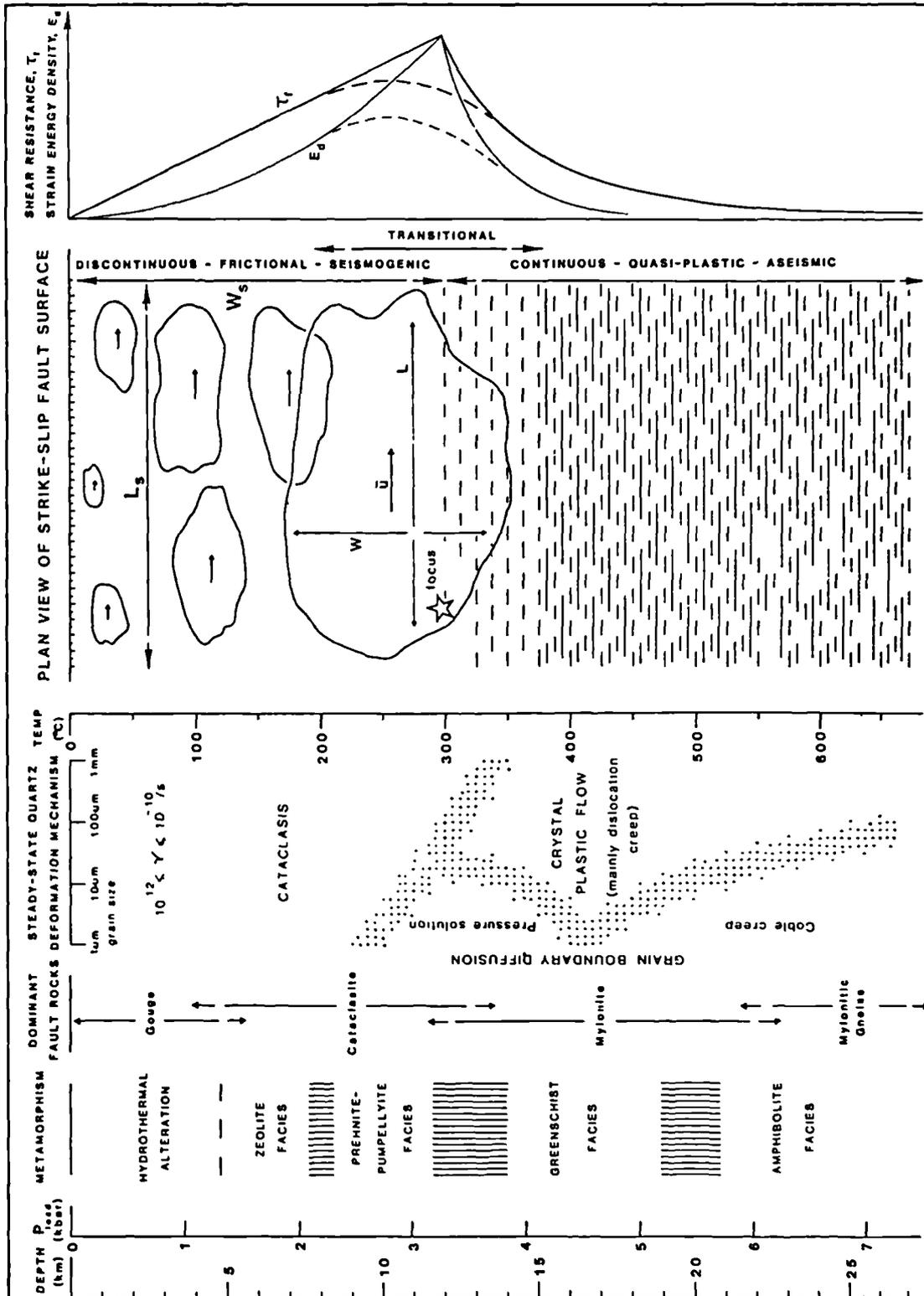
Figure 3.1. Conceptual model of a crustal fault zone (from Sibson, 1977).

3.2 Deformation mechanisms in shallow level fault zones

3.2.1 Crystal plasticity

Crystal plasticity can contribute to strain during deformation by internal deformation mechanisms in crystals such as the movement of dislocations and twinning. Twin glide and translation glide are important deformation mechanisms at low temperatures (usually <0.5 melting temperature at laboratory strain rates), where dislocation motion is confined to slip planes. Dislocation glide leads to dislocation tangles which restricts further dislocation motion and induces work-hardening (increased resistance to strain during deformation), (Atkinson and Meridith, 1987; Lloyd and Knipe, submitted). This type of deformation has been termed low temperature crystal plasticity, and has been found to be an important mechanism contributing to cataclasis during brittle faulting (Lloyd and Knipe, submitted). Crystal plasticity is important to the low-temperature ductile fracture (LTDF) mechanism (Lloyd and Knipe, submitted), and its role in fracturing will be discussed in detail in section 3.4.

High-temperature conditions (usually >0.5 melting temperature) result in dislocation climb (movement of dislocations out of their slip planes) and cross-slip (alteration of the slip plane used by screw dislocations). Dislocation motion during climb is diffusion controlled (White, 1973a, 1977). The mobility of dislocations can lead to microstructures characteristic of the processes of dynamic recovery and dynamic recrystallization. These processes are described in detail by Hobbs et al. (1972), Nicolas and Poirier (1976), Poirier (1985) and Urai et al. (1986), and the microstructures characteristic of these particular processes in quartz are documented and described by White (1973a, 1973b, 1976, 1977).

The process of dynamic recovery involves the reorganization of dislocations into lower energy configurations (White, 1977). The dislocations can be organized into walls bounding subgrains smaller than the original grainsize which are internally less deformed (White, 1977). Undulose extinction (areas of subparallel subgrain walls or forests of dislocations) and deformation lamellae are microstructures also associated with recovery processes (White, 1977).

Dynamic recrystallization can occur by subgrain rotation recrystallization and grain boundary migration (Hobbs, 1968; Nicolas and Poirier, 1976; White, 1973a, 1973b, 1976, 1977, 1979; Poirier and Guillope, 1979). During subgrain rotation recrystallization, dislocations are added to pre-existing subgrain walls, increasing the mismatch between subgrains until a new grain is formed. Hobbs (1968) suggested that this process is a continuation of the subgrain-forming recovery process. There is no universal agreement of the value of mismatch or misorientation across a boundary between two subgrains which determines when the boundary between them becomes a grain boundary (Urai et al., 1986). The misorientation across a subgrain boundary may increase during deformation by the presence of a static or mobile boundary (Urai et al., 1986). When the subgrain boundary stays fixed, the boundary can receive dislocations from subgrains on both sides. If the subgrain boundary is mobile, the boundary can migrate through the material and collect dislocations or other subgrain boundaries as it migrates. The main evidence for recrystallization by a subgrain rotation process comes from the core-and-mantle structures in partly recrystallized rocks (White, 1976). In this microstructure, cores of host grains are observed to have increasing subgrain development at their outer margins, or mantles, which are then surrounded by recrystallized grains with similar size and orientations to the nearby subgrains (White, 1976). In more completely recrystallized rocks, domains of recrystallized grains with similar orientations are sometimes observed and are interpreted by Poirier and Nicolas (1975) to represent former single grains that recrystallized by a subgrain rotation process.

Strain energy differences between grains drives the process of grain boundary migration recrystallization (Nicolas and Poirier, 1976). In the case of two adjacent grains of different strain energy, the less strained grain can consume a more strained grain by the migration of the boundary between the two grains into the more strained grain (White, 1973b, 1977). Urai et al. (1986) emphasized the relationship between the subgrain rotation and the grain boundary migration processes by showing that grain boundary migration can occur from the presence of newly nucleated grains or from strain free grains created by the subgrain rotation mechanism. Sutured boundaries are characteristic of the grain boundary migration process (White, 1973a).

Stress levels operating in ductile deformation zones can be estimated from microstructures resulting from dislocation creep and twinning, as they are related to the flow stress level (Groshong, 1972; White, 1979a; Ord and Christie, 1984; Etheridge and Wilkie, 1981; Twiss, 1977). Dislocation creep features such as dislocation density, sub-grain size and the size of recrystallized grains are all related to flow stress level, although recent work (White, 1979b; Ord and Christie, 1984; Twiss, 1977) shows some discrepancies which suggest more work is needed to clarify the detailed relationships, including recognition of the stability of these microstructural features (Knipe, 1989a). It has been suggested that subgrain size may reflect the maximum stress in a deformation history of variable stress magnitudes (Poirier, 1985). The size of dynamically recrystallized grains is inversely related to differential stress in single-phase materials (Twiss, 1977; Ord and Christie, 1984; Poirier, 1985).

3.2.2 Diffusive mass transfer (DMT)

Diffusion mass transfer involves the redistribution of material during deformation by diffusion processes. The transport of material can occur along various mass transfer paths, such as a. the bulk crystal structure (Nabarro-Herring creep; Poirier, 1985); b. diffusion along distorted and disordered crystal structures of grain boundaries (Coble creep; Poirier, 1985); c. diffusion along a thin fluid film present within grain boundaries ('pressure solution'; Rutter, 1983); and, d. transport in fluid which may itself be experiencing flow, producing infiltration of material (Etheridge et al., 1984; Gratier and Guiguet, 1986).

Knipe (1989a) outlined a three-stage classification of the processes involved in deformation induced by DMT: i. source mechanisms; ii. migration or diffusion mechanisms; and, iii. sink processes. As summarized by Kerrich (1978) and Rutter (1983), these processes represent the transfer of material away from zones of relatively high intergranular normal stress, to interfaces with low normal stress. Source mechanisms control the processes by which the material enters a diffusion path, the activation of diffusion through the crystal structure and along surfaces such as grain boundaries, and also those related to corrosion and reaction processes (Knipe 1989a).

Etheridge et al. (1983) and Etheridge et al. (1984) emphasized the role of high fluid pressure and mass transport by fluid advection during metamorphism (see also Chapter 4). Etheridge et. al. (1984) reviewed the importance of fluids in both prograde and retrograde metamorphic processes, and explored in detail the consequences of the structure of grain boundaries on processes in which fluids are involved.

3.2.3 Frictional sliding

At shallow levels in the crust, frictional grain boundary sliding is a mechanism commonly active during deformation of partially or unlithified sediments (Maltman, 1984; Jones and Preston, 1987). The friction between grains in these uncemented aggregates, particularly under the influence of low confining pressures and high pore fluid pressures is easily overcome, and sliding can be initiated. As a result, the aggregate can change shape without changes in the forms of individual crystals, grain shapes and sizes. This type of deformation can result in a grain fabric and texture which appears identical to that of the starting material, and therefore the operation of grain boundary sliding is often difficult to identify. Borradaile (1981) termed the deformation mechanism 'independent particulate flow'.

The microstructures found in partially lithified sediments recovered from D.S.D.P. cores adjacent faults and veins indicate that frictional grain boundary sliding is an important mechanism involved in their development. In addition, it has been shown that fluid influx through these zones can result in the complex interaction between fluid pressures, lithification and strain rate (Knipe, 1986a, 1986b; Moore et al., 1986; Agar et al., in press; Prior and Behrmann, in press a). High pore fluid pressures can promote significant dilation, and Knipe (1986b) has found that late stage loss of fluids can result in volume loss and preferred alignment of grains during the porosity collapse of the grain framework. These processes have been inferred to have operated during the development of scaly fabrics frequently described from these environments (Knipe, 1986a, 1986b; Moore et al., 1986; Agar et al., in press; Prior and Behrmann, in press a and b). However, microstructural analysis has shown that care must be taken in the classification and interpretation of scaly fabric development, since despite the mesoscopic similarity of certain scaly fabrics, the detailed geometry of

the microfabric suggests that different deformation mechanisms have contributed to their development (Agar et al., in press). Their work has shown that the mesoscopic and microscopic fabrics of tectonized fine-grained sediments can relate to different processes of rock evolution. Macroscopically defined scaly fabrics are found which do not have a microscopically preferred alignment (Prior and Behrmann, in press a).

The geometry of mesoscopically anastomosing fabrics can be described with terms such as 'anastomosing', 'parallel', and 'sinuous', as suggested by Borradaile et al. (1982). Therefore, Agar et al. (in press) have suggested that whilst the term 'scaly fabric' is still appropriate as a field description, it is important that the term is not used to refer to fabrics on the scale of grains, so as not to infer mechanisms of their development.

3.3 Fracture and cataclasis

3.3.1 Definition of fracture mechanics

It is appropriate here to reiterate the definition of fracture mechanics, as quoted in Atkinson (1987):

".... the fracture of materials in terms of the laws of applied mechanics and the macroscopic properties of materials. It provides a quantitative treatment, based on stress analysis, which relates fracture strength to the applied load and structural geometry of a component containing defects".

The classic paper of Griffith (1920) provided the basis for the development of fracture mechanics theories. Griffith's (1920) approach is on the scale of dislocations: crystalline solids are not ideal but contain defects or flaws. The defects or flaws act as stress concentrators. The defect is usually modelled as a crack, but it could be a pore or other non-linear defect. The influence of applied loads on crack extension can then be described in terms of parameters which characterize the stress and strain intensity near the flaw (crack tip). Crack propagation in various materials is described by the stress-intensity factor, K, and cracks always propagate when $K > K_c$ (the critical stress-intensity factor).

3.3.2 Fracture mechanisms

A range of intragranular and intergranular fracture mechanisms which can operate in rocks have been recognized, and each are described separately below. Sub-critical crack growth is an important fracture mechanism in the Earth's crust, particularly in the presence of fluids, and is also discussed. Knipe (1989a) has assessed fracture mechanisms in rocks on the range of pre-failure processes which influence or control the propagation of fractures. Fracture mechanism maps (Ashby et al., 1979; Ghandi and Ashby, 1979; Dennis and Atkinson, 1981) show the environmental conditions under which different mechanisms of fracture produce failure in the shortest time, i.e., are dominant (fig. 3.2). From these maps, it is inferred that for the upper 20 km. of the earth's crust, cleavage 1 or brittle intergranular fracture (BIF) 1 will be the most important mechanism of fracture in quartz (Atkinson and Meridith, 1987). These mechanisms will be discussed in the next sections.

3.3.2.1 Intragranular mechanisms

Fracture at the ideal strength, cleavage fracture, low temperature ductile fracture, and transgranular creep fracture are intragranular or transgranular fracture mechanisms which are discussed in this section.

Fracture at ideal strength is extremely unlikely as it is theoretically modelled as rupture in perfect crystals, which requires an applied stress greater than the interatomic attractive forces. Cleavage fracture mechanisms I, II, or III occur if the bulk resistance to plastic shear exceeds the cohesive strength on cleavage planes within a mineral (a cleavage plane being any plane in the crystal lattice along which the atomic bonds can be broken). Depending on the specific fracture nucleation process, one of the three cleavage fracture mechanisms can occur, as follows: i. Type I, controlled by pre-existing flaws which allow crack propagation at stresses less than those required for crystallographic slip or twinning. Fracture strength is dependent on the largest flaw size and there is no macroscopic flow, however, crack-tip plasticity is possible. ii. Type II, generated through microplasticity involving strains of <1%.
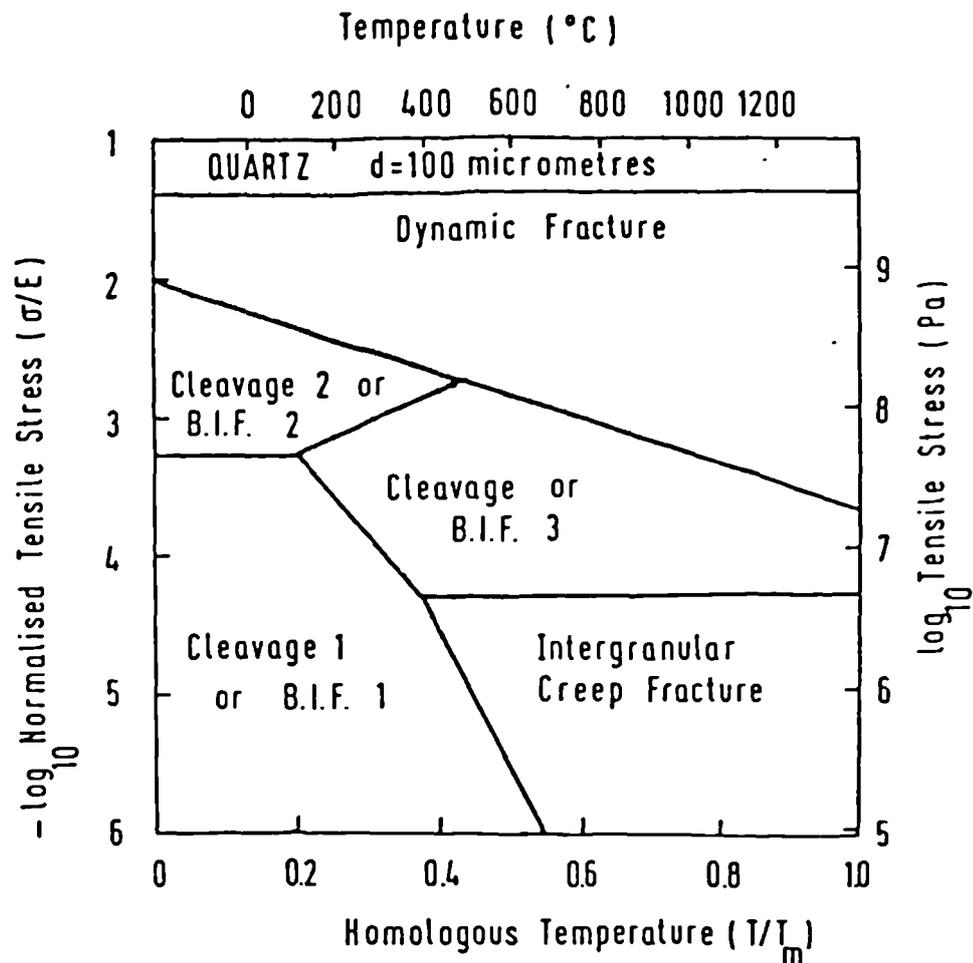
Figure 3.2. Fracture mechanism map for quartzite with 100 μm grain size. The stress axis in the map is truncated by the stress required to overcome the interatomic forces in a perfect crystal, given by σ_{ideal} = E/10. At stresses immediately below σ_{ideal} lies the region of dynamic fracture where the initial load must be described in terms of the propagation of an elastic wave through the material. Map infers that in the upper 20 km. of the earth's crust, cleavage I or BIF I will be the most important mechanism of fracture in quartz. From Atkinson & Meridith (1987), after Ashby et al. (1979) and Ghandi and Ahsby (1979) .

Type II cleavage fracture is modelled as resulting from a very small inherent flaw size, allowing the applied stress to exceed the levels required for crystallographic slip. The key idea here is the concept that slip could occur on a limited number of independent systems, associated with limited plastic strains (i.e. < 1%), such that internal stresses are generated from dislocaton pile-ups at grain boundaries, resulting in crack nucleation. iii. Type III cleavage fracture can involve up to 10% plastic strain prior to fracture, and is controlled by cracks generated by grain boundary sliding or crystal plasticity. Flow stress decreases with increasing temperature, therefore this fracture mechanism is temperature dependent. The flow mechanisms act to increase the materials resistance to fracture by crack-tip blunting, however, the flow can eventually generate larger cracks or cause pre-existing cracks to grow such that the cracks propagate unstably.

Low temperature ductile fracture (LTDF) has now been recognized as a geologically important mechanism contributing to brittle faulting in the upper crust (Lloyd and Knipe, submitted). Large strains (10-100%) can result from plasticity without cleavage fracture. Crack nucleation is commonly associated with voids or inclusions, and growth of the cracks occurs by plasticity. During transgranular creep fracture, crack nucleation and propagation is very similar to LTDF, however, the associated creep deformation is a temperature dependent mechanism. Large plastic strains can occur, and therefore the mechanism is generally time dependent (Atkinson and Meridith, 1987).

3.3.2.2 Intergranular mechanisms

Dynamic fracture, brittle intergranular fracture, and intergranular creep fracture mechanisms are considered in this section. Concepts of dynamic fracture are of great interest to geophysics in the study of rapid fault motion and seismic wave generation (e.g. Aki and Richards, 1980). For the dynamic stress intensity factors, the stress distribution around crack tips must be calculated using the equations of motion, rather than the equations of equilibrium, as in all of the previous cases described above, the state of stress is assumed to be that for a stationary crack and kinetic energy is not considered (Atkinson, 1987). For elastic analysis of the strain energy release rates, kinetic energy must be considered.

The stress required to cause a mineral grain to cleave is delicately balanced by the stress required to cause brittle grain boundary cracking (Atkinson and Meridith, 1987). The fracture mechanism which occurs is determined by temperature, impurity content, and the rock composition and texture, including the important aspect of cement mineralogy and texture. Fractures which occur along a grain boundary have been termed brittle intergranular fracture by Ghandi and Ashby (1979). They recognize three types of brittle intergranular fracture: BIF I, BIF II and BIF III, which are analogous to the particular cleavage mechanisms described above.

Failure associated with high temperatures and low stresses always occurs by intergranular creep fracture (Ghandi and Ashby, 1979). This mechanism is associated with the nucleation and growth of voids or wedge cracks at grain or phase boundaries. The nucleation of the crack is most likely controlled by dislocation creep, but with small cracks, growth can occur by local diffusion (Atkinson and Meridith, 1987). Linking of voids or cracks associated with the fracture is associated with low (<10%) plastic strains, even after long periods of creep deformation, as stresses are small.

3.3.2.3 Subcritical crack growth

Fracture mechanics infers that fracture occurs by propagation of pre-existing cracks. As discussed earlier, cracks always propagate when $K > K_c$. However, stress corrosion, dissolution, diffusion, ion-exchange and microplasticity are mechanisms by which cracks can grow subcritically (Atkinson, 1984, 1987). The important chemical effects of pore water, almost ubiquitous in the crust, influence these mechanisms, each of which are described briefly here.

As K decreases, the rate of crack propagation decreases as well, such that a threshold level of K, there exists a value of K (K_{th}) below which no propagation occurs. K is dependent on composition, and stress corrosion can reduce K_{th} by the presence of reactive species at crack tips promoting weakening reactions. Dissolved impurities can also contribute to these weakening reactions, more likely at high temperatures, as diffusion is involved. If ion exchange from chemical species with species from the solid

phase results in a gross mismatch in the size of the different species, lattice strains can occur which facilitate crack extension.

Microplasticity can also give rise to subcritical crack growth. In the stress field ahead of an initially stable macrocrack tip, a damage zone can develop where microcracks of various orientations can nucleate by inhomogeneous plasticity wherever the local conditions for slip or twinning are satisfied (Atkinson and Meridith, 1987). Linking of grain boundary and cleavage microcracks will allow macrocrack extension. This process is episodic, involving periods of rapid crack extension followed by periods of relative crack stability. Macroscopically then, it appears as quasi-static subcritical crack growth. The processes involved in this type of crack growth are most easily activated under conditions of relatively high temperatures and low strain rates.

3.4 Experimental work on microcracking

This section discusses the important experimental work done on microcracking. Only the most relevant and recent work will be reviewed from the significant amount of work in this field.

Kranz (1983) presents a review of this subject. He classifies microcracks into grain boundary cracks, intracrystalline cracks, intercrystalline cracks, and cleavage cracks. Tensile microcracks often observed in experimental work are referred to as 'axial' cracks, and several examples of impingement-induced microcrack experiments are discussed below. A classic experiment by Gallagher et al. (1974) used photoelastic techniques to demonstrate the formation of microcracks perpendicular to σ_3 in tensile stress fields developed by impingement of grains (fig. 3.3). Stress concentrations at grain contacts were connected by microfractures which followed the maximum principal stress trajectory which connects the 'critical' contacts, propagating through the points where the magnitude of the local maximum stress difference is the greatest. Positioning of the critical contacts is dependent on sorting, grain shapes, packing, and the boundary load conditions applied to the aggregate. Microfracture orientation is random in poorly sorted aggregates, and is influenced by packing in well-sorted aggregates.
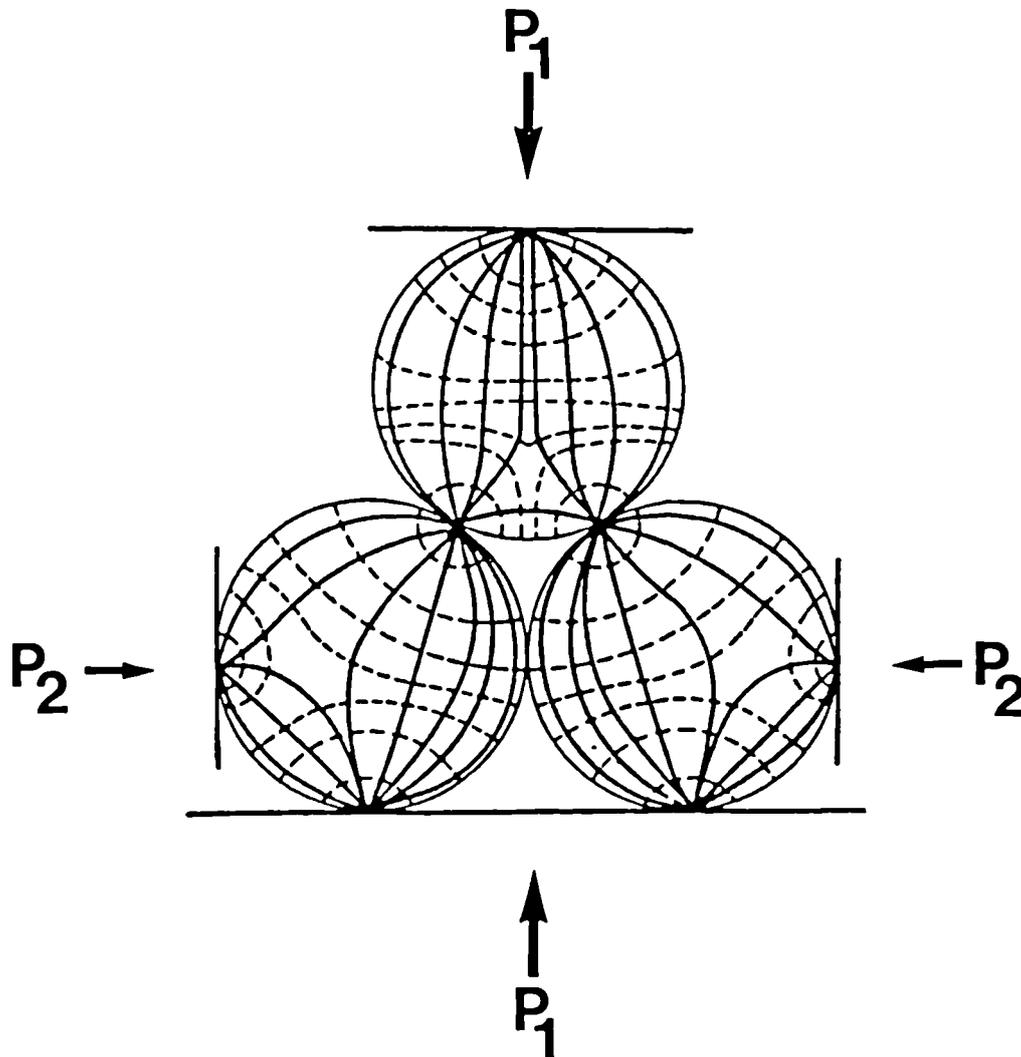
Figure 3.3. Schematic diagram of the principal stress trajectories prior to failure in a three-disc model, from the experimental observations of the stress fields developed by impingement of 'grains' (perfectly elastic discs) subjected to a load. The load is applied both vertically (P_1) and horizontally (P_2), with $P_1 >> P_2$. The greatest principal stress trajectories are indicated by solid lines which also are extension fracture trajectories. Dashed lines indicate trajectories of the least principal stress (from Gallagher et al., 1974).

Similar impingement-induced microcracking can be produced thorugh indenter experiments (Swain and Lawn, 1976; Swain and Atkinson, 1978; Atkinson and Avdis, 1980). These workers developed a theoretical framework for the sharp-indenter technique. The load beneath a sharp indenter is compressive. However, the stress field produced contains a significant tensile component which determines the crack-driving force. The fracture parameters derived from indenter tests thus relate to mode I cracks, and can be therefore compared with mode I analyses elsewhere using other methods (Ferguson et al., 1987).

Lindquist et al. (1984) used tungsten carbide indenters in samples of limestone, marble and granite. Fracture patterns were compared directly with the theoretical predictions of indent patterns by Lawn and Wilshaw (1975). Lindquist et al. (op.cit.) observed radial cracks, perpendicular or sub-perpendicular to the load, with a zone of `crushed' material under the indenter. An interesting aspect of their experiments is the modification of fracture patterns with the microstructure of the samples. Straight and continuous cracks in the fine-grained (< 0.007 mm) dense limestones, compared with the more irregular, discontinuous fractures in the medium grained marble (0.27 mm). Grain boundaries and cleavage affected crack path in the latter example. In the medium grained granite (0.37 mm), a few cracks developed similar to those in the calcareous rocks, but these subsequently multiplied into lower-angled, shorter cracks. The general pattern of the radial cracks agreed well with the simple elastic fields predicted by the configurations described by Lawn and Wilshaw (1975), however the transgranular fractures were often strongly influenced by pre-existing flaws and microstructure.

A conventional Vickers microhardness test used to determine mode I ing) fracture toughness, K_{ic}, and hardness, H, in quartz was combined with detailed SEM and TEM study to determine the deformation processes in natural quartz resulting from indentation experiments by Ferguson et al. (1987). Their study provided a unique example of the application of fracture mechanics and microstructural analysis in evaluating the mechanics of fracture in sharp-indenter experiments. One important observation was revealed by extensive SEM study of the three-dimensional indent-fracture morphology. Ferguson et al. (1987) found a region of high back-scattered

electron contrast immediatley adjacent to the indenter contact. TEM analysis determined that the zone is an intensely deformed area with very high fracture density. The detailed study revealed evidence for partial melt along some fractures, particularly those parallel to the indent impression edges. Ferguson et al. (op.cit.) suggest that this is the result of rapid displacement rates along shear fractures in which the forward motion of the indenter was accommodated. A submicrometer-scale blocky structure is observed between fractures, possibly originated by cataclasis. However, no voids were observed in this zone, suggesting that some crystal plasticity may be involved as an accommodation process contributing to the deformation. An important conclusion in this study is that the 'plastic' deformation associated with indentation in quartz is shown to be controlled largely by fracturing. In terms of the fracture parameters in the fracture mechanics analysis of the experiments, the increase in hardness with decreasing load which they observed is therefore to be expected. The energy available for fracture increases with the cube of a characteristic dimension, whereas that required increases only with the square. They note that a similar hardness-load relationship is observed in many materials, suggesting that fracture may be a more important process in low-temperature 'plasticity' than previously recognized.

Microfractures induced from shear fault experiments were identified by Friedman and Logan (1970) as 'microscopic feather fractures,' observed oriented parallel to σ_1 and exclusively related to shear faults. Teufel (1981) observed micrscopic feather fractures on pre-cut Cocconino sandstone, in an experiment which confirmed a density increse with displacement and normal stress, and a crack length increase with the same parameters.

More recently, a significant contribution to the theory of microcrack experiments was presented by Hori and Nemat-Nasser (1985). Their model is for progressive microcrack growth and microcrack interaction, based on experimental observations of the process of crack growth along a defect. The results agree with that of the experiments of Brace and Bombalakis (1963), where the stressing of an inclined crack results in growth in a curved path towards the direction of applied compression. Hori and Nemat-Nasser's experiments also confirmed that the slightest lateral tension causes crack growth to become unstable after a critical crack length.

A topic following on from the above is the influence of initial microstructure and failure conditions on microcracking mechanism. Some experiments which demonstrate this are described here.

Textural changes through failure are similar to the effects of confining pressure. Crack densities at failure increase with confining pressure, as shown by Hadizadeh (1980), Friedman and Logan (1970), and Teufel (1981). Hadizadeh (1980) also demonstrated that microcrack length increases with confining pressure. Dunn et al. (1973) studied the influence of microstructure on microcrack mechanism. An inverse power-law relationship was found between strength and porosity in sandstones and quartzites. The higher porosity, lower strength rocks generated a wide zone of cataclasite with less grain fracturing compared to the low porosity, high-strength rocks.

Hadizadeh (1980) classified failure into two types, governed by what he termed Type I and II microstructures. Well-cemented, interlocking, low-porosity microstructures are described as type I. The stress distribution is initially homogeneous, and shear-mode grain boundary cracking is favoured until the microstructure is 'loosened' sufficiently for impingement-induced microcracks. Poorly-cemented, high-porosity polyphase rocks have type II microstructures, where the initial stress distribution is very inhomogeneous, and impingement microfractures are favoured. Blenkinsop and Rutter (1986) suggested that the microstructure of the Cambrian Pipe rock quartzite of N.W. Scotland was similar to that of the type II microstructure at the time of deformation. The classification into two types of deformation sequences is therefore based on the homogeneity of the initial stress distribution, which controls the sequence of microcrack mechanisms and fracture type.

3.5 Cataclasis and fault rock nomenclature

This section describes field and microstructural studies of cataclastic fault rocks in both nature and experiment, including discussion of the fault rock nomenclature used in the studies described below.

Sibson's (1977) textural classification for the distinctive rock types found in zones of shear dislocation at both high and low crustal levels considered the range of fault rocks which could occur (fig. 3.4). The classification avoids genetic connotations, and is divided by the recognition of the following two significant features: firstly, the separation of fault rocks which are essentially random in shape and crystallographic fabric from those which are foliated, and secondly, the presence or absence of cohesion. Cohesive fault rocks are then subdivided on the nature of their matrix. Sibson's scheme is easily used in the field, as it relies on two easily identified discriminant features, foliation and cohesion, and the quantified estimate of matrix to clast ratio.

Rutter and White (1979) first provided insights into the detailed microstructure of fault gouge from experimental studies. Stress relaxation tests were performed by Rutter and Mainprice (1978) on pre-faulted and intact samples of impure quartz sandstone deformed in both dry and wet conditions at temperatures of 300-400°C. The microstructures of the fault gouge studied by Rutter and White (1979) are highlighted here. The initial faulting at 20°C produced an affected zone up to 20 grain diameters wide, with the main fault 1 grain-diameter wide. Within the fault zone, coarse fragments of 20-50 μm are interspersed with a matrix of fine fragments of 1-5 μm range. TEM shows two important observations which are the result of processes occurring during deformation of the sandstone at 300-400°C in the wet experiments: i. the recrystallisation of pre-existing deformed illite and kaolinite, which then formed oriented aggregates of small micas, and the segregation and growth of mica beards, and ii. syntectonic formation of quartz overgrowths and new grains. The observations indicate the importance of diffusive mass transfer processes in the experiments, which may correspond to the processes involved in the healing of natural fault zones after slip, leading to time-dependent modification of the physical properties of fault zones (Rutter and White, 1979).

RANDOM - FABRIC	FOLIATED

INCOHESIVE

| FAULT BRECCIA (visible fragments >30% of rock mass) | ? |
| FAULT GOUGE (visible fragments <30% of rock mass) | ? |

COHESIVE

Glass/devitrified glass

| PSEUDOTACHYLYTE | ? |

NATURE OF MATRIX

Tectonic reduction in grain size dominates grain growth by recrystallisation & neomineralisation

CRUSH BRECCIA	(fragments > 0.5 cm)	0 - 10%
FINE CRUSH BRECCIA	(0.1cm < frags. < 0.5cm)	
CRUSH MICROBRECCIA	(fragments < 0.1 cm)	

PROTOCATACLASITE	PROTOMYLONITE	10 - 50%
CATACLASITE	MYLONITE	50 - 90%
ULTRACATACLASITE	ULTRAMYLONITE	90 - 100%

Cataclasite Series

PHYLLONITE VARIETIES

Mylonite Series

PROPORTION OF MATRIX

Grain growth pronounced

| ? | BLASTOMYLONITE |

Figure 3.4. Textural classification of fault rocks (from Sibson, 1977).

House and Gray (1982) used Sibson's (1977) textural classification to describe cataclasites adjacent the Saltville Thrust, a major regional thrust of the Southern Appalachian fold and thrust belt in the U.S. The amount of matrix is used to distinguish between crush breccias (<5% matrix), cataclasites (50-70% matrix), and ultracataclasites (90% matrix). The fault rocks are viewed as a progressive and sequential series resulting from communition by fracturing and grinding along intersecting fractures. The fault zone initiates by microfractures which coalesce to form conjugate shear fractures. A gouge with the matrix composition of an ultracataclasite is formed from continued frictional grinding and grain size reduction. The continuous reduction in grainsize is coupled with a changing proportion of matrix content in the fault rock. The overprinting of secondary shear zones, stylolites and veins subsequent to the development of the cataclastic fabric is observed. House and Gray (1982) note that the simple textural evolution inferred from the finite microfabrics of the fault rocks is problematic considering the very large number of stress cycles the rocks along seismically active fault zones must have experienced.

Olgaard and Brace (1983) report a study on fault gouge from two mining-induced shear fractures. Two samples of gouge were collected: the 'old' gouge sample was collected from a shear zone that formed during an earthquake of magnitude 2.1 at a depth of 2 km. The width, displacement, area and driving stress were measured at this locality. The 'fresh' sample was collected from the same area but from a smaller, unrelated fracture. SEM and TEM observations showed that: 1. the particles range in size from the original grain size of the Witwatersand quartzite (+0.5 mm.) to less than 0.05 μm, and X-ray sedimentation data indicate that the particles follow a log-normal size distribution between 1 and 50 μm; 2. the particles larger than 1 μm. are slightly rounded, nearly equant in shape and conchoidally fractured; 3. TEM study indicates that the submicron-sized quartz particles are highly angular and plately and commonly show basal plane cleavage; and, 4. misorientations between cleavage plates they suggest imply that the plates have been separated.

Olgaard and Brace (1983) calculated surface area measurements from the X-ray sedimentation and nitrogen adsorption techniques, and found that in the old gouge, specific surface area is 2.0 m^2/g, and in the fresh gouge, it

is 0.7 m^2/g. From these measurements and their assumptions of fault parameters, the surface energy was calculated to be 1-10% of the total energy released during an earthquake, and therefore, of the same order as the seismic energy. If the area between the cleavage plates observed on the TEM is considered, a factor of 2 or higher is obtained for surface energy.

Rutter et. al. (1986) report an important comparison of structural and microstructural features of experimentally and naturally produced fault gouge, emphasizing their geometrical similarities. The importance of cementation affecting the strength and frictional characteristics of a fault zone was also highlighted (see also Rutter and White, 1979).

Blenkinsop and Rutter (1986) describe pervasive brecciation in Cambrian Quartzite from the Moine Thrust Zone in NW Scotland resulting from folding, and distinguish the breccias from cataclasites resulting from localized strain along the Ord Thrust Plane. They emphasize that their descriptions, based on field and microstructural observations, are not intended as a comprehensive classification of fault rocks. As with House and Gray (1982), Blenkinsop and Rutter (1986) use the amount of matrix present in the rocks to distinguish between intact quartzite (relatively undeformed quartzite), breccia (25-75% intact quartzite), and ultrabreccia (<25% intact quartzite). They propose that the fault rocks represent a sequence of progressive deformation involving three processes: 1) development of extension microcracks; 2) development of shear faults by linking of and shearing along extension microcracks; and 3) development of breccias and ultrabreccias as large-scale analogues of the shear faults. The matrix is described as fine-grained, consisting of fragmented grains, iron oxides, and non-luminescing cement.

Using field and optical microscopy techniques, Chester and Logan (1986) described gouge from the Punchbowl Fault Zone, an inactive trace of the San Andreas. Microscopically, the gouge is described as approximately 70% brown "matrix" composed of grains less than 10 μm in size. Matrix grains are typically equant, angular porphyroclasts of quartz or feldspar. Porphyroclasts larger that 10 μm constitute 5% of the gouge. The gouge also contains microcrystalline quartz or calcite, appearing as sealed fractures or irregularly shaped porphyroclasts. Chester and Logan (1986) conclude that

at least 30% of the gouge was precipitated form a fluid phase, and that the presence of a significant amount of cement and cataclastically deformed cement suggests that the gouge was repeatedly cemented and fractured during faulting.

More recently, particle size distributions found in cataclastic fault gouges were the focus of investigations looking into the mechanical processes operating during cataclastic grain size reduction (Sammis et al., 1986, 1987). The self-similar (log-normal) particle size distributions found in the studies of Sammis et al. (1986, 1987) were interpreted to infer a self-similar process of cataclastic gouge formation; that is, the inference that a consistent mechanical process operated at each scale of measurement in a particular gouge sample, and moreover, that this process was unchanged throughout the evolution of the fault gouge. In these studies, it was noted that both natural and experimentally produced fault gouges from sandstone failed to exhibit a self-similar particle size distribution. Sammis et al. (1987) suggest that this is a result of a breakdown of self-similar microfracturing at the scale of the pores. The range of scales to which the self-similar processes are consistent remains under question, as the larger field scale observations of self-similarity have not been tested with those of the microstructural scale. Note that although the studies of Sammis et al. (1987) covered particle size distributions over nearly three orders of magnitude, the maximum magnification used in the optical and SEM study of the fault gouges was 1600x.

The detailed information obtained from the TEM observations of the experimental and natural fault gouges by Rutter and White (1979) and Rutter et al. (1986) highlight a range of processes which are of importance during cataclastic grain size reduction. TEM investigations of natural cataclastic fault rocks are thus extremely important in the understanding of the processes involved in cataclasis during tectonic events, but published studies are limited. However, Knipe (1989b) and Lloyd and Knipe (submitted) have presented detailed microstructural data from the study of cataclastic fault rocks in the Moine Thrust Zone, NW Scotland. Knipe (1989b) described a range of microstructures preserved in fault rocks developed along major thrusts in the Assynt region, each of which have experienced a different range of metamorphic conditions. These microstructures are discussed next.

Quartzites from the upper parts of the Assynt Thrust sheet contain a three dimensional network of transgranular fractures separating blocks which contain crystal plastic deformation features. Knipe (1989b) distinguishes between microbreccias (where the fine-grained matrix is less than 40% of the zone volume and the larger detrital grain fragments are extremely poorly sorted in terms of grain size), and cemented gouges (where the matrix accounts for more than 85% of the fracture zone volume and the detrital grain fragments are well sorted with an extremely small range in size). The detrital grain fragments in the gouges contain dislocation densities greater than 3 x 10^9/cm^2. The matrix grains are 2-5 μm in diameter, and are roughly hexagonal in shape. The matrix grains contain internal dislocation substructures, but dislocation densities are usually lower than 3 x 10^8/cm^2, and the dislocations form a more ordered array, indicative of recovery.

Knipe (1989b) notes that the gouge zones are banded, with individual bands showing different clast sizes, different degrees of sorting and different fragment/matrix ratios. The detrital grain fragments again contain high dislocation densities, but have extremely irregular margins indicative of corrosion by fluids in the fault zone. TEM observations of the matrix in the gouge zones again shows grain sizes ranging from 2-5 μm, and the internal features within these grains again contrasts with that of the larger detrital grain fragments. The larger grains have internal microstructures ranging from high dislocation densities of >3 x 10^9/cm^2, to cells with lower internal dislocation densities and dislocation walls. The smaller grains contain few defects and are defined by approximately straight grain boundaries with irregular hexagonal shapes. Knipe (1989b) infers that the small grains represent the end product of a recovery process which changes the high dislocation densities into cells and then into strain-free grains.

The detailed microstructural analysis of the cataclastic fault rocks along a minor backthrust in the lower Sole Thrust system of the Moine Thrust Zone is the topic of another paper by Lloyd and Knipe (submitted). With the use of the fracture mechanics approach, their microstructural observations represent a significant increase in the understanding of the development of microbreccia/cataclastic displacement zones. Lloyd and Knipe propose that

fracture dominated deformations can experience grain-size, shape and packing induced localisation of stress and strain-rate variations. Thus, the partitioning of different deformation mechanisms can occur, and will have an important influence on microstructural development. The detailed fracture mechanics approach used in their study has allowed them to conclude that the inherited microstructures can result in a heterogeneous distribution of fracture strengths in an aggregate, and that this can then control some of the linking of microfractures into more extensive fracture arrays and the structure of cataclastic zones.

In Lloyd and Knipe's study, intragranular microfractures preserved in the relatively undeformed parts of the quartzite away from the main displacement zone, or in relict low deformation zones, link grain contacts exactly as predicted by Gallagher et al. (1974), and as observed in experiment (Teufel, 1981) and in nature (Blenkinsop and Rutter, 1986). Lloyd and Knipe suggest that the intragranular microfractures are simple extension fractures. With the observations of the intragranular microfracture microstructures and the characteristics of possible fracture mechanisms, they infer that where there does not appear to be any general plasticity associated with the fractures. The fractures are primarily cleavage 1, and possibly cleavage 2 fractures (in small proportions). Through-going fractures with little displacement (<20 μm) and no microbreccia/cataclastic infilling are considered to be extensional fractures developed by linking of earlier isolated fractures. There is an overall scarcity of grain boundary fractures, suggesting that the boundaries had higher fracture stresses, acted as barriers to fracture propagation, and therefore suppressed brittle intergranular fracture mechanisms relative to cleavage mechanisms. Lloyd and Knipe are able to conclude that generally, the initial fracturing and the development of through-going extension fractures involves the cleavage 1 fracture mechanism, while cleavage 2, brittle intergranular fracture (BIF) and low temperature ductile fracture (LTDF) make only minor contributions. They observe that the propagation of extensional fractures through grains involved some microplasticity, shown by the presence of dislocation substructures adjacent to such fractures. With these TEM observations, they are able to suggest that this probably represents a transition from cleavage 1 to cleavage 2 fracture, possibly even to cleavage 3.

Lloyd and Knipe (submitted) then describe the development of microbreccia/cataclastic filled zones which show displacments of >100μm. They suggest that the zones represent the end product of the development of the fault microstructures, and probably develop from the through going extensional fractures described above. They observe that the effective fracture width of the early extensional fractures extends over several grain diameters. This weakness lowers the shear yield/fracture strength, and therefore shear deformation and subsequent displacement is localized along the through-going extension fractures. The effective fracture width and characteristic irregular fracture traces accompanied by the shear displacement induces local regions of extension and/or compression, interfacial friction and grain communition by irregular fracturing. This leads to the formation of open but narrow microbreccia filled through-going fracture zone (as also described by Pollard and Segall, 1987). In order to accommodate displacement form shearing along the initial low-displacement through-going fractures, wing cracks can be formed by further extension fracturing at high angles to the shear direction (see also Adams and Sines, 1978; Horii and Nemat-Nasser, 1986; Pollard and Seagall, 1987). Therefore, the wing cracks can then be exploited by shearing and microbreccia formation, resulting in discrete blocks of rock bounded by gouge-filled fractures.

Lloyd and Knipe note that the through-going fractures in the fault zone tend to develop with increasing displacement towards a fine-grained/ultra fine-grained cataclasite with progressively smaller and fewer clasts. They emphasize that this is not a simple progressive development, as there are examples where small displacement zones contain fragments greater than 50 times the matrix grain size, while there are also zones of larger displacements which contain more than 50% of grains this size. However, Lloyd and Knipe suggest that the general decrease in average grain size in the cataclastic/microbreccia zones does reveal that progressive fracturing does accompany displacement.

The detailed study by Lloyd and Knipe (submitted) emphasizes several important and significant conclusions which are relevant to this study: 1) Individual fractures are not only produced by different processes, but there is evidence that a transition from cleavage 1 and 2 to BIF can occur. 2) The

inherited microstructures can greatly influence fracture processes, and the distribution of the different initial microstructures will give rise to a heterogeneous distribution of fracture strengths in an aggregate. 3) Low temperature plasticity (LTP) and low temperature ductile fracture processes (LTDF) are important processes occurring during faulting at upper crustal conditions. 4) The heterogeneous fracture strength in grains resulting from different initial microstructures, different orientations, different packing, sorting and sizes, together with the different pre-fracture deformation responses can control some of the linking of microfractures into more extensive fracture arrays and the structure of cataclastic zones. In addition, TEM observations in the gouge zones show new quartz overgrowths on cataclastic fragments, and phyllosilicate inclusions in areas of quartz cement, both which represent late stage events in the gouge evolution. Deformed cement areas precipitated during an earlier deformation event now contain high dislocation densities, as with detrital grain fragments. These observations highlight the important role of both dislocation and diffusive mass transfer processes within the fault zone.

Chapter 4. A Review of Fluid Flow and Faulting
in Sedimentary Basins

4.1 Introduction

Faults can influence fluid flow pathways in basins: they can either segment oil fields (i.e. 'seal'), or they can allow migration of fluids vertically up or down the stratigraphy. A fault may act as a conduit when moving, but may be sealed when passive. The reverse may also be true. Thus, the processes involved in faulting can contribute to the transmissability of fluid flow in fault zones. The effects of fluid flow and faulting in sedimentary basins as emphasized in this thesis has direct implications for the assessment of the processes involved in fault sealing, as the products of faulting have long been known to have the capability to trap hydrocarbons (Harms, 1966; Smith, 1966, 1980; Berg, 1975; Weber and Mandl, 1978; see also Schowalter, 1979; Harding and Tuminas, 1988; Watts, 1987). This chapter discusses examples of localized fluid flow along faults (section 4.2), large-scale hydrogeological regimes in sedimentary basins (section 4.3), hydrocarbon migration and entrapment (section 4.4), and the effect of deformation on capillary pressures (fault seals) (section 4.5).

4.2 Localized fluid flow along faults

Many examples exist of faults acting as barriers to all types of fluids, however, there is much evidence that many faults do not seal, and in fact, act as conduits for fluid migration (Smith, 1966, 1980; Seeburger, 1981). The volumes of fluids transported along faults has in many instances been proved to be quite large (Briggs and Troxell, 1952; Swensen, 1964; Wood et al., 1985; Burley et al., 1989). In addition, certain faults have been identified as behaving as both conduits and barriers to fluid flow at different times during the fault movement history or during the history of fluid migration. Recent data from fluid inclusion studies has provided direct evidence for the cyclic transport of fluids along faults (Grant, 1989; Grant et al., in press; Burley et al., 1989). This has been explained with the dynamic seismic pumping and seismic valve mechanisms, as described by Sibson et al. (1975), and Sibson (1981, 1987, 1988). Although the two mechanisms differ in detail, both emphasize the link between the dynamic effects associated with earthquake faulting with fluid flow.

During seismic pumping, the build up of elastic strain prior to an earthquake results in microcracks that then close when the stress is relaxed during slip on the fault. The closure of cracks expels the pore water and generates overpressure. Episodic hydrofracturing then occurs in the fault zone. During rupture propagation, dilational jogs are favorable sights for the influx of mineralizing fluids due to the fluid-pressure differentials which arise due to seismic pumping (Sibson, 1986, 1987). In the fault valve mechanism, high-angle reverse faults may act as fluid-activated valves which promote large cyclic fluctuations in fluid pressure (Sibson, 1988). A structural cycle related to major seismic failure episodes on a steep existing fault system occurs such that reactivation of faults in this orientation can only occur when fluid pressure exceed the lithostatic load. At fault failure, fracture permeability created within the rupture zone allows sudden draining of the geopressured reservoir at depth. Therefore, in a fault flat/fault vein system, the opening of flats is attributed to the prefailure stage of supralithostatic fluid pressures, and the deposition within fault veins is attributed to the immediate post-failure discharge phase. The hydrothermal 'self-sealing' leads to a rise in fluid pressure and a repetition of the cycle.

In sedimentary basins, it is known that faults can act as conduits for fluids which effect diagenesis in sediments. Flourney and Ferrell (1980) documented preferential precipitation around faults in the Lirette field of Louisiana, and evidence for faults transporting acidic fluids and hydrocarbons in the Spindle field of Colorado has been presented by Porter and Weimer (1982). Jourdan et al. (1987) argue that hot fluid circulation along major bounding faults at temperatures of between 120-140°C induced extensive diagenetic alteration of Jurassic Brent reservoirs in the East Shetland Basin of the Northern North Sea. The study by Burley et al. (1989) suggests that faults in the Tartan Reservoir in the North Sea were conduits for migrating hot fluids responsible for the generation of widespread secondary intergranular porosity within the Piper Formation sandstones. Lee et al. (1989) found localized intense illite formation in the Rotliegende sandstone adjacent to a fault in the Southern North Sea. They speculate that fault activity may have promoted the circulation of fluids which provided a greater supply of the constituents necessary for illite growth.

The studies discussed above demonstrate the influence of faults on localized fluid flow.   Faults can also alter fluid flow regimes basin-wide. Basin-scale fluid flux controls not only the diagenetic aspects of sediments, but also has much influence on the migration of hydrocarbons.   Therefore, section 4.3 discusses basin hydrodynamics, as understanding fault-related affects on basin-scale fluid flow is dependent upon the concepts of intrabasinal fluid regimes.

4.3   Hydrogeological regimes in sedimentary basins

This section covers the basic concepts of the subsurface hydrogeologic system of large, depositionally active sedimentary basins.   It is widely viewed that static conditions rarely, if ever, exist in subsurface fluid flow systems in such basins (Galloway, 1986).   The flow dynamics and fluid chemistries evolve through time and complicate interpretation of diagenetic histories of sediments within a basin.   The interaction of major faults within basin flow regimes is a topic which has only just recently received attention, despite its implications on diagenesis and hydrocarbon migration pathways, as demonstrated by Burley et al. (1989).

Subsurface waters of whatever origin moving in several different regimes can be termed ground water (Bogomolov et al., 1978;   Galloway, 1986) (fig. 4.1).   These regimes (Galloway, op.cit.) represent end members to a continuum ultimately controlled by the structural position, hydrochemistry and flow dynamics.

The meteoric regime encompasses the shallow portions of the basin fill (fig. 4.1). Fluid influx occurs by infiltration of precipitation and surface waters down the topographic gradient in the direction of decreasing gravitational potential energy, followed by repeated vertical discharge at hydrological base level (fig. 4.1; Galloway, 1986).   Hydrologic base level is commonly determined by sea or lake level.   Once the fluids reach base level, there is little potential for additional lateral flow beneath the subaqueous basin centre, as there is no hydrodynamic head.   The shoreline is typically a major discharge area for meteoric aquifers, and the circulation of these fluids is rapid on a geologic time scale.   The pathway taken by meteoric fluids will strongly influence the early diagenetic history of sediments at shallow levels in basins.
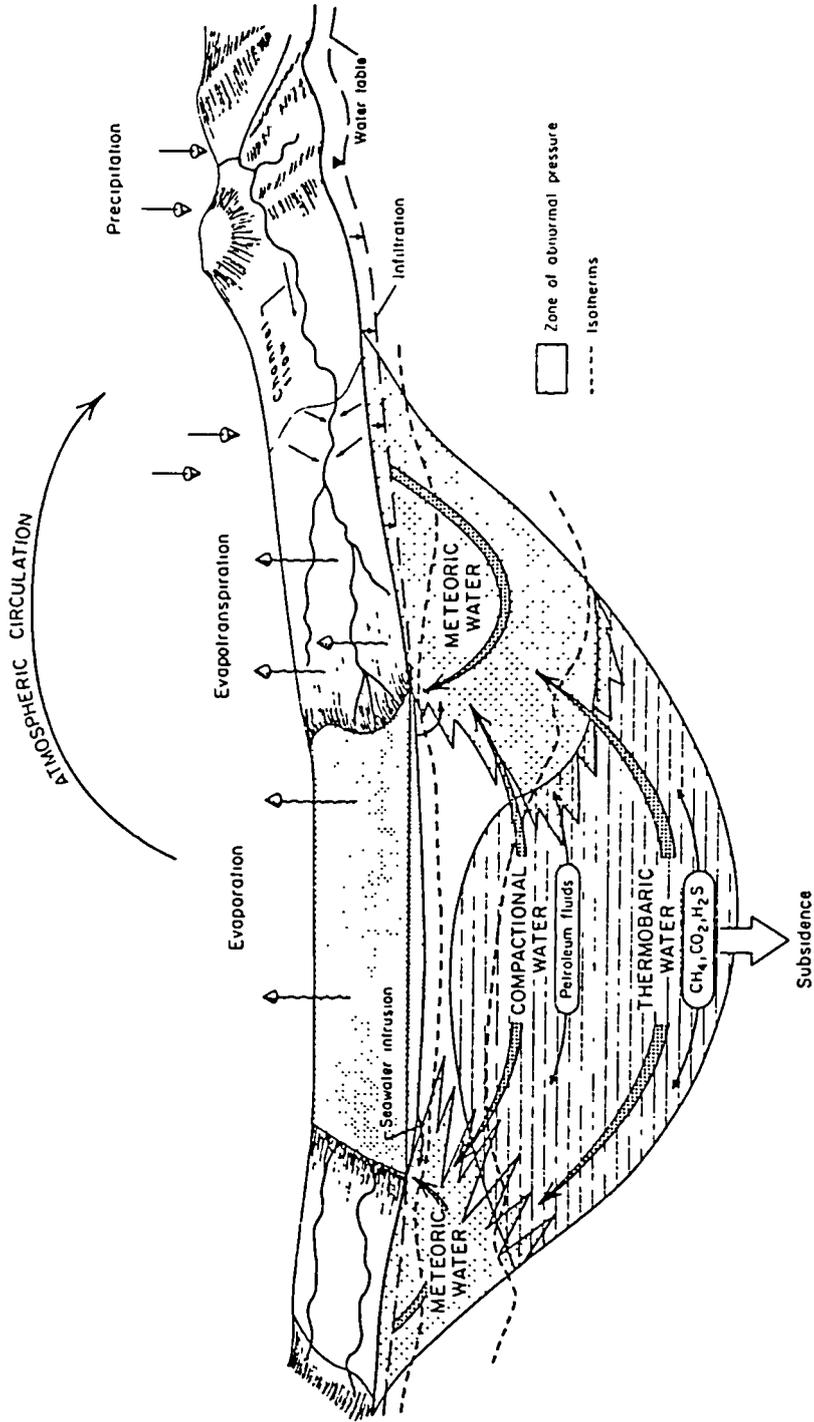
Figure 4.1. Hydrologic regimes of a large, subsiding depositional basin (from Galloway, 1986).

The compactional regime (Galloway, 1986) is characterized by the upward and outward expulsion of pore waters trapped within the compacting sediment pile (fig. 4.1). Pressure head is the driving mechanism for flow, and lithostatic loading can create increased pressure. The thermobaric regime (Galloway, op.cit.) lies in the deepest portions of the basin fill where temperature and pressure are at their greatest. Fluids flow occurs in response to pressure gradients created by phase changes, including the generation of hydrocarbons or the release of mineral-bound water (as in the dehydration reaction of clay minerals or other hydrous mineral phases), and by continued lithostatic loading. Galloway (op.cit.) suggests that the extremely low permeability of the compacted sediments can restrict the rate of water movement over geologically significant time spans. This can lead to overpressuring, resulting in hydrofracture or establishment of a closed aquifer system(as in the Jurrasic of the North Sea).

Galloway (op.cit.) suggests that there is considerable mixing and interaction of waters from each regime. This is evidenced by the pervasive zones of leached porosity, and thermal, pressure and salinity anomalies observed within his study of the Frio Formation. He notes that cross-cutting growth fault zones and diapirs can provide avenues for vertical fluid movement and mixing. He speculated on the importance of deep fluids within the basin flow regimes, and this has now been illustrated by the work of Burley et al. (1989).

Recently, thermally driven convection of waters within aquifers has been proposed as a possible mechanism of fluid mass-transfer within sedimentary basins (Wood and Hewett, 1982). Their study showed that fluid velocities in large sand bodies, although on the order of 1 meter per year when in the presence of normal geothermal gradients (25° C/km), are enough to produce significant porosity changes over a time span of several million years.

Etheridge et al. (1983), and Etheridge et al. (1984) emphasized the role of high fluid pressure and mass transport by fluid advection during metamorphism. Due to enhanced permeability and pressure gradients that would be expected at very high fluid pressures, Etheridge et al. (1983) conclude that advective mass transport dominates regional metamorphism.

Etheridge et. al. (1984) emphasize and review the importance of fluids in both prograde and retrograde metamorphic processes, and explore in detail the consequences of the structure of grain boundaries on processes in which fluids are involved. The driving force for fluid motion during regional metamorphism is of two main types: 1) large-scale buoyancy forces arising from the enhanced thermal gradient, and 2) local gradients in pore fluid pressure between dilatant zones (for example, hydraulic fractures, fault zones and other high strain rate zones), and the ambient pore fluid pressure in the bulk of the rock mass.

Giles (1987) has further emphasized the importance of flow rate, reaction rates, specific surfaces and temperature in controlling the areal extent of leaching during secondary porosity creation. He suggests that wide leaching zones are related to high flow rates, which promote a high throughput of undersaturated fluid, and are favored by low reaction rates occurring at low temperatures. Lower flow rates and higher temperatures encountered during deep burial diagenesis result in narrower and more intense leaching zones.

Magara (1976) suggested that most water expelled from sediments moves horizontally in an interbedded sand-shale sequence, and vertically upward in a continuous shale sequence. In addition, Magara (op.cit.) has argued that the volumes of water expelled from compacting sediments and moving through sand-shale sequences is a contolling factor in hydrocarbon occurrence in the Gulf Coast. Magara (1987) has also calculated the rate of increase of fluid pressure (psi/Ma) in excess of hydrostatic generated during sediment loading from sedimentation rate (ft/Ma) of a formation and its average bulk density. The directions of horizontal migration of the compaction fluid can then be inferred from the first derivative of the rate of increase of the fluid pressure (psi/Ma/mile). He suggested that the horizontal fluid movement may be essential for driving hydrocarbons towards a trapping position during the primary stages of migration. The next section discusses petroleum migration in context of these hydrodynamic factors.

4.4 Hydrocarbon migration and entrapment

It is generally accepted that most oil forms at temperatures between 60 and 150° C, corresponding to burial depths of about 1500 to 4500 meters in areas of normal geothermal gradients (Philippi, 1965; Tissot et al., 1971; Cordell, 1972; Dickey, 1975; Hunt, 1975; McAuliffe, 1979). Subsequent to the generation period, primary oil migrates from the source rock to the reservoir rock, followed by secondary migration through the reservoir rocks to trapping conditions. Schowalter (1979) defines primary migration as "the movement of hydrocarbons from mature organic-rich source rocks to an escape point where the oil and gas collect as droplets or stringers of continuous-phase liquid hydrocarbon and secondary migration can occur". The escape point is the point at which the hydrocarbons can migrate as a continuous-phase fluid through water-saturated porosity, whether it be a reservoir rock, an open fault plane, or open fractures.

Many mechanisms have been proposed for primary hydrocarbon migration, including solution in water, diffusion through water, dispersed droplets, soap micelles, and continuous-phase migration through water-saturated pores (Price, 1976; Baker, 1959, 1960, 1962; Cordell, 1972). Early ideas favored the early expulsion of hydrocarbons with the water phase of compacting sediments, however, geochemical evidence summarized by Cordell (1972) suggests that oil is formed at depths where the source rocks have lost most of their pore fluids by compaction. Wilson (1975) discusses this paradox of the time of inception and duration of oil expulsion from source rocks to its accumulation in reservoir rocks, assessing the arguments of both early and late expulsion theories. He calls attention to the fact that maturation of hydrocarbons can take place with time and depth in source rocks and entrapped accumulations alike. Wilson (1975) concludes that the problems of the timing and mechanisms of primary hydrocarbon migration remain unresolved, despite the volume of data on the subject. Further discussion of this topic will not be presented in this thesis. The formation of a commercial oil or gas accumulation necessitates secondary migration through reservoir beds, and more relevent to this study, entrapment of the hydrocarbons in the subsurface. Therefore, the remainder of this section concentrates on the mechanisms of secondary hydrocarbon migration and entrapment.

Schowalter (1979) outlines the detailed mechanisms of secondary migration, as the hydrocarbons move as a continuous-phase fluid through water-saturated rocks, faults, or fractures, and the concentration of the fluid occurs in trapped accumulations of oil and gas. Under hydrostatic conditions, the main driving force for secondary migration is buoyancy. With known water and hydrocarbon densites, the magnitude of the buoyant force can be determined for any hydrocarbon column in the subsurface. The range of oil and water densities in the subsurface suggests that there are differences in the ability of oil in different oil-water systems to migrate through a given reservoir rock, or more importantly in this study, to be trapped by a given seal (Smith, 1966; Schowalter, 1979).

For static continuous hydrocarbon columns, the buoyant force increases vertically upward through the column. The effect of hydrodynamic conditions is to change the buoyant force in the subsurface, and therefore the migration potential for a given hydrocarbon column (Schowalter, 1979). Downdip flow reduces buoyancy or migration potential, while updip flow increases buoyancy or migration potential for any given oil filament (fig. 4.2; Schowalter, op.cit.).

Hydrodynamic conditions in the subsurface also alter the lateral seal capacity in the stratigraphic entrapment of hydrocarbons. Downdip flow increases the seal capacity of a given lateral confining bed along a migration path by reducing the buoyant pressure of any hydrocarbon filament through a reservoir, while updip flow effectively reduces lateral seal capacity in a given zone, as the buoyant force would be increased from the hydrostatic (Schowalter, 1979). Hubbert (1953) discussed in detail the importance of hydrodynamics with regard to oil entrapment in structural traps. Without further expansion on the complex hydrodynamic situation, the critical factors involved in entrapment of hydrocarbons will be briefly mentioned, as outlined by Schowalter (1979).

For structural traps, the critical factors are the seal capacity of the reservoir caprock, the structural configuration at the base of the seal, and in the case of hydrodynamic conditions, the tilt of the oil-water contact (Schowalter, 1979). For stratigraphic traps, the location, configuration, and seal capacity of a lateral barrier to oil or gas migration along a carrier bed are critical. In terms of vertical hydrocarbon columns, the seal capacity of the barrier will be affected by the density of the hydrocarbon and water

55
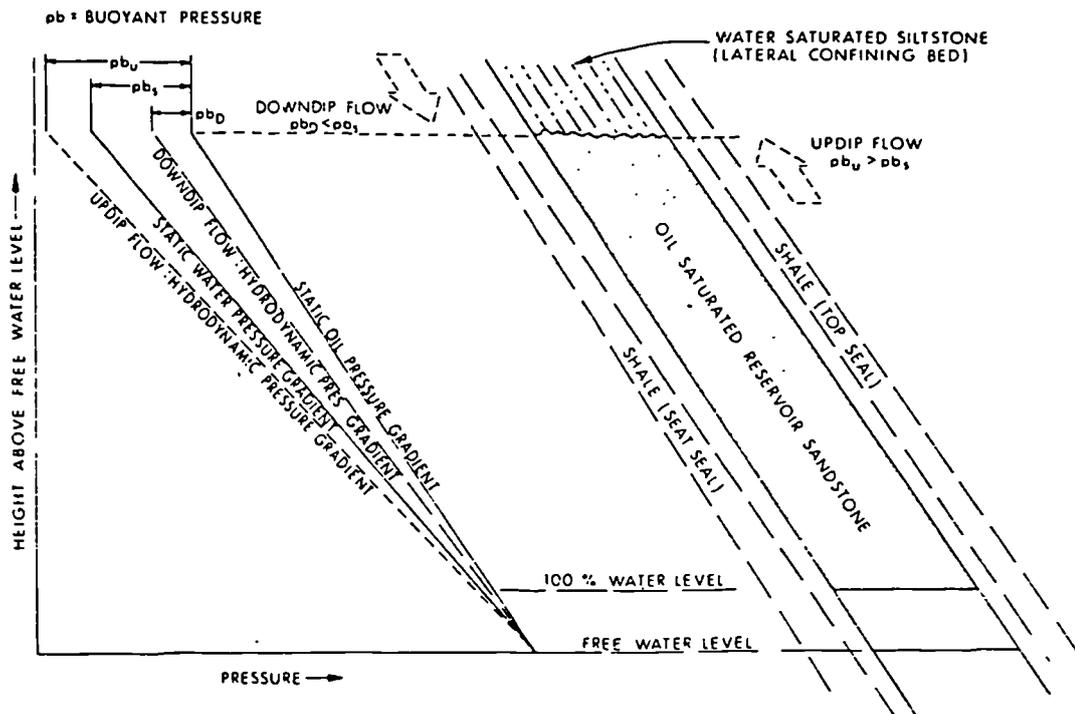
Figure 4.2. Effect of hydrodynamics on buoyant force in oil reservoir for constant hydrocarbon column height (from Schowalter, 1979). Note that downdip flow results in a greater hydrodynamic pressure gradient, thereby reducing buoyancy or migration potential, while updip flow results in a lower hydrodynamic pressure gradient, increasing the buoyancy or migration potential for any given oil filament.

phases, the hydrodynamic conditions of the carrier bed, the radius of the pore-throats of the barrier, the interfacial tension of hydrocarbon-water phase and the wettability of the rock. In combination, the last three factors listed determine the 'capillary pressure' of a given rock. Capillary pressure was defined by Leverett (1941) as the pressure difference between the oil phase and the water phase across a curved oil-water interface. The capillary pressure, or hydrocarbon-water displacement pressure of a rock is defined by:

$$P_d = \frac{2\gamma \cos \Theta}{R}$$

where γ = oil-water interfacial tension; Θ = contact angle of oil and water against the solid, and; R = radius of the pore throat (fig. 4.3; Schowalter, 1979). Schowalter notes that the dip of a reservoir will not affect seal capacity but will affect the volume of hydrocarbons trapped.

Capillary pressure is a critical factor in the discussion of seals in the entrapment of hydrocarbons. An elaborate discussion of capillary pressure is presented by Berg (1975), who combined the work on capillary pressures and hydrodynamic drive to predict the height of an oil column that is contained in a stratigraphic trap.

More recently, Davis (1987) evaluated the sensitivity of entrapment processes to variations in temperature, fluid densities and geologic parameters. In respect to capillary pressure, variations in oil/water density differences have little effect upon threshold capillary pressures (the pressure at which the forces driving the oil globule first overcome interfacial tension and move the globule through a pore throat). In addition, Davis (op.cit.) found that increases in capillary pressure sufficient to cause petroleum entrapment are only important when porosities drop below 5%. At porosities of less than 5%, permeability values in most strata become negligible, and resistance to oil migration due to capillary pressures increases dramatically. This observation is of great importance when considering the seal capacity of faults, as the porosity and permeability of fault rock products varies greatly. The next section considers the important aspects of fault seals which occur in the subsurface.

THE HYROCARBON-WATER DISPLACEMENT PRESSURE OF A ROCK IS
A FUNCTION OF HYDROCARBON-WATER INTERFACIAL TENSION,
WETTABILITY, & RADIUS OF THE PORE THROAT.
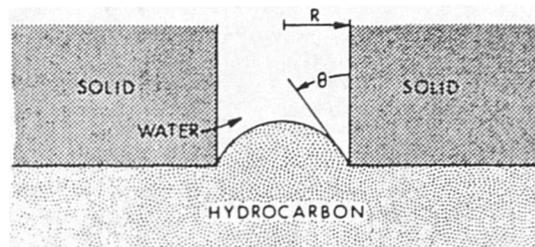
$$pd = \frac{2\gamma\cos\theta}{R}$$

WHERE pd = DISPLACEMENT PRESSURE
  γ = OIL-WATER INTERFACIAL TENSION
  θ = CONTACT ANGLE OF OIL AND WATER AGAINST THE SOLID
  R = RADIUS OF THE PORE THROAT

AS γ INCREASES pd INCREASES
AS θ DECREASES pd INCREASES
AS R DECREASES pd INCREASES

Figure 4.3.   The hydrocarbon-water   displacement   pressure   (capillary
pressure) of a rock: the resistant   forces   in   secondary   hydrocarbon
migration (from Schowalter, 1979).

4.5 Fault seals and capillary pressure

Generally, hydrocarbon-producing plays are ranked from basin history assessments, which include burial and thermal histories for certain horizons, such as described by Galloway et al. (1982) and Guidish et al. (1985). Fault geometries, kinematics and histories are generally integrated into the basin history from information derived from seismic data, such that many prospective plays adjacent faults are assessed purely on the basis of the relative timing of hydrocarbon formation, migration, and faulting, and estimates of the amounts of oil and gas expelled from the source rock into the porous reservoirs. Plays which rely on the sealing capability of a fault have to be judged in some way without exact knowledge of the detailed fault zone characteristics. Therefore, the present 'static' properties of a fault are critical in predicting not only sealing probabilities, but in quantifying the column of gas or oil trapped by the fault. Direct access to fault rocks which can identify specific fault/fluid relationships is rarely available. Therefore, detailed field and micro-scale studies of fault rocks within sedimentary basins can provide a basis in which to extrapolate predictive modelling of sealing mechanisms and processes along fault systems observed in seismic data during hydrocarbon exploration.

Smith (1966) relates the general theories of hydrocarbon entrapment to investigate theoretical cases of faults acting as barriers or paths to hydrocarbon migration. Smith (op.cit.) states that there are two ways in which a boundary to lateral migration of hydrocarbons might result from faulting: 1. by juxtaposed sedimentary lithologic types of different capillary properties and, 2. by emplaced fault-zone material formed by "mechanical or chemical processes related directly or indirectly to faulting." The trapping-capacity limit of the 'boundary material' is determined by the elevation at which the capillary pressure equals the displacement pressure of the boundary. In addition, the maximum thickness of hydrocarbons that can be trapped by the boundary is related to the difference in the displacement pressures of the boundary rock and the reservoir rock (Smith, op.cit.). He states that hydrocarbons cannot be trapped unless there is a difference in displacement pressures at the interface of the media. Smith (op.cit.) also notes that the distribution of the boundary material, as well as its displacement pressure will govern the maximum height of hydrocarbon column that can be trapped at a fault.

The equations derived by Smith (1966) were developed for determining the boundary trapping capacity under hydrostatic conditions. As he notes, the principles of entrapment by differences in displacement pressure are valid for hydrocarbons in both hydrostatic and hydrodynamic environments. However, the determination of capillary pressure for the hydrodynamic case is more difficult than for the hydrostatic case (Smith, op.cit.). Pressure in the oil phase is determined by equations as in the hydrostatic situation, however, water phase pressure must be based on a detailed knowledge of the vertical pressure distribution in the dynamic situation, which can differ significantly from the vertical distribution in a static situation (Hubbert, 1953; Smith, 1966, 1980; Watts, 1987). Examples of this problem are illustrated by Smith (1966), and demonstrate that a fault can be non-sealing to water movement without necessarily being non-sealing to hydrocarbon movement. Finally, Smith (1966) states that application of the theories of entrapment could resolve many aspects of the fault-seal problem if data were available on the capillary properties of the "media in contact at the fault."

Later, Smith (1980) reports a study in the Louisiana Gulf Coast salt basin undertaken to determine the different situations of fault entrapment of hydrocarbons in Tertiary sediments of the Gulf Coast, and to investigate their role of juxtaposed sediments in a sandstone-shale sequence in creating sealing and non-sealing faults. His investigations were limited to traps associated with faults which restrict vertical migration of hydrocarbons, in other words, where an accumulation is in contact with the fault. Different fault-lithology-accumulation relationships were observed (fig. 4.4), in some cases all relations were found present at different levels along the same fault. In all the examples studied, only faults nonsealing to lateral migration were observed where parts of the same sandstone body are juxtaposed across a fault. Juxtaposed sandstone bodies of different ages were found to be sealing and others non-sealing to lateral migration. In general, sealing faults were the most common. Smith (op.cit.) suggests that the fault seal "apparently results from the presence of boundary fault-zone material emplaced along the fault by mechanical or chemical processes related directly or indirectly to faulting." He observes that the distribution and displacement pressure of the 'unidentified' fault zone material governs the maximum thickness of the hydrocarbon column that can be trapped at a fault. This highlights the need for detailed microstructural analysis of fault rocks in order to better understand their sealing capabilities.

HYPOTHETICAL SITUATION	ANALYSIS OF FAULT SEAL	
	VERTICAL MIGRATION	LATERAL MIGRATION
(a) SAND OPPOSITE SHALE AT THE FAULT. HYDROCARBONS JUXTAPOSED WITH SHALE.	SEALING	**SEALING** RESERVOIR BOUNDARY MATERIAL MAY BE THE SHALE FORMATION OR FAULT ZONE MATERIAL.
(b) SAND OPPOSITE SAND AT THE FAULT. HYDROCARBONS JUXTAPOSED WITH WATER.	SEALING	**SEALING** SEAL MAY BE DUE TO A DIFFERENCE IN DISPLACEMENT PRESSURES OF THE SANDS OR TO FAULT ZONE MATERIAL WITH A DISPLACEMENT PRESSURE GREATER THAN THAT OF THE SANDS.
(c) SAND OPPOSITE SAND AT THE FAULT. COMMON HYDROCARBON CONTENT AND CONTACTS.	SEALING	**NONSEALING** POSSIBILITY IS REMOTE THAT FAULT IS SEALING AND THE RESERVOIRS OF DIFFERENT CAPACITY HAVE BEEN FILLED TO EXACTLY THE SAME LEVEL BY MIGRATING HYDROCARBONS.
(d) SAND OPPOSITE SAND AT THE FAULT. DIFFERENT WATER LEVELS.	SEALING	**UNKNOWN** NONSEALING IF WATER LEVEL DIFFERENCE IS DUE TO DIFFERENCES IN CAPILLARY PROPERTIES OF THE JUXTAPOSED SANDS. SEALING IF WATER LEVEL DIFFERENCE IS NOT DUE TO DIFFERENCES IN CAPILLARY PROPERTIES OF THE JUXTAPOSED SANDS.
(e) SAND OPPOSITE SAND AT THE FAULT. COMMON GAS-OIL CONTACT, DIFFERENT OIL-WATER CONTACT.	SEALING	**NONSEALING** POSSIBILITY IS REMOTE THAT FAULT IS SEALING AND MIGRATING GAS HAS FILLED THE RESERVOIRS OF DIFFERENT CAPACITY TO EXACTLY THE SAME LEVEL.
(f) SAND OPPOSITE SAND AT THE FAULT DIFFERENT GAS-OIL AND OIL-WATER CONTACTS	SEALING	**SEALING** A DIFFERENCE IN BOTH GAS-OIL CONTACT AND OIL-WATER CONTACT INFERS THE PRESENCE OF BOUNDARY FAULT ZONE MATERIAL ALONG THE FAULT
(g) SAND OPPOSITE SAND AT THE FAULT. WATER JUXTAPOSED WITH WATER.	UNKNOWN	UNKNOWN
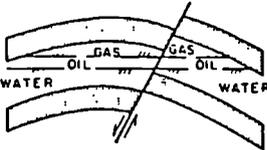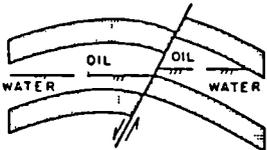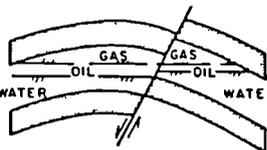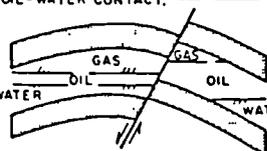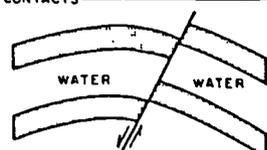
Figure 4.4. Analysis of vertical and lateral migration of fault seal for hypothetical fault-lithology-accumulation relations (from Smith, 1980).

Pittman (1981) noted that 'granulation" caused by cataclasis reduces porosity and permeability in quartz sandstones of the Simpson Group, (Ordovician), Oklahoma. The reduced pore aperature size in the rock also leads to a bimodal distribution of grain sizes, and he suggests the mechanical reduction in pore aperature size creates the potential for fault sealing traps. However, in the friable sandstones studied, the significant reduction in pore aperature size due to faulting is not sufficient to constitute a seal, although the faults certainly influence local entrapment of hydrocarbons. It is interesting to note that porosities in the first case are reduced from 8.2% in the undeformed rock, to 5.1% in the faulted sandstone. However, in the second case of the friable sandstones, the porosities are reduced from 25.5% to 15.8%. These values correspond well with Davis' (1987) calculations that capillary pressure increases sufficient to cause entrapment of hydrocarbons only occur when porosities drop below 5%.

Seeburger (1981) studied the distribution of pore space in crustal rocks, and the transport properties of that pore space, particularly adjacent faults. The first part of the study used an ultrasonic borehole televiewer to observe in situ fracture distribution in ten wells near Palmdale, California (five wells); Hollister, California (three wells); and Monticello Reservoir, South Carolina (two wells). All but one of the wells were drilled in granitic rock. Seeburger found that the number of fractures observed was relatively independent of depth; steeply dipping fractures were found throughout the wells. He also found that statistically significant fracture orientation could not be related to the measured orientation of the regional stress field. Seeburger concludes that the data indicates a local rather than regional effect on the distribution and orientation of natural fractures, and therefore, that it is often not possible to predict the fracture distribution and orientations that would be encountered in a well simply from an analysis of the tectonic stress field and the regional geology.

More directly related to this study, the second section of Seeburger's (1981) thesis consists of an examination of the characteristics of fluid flow around fault zones. Several direct fault zone observations are cited by Seeburger; his assessment and conclusions are based on case studies presented from other workers. Seeburger (op.cit.) suggests that in the often found case of a fault acting as a conduit and barrier to fluid flow, the required permeability is highly anisotropic. High permeability is found parallel to the fault plane in the hangingwall and the permeability

perpendicular to the fault plane is low. He notes that Weber et al. (1978) observed a zone of dilation or pore increase on the downthrown side, and compaction or pore decrease on the upthrown side of faults formed in ring-shear apparatus experiments, and along small natural shear faults. It was concluded that such a system could facilitate fluid movement along the downthrown (hangingwall) side of faults.

Seeburger (op.cit.) concludes that the high permeability zone is a result of increased fracturing and porosity, while the low permeability zone is a result of porosity reduction, grain size reduction, and a lessening of the degree of sorting in fault zone material. He cites observations in mines and in cores which are in good agreement with this predicted structure: highly fractured (permeable) zones are found parallel to fault zones and very often in the hangingwall side of the zone, while low permeability gouge is very often found on the footwall side of the fault zone. Based on general relations between porosity, sorting, pore and grain size, and permeability, Seeburger suggests that the structural characteristics of the 'observed fault zones' are consistent with the permeability distribution near faults.

More recently, Watts (1987) describes an elegant theoretical analysis of cap-rock and fault seals for single- and two-phase hydrocarbon columns. He divides cap-rock seals in to those that fail by capillary leakage (membrane seals) and those whose capillary entry pressures are so high that seal failure preferentially occurs by fracturing and/or wedging open of faults (hydraulic seals). Modelling studies of membrane seals were represented by using pressure/depth (P/D) profiles through sealed hydrocarbon columns (fig. 4.5). With the use of these profiles, Watts (op.cit.) was able to determine that a given membrane seal can trap a larger oil column than gas column at shallow depths, but that below a critical depth, gas is more easily sealed than oil. He found that this criticial depth increases with lower API gravity and overpressured conditions (for the gas phase). Also, the P/D diagrams have shown that at seal capacity, a two-phase column will always be greater than if only oil or gas occurs below the seal.

Watts (1987) concludes that for hydraulic seals, the seal capacity to oil always exceeds that for gas. More interestingly, a trapped two-phase column at hydraulic seal capacity will be less than the maximum-allowed oil-only column, but more than the maximum gas-only column. Watts suggests that unlike membrane seals, hydraulic seal capacity is related to cap-rock
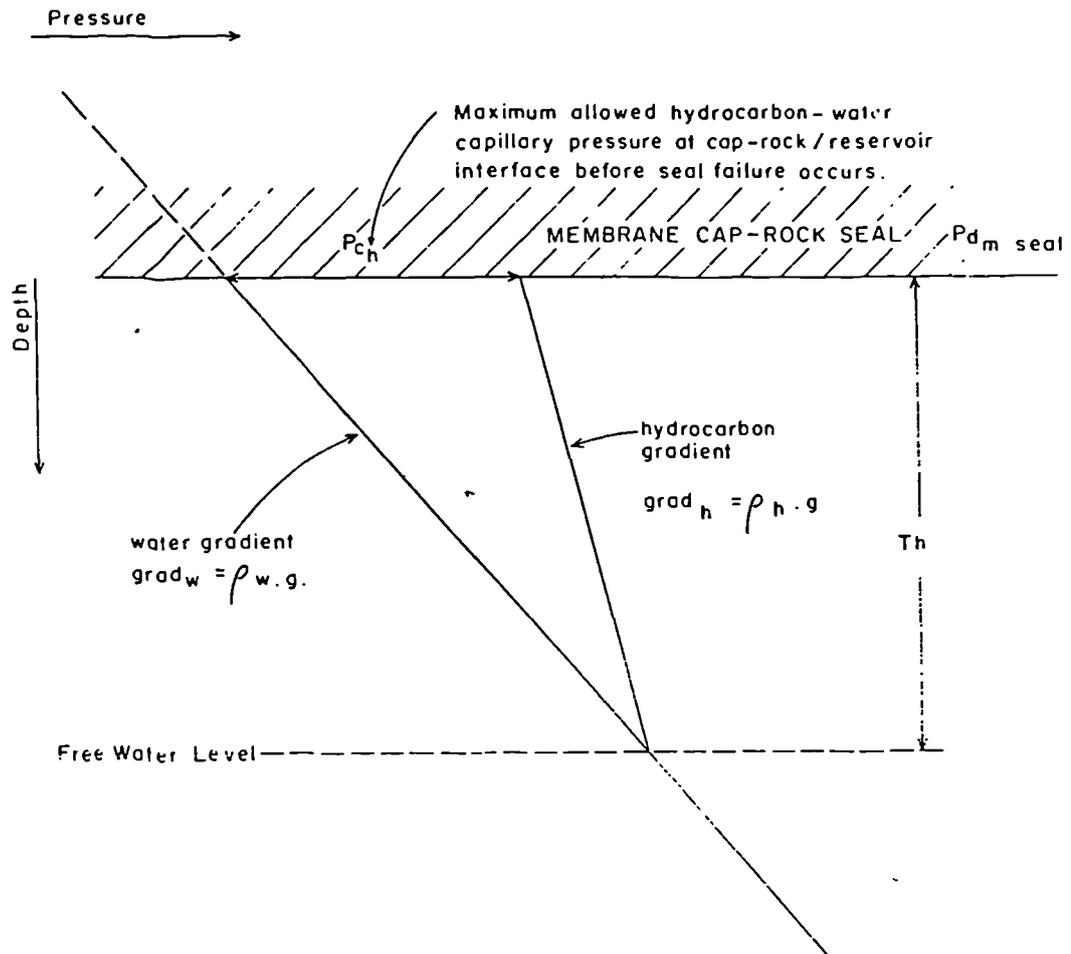
Figure 4.5. Pressure/depth (P/D) profiles through a membrane sealing cap-rock (of entry pressure Pd_m) which is sealing a maximum allowed hydrocarbon column T_h. The difference between the water and hydrocarbon gradients ($grad_w$ and $grad_h$) at the cap-rock/reservoir interface is the maximum allowed capillary pressure that the seal can support before leakage (Pc_h). Consequently, at seal capacity, $Pc_h = Pd_m$ and simple geometrical construction results in the derivation of the overall membrane seal equation (from Watts, 1987).

thickness, in addition to the magnitude of the minimum effective stress in the sealing layer and the degree of overpressure development in the sequence as a whole.

Watts (op.cit.) states that fault-related seals are effectively analogous to membrane cap-rocks which have been tilted to the angle of the fault plane. Therefore, all the above conclusions derived for membrane cap-rocks apply to both sealing faults sensu stricto (fault plane seals) and juxtaposition faults (hydrocarbon trapped laterally against a juxtaposed sealing unit). An important finding is that the maximum-allowed two-phase column trapped by a sealing fault is greater than that for an equivalent single-phase column, but less than that predicted for a horizontal membrane cap-rock under similar conditions.

The membrane sealing theory developed by Watts (op.cit.) assumes that all reservoirs are water-wet and no hydrodynamic flow exists. Watts suggests that the conclusions he draws on membrane seal capacity place constraints on the migration efficiency of gas along low-permeability paths at depth where "fracturing, wedging open of faults and/or diffusion process" may be more important. Contrary to previous assertions, Watts speculates that leakage of hydrocarbons through membrane seals occurs in distinct pulses such that the seal is at or near the theoretically calculated seal capacity, once this capacity has been initially attained.

One recent approach to predicting the longitudinal and transverse closure properties of faults has been through assessment of the large-scale deformation adjacent faults of varying kinematics (in the particular case described here, those faults with reverse or strike-slip components of movement), in combination with identification of the juxtaposition of older, less permeable rocks or 'impermeable material' within the fault zone (Harding and Tuminas, 1988). They note that fault zone barriers to fluid flow can include shaly smear gouge, cataclastic gouge, mineral deposits, or asphalt or tar impregnation. They also state that factors most likely to increase the incidence of leakage up the fault are permeable gouge, fractures, and fault 'rejuvenation.' Harding and Tuminas (op.cit.) state an observation also suggested by other workers that smear gouge having a large sand fraction is the most prone to promote leakage up the fault (Weber et al., 1978), and shaly smear gouge is the least likely (Weber and Daukoru, 1975; Weber et al., 1978; Smith, 1980). Harding and Tuminas (1988) infer that

in general terms the possibility of leakage may decrease with older faults, as with time, fractures may gradually fill with cements and cease to be conduits for fluid migration.

Further studies by the same group (Exxon Production Research Company, Houston, Texas) identified the importance of defining the "impermeable material" more accurately, and based the sealing properties along a fault on the relationship of the amount of 'mixing' which has occurred in the fault zone during juxtaposition of sediments with different sealing properties, for example, porous sandstone and less-permeable shales (Dengo, pers. comm., 1988). The calculation is dependent on the displacement of each horizon along the fault, and therefore the amount of mixing which has occurred is assessed by the displacement of specific reservoir rocks. A computer program was developed by the group which quantifies the sealing capability along the vertical extension of the fault from core, well-log, and seismic data (Dengo, pers. comm., 1988). However, there may be drawbacks to this type of calculation, as the exact mechanisms operating during the 'mixing' are not well-defined; the faulting mechanisms operating under different conditions are known to be complex (Knipe, 1986a, 1986b, 1989a; Lloyd and Knipe, submitted), and result in a wide range of fault rock products, each of which will vary in sealing capability.

Mitra (1988) assessed finite strain associated with various deformation mechanisms, and related the strain with significant alteration of porosity and permeability of reservoir rocks, in this case, in the Central Appalachan Overthrust Belt. His work demonstrates that the emphasis on integrating diagenetic histories and the relative timing of each deformation mechanism with the migration of hydrocarbons is critical to the correct interpretation of reservoir quality, in this case, to changes in porosity. He states that the diagenetic history determines the rock fabric prior to deformation and therefore influences the style and intensity of fracture fillings.

Mitra (op.cit.) concludes that mechanisms such as pressure solution and cataclasis reduce porosity and permeability, whereas extension fracturing and brecciation increase them. A more detailed assessment of the exact mechanisms responsible for porosity change resulting from cataclasis is needed in order to clarify the role of cataclasis in porosity and permeability reduction or enhancement in reservoir rocks such as those studied by Mitra (1988).

4.6 Summary

From the above discussions, it is evident that fault zone structure clearly determines permeability anisotropies which can control fluid migration directions in every hydrological regime of a sedimentary basin, and the sealing capabilities of a fault. Therefore the following chapters will focus upon identifying the deformation processes involved in the evolution of fault zones, with the aim of outlining how fault rock development can influence fluid flow and sealing in fault zones.

Chapter 5. The Orcadian Basin

5.1 Introduction

This chapter presents new structural data from selected coastal sections on the Mainland, Orkney, with the aim of constructing a deformation history for the Orcadian Basin in the Orkney area. The coastal sections provide examples of a range of intrabasinal fault geometries and inversion-related structures which can be mapped in detail in order to constrain fault histories during basin evolution and inversion. In addition, the well-exposed fault zones have allowed detailed examination and collection of fault rocks for microstructural analysis in order to provide insight to fault rock development along a range of fault geometries.

First, in order to provide a framework in which to discuss the data, section 5.2 describes the regional setting of the study area, and section 5.3 presents a review of the previous work in the Orcadian Basin. Sections 5.4, 5.5 and 5.6 describe in detail the structures mapped along three selected coastal sections on the Mainland (fig. 5.1). Each of the sections correlate with 1:5000 scale maps found in the back pocket of this thesis and located on fig. 5.1. The maps are intended primarily for reference, and to give an overall impression of the fault zone exposures and location of specific exposures discussed in the text. Each section contains a discussion integrating the field and microstructural data, and lists specific conclusions for the area described. These conclusions will be used to construct a basin history presented in the synthesis in Section 5.7. Section 5.8 summarizes the development of fault rocks along the major faults in the Orkney area.

5.2 Regional setting

Coward and Enfield (1987) and Enfield and Coward (1987) have demonstrated the influence of Caledonian structures upon the development of the Devonian West Orkney and Orcadian Basins in North West Scotland, at least during initial extension in the region. Several other basins have been documented as forming by the reactivation of Caledonian compressional structures as extensional fault systems, notably those in Norway (Hossack, 1984; McClay et al., 1986; Norton, 1986; Scranne and Seguret, 1987).

Figure 5.1. Map showing major folds and faults on the Mainland, and index to the maps presented in this thesis.

Fig. 5.36

Fig. 5.35

ROUSAY

EDAY

Stromness Flags (MORS)

ORKNEY ISLANDS

MAINLAND

SHAPINSAY

Fig. 5.5

NORTH SCAPA FAULT

Fig. 5.4

Rousay Flags (MORS)

Fig. 5.3

EAST SCAPA FAULT

Fig. 5.23

Scapa Sandstone (?UORS)

HOY

?

BRING FAULT

Scapa Flow

Hoy Sandstone (UORS)

BURRAY

SCALE

0   5

km
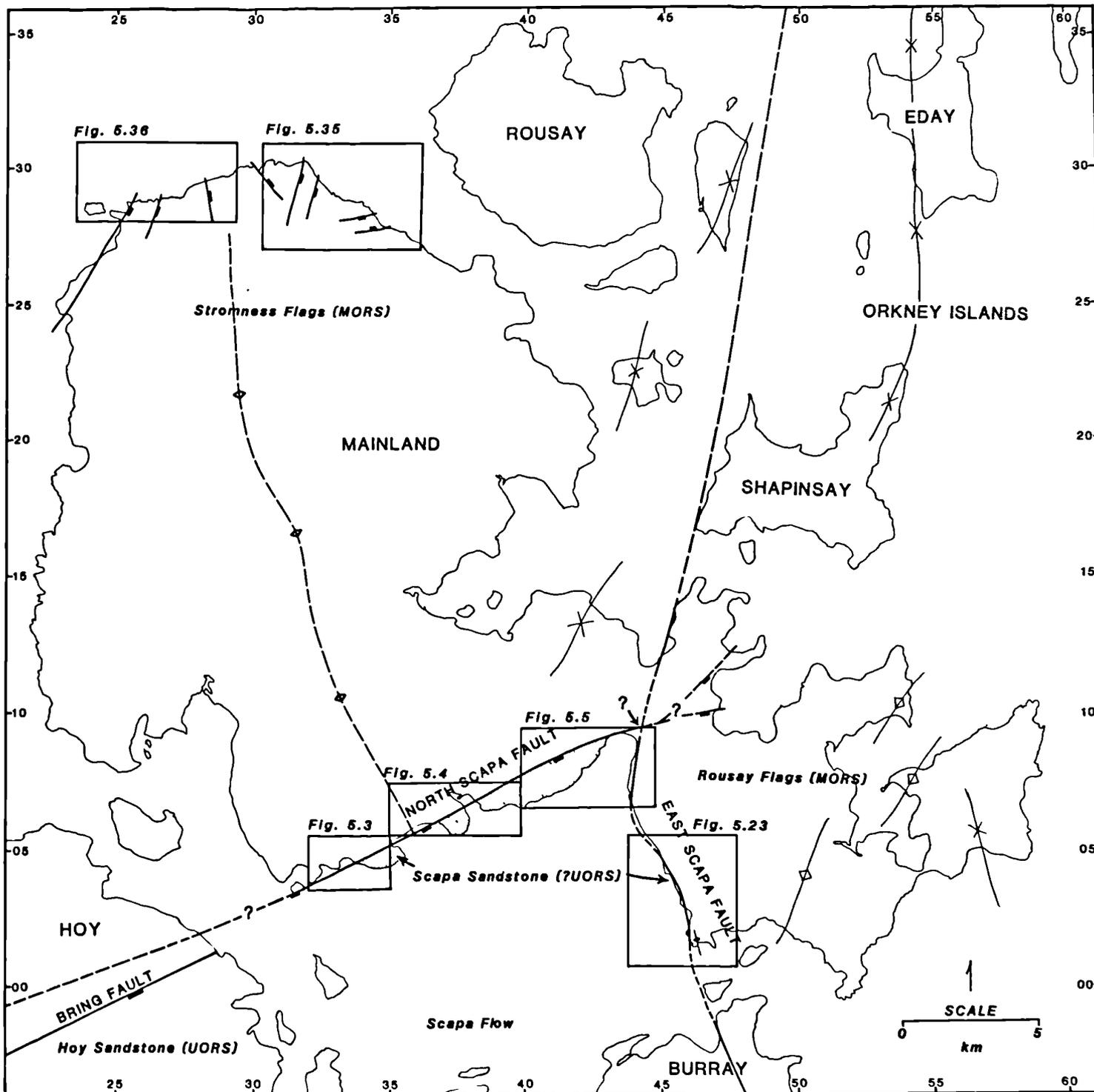
Exposures of the Orcadian Basin sediments now lie on the NE-SW trending Orkney-Shetland Platform (fig. 1.1), bounded to the east by the most important and fundamental tectonic feature of the area, the Great Glen Fault. The fault has incited many interpretations of the extent and timing of its large-scale strike-slip movements (Smith, 1977; VanderVoo and Scotese, 1981; Rogers et al., 1989). New mapping, facies analysis, aerial photo interpretation, palaeocurrent, conglomerate provenance and clast size data by Rogers (1987) shows that the Great Glen Fault and related strike-slip faults did not control the Old Red Sandstone (ORS) basins of northern Scotland. Rogers (1987) suggests that throughout ORS times, subsidence and paleogeography reflect NW-SE extension. Rogers' (1987) extensive data show compelling evidence for net post-ORS dextral motion on the GGF of only 25 km: 8 km. in the Mesozoic, and 17 km. in the latest Devonian to early Permian.

Post-ORS sediments are of only limited onshore outcrop in northern Scotland. The thin Permo-Triassic sandstones along the coast south of the Great Glen Fault are representative of the thicker deposits offshore in the Moray Firth area (Sunderland, 1972), as proven by boreholes. These are overlain by Jurassic sands and shales, preserved onshore in a small faulted graben south of Helmsdale (Pickering, 1984).

In summary, there is no evidence for there ever having been substantial accumulations of post-ORS sediments on the main massif. The massif acted as a stable block separating the rift systems of the North Sea and the Hebrides. In addition, Hillier and Marshall (1988) show that there appears to be no increase in organic maturity with depth, confirming that burial of the sediments has never been great.

5.3 Previous work on Orkney

The Geological Survey officers Wilson, Edwards, Jones, Knox and Stephens surveyed the Orkney Islands between 1927 and 1929; their map was published in 1932, and a descriptive memoir was published in 1935. Mykura (1976) published the last comprehensive memoir of the area, and based his account of the Orkneys on much of the work done by the geological survey and the more recent detailed sedimentological work which is discussed below.

5.3.1 Sedimentology and stratigraphy

The sediments have been sub-divided into the Lower, Middle, and Upper ORS (LORS, MORS, and UORS, respectively) groups largely as a result of the observations of earlier workers (e.g. Murchison, 1859), and the minor unconformities which are thought to separate the three groups (fig. 5.2). Basinwide correlation has depended almost entirely on the Achanarras/Sandwick fishbed horizon (Astin, in press). This is a deposit of a deep lake interpreted to have persisted for longer than usual and contains a distinct and diverse fish fauna (Rayner, 1963; Trewin, 1976; Westoll, 1979; Mykura, 1983; Trewin, 1985; Astin, in press). The bio-stratigraphic correlation is currently being refined by palynological studies (Allen and Marshall, 1981; Marshall and Allen, 1982; Marshall, 1988, 1989). The earliest ages placed on the ORS sediments are shown on fig. 5.2; the UORS may extend into, and may be stratigraphically continuous with the Lower Carboniferous (Astin, 1985). This section describes the previous work on the stratigraphy of the Orcadian Basin sediments exposed on Orkney, starting at the base of the section shown in fig. 5.2.

5.3.1.1 The Lower Old Red Sandstone

Near Yesnaby on the Orkney Isles, sediments of probable LORS age outcrop (Mykura, 1976). The Yesnaby Sandstone Group has been divided into two facies which are separated by the Garthna Geo Fault. At Harra Ebb, an angular discordance of approximately 6° can be seen separating the two formations, the upper Harra Ebb Formation from the lower Yesnaby Sandstone Formation (Mykura, 1976). The LORS is characteristically coarse, but commonly contains well-rounded and compositionally immature conglomerates with thin sandstone interdigitations (Mykura, 1983). The occurence of local thick fanglomerate deposits and the restricted depostional distribution of the LORS suggests deposition occured in small restricted basins, probably controlled by active fault topography (Mykura, 1976, 1983).

5.3.1.2 The Middle Old Red Sandstone

The base of the MORS is strongly diachronous, overstepping the LORS to the west onto Moinian basement both on the Scottish mainland, the Orkney and Shetland Isles (Mykura, 1976). The MORS is sub-divided into the Stromness Flagstone Group (containing the Sandwick fish beds), the Rousay Group, and the Eday Group (fig. 5.2). Each group is described separately below.
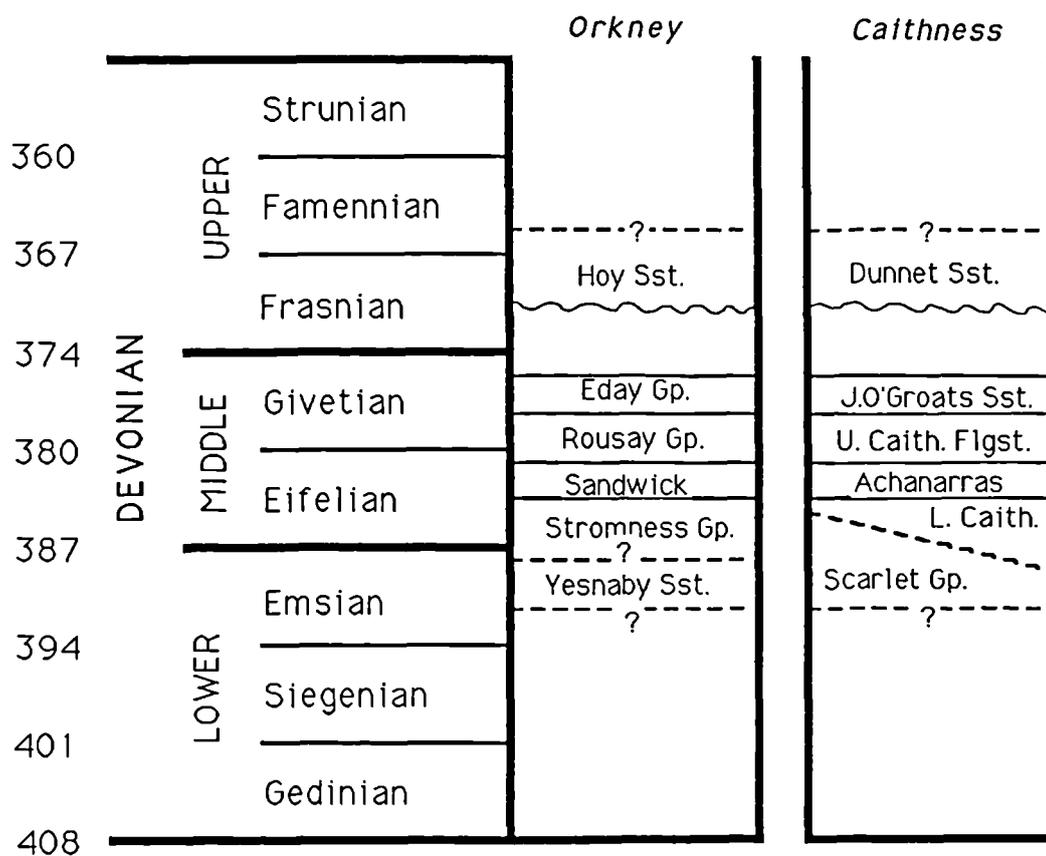
Figure 5.2. Present correlation of stratigraphy of the Old Red Sandstone on Orkney and Caithness, after Mykura, (1983, 1976) and Rodgers (1987). The extent, or existence, of the hiatus at the Middle to Upper Devonian boundary is unknown. The extent of the Upper Devonian succession is unknown.

Fannin (1970) identified 50 fluvio-lacustrine cycles in the Stromness Flagstones, and concluded that the cycles were formed by fluctuations in the level of a single large lake in the Orkney area, and that these transgressions were rapid. The base of each cycle is characterised by the deepest water lacustrine sediments, while the overlying beds indicate a sequence of progressively shallower lacustrine facies. These are in turn capped by fluvial sediments. Fannin concludes that towards the end of Stromness Flagstone times the lake was shallower and perhaps a number of isolated water bodies were developed. He also suggests that the center of the topographic basin appears to have moved northward with time. Fannin proved a thickness of 350 m. of Lower Stromness Flagstones.

The correlation and thicknesses of the Upper Stromness and Rousay Flagstones has been recently revised by Astin (in press), who found that the Upper Stromness Flagstone Formation is 325 m. thick, and the Rousay Flagstone Formation ranges in thickness from 170-215 m. The flagstones are followed by 800 meters of dominantly fluvial and aeolian sediments of the Eday Sandstone Group, consisting of three sand-rich formations separated by finer-grained formations (Astin, 1985). Astin (1985) has identified the deposits of two major river systems at this time. The northern system was at least 30 km. long, covering the area of the northern Orkneys, and was a fan spreading from an apex c. 15 km. NW of Eday. The southern system was at least 40 km. long, and flowed north from Caithness across southern Orkney.

Ridgeway (1974) studied the sedimentology of the Eday Group. At the base of the Group a series of transition beds marks the passage from dominantly lacustrine Rousay Flagstones, to the fluviatile Eday Group. The basal Lower Eday Sandstones include up to three facies, after which a relatively rapid transition to the Eday Flagstones occurs, in which rhythmic sedimentation is developed. The second coarse-grained formation follows, the Middle Eday Sandstones. The Eday Marl Formation marks a return to fine-grained sedimentation, which is followed by, and Ridgeway feels is penecontemporaneous with, the Upper Eday Sandstones.

Ridgeway (1974) interprets that the Lower Eday Sandstones were primarily laid down in braided river courses where deposition took place largely in channels. Flood plain lakes occurred during Eday Flags deposition in high sinuousity channels. In the Middle Eday Sandstone times, a return to braided streams enabled channel deposition to predominate again. The Eday Marls and Upper Eday Sandstone were deposited on a flat flood plain where shallow overbank lakes and channels were prevalent.

5.3.1.3 The Upper Old Red Sandstone

The thick sandstones and underlying volcanic rocks seen on the island of Hoy were once thought to be the only UORS rocks on Orkney (Mykura, 1976). However, Astin (pers. comm., 1989) has recently confirmed that the Eday Group sediments can be correlated with the UORS sediments on Hoy, and that the MORS-UORS sedimentation on Orkney is strongly diachronous.

The basic volcanic rocks on Hoy are alkaline lavas which rest directly on the supposed unconformity of the MORS rocks, forming the base of the UORS succession (Mykura, 1976). The alkaline lavas have been dated at about 370 My by Halliday et. al. (1977). The thickness of the sandstones on Hoy is uncertain, but are at least 1000 m. (Mykura, 1976).

McAlpine (1978) studied the UORS of Orkney and Caithness, and subdivided the Dunnet Head and Hoy Sandstone into nine lithostratigraphic members in which three lithofacies were recognized. Both the Dunnet Head and Hoy Sandstone have features indicative of distal, sandy deposits of wadi fans and the adjacent pediment of aeolian, sabkha and playa lake sediments. The palaeocurrents in the fluvial strata are consistent with them having been deposited in a braided system of wadi channels. McAlpine showed that the Orkney and Caithness UORS was deposited by a NE-ward flowing river system. Rogers (1987) suggested that since the UORS river system was similar in orientation, facies and position to the southern Eday Sandstone ("upper MORS") river system, there was little doubt that the same river system deposited, and catchment, fed both. Astin's (pers. comm., 1989) recent work on the Eday Group and UORS on Hoy has confirmed this.

5.3.1.4 Comprehensive ORS stratigraphic work

Rogers (1987) used new mapping, facies analysis and other techniques to compile a massive amount of data in revising the entire stratigraphy of the ORS around the SW Moray Firth, at the south end of the Orcadian Basin, astride the Great Glen Fault. The first important conclusion that is made is that although Rogers agrees to a post-UORS compression, the previous notions of regional Lower-Middle and Middle-Upper ORS unconformities associated with Middle Devonian compression are disproved. He emphasized that strike-slip faults did not control the ORS basin; the ORS subdivisions, subsidence and palaeogeography reflect NW-SE crustal extension. Transfer faults which separated half-graben acted as lines of differential subsidence and of access for drainage to the basin. At least in the southern Orcadian

Basin, syn- and antithetic faulting caused uplift of previously subsiding areas to supply ORS clasts to later ORS alluvial fans. The Orcadian Lower, Middle and Upper ORS should be recognized as facies representing partly diachronous stages in the interaction of drainage, sea level, and extensional tectonics. The reported unconformities between the Lower, Middle and Upper ORS, if present, are extremely localized features, perhaps only due to localized uplift in footwalls adjacent the major growth faults. This should be considered in context of the conclusions made from the structural observations described in the next section.

5.3.2 Structure

Early structural work on Orkney was limited. Mykura (1976) noted the near northerly trend of the axial traces of the large open folds exposed over the north-south extent of the Islands, such as the northerly plunging Eday Syncline, the West Mainland Anticline and the Deerness Syncline (figs. 1.1 and 5.1). Mykura divided the faults into three systems according to their trend: a. the ENE-NE trending faults, such as the North Scapa Fault, b. northerly faults, such as the East Scapa Fault, and c. the less common northwesterly faults.

The work of Coward and Enfield (1987) and Enfield and Coward (1987) focused upon the timing and style of extension in the West Orkney Basin, based on commercial, speculative and deep seismic data. An attempt was also made to link the offshore data with observations onshore in Caithness and Orkney, to better constrain the timing of the tectonic events.

Coward and Enfield (1987) found that the West Orkney Basin, and the related Outer Isles and Minches Basins, are characterized by half-grabens formed on large growth faults with up to 10 km. displacement, and these faults detach within the Caledonian basement. They also suggest, through the use of restoration techniques, that the extension within the West Orkney Basin can be seen as occurring on two different types of faults, and furthermore, with the use of field data, at two different recognisible times. Initial extension occurred on listric faults soleing onto high-level detachments, interpreted as the offshore continuation of the Caledonian Thrusts. Further extension seen on seismic data is interpreted to occur on a more widespread system of approximately planar faults, which breach the early system to detach at mid-crustal levels, along deeper Caledonian thrusts. Overall, extension occurred in a NW-SE direction.

Coward and Enfield (op.cit.) also suggest that the Devonian Basins have undergone several episodes of inversion: during the Middle Devonian, where sedimentary patterns were affected within the ORS basins; during the Carboniferous, related to Variscan deformation; and also within the Mesozoic. A change in sedimentation patterns is seen in the seismic data, such that the lower sedimentary sequences thicken toward the NW, into the major Devonian growth faults (direction of onlap to the SE), above which a disconformity separates a depositional pattern where the onlap is to the NW, and thickening of the sedimentary package is to the SE. They admit that this cannot be accurately dated because of the lack of stratigraphic control within the basin. They relate the change in sedimentation pattern to tectonic inversion caused by uplift and tilting of the fault blocks, either by oblique or reverse displacement on the faults.

Coward and Enfield (op.cit.) suggest that a reversal in the sedimentation pattern related to inversion would be observed as a phase of strike/oblique slip reactivation of NNE-NE trending Devonian faults in Orkney and Caithness. The kinematics and timing of these episodes of fault reactivation and basin inversion was then determined by field work. In particular, evidence for strike-slip reactivation along large faults on Orkney was found which suggested early sinistral displacement, and also two episodes of later dextral displacements on N-S trending faults (the Brims-Risa and East Scapa Faults). Late Permian dykes (Brown, 1975; Rock, 1983; Baxter and Mitchell, 1984) were used to date relative movement on major faults: the dykes cross-cut folds associated with the sinistral movements, and intrude the planes of dextral strike-slip faults and therefore post-date the sinistral and earliest dextral deformation. The early dextral strike-slip deformation is thought to be related to Variscan deformation and inversion, which juxtaposed the ORS basins of Shetland by displacements of tens of kilometers on the Walls Boundary Fault-Great Glen Fault system (Coward et al., 1989). Coward and Enfield (op.cit.) state that later, dextral-slip movement appears to have reactivated faults on Orkney in a transtensional sense, deforming the Permian dykes. The transtensional displacement shows extension down to the east, and is perhaps related to basin development in the Moray Firth during the Mesozoic. Enfield (1988) used the obliquity of folds on Orkney to assess the displacement senses associated with the various phases of strike-slip faulting. However, the age relationships of the folding and faulting on Orkney are not well-constrained. This will be discussed in more detail in sections 5.6 and 5.7.

5.4 North Scapa Fault Section

5.4.1 Introduction

This section presents field and microstructural observations from the North Scapa Fault (NSF), which is exposed in several bays along the north coast of Scapa Flow, Mainland, Orkney (figs. 5.3, 5.4 and 5.5). A particularly well-exposed section through the NSF occurs in Orphir Bay [HY 335045] (fig. 5.6). At this locality, detailed analysis of the microstructures and fracture arrays in the sandstone in the hangingwall of the fault has revealed the sequence of faulting and related fluid flow events which have occurred during initial extension and later reactivation along the fault. This has allowed a fault history to be established, and this history has been placed into context of a burial history for the sediments in the Orkney area recently presented by Astin (in press), in order to better constrain the timing of the faulting events (section 5.4.5.2).

The NSF trends SW-NE from Houton Head [HY 306035] to the northern part of Scapa Bay [HY 435090], where its intersection with the East Scapa Fault is obscured (fig. 5.4). Extension of the fault to Sea Geo [HY260025] on the north east coast of the island of Hoy has been inferred by the Geological Survey (1932) (fig. 5.1). Along its entire length on the Mainland, the NSF separates Upper Stromness (MORS) lacustrine facies rocks from fluvial facies North Scapa Sandstone in its hangingwall. The age of the North Scapa Sandstone has been under debate because of the nature of the unexposed contacts the sandstone has with the rest of the stratigraphy along the fault. Ridgeway's (1974) stratigraphic work on the North Scapa Sandstone suggested that it was of MORS age, as its facies was most similar to the facies of the Eday Sandstone beds observed elsewhere on the Islands. Ridgeway (1974) also found an unusual thickness of the sandstone in the hangingwall of the NSF (500 meters instead of the usual 200-300 meters found elsewhere on Orkney). From the thickening of the sediments, it was inferred that the NSF was active during deposition of the Eday Sandstone, which suggests the earliest fault movement occurred during the upper MORS.

Astin's (1985) sedimentological work also supported the idea that the fault was active during deposition. However, Astin (1985) and Rogers (1987) both strongly suggested that the North Scapa Sandstone facies is extremely similar to that of the UORS sandstone facies on Hoy, and that the North Scapa Sandstone is of UORS age.

Figure 5.6. Photomontage of domains 2-4 in the hangingwall of the North Scapa Fault, Orphir Bay, Mainland, Orkney [HY 335045]. Fault plane (FP) dips 65° ESE. Domains as labelled. Umbrella 1 m. long. See fig. 5.7 for line drawing of features and sample locations.

As discussed in section 5.3.1.3, recent work on the Eday Group sediments, including the North Scapa Sandstone, has confirmed that the "upper MORS" Eday sediments can be correlated with the UORS sediments of Hoy (Astin, pers. comm., 1989). Astin's work also confirmed considerable thickening of the North Scapa Sandstone in the hangingwall of the NSF; a minimum 55 metres of thickening occurred during deposition of the first half of the Eday Group (Astin, pers. comm., 1989). However, the exact age of the Eday Group is uncertain due to the diachronous MORS-UORS sedimentation (Astin, pers. comm., 1989). Thus, the first movements on the North Scapa Fault occurred sometime in the MORS to UORS (Middle Devonian). Microstructural work in this thesis does suggest the fault was active early in the burial history of the sediments in its hangingwall, agreeing with Astin's work (see discussion below). This study will refer to the sediments in the hangingwall of the NSF as the North Scapa Sandstones.

5.4.2 Orphir Bay [HY 335045]

This section describes a detailed analysis of the NSF zone in Orphir Bay [HY 335045]. The fault is shown in fig. 5.6, and a detailed line drawing of the structure is shown in fig. 5.7. The fault plane strikes 048° and dips 60-70° southeast. Slickensides on the fault surface plunge consistently 60° to the southeast, indicating sinistral, oblique-slip faulting during the last phase of movement. Fractures developed in the hangingwall of the fault related to this last phase of movement will be discussed below. As discussed above, previous work suggests that there was fault activity prior to the later sinistral movement, in a dominantly extensional movement sense, at some time during the MORS-UORS. Structural evidence for this early movement is discussed below.

5.4.2.1 Footwall deformation

Deformation in the Upper Stromness flagstones (MORS) in the footwall of the NSF is shown in figs. 5.7 and 5.8a. The beds are gently folded into the fault, and 1-2 meters of incohesive fault gouge occurs in the footwall block. The footwall deformation is characterized by packets of strata bounded by minor slip surfaces, often in conjugate pairs. Conjugate fractures are also seen on the smaller scale within the packets, with each packet showing a different range of orientations for the fractures (figs. 5.7 and 5.9). This suggests the minor 'interpacket' fractures formed earlier than the through-going slip surfaces and were then rotated within the blocks.

Figure 5.7.   Line drawing of the North Scapa Fault, Orphir Bay, Mainland, Orkney [HY 335045], as shown in fig. 5.6.   Length of drawing not exact due to distortion on photomontage.   Sample locations and fracture analyses details are labelled in the hangingwall.   The well-bedded flagstones in the footwall are separated into blocks (labelled A-D) with variable fracture orientations as shown in fig. 5.9a-d.   Bedding in the hangingwall is not discernable closer than 10 m. to fault.   See text for discussion.

NORTH SCAPA FAULT SECTION

Orphir Bay (HY336042)

SW Mainland, Orkney

CLIFF TOP

BEDDING

(Limit of exposure)

NW

Upper Stromness Flags

FAULT PLANE

49519 49524 49520 49521

BRECCIA ZONE

BRECCIA ZONE

CLIFF BOTTOM 49526

49517 SE

DOMAIN 4 DOMAIN 3 DOMAIN 2

Scapa Sandstone

SCALE

0 meters 5

TRACE OF BEDDING IN FLAGS; FRACTURE ARRAY IN SANDSTONE

TRACE OF LINE TRAVERSE FOR FRACTURE ANALYSIS IN HANGINGWALL

BRECCIA ZONES

49519 ■ SAMPLE LOCATIONS /SAMPLE NO.

LOCATION OF FRACTURE DENSITY ANALYSIS IN HANGINGWALL

A-D LOCATION OF FRACTURE ANALYSIS IN FOOTWALL

Figure 5.8. Photographs of deformation adjacent to the North Scapa Fault, Orphir Bay, Mainland, Orkney [HY 335045]. a) Folding and fracturing in Upper Stromness Flagstones in footwall of fault. Fractures offset 'packets' of bedding, and contribute to the rotation of bedding during folding. Hammer 50 cm. long. Looking WNW. b) Shiny, slickensided slip plane parallel to bedding in Upper Stromness Flagstones, used to accomodate folding in footwall during faulting. Ten pence piece for scale. c) Detailed view of fault-parallel breccia zone separating domains 2 and 3 in the hangingwall Scapa Sandstones. Note angular to rounded clasts, many darkened to indicate evidence for hydrocarbon migration pre-dating breccia development. Pencil 15 cm. long. Looking WNW. d) Detailed view of fault-parallel breccia zone separating domains 3 and 4 in the hanginwall Scapa Sandstones. Note angular to rounded clasts of white sandstone from domain 4 in darkened matrix. Pencil 15 cm. long. Looking WNW.
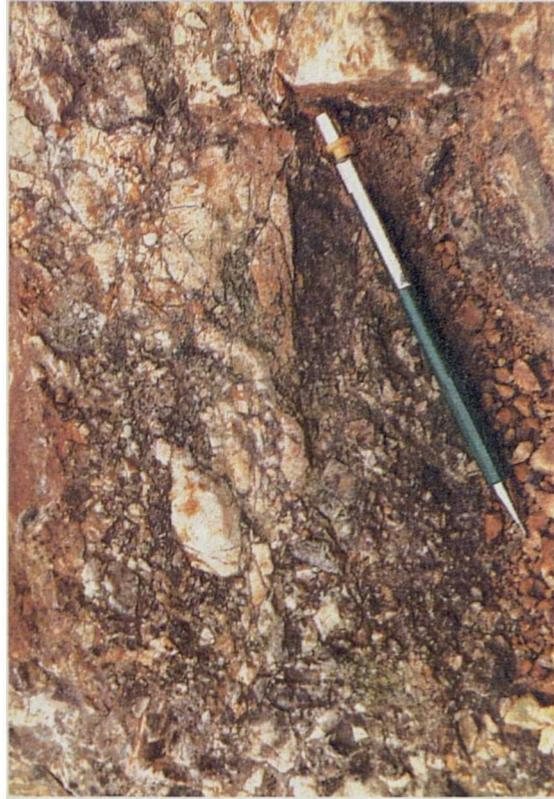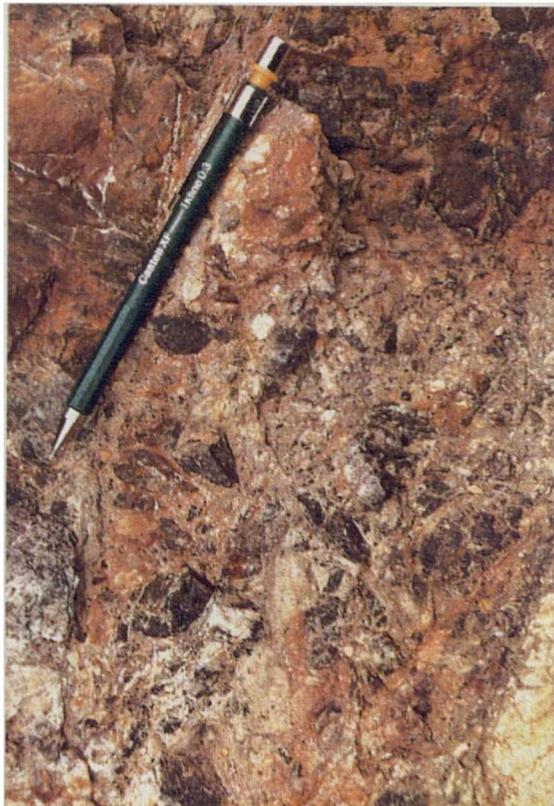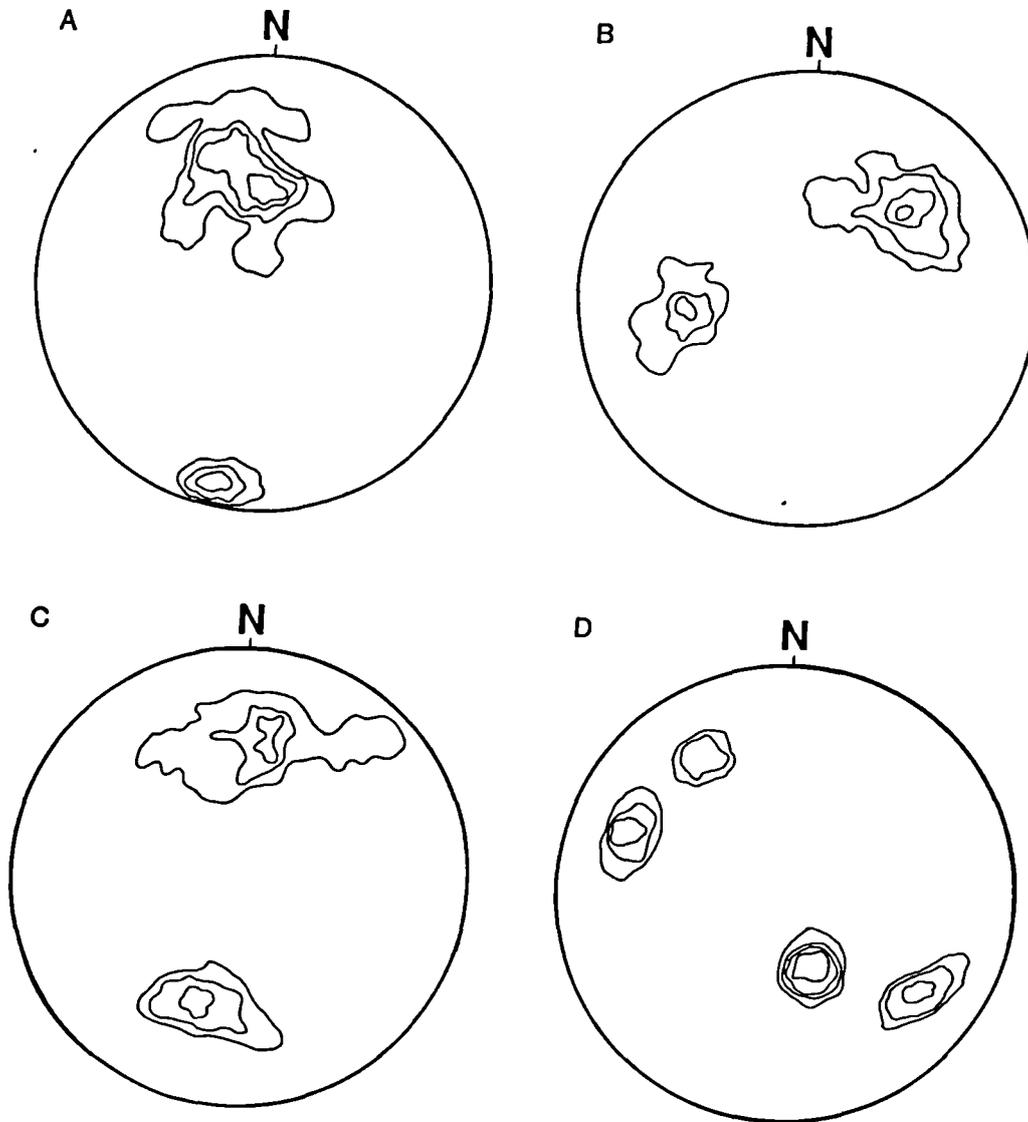
Figure 5.9. Lower-hemisphere, equal-area, contoured stereoplots of poles to fracture orientations in Stromness Flagstones in footwall of North Scapa Fault, Orphir Bay, Mainland, Orkney [HY 335045]. Location of fracture analysis shown as A-D on fig. 5.7. a.) Fractures in block A; contours 33, 16, 8, and 4% per 1% area, n=34. b.) Fractures in block B; contours 25, 17, 9 and 5% per 1% area, n=52. c.) Fractures in block C; contours 10, 8, and 4% per 1% area, n=48. d.) Fractures in block D; contours 33, 25, 16 and 8% per 1% area, n=22.

Folding was accommodated by slip along the conjugate fractures, together with slip along bedding-parallel surfaces, creating a shiny slickensided surface (fig. 5.8b), similar to the scaly fabrics described mesoscopically in DSDP cores (Moore et al., 1986; Prior and Behrmann, in press; Agar et al., in press). The bedding-parallel slip surfaces occur within 10 meters of the fault on most planar surfaces observed. The line drawing (fig. 5.7) summarizes the deformation within each of the packets of strata in the footwall of the NSF.

5.4.3 Hangingwall deformation

Outcrop analysis of the hangingwall has revealed four domains which reflect the relative deformation state of the North Scapa sandstone. The domains have been divided on the basis of the relative intensity and orientation of fracture development, the cohesiveness of the sandstone (degree of cementation), and the presence of a darkened sandstone in domain 3.

Domain description	Distance from fault
1) Well-bedded, undeformed sandstone (parent rock)	15 meters
2) Fractured, blocky sandstone	3-15 meters
3) Extremely fractured, darkened sandstone	1-3 meters
4) Well-cemented, cataclastic lensoidal sandstone	0-1 meters

Although these general descriptions indicate an overall increase in deformation adjacent toward the fault, the character and distribution of the deformation is different in each domain, and this is considered in detail in the next section. These domains will be referred to throughout the fault zone descriptions. Fault-parallel breccia zones occur between domains 2 and 3, and between domains 3 and 4 (fig. 5.7).

5.4.3.1 Macroscopic fracture array

The relationship of minor fracture arrays to major faults has long been of interest to geologists, and has been studied both in the field (e.g., Engelder, 1974; Thompson and Burke, 1974; Aydin, 1978; Brock and Engelder, 1977; Bruhn and Pavlis, 1981; Jamison and Stearns, 1982; House and Gray, 1982), and theoretically (Reches, 1978, 1983). The field studies listed above found a range of fracture orientations and densities in relationship to the fault geometries. One of the more important aspects of studies such as these is the relationship between fracturing and permeability. This relationship

is directly relevant to the oil industry, as fracture permeability can greatly increase reservoir potential in an otherwise low porosity sandstone, and provide pathways for hydrocarbon migration. As discussed in Chapter 4, Seeburger (1981) concluded that high permeability zones found adjacent faults is a result of increased fracturing and porosity. However, other studies have found that fracture and cataclasis associated with faulting can lead to a decrease in permeability. For example, in the Jamison and Stearns (1982) study, increasing fracture density adjacent an extensional fault correlated with, and caused a decrease in permeability.

The fault zone exposure in Orphir Bay provides and ideal location to study fracture array development in the sandstone in the hangingwall of the fault. In addition, this data can be then integrated with microstructural data in order to provide information regarding the relationship between fracturing and fluid flow adjacent the fault. This relationship will be discussed in section 5.4.4.

A line-traverse of the macroscopic fractures in the hangingwall of the fault was carried out 1-15 meters from the fault plane to obtain information of the dominant fracture orientations, and the fracture spacing (the location of line-traverse is shown on fig. 5.7). Up to 1 meter from the fault, the fractures were of consistent orientation and spacing, and therefore were not included in the line-traverse. The orientation and spacing of all fractures encountered in the line traverse were measured, regardless of length, which varies from several cm. to several meters. Due to the deformation, bedding is obliterated up to 10 meters from the fault plane, therefore assessing the offsets along the fractures was in most cases not possible.

In addition, information about the fracture density adjacent the fault was obtained using the following method. Photographs were taken of 0.5 meter^2 areas along the same traverse, the tracings were then digitized, and the three-dimensional fracture density was calculated from a computer linked to the digitizer. The assumptions, problems, and errors involved in the methods of fracture array measurement are described in Appendix 2.

5.4.3.1a Fracture orientations

The fractures in the first 15 meters from the fault plane can be separated into two groups: 1) those from 1-15 meters from the fault plane (domains 2 and 3), defining angular blocks of sandstone ranging from 1-2

cm. in length, to 10-15 cm. in length with increasing distance from the fault plane, and; 2) those in the first meter from the fault plane (domain 4), oriented sub-parallel to the fault, spaced 2-10 cm. apart, which create an anastomosing fracture array, defining lensoidal-shaped blocks of cemented sandstone. Both groups developed during the last phase of deformation, as they cross-cut all other deformation features in the fault zone, and breccias developed as a result of the fracturing contain clasts of previously developed cataclasites from domain 4 (see discussion below).

Contoured plots (lower-hemisphere, equal-area) of the poles to the fracture planes are shown in fig. 5.10. The group of fractures in domains 2 and 3 define an assemblage of three sets of orientations (fig. 5.10a). The mean attitude of two of the sets ($223^{\circ}/28^{\circ}$ and $059^{\circ}/43^{\circ}$), define a conjugate set, intersecting in an acute angle of 60° or less. One of these sets ($223^{\circ}/28^{\circ}$) is nearly parallel to the bedding in the Scapa Sandstone outside of the fault zone. The other set ($059^{\circ}/43^{\circ}$) trends sub-parallel to the fault plane, and is coincident with dark, anastomosing seams containing hydrocarbon, discussed in section 5.4.3.2. The third set, less well-developed but still prominent, trends perpendicular to the conjugate set, but its orientation is much steeper ($140^{\circ}/80^{\circ}$). Slickensides are rarely (<10%) observed on the fractures from group two, but when they are observed, or a feature can be used to assess the offset along the fracture, the fractures belonging to the conjugate set show extensional offsets. The fractures in domain 4 have a mean attitude of $063^{\circ}/60^{\circ}$ (fig. 5.10b). The abrasive slickensides on the fracture surfaces are consistent with that of the fault plane, plunging 60° to the north east, also indicating sinistral, oblique-slip movement.

5.4.3.1b Interpretation of fracture orientations

The first group of fractures in domains 2 and 3, which shows three well-developed sets, possesses mutual cross-cutting relationships, and thus must have developed to accommodate strain during part of the same faulting event. Thompson and Burke (1974), Aydin (1978), and Bruhn and Pavlis (1981) have all described the penecontemporaneous development of three or four sets of faults in the field. Reches (1978) has shown theoretically that the development of four sets of faults with orthorhombic symmetry occurs in a three-dimensional strain field whereas two sets of faults with a conjugate pattern arise as a result of plane strain. Three-dimensional strains are the general case in nature, and Reches (1983) has shown that four sets of faults are required in this situation. The fracture array from Orphir does not fit the theoretical analysis.
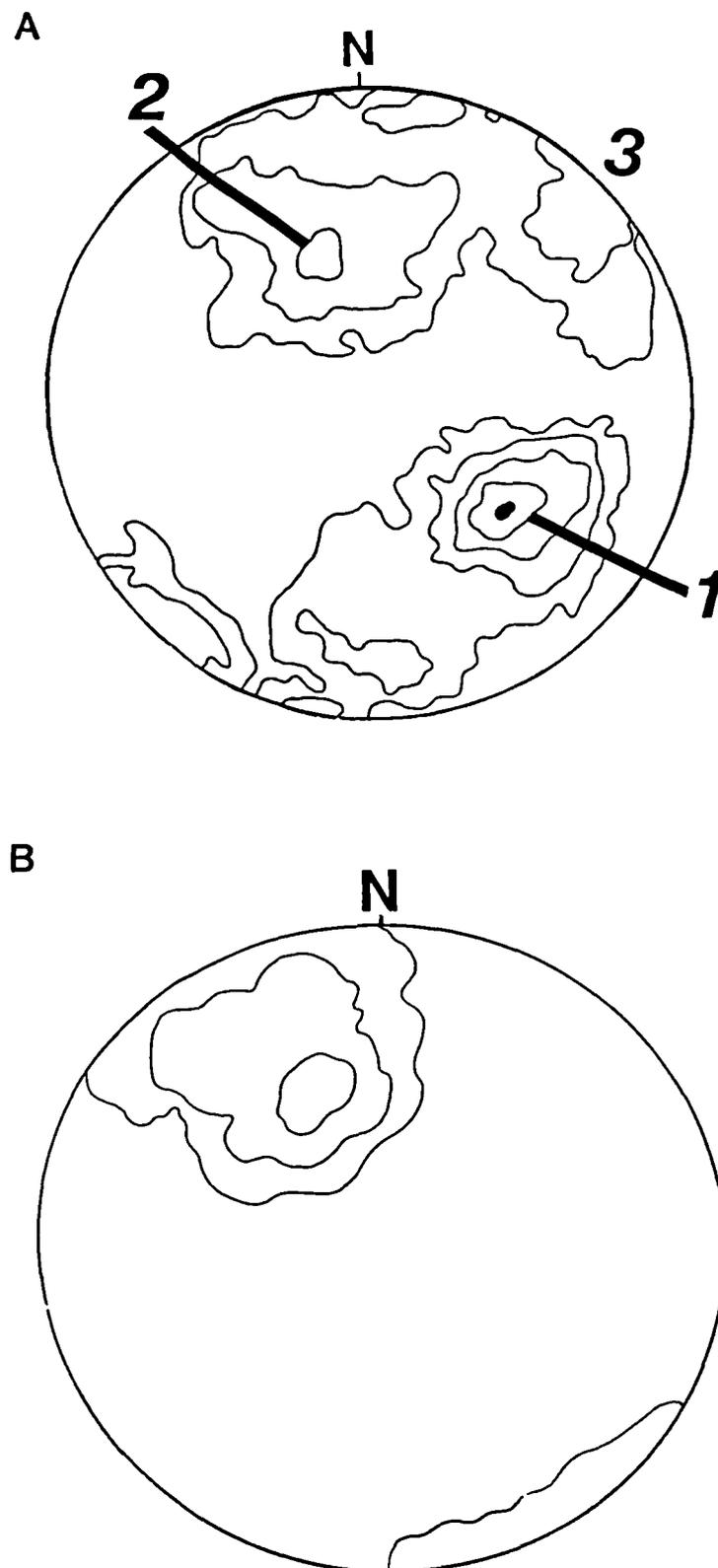
Figure 5.10. Lower-hemisphere, equal-area, contoured stereoplots of poles to fracture orientations in Scapa Sandstone in hangingwall of North Scapa Fault, Orphir Bay, Mainland, Orkney [HY 335045]. a) Fractures from line traverse in domains 2 and 3; contours 10, 7, 4, and 2% per 1% area, n=488. b) Fractures in domain 4; contours 24, 10, and 2% per 1% area, n=43.

Other field studies (Aydin, 1977; Bruhn and Pavlis, 1981) which have found the development of just three fault sets have suggested that pre-existing structures could affect the fault array development. The fracture array in the Scapa Sandstone appears to represent a modified conjugate fracture pattern. This could have resulted from the presence of an anisotropy in the sandstone, such as bedding. Indeed, the bedding in the hangingwall is oriented nearly parallel to the most frequently observed fracture set in domains 2 and 3.

As described above, the fractures in domain 4 create an anastomosing array defining lensiodal sandstone bodies, and show the same movement indicators as that of the fault plane. The evolution of the anastomosing fracture array is analogous to the development of a throughgoing fault zone with shear lenses as described by Naylor et al. (1986) (fig. 5.11). In the model, Riedel shears are first developed slightly oblique to the fault. During continued displacement, first splays, lower angle shears, P shears and then the first shear lenses are developed, resulting in a fault zone with shear lenses, each of which contain surfaces which show the same movement indicators (slickensides) with that of the main fault (fig. 5.11). Note that during the deformation, certain shear planes can become inactive and the displacement can be transferred to another shear plane.

The question remains as to why different fracture patterns are observed in domains 2 and 3 from that observed in domain 4. It is suggested below that the cohesive cataclastic sandstone in domain 4 is the result of an earlier faulting event, as it predates hydrocarbon migration (see discussion below), found to be coincident with later reactivation of the fault which produced the fracture arrays described here. Therefore, at the time of the fracture development, the bedding which was present as an anisotropy in domains 2 and 3 was not present in domain 4. The development of the shear lenses in domain 4 could have resulted due to the homogeneous, fine-grained nature of domain 4 at the time of fracturing. Futher discussion of this is presented in section 5.4.4, after the microstructures of each domain are described.

5.4.3.1c Fracture spacing and density

The line-traverse shown in fig. 5.7 not only determined the dominant fracture orientations, but also the fracture spacing (fig. 5.12a). The three fracture orientations in the group 2 fracture array described above were observed up to 100 meters from the fault plane. In general, the fracture spacing increases away from the fault plane.

Shear lens development in sandstone

(section perpendicular to fault plane)
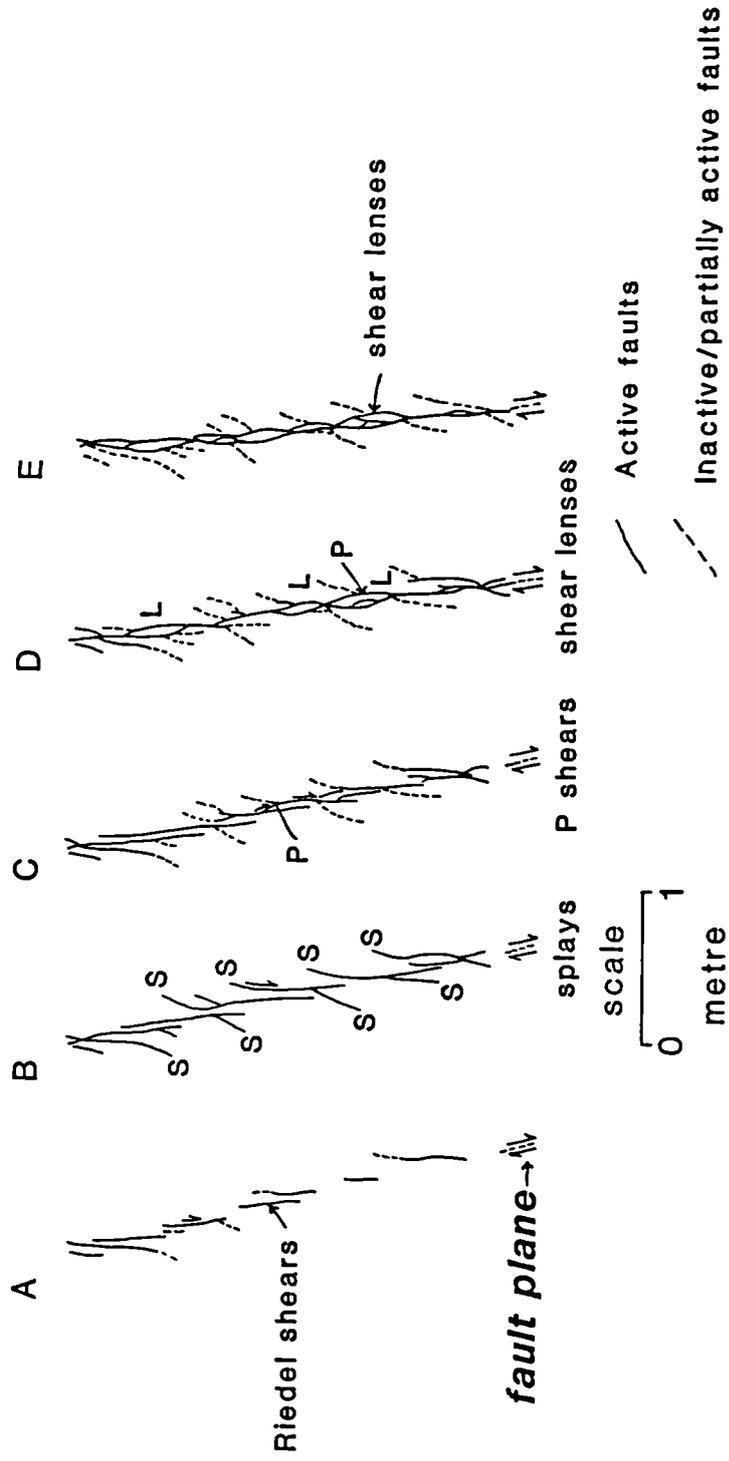
Figure 5.11. Model for the development of shear lenses adjacent to the North Scapa Fault in domain 4. Development of: a) Reidel shears; b) Reidel shears and first splays; c) Lower angle shears/first P Shears (P); d) More P shears; first shear lenses (L), and; e) throughgoing fault zone with shear lenses. After Naylor et al., (1986).

A

B
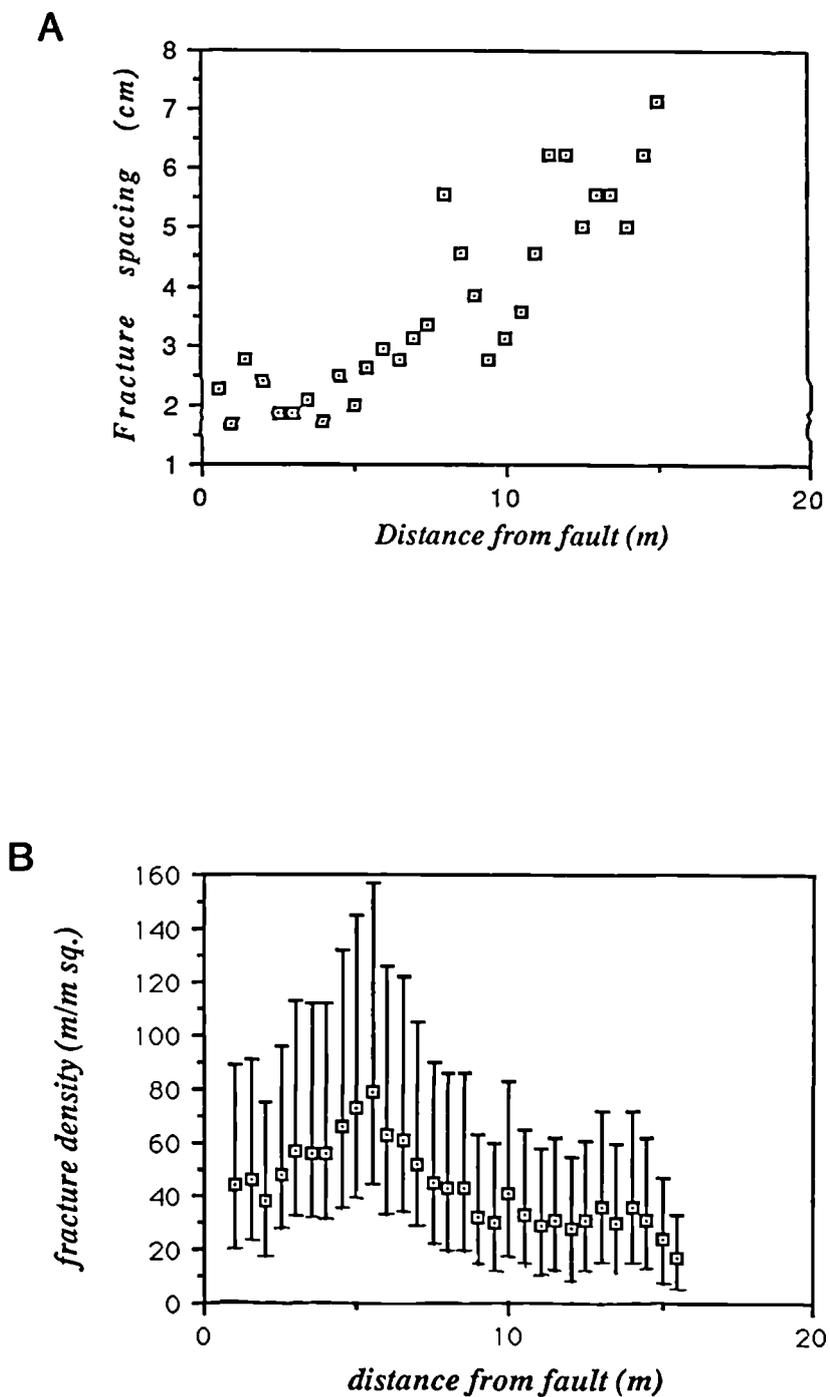
Figure 5.12. Graphs of: a.) fracture spacing, and; b.) fracture density in the North Scapa Sandstone in the hangingwall of North Scapa Fault, Orphir Bay, Mainland, Orkney. See text for discussion.

The data calculated at 0.5 m. intervals is displayed in fig.5.12a, and shows that the spacing increases from 1.7 cm. to 7.1 cm. at 15 meters from the fault, and a decrease in spacing corresponds with the development of breccia zones, particularly those mentioned above at 1 and 3 meters from the fault. Fracture densities have also been calculated from tracings of photographs taken perpendicular to the fault plane (fig. 5.13). The calculated fracture densities correspond well with the calculated fracture spacings (fig. 5.12b). As expected, the fracture density decreases away from the fault. The exception is the breccia zone separating domains 3 and 4, where the fracture density is at its maximum.

The fault-parallel breccia zones at 1 and 3 meters are not delineated by slip surfaces at their margins. The breccia zones correspond to an increase in fracture density (fig. 5.12b). The clasts in the breccias range in shape from rounded to sub-angular, and <1 cm. to 5 cm. in diameter (fig. 5.8c and d). The clast types found in the breccia zones are either fragments of a very grey to black sandstone found only in domain 3 of the fault zone (fig. 5.8c), or a very fine-grained white sandstone found only in domain 4 (fig. 5.8d). The matrix zones in the breccias range from a fairly incohesive, fine-grained gouge, to a hardened (well-cemented) grey/black material. The importance of the high fracture densities and breccia zones for providing fluid pathways will be discussed in section 5.4.5.

5.4.3.2 Hydrocarbon migration pathways:gas chromatograph data

The occurrence of hydrocarbons in the Orcadian Basin is summarized by Parnell (1983, 1985). Parnell (1985) reported the occurrence of hydrocarbon staining in the coarser-grained sandstones in the Orcadian Basin, notably along the major faults in Orkney such as the Brims-Risa (for location see fig. 1.1) and North Scapa Fault. Exposures at Orphir Bay show the presence of bitumens adjacent the NSF and occasionally along cross-bedding outside the fault zone. The relationship between the fracture array orientation, spacing, and density with the hydrocarbon migration has been deduced by integrating data obtained by detailed microstructural analysis of the sandstone in each domain of the fault. This has allowed the timing of the hydrocarbon migration in relationship within the fault history to be deduced, and the discrete hydrocarbon migration pathways to be identified. This will be discussed in section 5.4.5.

Figure 5.13. Line drawing of fractures in the North Scapa Sandstone in the hangingwall of the North Scapa Fault, Orphir Bay, Mainland, Orkney. Each block represents 0.5^2 m. Drawn from photographs taken parallel to outcrop face, which is oriented approximately perpendicular to the fault.

Fracture density
(m/m sq.)

Distance from
the Scapa Fault
(meters): 1

0.5 m

44.3 45.5 37.6 47.9 56.6 55.8 56.2 66.0 72.6 78.7

63.1 61.1 52.3 44.9 43.0 43.2 31.6 30.2 41.3 32.7

29.2 31.0 27.5 30.6 35.9 30.1 36.1 30.8 23.6 16.6
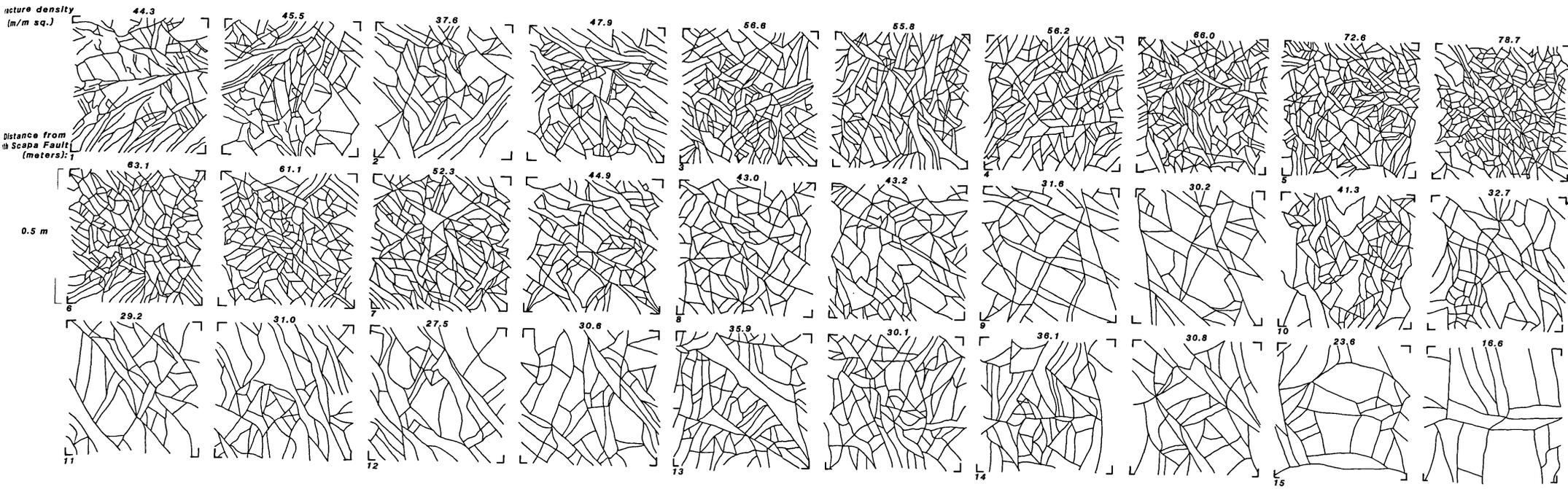
The hydrocarbons are observed in domain 3, 1-3 meters from the fault, and not directly adjacent to the fault in domain 4 (fig. 5.14a). They are observed as grey/black zones trending sub-parallel to the fault, in narrow anastomosing bands, 1cm. to several cm. wide (fig. 5.14b). The bands are parallel to one of the fracture sets ($059^{\circ}/43^{\circ}$) described in section 5.4.3.1a. Outside domain 3, hydrocarbons are observed trending along cross-lamination surfaces (fig. 5.14c). Weber (1980) described the influence of small-scale sedimentary features in controlling anisotropic horizontal fluid flow permeability. In the case of cross-bedding, while the original permeability anisotropy is usually quite low, diagenesis will enhance the permeability differences between the coarse and fine laminae found along the cross-beds. Thus, this anisotropic horizontal permeability must have been present at the time the hydrocarbons migrated through the sandstone outside the fault zone.

Microelemental analyses by gas chromatography was undertaken to obtain information of the total organic carbon present in samples from domains 3 and 4. Table 5.1 summarizes this data, which shows that neglible organic carbon is present in domain 4, while domain 3 contains a significant amount of organic carbon.

Total carbon content - North Scapa Sandstone			
Sample Location	Crushed	Acid Washed	A.W. & Filtered
Domain 4 in fault zone	0.0797	0.0651	0.0576
Domain 3 in fault zone	0.2926	0.2908	0.2937

Table 5.1. Gas chromatograph data for the North Scapa Sandstone in the hangingwall of the North Scapa Fault, Orphir, Orkney.

Figure 5.14.   Photographs of hydrocarbon migration pathways in the North
Scapa Sandstone in the hangingwall of the North Scapa Fault, Orphir Bay,
Mainland, Orkney.   In all cases, pencil is 15 cm. long. a)   Fault plane
(arrowed, FP), and junction between domains 3 and 4;   domain 4 (yellow
sandstone) seen in foreground;   domain 3 (darkened sandstone) seen above.
Separated by narrow (10 cm.) cataclastic zone.   Looking ESE.   b)   Detailed
view of of hydrocarbon migration pathway in domain 3.   Looking WNW.   c)
Detail of hydrocarbon migration pathway outside of fault zone in domain 1,
parallel to cross-bedding.   Looking WNW.
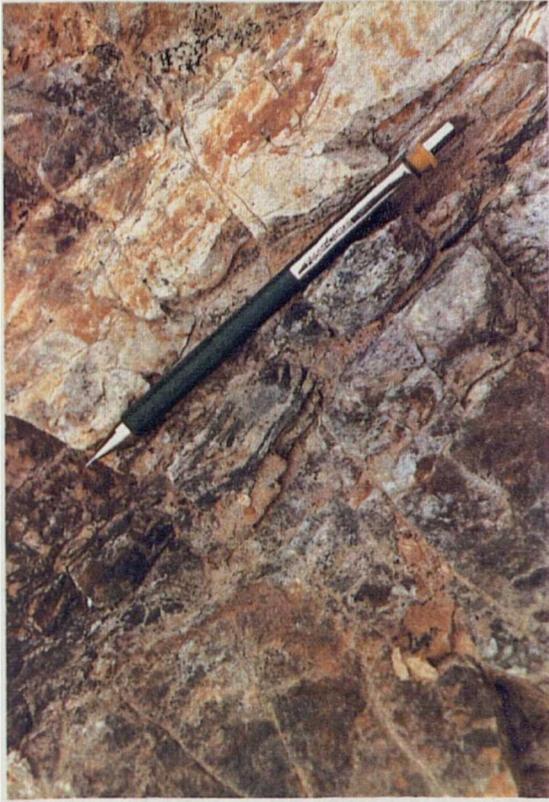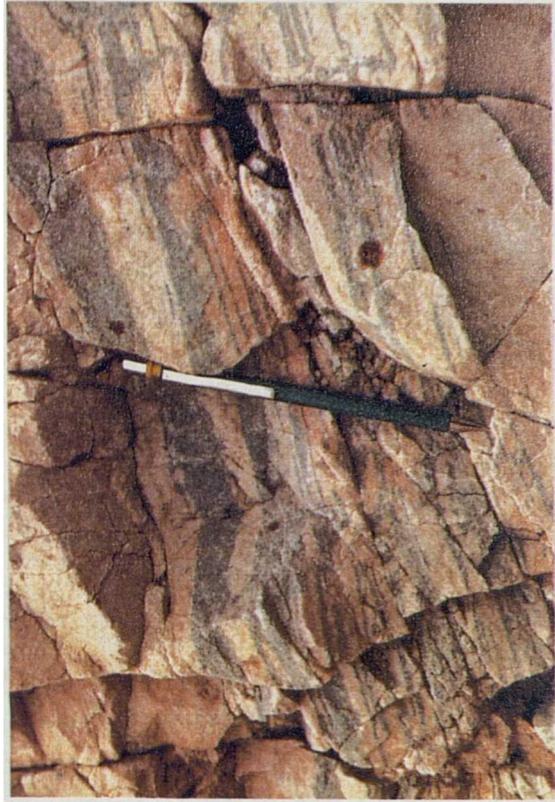
5.4.3.3 X-ray diffraction data

X-ray diffraction (XRD) of grain size separates from inside and outside the fault zone was undertaken to identify the dominant clay phases present in the undeformed Scapa sandstone, and in the deformed sandstone adjacent to the NSF. Both <2 μm. and 2-6 μm. grain size fractions were analysed. TEM shows that the grain size of the pore-filling kaolinite commonly observed in the undeformed sandstone is 2-6 μm (see section 5.4.3.4a below). Therefore, the XRD data obtained from the 2-6 μm analyses is thought to be the most accurate indicator of the clay phases which are present in the samples, and are shown here. The methods used in the analyses, and the full data set are shown in Appendix 3.

Fig. 5.15a shows that kaolinite (K) is the dominant clay in the parent rock outside the fault zone (domain 1). Figs. 5.15b and c indicates that in domain 3, the darkened zone, kaolinite is still present. Figs. 5.15d and e shows that in domain 4, however, illite (I) is the dominant clay phase, and kaolinite is extremely rare or absent. The unmarked large peaks are quartz. The XRD data demonstrates that the precipitation of certain clay phases was influenced by the deformation adjacent to the fault. The microstructures associated with the occurrences of the illite and kaolinite are described in the next section. The probable sequence of diagenetic events which occurred in the North Scapa Sandstone adjacent to the NSF are then discussed in section 5.4.5.

5.4.3.4 Microstructures and grain size data

Two perpendicular thin sections were cut from samples from each domain (see Appendix 1 for details). The thin sections were used for point counting in domain 1, and grain size analysis and assessment of the deformation microstructures in domains 1-4. Point count measurements of the undeformed North Scapa Sandstone from domain 1 were averaged from four thin-sections, 450 points per section. Grain size data was obtained by digitizing 100 grains from a tracing of each section at 50x magnification, and the mean calculated from the digitized data by a computer linked to a digitizer. The grain size measurements shown have been plotted using the √d distribution in order to obtain an approximately normal distribution. Examples in which normal distributions are not observed will be discussed in the appropriate sections. Appendix 5 discusses the methods and calculations used to obtain the grain size means quoted.

K   K

10   20   30   40   50   60

A
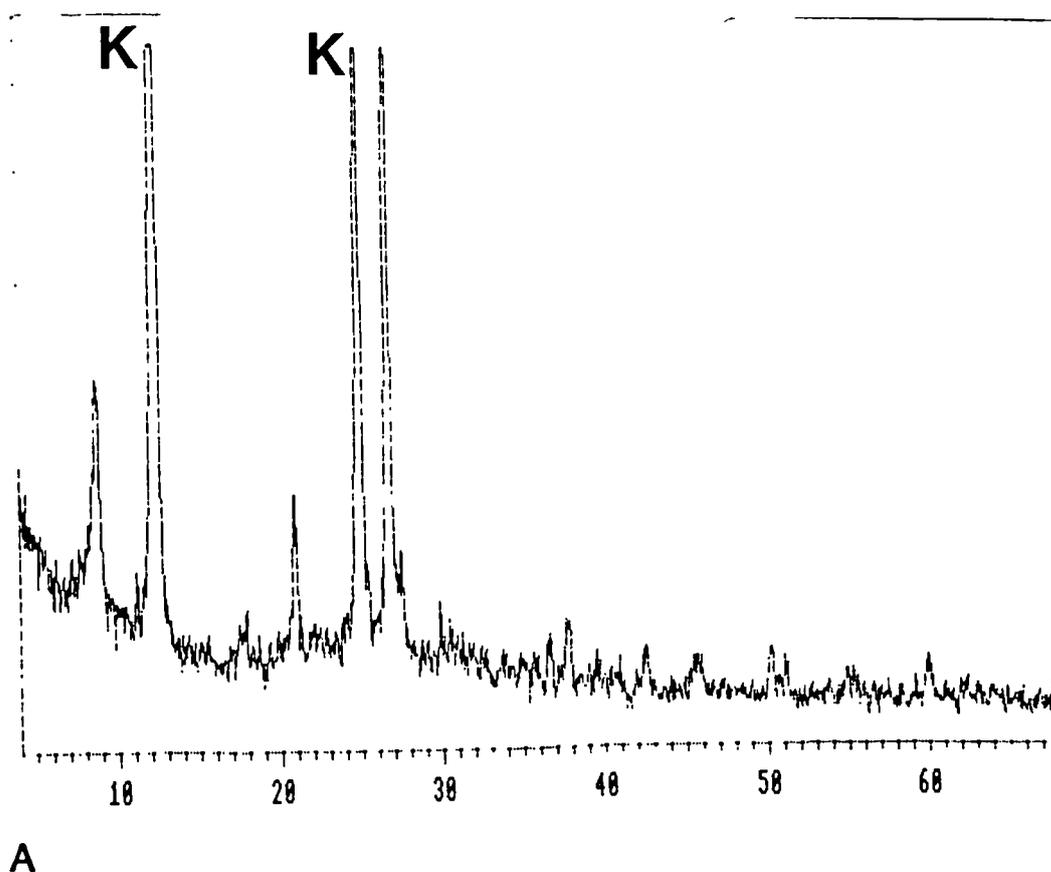
Figure 5.15. X-ray diffraction patterns from domains 1, 3 and 4. In all cases, large unmarked peaks are quartz. a) Data from domain 1, (sample 49517) outside of fault zone. Note kaolinite peaks and absence of illite peaks. Glycolated and heat treated 2-6 µm grain size fraction. b) Data from domain 3 (darkened zone adjacent domain 4, sample 49520). Untreated 2-6 µm grain size fraction. Note kaolinite (K) peak and absence of illite peaks. c) Data as from b. (sample 49520), except glycolated and heat treated. d) Data from domain 4, adjacent the fault (sample 49519), untreated 2-6 µm grain size fraction. Note illite peaks (I). e) Data from domain 4, adjacent the fault (sample 49519), glycolated and heat treated. 2-6 µm grain size fraction. Note illite peaks (I). See Appendix 3 for full data set.
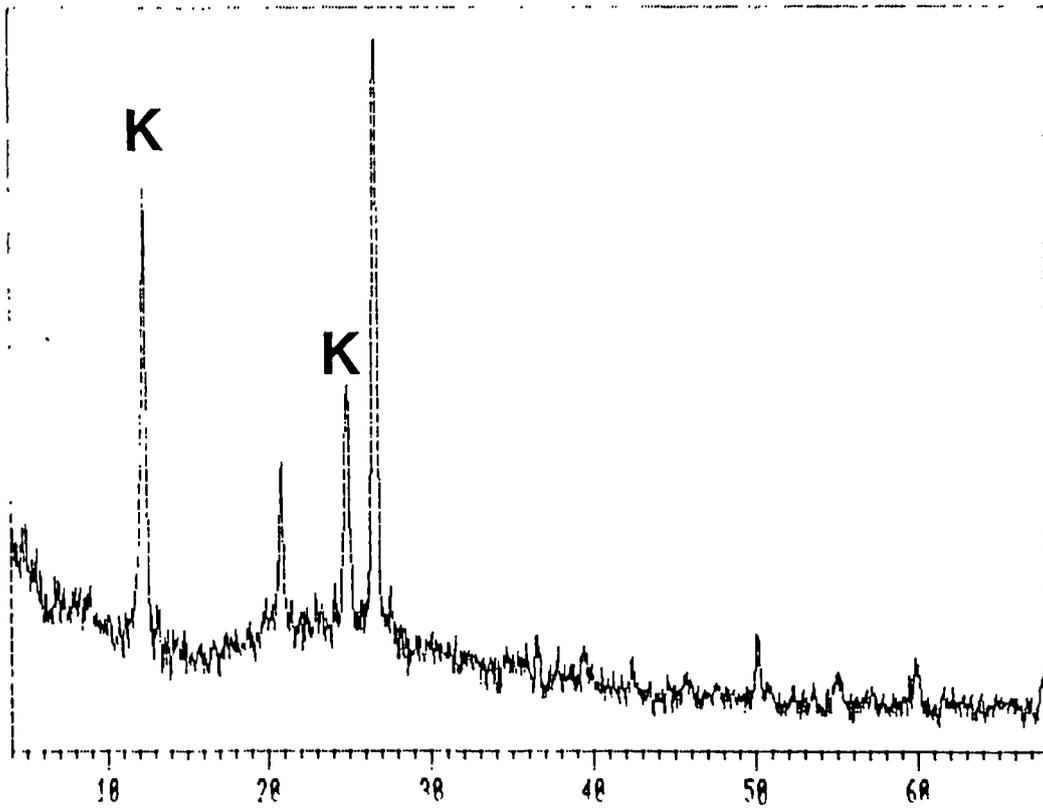
B
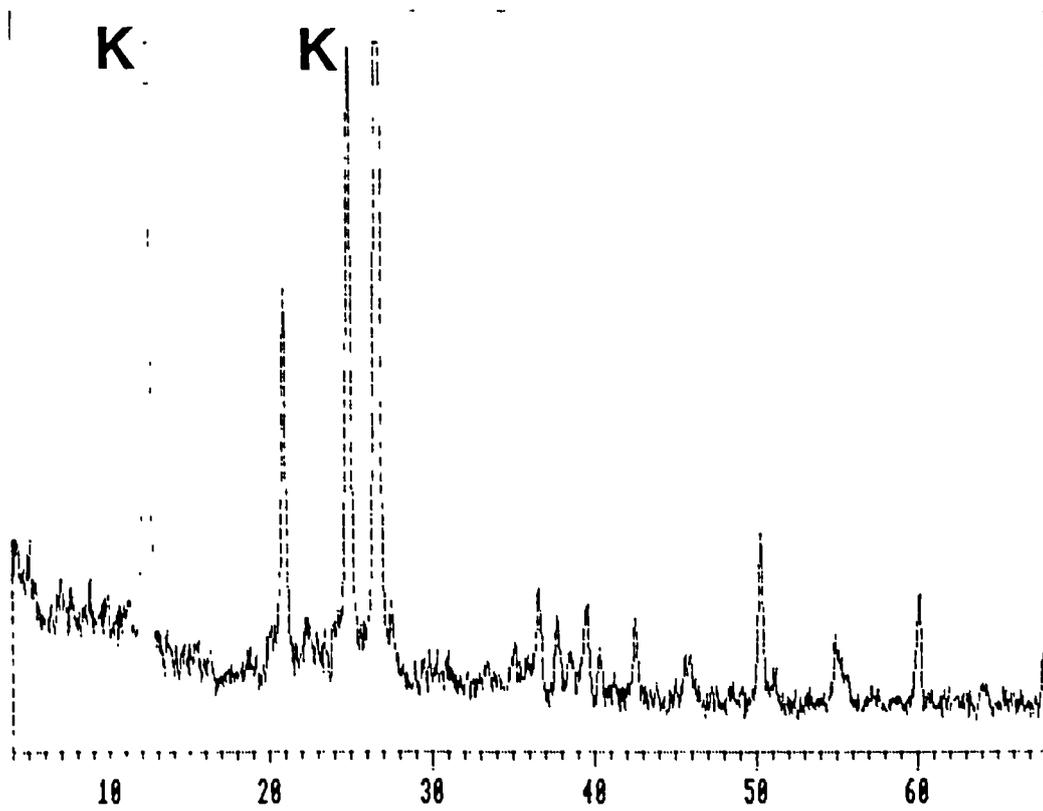
C
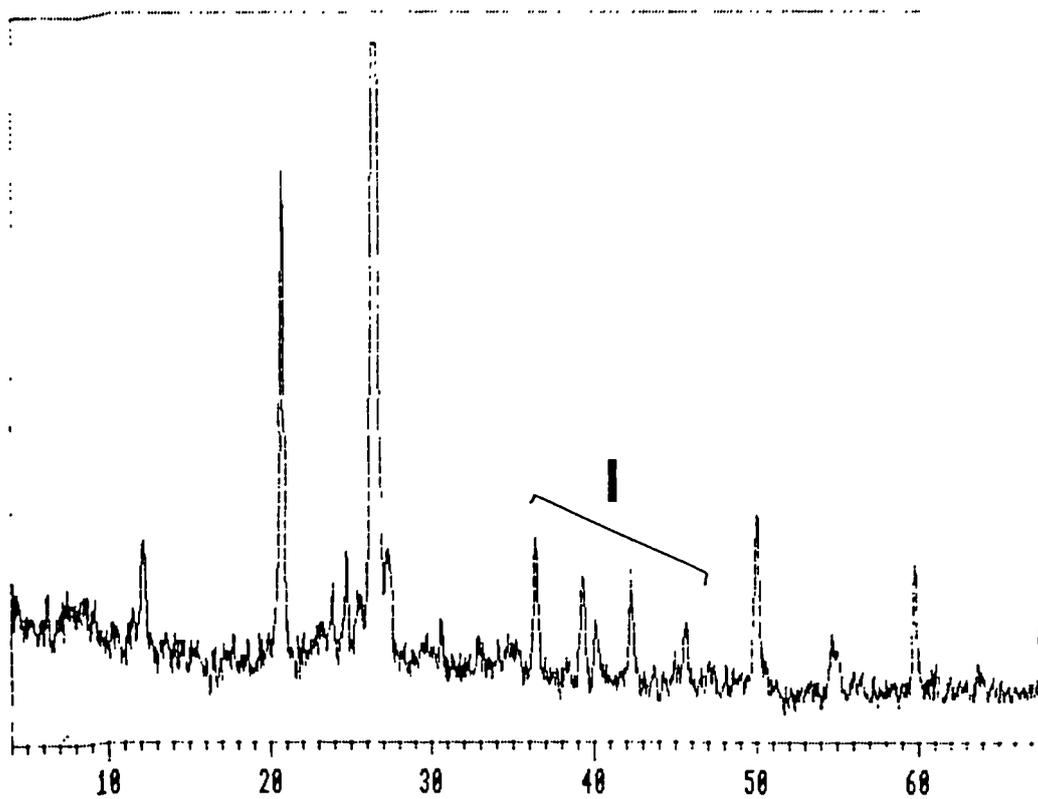
D
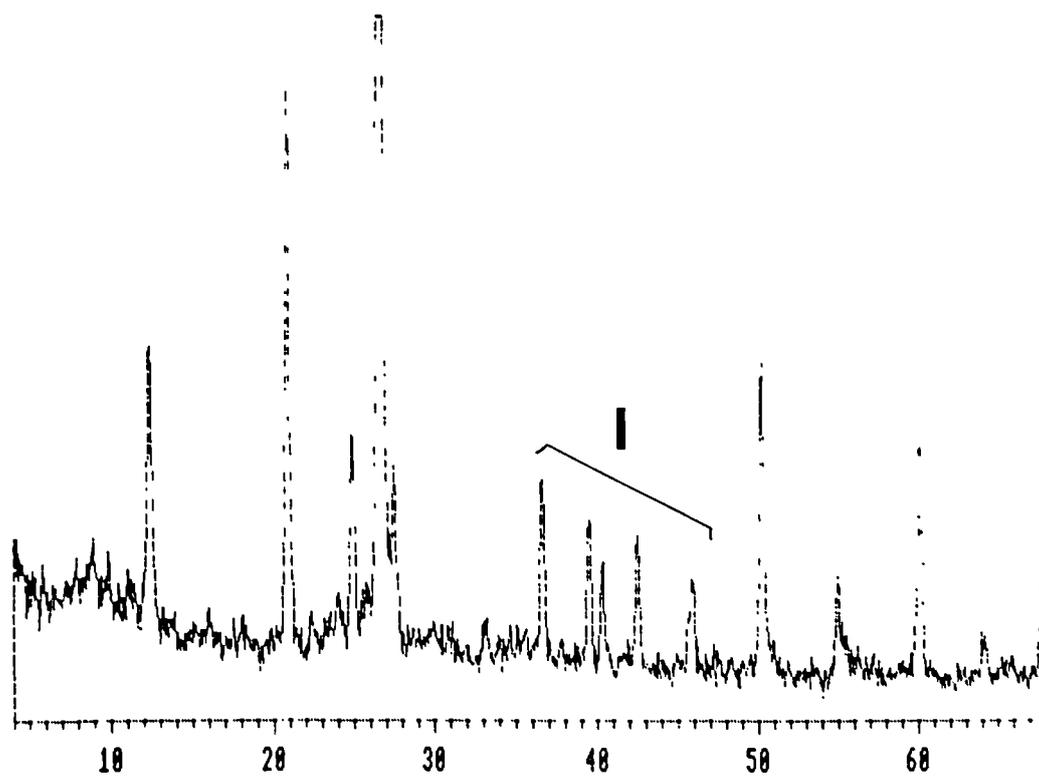
E

This section first describes the original undeformed microstructure of the North Scapa Sandstone, and then outlines the deformation microstructures in each domain of the fault zone. An interpretation of the deformation mechanisms and diagenetic processes which contributed to the final microstructure in each domain will be discussed in section 5.4.5.

5.4.3.4a. Domains 1 and 2

Fig. 5.16a shows the undeformed North Scapa Sandstone just outside the fault zone in Orphir Bay. Point counting reveals an average of 73% quartz, 8% polycrystalline quartz, less than 7% feldspar, 10% kaolinite, and 2% illite. Detrital mica is also present but is rare. The typical morphology of the pore-filling kaolinite in the undeformed sandstone is shown in the TEM montage in fig. 5.17, and reveals that the kaolinite grain size ranges from 2-6 μm. In domain 1 (15 metres from the fault), the parent rock has a mean apparent quartz grain diameter ranging from 189.9 +51.0/-44.9 μm to 194.6 +57.9/-50.6 μm (fig. 5.18a and b). The grains appear to be fairly well-rounded, although this is often difficult to assess, as physical and chemical compaction has resulted in sutured contacts, obliterating many of the original grain boundaries. Quartz overgrowth rims are common. Present day porosity in the undeformed sandstone ranges from 5-10% (Ridgeway, 1974). The Scapa Sandstone from domain 2 (10 metres from the fault) is very similar to that described in domain 1 above. The mean apparent grain diameter in domain 2 ranges from 164.8 +43.4/-38.2 μm. to 209.4 +49.0/-43.1 μm, relatively unchanged from that of domain 1 (fig. 5.18c and d).

5.4.3.4b. Domain 3

The mean grain size of the sandstone in domain 3 (2 metres from the fault) ranges from 158.7 +46.6/-40.6 μm to 171.6 +52.2/-45.3 μm (fig. 5.18e and f), only slightly reduced. However, there are zones of finer grain size. Fig. 5.16b shows an optical micrograph of a fault-parallel grain size reduction zone, observed in the field as the fault-parallel darkened zones which contain bitumen, as described in section 5.4.3.2. These zones are sub-parallel to one of the fracture sets described in section 5.4.3.1a. The zones have a mean grain size of 50.6 +23.4/-19.1 μm to 76.8 +42.3/-32.6 μm (fig. 5.18g and h). Note, however, that the grain size data is no longer normally distributed. The limit of resolution for the optical measurement of the grain size within the cataclastic zones is apparent by the absence of measurements less than 25 μm, and is marked by a dashed line on the graph.

Figure 5.16. Optical micrographs of North Scapa Sandstone adjacent to the North Scapa Fault, Orphir Bay, Mainland, Orkney. a) Sample from outside of fault zone in domain 1 (sample 49517A). Note 150-200 μm diameter quartz grains with quartz overgrowths (O), and 'pore space (blue) most probably preserved from secondary porosity. Also note organic matter in pore space at top left. PPL. Scale bar 0.25 mm. b) Sample from domain 3 showing fault-parallel cataclastic zone (sample 49520A). Note the grain size reduction zone contains clays (brown) and very small 'specks' of black organic matter. PPL. Scale bar 0.5 mm. c) Sample from fault-parallel breccia zone separating domains 3 and 4 (sample 49524A). Note cemented clasts of sandstone in organic-rich matrix (darkened zones). PPL. Scale bar 0.5 mm. d) Sample from domain 4 directly adjacent fault (sample 49519A). Note wide range of grain sizes, with large 150-200 μm. grains completely surrounded by fine-grained quartz/clay matrix. Also note irregular, corrosive boundaries on quartz grains. XP. Scale bar 0.25 mm.
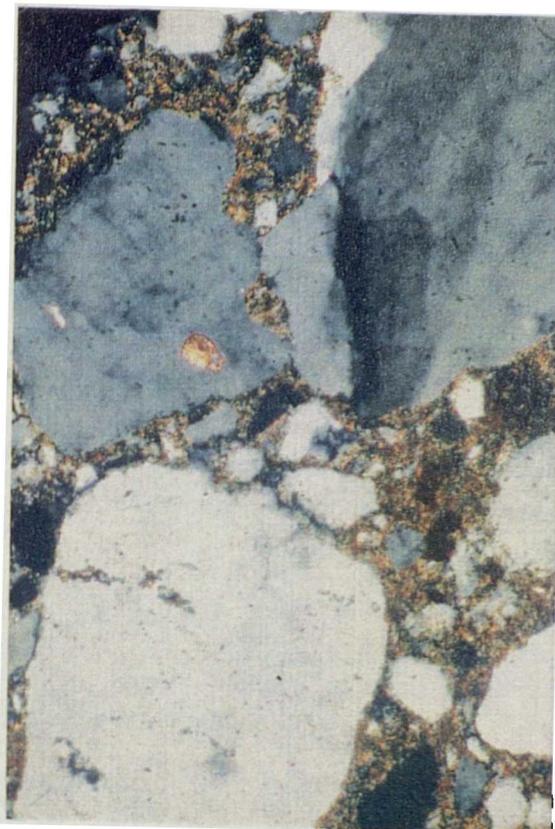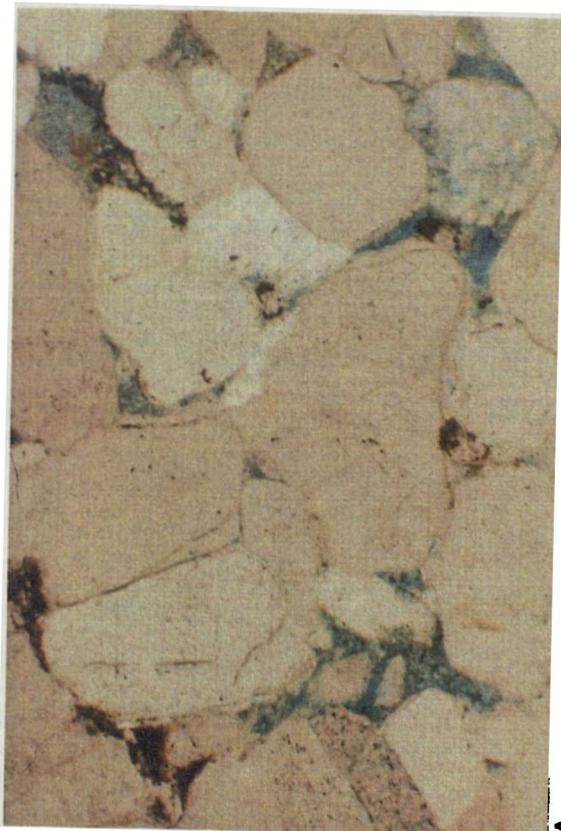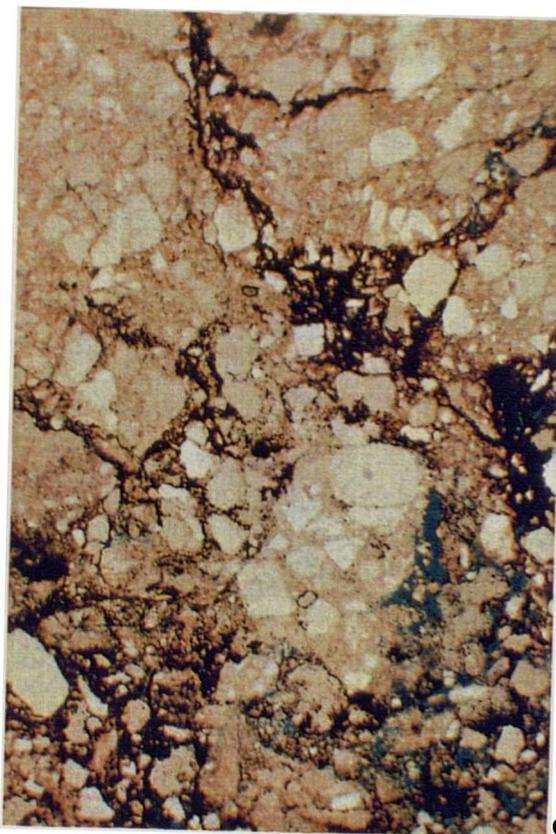
Figure 5.17. TEM montage showing cross-sectional morphology and size of typical kaolinite grains observed in pore space in samples outside of domain 4 (sample 49517A). Identifed by qualitative microanalyses. Scale bar 2 μm.

Figure 5.18.   Grain size data for the North Scapa Sandstone in the hangingwall of the North Scapa Fault.   a.   Fault-parallel section from domain 1 (sample 49517A).   b.   Fault-perpendicular section from domain 1 (sample 49517B).   c.   Fault-parallel section from domain 2 (sample 49526A). d.Fault-perpendicular section from domain 2 (sample 49526B). e.Fault-parallel section from domain 3 (sample 49521A). f.Fault-perpendicular section from domain 3 (sample 49521B). g.Fault-parallel section from narrow cataclastic zone in domain 3 (sample 49520A).   h.   Fault-perpendicular section from narrow cataclastic zone in domain 3 (sample 49520B).   i.   Fault-parallel section from domain 4 (sample 49519A).   j.   Fault-perpendicular section from domain 4 (sample 49519B).   k. Fault-parallel section from fine-grained matrix in domain 4 (sample 49519A).   l.   Fault-perpendicular section from fine-grained matrix in domain 4 (sample 49519B).   Dashed line at 20-25 μm. on graphs g, h, k. and l indicates limit of resolution for the optical microscope of grain size measurements in the matrix zones of the cataclasites.

A grain size, d (μm)

189.9
+51.0
-44.9

B grain size, d (μm)

194.6
+57.9
-50.6

C grain size, d (μm)

164.8
+43.4
-38.2

D grain size, d (μm)

209.4
+49.0
-43.1

I

grain size, d (μm)

0 25 100 225 400 625

20

161.8
+51.6
−44.9

frequency

10

0

0 5 10 15 20 25

√d

J

grain size, d (μm)

0 25 100 225 400 625

20

180.2
+53.6
−46.8

frequency

10

0

0 5 10 15 20 25

√d

K

grain size, d (μm)

0 25 100 225 400 625

30

72.3
+26.3
−22.2

frequency

20

10

0

0 5 10 15 20 25

√d

L

grain size, d (μm)

0 25 100 225 400 625

20

87.9
+41.4
−33.4

frequency

10

0

0 5 10 15 20 25

√d

TEM of the fine-grained matrix in the cataclastic zones reveals that extensive grain size reduction has occurred within these narrow zones, as quartz grains 3-5 μm in diameter are observed (fig. 5.19a). Therefore, the mean grain sizes quoted for the cataclastic zones are biased by the resolution problem for grains <25 μm in size, of which account for approximately 50% of the cataclastic zones (fig. 5.16b). From these observations, the amount of grain size reduction within the cataclastic zones ranges from 1 to 2 orders of magnitude.

The growth of new clays within the cataclastic zones is seen on the TEM (fig. 5.19a), in this case, kaolinite has precipitated in the newly-developed pore space (the clay was identified by qualitative microanalysis on the TEM). New quartz cements are observed on the TEM within the cataclastic zones, shown by growth dislocations trending perpendicular to the fracture walls (fig. 5.19b). Fig. 5.16c is an optical micrograph of the pervasive breccia zone from the boundary between domains 3 and 4: clasts of cemented sandstone, 0.5-2 mm. in diameter, are contained in a matrix of organic-rich material. The fragments of sandstone within the clasts are angular and variable in size, suggesting that they represent a cemented cataclasite which has been 're-worked' into the breccia zone.

5.4.3.4c. Domain 4

In contrast to the other domains, fig. 5.16d shows the wide range of grain sizes characteristic of the sandstone in domain 4. Large, <200 μm-diameter quartz grains are typically surrounded by an extremely fine-grained matrix. The mean grain size of the large quartz framework grains in domain 4 (1.0 metre from the fault) remains relatively unchanged from that of the other domains, ranging from 161.8 +51.6/-44.9 μm to 180.2 +53.6/-46.8 μm (fig. 5.18i and j). However, the matrix, which under the optical microscope appears to consist of fine-grained quartz and clay, has a mean grain size of 72.3 +26.3/-22.2 μm to 87.9 +41.4/-33.4 μm (fig. 5.18k and l). As with domain 3, the grain size data is no longer normally distributed. The limit of resolution for the optical measurement of the grain size within the fine-grained matrix is apparent by the absence of measurements less than 25 μm, and is marked by the dashed line on the graph. TEM reveals that the matrix consists of quartz grains 2-4 μm in diameter, surrounded by a pore-bridging illite (fig. 5.20a). Thus, up to 2 orders of magnitude reduction in grain size has occurred. Pore space is non-existent in this domain, as TEM observations detect pervasive microfibrous illite cement filling even the smallest pores (fig. 5.20b).

Figure 5.19. TEM micrographs of cataclastic seams and fractures from domain 3 (sample 49521A). a) 3-5 μm. quartz grains with straight, boundaries and occasionally 120° junctions, within matrix containing kaolinite grains (arrowed) freely growing in pore space; note undeformed nature of kaolinite. Phases indentified with qualitative microanalyses. Scale bar 1 μm. b) Iron-rich quartz fracture fill containing growth dislocations oriented perpendicular to fracture boundary. Scale bar 1 μm.

A

B

Figure 5.20. TEM micrographs of fine-grained matrix zone from domain 4 (sample 49519B). a). 2-3 µm. rounded quartz grains adjacent to larger grains, each completely surrounded by pore-bridging illite (arrowed). Identified by qualitative microanalyses. Scale bar 2 µm. b) Morphology of pervasive hairy illite cement. Note deformed nature of grains. Identified by qualitative microanalyses. Scale bar 0.5 µm.
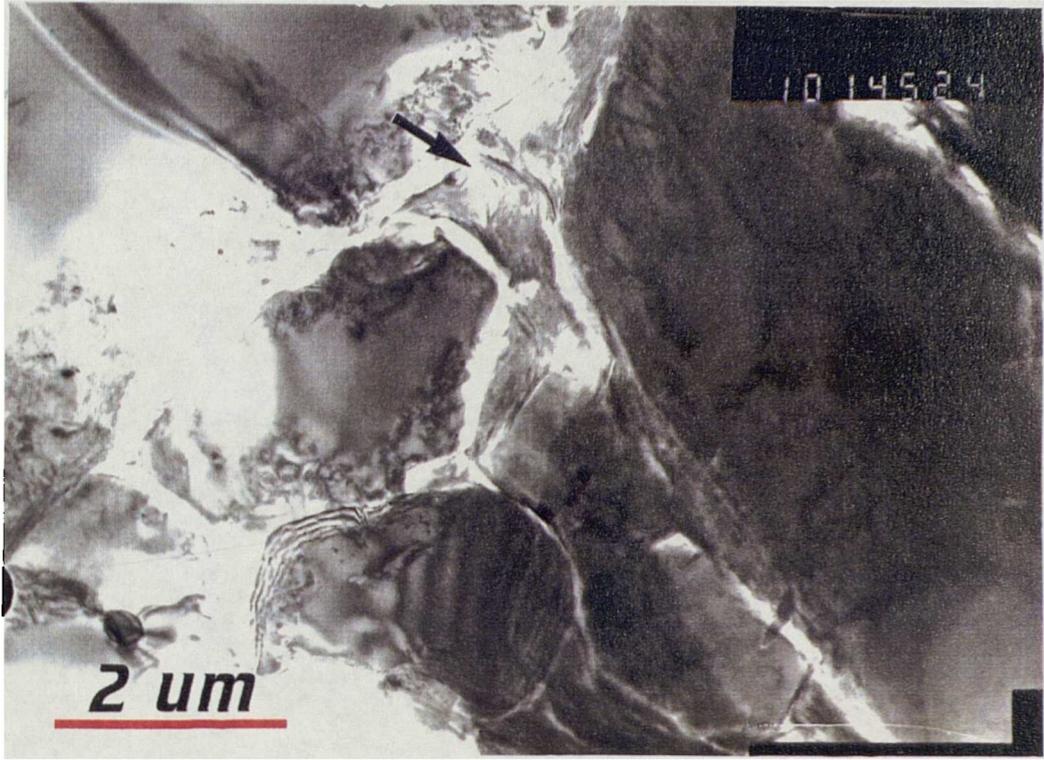
A
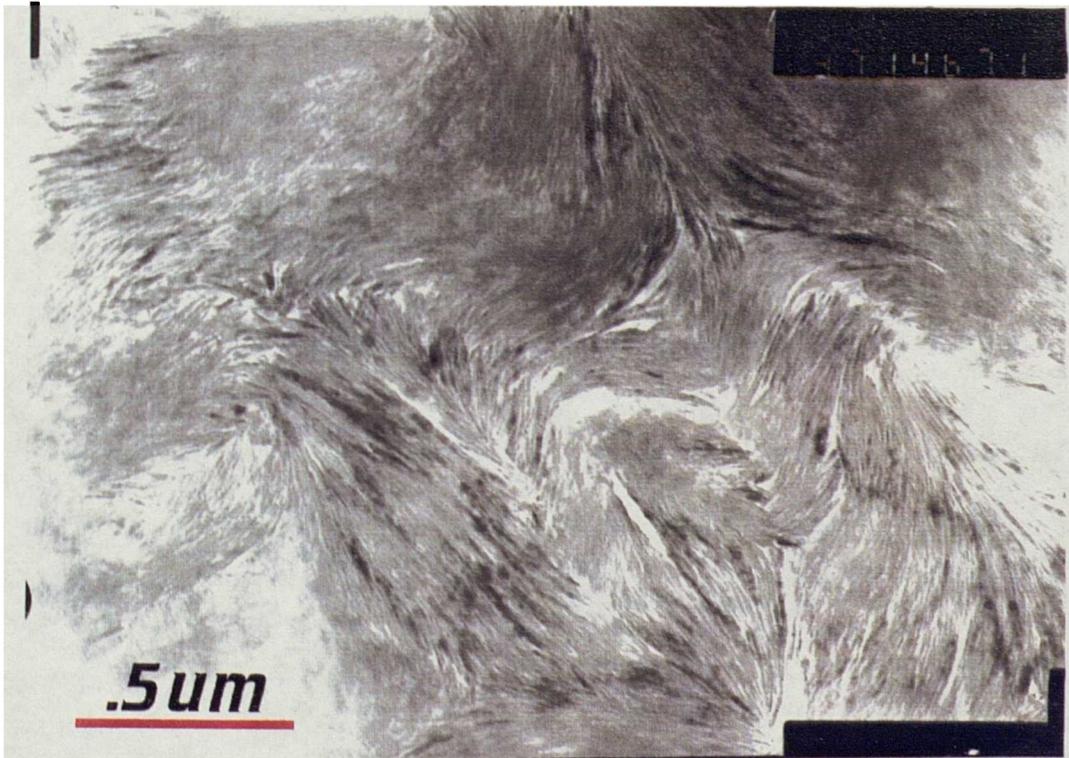
B

5.4.4 Fracture mechanisms involved in the grain size reduction

The previous section described the microstructures in the cataclastic zones adjacent to the NSF. This section discusses the possible fracture mechanisms which operated during the grain size reduction observed in domains 3 and 4.

Detailed investigation of the narrow cataclastic zones in domain 3 shows both isolated grains and angular fragments floating in bitumen (fig. 5.21a). Individual grains appear to have been incorporated into this 'matrix' by grain boundary fracture (fig. 5.21a and b). Once the clasts have been incorporated, there is evidence that transgranular fracturing has operated to produce the smaller, angular fragments again floating in the bitumen matrix (fig. 5.21a). Evidence for both grain boundary and transgranular fracture processes operating during faulting and coincident with hydrocarbon migration can be seen clearly in fig. 5.21b. Note, however, that many of the grains and fractures have boundaries which are irregular and/or dentate (fig. 5.21a and b). In addition, the walls of the transgranular fractures cannot be 'fitted back together' in a simple manner. Material therefore appears to have been removed (fig. 5.21b). These observations suggest that a fluid was present at the time of faulting which corroded material from along the grain and fracture boundaries. As the cataclastic zones are coincident with one of the dominant fracture sets in the fault zone, it is also probable that the corrosive fluid was channelled along the macroscopic fracture path. Thus, fractures on all scales acted as pathways for fluids, aiding the corrosion of rock fragments.

Due to the pervasive post-faulting cementation in domain 4, direct evidence for specific fracture mechanisms which might have operated has not been preserved. However, the large framework quartz grains floating in the matrix in fig. 5.16d have sub-rounded grain boundaries which appear to represent original grain boundaries (e.g. see fig. 5.16a). The absence of planar boundaries along the larger clasts in the cataclasite may indicate that the grains were easily disaggregated by fracture along their boundaries, such that disaggregation took place in a weakly lithified sediment. Transgranular fractures are occasionally observed in domain 4 (fig. 5.21c). TEM observations reveal extremely fine (2-4 μm) quartz grains in the cataclasite matrix, which suggests that transgranular fracture contributed to further grain size reduction in domain 4.

Figure 5.21. Optical micrographs of fractures in North Scapa Sandstone in the hangingwall of the North Scapa Fault. a.) Sample 49520A from domain 3. Fractures along grain boundaries (arrowed) adjacent to bitumen-filled matrix zone. Note irregular and dentate grain and fracture boundaries. XP, ST. Scale bar 0.5 mm. b.) Sample 49520A from domain 3. Transgranular fractures in quartz grains floating in bitumen. Note irregular fracture boundaries. XP, ST. Scale bar 0.25 mm. c.) Sample 49519A from domain 4. Transgranular fracture in quartz grain. XP, ST. Scale bar 0.25 mm.
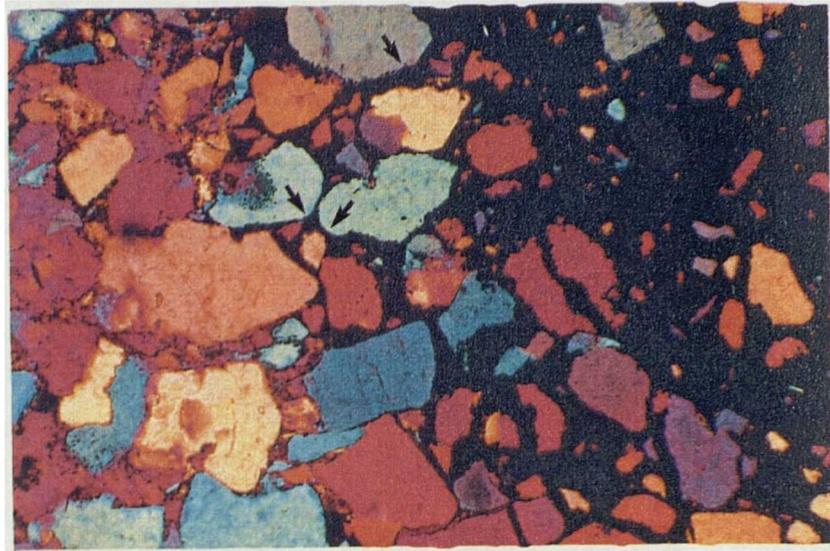
A
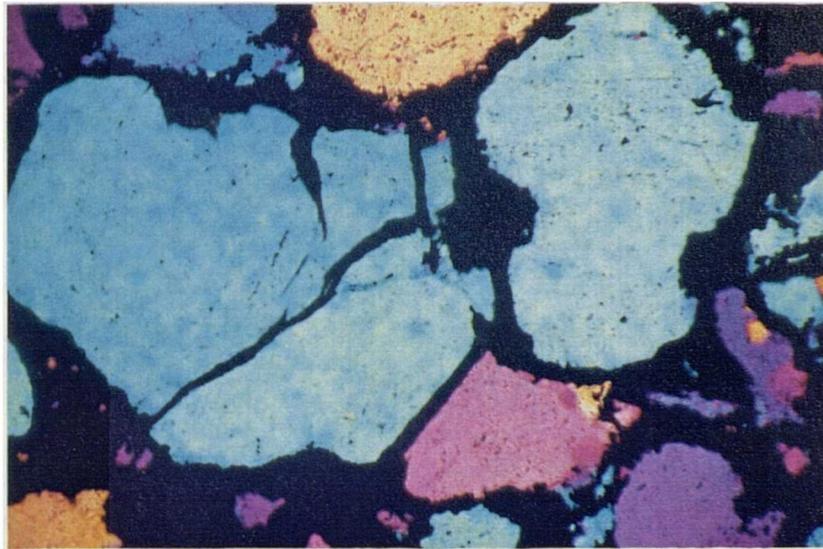
B
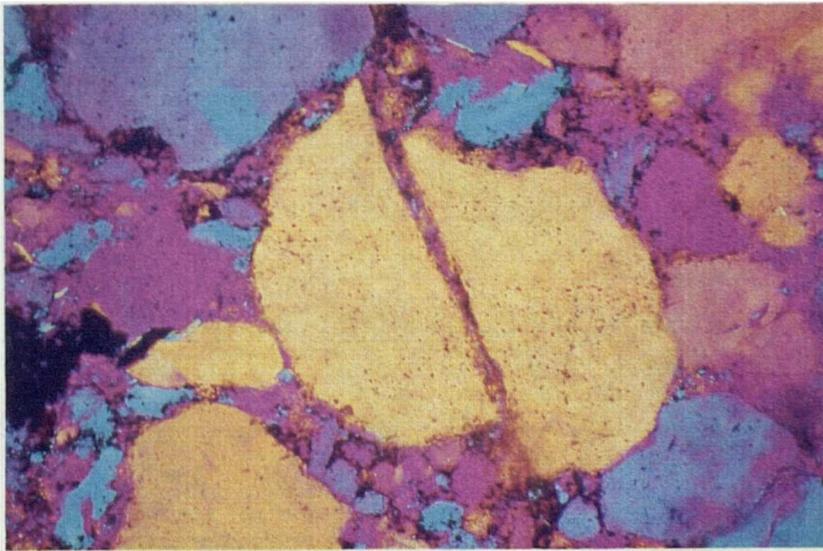
C

5.4.5 Discussion

5.4.5.1 Fault history and fluid flow events

This section discusses the deformation mechanisms which operated during evolution of the North Scapa Fault Zone by reviewing the important microstructural observations, together with the XRD, gas chromatography and grain size data presented. A fault history is presented for the fault, which integrates evidence for specific fluid flow and diagenetic events adjacent to the fault. The fault history is then compared and placed into context of a burial history for the sediments, recently presented by Astin (in press) (section 5.4.5.2). Evidence for the earliest movements along the North Scapa Fault are discussed first.

It was suggested in section 5.4.4 that during initial faulting, grain boundary fracture operated in domain 4 to initially disaggregate grains in a weakly lithified sediment, and that further grain size reduction was accomplished by transgranular fracture. This has resulted in a cataclasite with extremely variable fragment sizes. Quartz fragments exist within the matrix in domain 4 which are an order of magnitude or more smaller than the larger framework quartz grains (fig. 5.20a). The porosity and permeability in a cataclasite with a highly variable fragment size can be compared to that of a poorly-sorted sandstone. A decrease in sorting has long been known to decrease both porosity and permeability in sandstones (Rogers and Head, 1961; Beard and Weyl, 1973).

The extreme grain size reduction was also accompanied by the preferential precipitation of fine-grained illite cement in domain 4. Intense localized growth of illite adjacent to a major fault has also been observed by Lee et al. (1989), as discussed in Chapter 4. Lee et al. (op. cit.) suggested that the illite growth was enhanced by the circulation of fluids adjacent to the fault due to fault activity. There can be little doubt that fluid flow adjacent to the North Scapa Fault also influenced the illite precipitation early in the burial history of the sediment. Pervasive illite grain coatings have also been shown to increase the amount of intergranular pressure solution and cementation occurring during diagenesis (Heald and Larese, 1974; Houseknecht, 1988). It is probable that in domain 4, compaction subsequent to faulting played an important role in the preferential cementation of the cataclasite by quartz directly adjacent to the fault.

The occurrence of illite is also known to significantly reduce permeability in reservoir rocks (Sommer, 1978; Rossel, 1982). Therefore, the variable fragment size within the cataclasite, together with the precipitation of the microfibrous illite surrounding even the finest grains, significantly reduced the porosity and permeability in the North Scapa Sandstones adjacent to the North Scapa Fault early in the diagenetic history of these sediments.

This initial faulting event correlates with Astin's (pers. comm., 1989) recent confirmation of initial extension along the fault during deposition of North Scapa Sandstone. The absence of pore-filling kaolinite in domain 4 suggests that the deformation and cementation in domain 4 took place before the diagenetic event responsible for the kaolinite precipitation occurred.

Domain 3 is dominated by the presence of fault-parallel migration pathways through which hydrocarbons have been channelled. The migration pathways are coincident with narrow, intense zones of cataclasis in which the grain size has been reduced by 1 to 2 orders of magnitude. These zones of cataclasis are also coincident with one of the fracture sets measured in the line-traverse and discussed in section 5.4.3.1a. Grain boundary fracture and transgranular fracture operated within the cataclastic zones in domain 3 in the presence of a corrosive fluid. Bitumens are also present in the pore space surrounding cemented clasts of sandstone in a fault-parallel breccia zone separating domains 3 and 4. This suggests that the dilatancy associated with the cataclasis directly influenced the fluid pathways.

It is inferred that the faulting event which influenced the hydrocarbon pathways proceeded the faulting which resulted in the precipitation of the illite and quartz cement in domain 4. This is evidenced in the fact that the hydrocarbons are not observed within the 1-meter wide, high-strain zone in domain 4, which acted as a seal to the hydrocarbons. In addition, clasts of the cataclastic cemented sandstone from domain 4 are contained in the fault-parallel breccia zone bounding domain 3. Pore-filling kaolinite occurs in domain 3, despite the presence of hydrocarbon in many of the pore spaces. This suggests that the diagenetic event responsible for the precipitation of the kaolinite must have occurred prior to the hydrocarbon migration, and thus the later faulting event.

The fault reactivation, which acted to channel the hydrocarbons through dilatant zones associated with cataclasis, did not damage the existing seal in domain 4. This is not suprising, as under all environmental conditions, clay-bearing gouges exhibit strain hardening (Rutter et al., 1986; see also Summers and Byerlee, 1977; Logan et al., 1981; Morrow et al., 1982). The faulting which proceeded the development of the seal was therefore accommodated by strain distributed in other domains, namely cataclasis and brecciation, as shown by the fault-parallel breccia zones and high fracture densities outside of domain 4.

These observations are similar to those of Aydin (1978) and Aydin and Johnson (1978, 1983), who found that continued strain in porous sandstone resulted in the formation of new deformation bands instead of the localisation of displacement into one band, which they interpreted as strain hardening. Jamison and Stearns (1982) also found that a decrease in porosity and permeability in microfaults resulted in strain hardening in the Wingate sandstone.

The different fracture arrays developed in domains 2 and 3, from that of domain 4, might be explained by the presence of the strain-hardened domain 4, and the models discussed above for their development. In the shear lens model, certain shear planes can become inactive during displacement as others develop. This is likely to occur in a previously strain hardened zone where displacement is not able to localize. In the development of the three penecontemporaneous fracture sets, all of the fractures contributed to accommodate displacement simultaneously. Thus, strain might have been more efficiently accommodated during the development of the three fracture sets, rather than by the anastomosing fracture array in domain 4.

5.4.5.2 The fault history in context of the burial history

The fault movements outlined above indicate a history of initial extension along the North Scapa Fault, early in the burial history of the North Scapa Sandstone, followed by later reactivation of the fault during which hydrocarbons were mobile. The probable age of the reactivation event can be better constrained if the burial history presented by Astin (in press) is considered. The relative sequence of fault movements and diagenetic events which occurred in the North Scapa Sandstone adjacent to the North Scapa Fault have been plotted on a modified version of Astin's burial history curve (fig. 5.22).
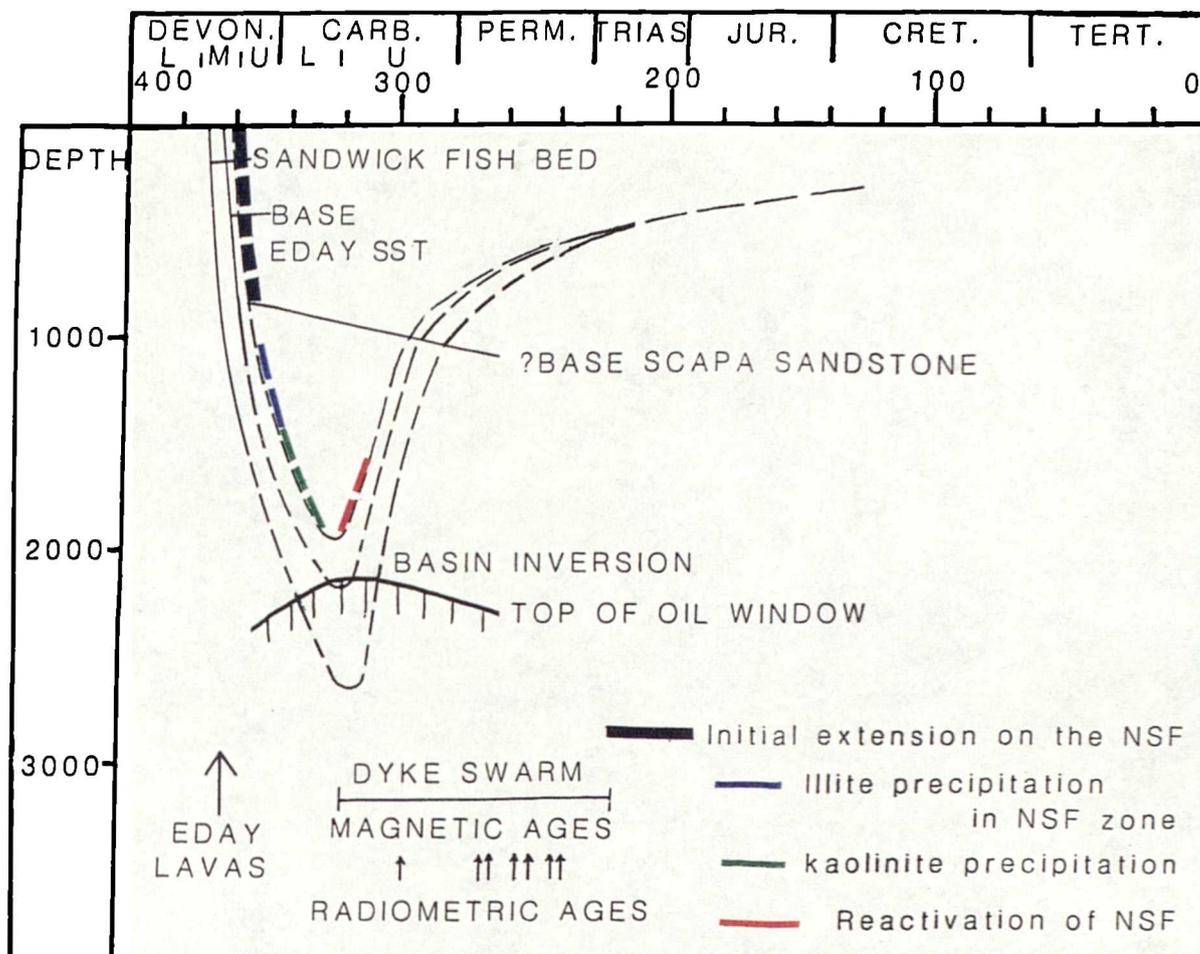
Figure 5.22. Burial history diagram from Astin (in press) for the upper MORS to UORS, using revised thicknesses for the Stromness and Rousay flagstones between the Sandwick Fish Bed and the base of the Eday Sandstone, and allowing for the presently compacted state of the sediments. New data from Astin (pers. comm., 1989) suggests that the base of the Scapa Sandstone is probably slightly younger than the base of the Eday Sandstone as indicated on the diagram, but deposition of the sediments is probably diachronous. Dashed lines assume 1000m. of Carboniferous sediments in the region. Ages of dykes from Brown (1975), Halliday et al. (1977), Mykura (1976), and Baxter & Mitchell (1984). The dyke magnetic ages preserved in the Eday group come from Robinson (1985, 1986). Probable time span over which the illite and kaolinite precipitation took place in the North Scapa Sandstone in the hangingwall of the North Scapa Fault, and the reactivation of the North Scapa Fault indicated on the burial history for the Scapa Sandstone.

The age of the initial extension on the NSF is still under question, but occurred at some time during the upper MORS to UORS (fig. 5.22). Illite precipitation in the fault zone occurred subsequent to the initial faulting, at some time prior to hydrocarbon migration. Diagenetic kaolinite is present in all domains except domain 4. It is suggested that the precipitation of kaolinite occurred subsequent to the illite precipitation, but prior to hydrocarbon migration (fig. 5.22).

Astin (in press) has suggested that the source rocks (lacustrine facies Stromness and Rousay Flagstones) in the Orcadian Basin reached maturity at the top of the oil window during the Carboniferous, just prior to basin inversion (fig. 5.22). This corresponds to a depth of 2-3 km. The presence of hydrocarbons in the breccias and cataclastic zones suggests that the latter faulting event took place at some time during, or just after, oil generation, at less than 2.5 km. depth. Permo-Carboniferous dykes (Brown, 1975; Rock, 1983; Baxter and Mitchell, 1984) adjacent to the fault are undeformed during the latter faulting event. Thus, reactivation of the fault most probably correlates with inversion of the basin, at some time during the Carboniferous. Reactivation of other faults in the basin at this time will be considered further in sections 5.5 and 5.6.

5.4.5.3 Fracture permeability and fault seal mechanisms

The fracture array and microstructural data presented above provides insight to the relative amount of fracture permeability in each domain adjacent to the fault, and to the mechanisms responsible for creating, and preserving, the fault seal in domain 4.

It is important to point out that while the three fracture sets in domains 2 and 3, and the anastomosing array in domain 4 formed during the same faulting event, the microstructural data indicates that while the former sets provided pathways for fluids, the latter array did not, as the fault seal which existed in domain 4 was not damaged. It is apparent that the existence of a strain hardened zone (due to the earlier deformation) acted to preserve the low permeability domain adjacent to the fault. The highest fracture densities, found in domain 3, are directly coincident with the hydrocarbon pathways, and zones of microporosity in which new clay phases (kaolinite) precipitated. Thus, the highest fracture permeabilities must have existed in the zones of highest fracture density and breccia development in domain 3.

The detailed TEM data has revealed the mechanisms and processes of fault seal in this example. Fracture and cataclasis in the sandstone has resulted in a cataclastic rock of extremely variable fragment size, in which fine-grained (<25 μm) matrix zones account for approximately 50% of the cataclasite. This, together with the preferential precipitation of the quartz and illite cement in the cataclasite, has acted to seal the fault. There is no evidence on the outcrop scale for mixing of the footwall sediments with the hangingwall sediments, i.e., clasts of the fine-grained lacustrine facies rock are not observed in the hangingwall.

In addition, there is no evidence microstructurally for mixing of the sediments on the grain or fine aggregate scale. Thus, the 'mixing' model for fault sealing, as discussed in Chapter 4, does not appear to be responsible for creating the fault seal in this example. This has important implications for fault seal models which suggest that the presence of an impermeable cap rock directly adjacent to the fault is necessary in many cases to act as the fault seal, either to provide a 'shaly' barrier which is 'smeared' into the fault zone, or simply to act as a cap rock seal which has been juxtaposed against the reservoir rock (e.g., Smith, 1980; Harding and Tuminas, 1988). In this case, cataclasis of the hangingwall sandstone, together with the precipitation of the quartz and illite cement, has provided the low permeability barrier needed to seal the fault.

5.4.6 Conclusions

In summary, the NSF fault is characterised by fault-parallel domains which differ in terms of the distribution of cataclasis (including fracture orientation and spacing), organic carbon content, dominance and distribution of clay phases, and microstructure. The distribution of the cataclastic deformation appears to have controlled fluid pathways which contributed to the diagenetic events and governed hydrocarbon pathways adjacent to the fault during the basin history.

Evidence for the first fluid flow/faulting event is seen in domain 4 (directly adjacent to the fault), where significant grain size reduction, and the preferential precipitation of a fine-grained illite cement occurred. The precipitation of the cement, coupled with the grain size reduction, resulted in sealing of the fault. This event most probably correlates with the early extensional event confirmed by the sedimentological data of Astin (pers. comm., 1989).

Further movement on the fault, most probably during the Carboniferous, controlled hydrocarbon migration pathways. However, the fault seal represented by domain 4 was not damaged during the later cataclastic faulting. This is explained by the strain hardening of domain 4 resulting from the earlier faulting.

The last movement was sinistral and oblique-slip in sense. Breccia zones developed outside of domain 4 as a result of this last fault movement, and contain clasts of both the white, cemented sandstone from domain 4, and the darkened, bitumen-filled sandstone from domain 3. This is further evidence that the earliest fluid flow event creating the seal preceeded the later cataclastic faulting event. Fracture densities are 70 m^{-1} within breccia zones, and decrease rapidly 10-15 meters from the fault plane to less than 20 m^{-1}. Calculated fracture spacing from the line traverse correlate with the calculations of fracture density from the two-dimensional fracture tracings.

5.5   East Scapa Fault Section

5.5.1   Introduction

The total extent of the N-S trending East Scapa Fault in the Orkney Island area is 23 km., from the northern island of Eday, across the eastern Mainland, to the southern islands of Glims, Burray and South Ronaldsay. This section describes a traverse parallel to the strike of the fault, adjacent to the east coast of Scapa Flow, from St. Mary's [HY 475015] to Upper Scapa Bay [HY 435090] (fig. 5.23). The fault trace is not linear, and changes in fault strike correspond with changes in fault zone structure and fault rock development (figs. 5.23). The traverse allows detailed mapping and microstructural analysis of the fault rocks, in order to provide additional data regarding the deformation history and fluid flow events in the Orkney area, in which the data obtained from the North Scapa Fault zone can be integrated. In addition, the development of fault rocks along a fault with differing geometry and deformation history from that of other faults within the basin (i.e., the North Scapa Fault) can be investigated and compared.

Present-day fault geometry indicates a net reverse stratigraphic displacement along the length of the East Scapa Fault, with the older Rousay Flagstones juxtaposed in the hangingwall against the younger Eday Group sediments in the footwall. The age of the Eday Group sediments in the footwall of the East Scapa Fault, like those in the hangingwall of the North Scapa Fault, is under question (Astin, 1985; Rogers, 1987). Astin (pers. comm., 1989) has recently confirmed that the Eday Sandstones in the hangingwall of both faults can be correlated with the facies of the UORS sandstones seen on Hoy. However, the upper MORS-UORS sedimentation is strongly diachronous, and thus, the exact age of the Scapa sediments is uncertain. This thesis will use the term East Scapa Sandstone for the Eday Sandstones in the hangingwall of the East Scapa Fault.

Despite its present-day reverse geometry, the large-scale and small-scale structures associated with the East Scapa Fault indicate a long and complex displacement history for the fault (Enfield, 1988). Astin (pers. comm., 1989) has confirmed that the East Scapa Fault was part of a fault system in the basin which controlled the deposition of the 'Eday Group' sediments, and inferred that the fault was an active normal fault during this time.

Enfield (1988) has used regional structures (large folds) as kinematic indicators to assess the displacement sense on the East Scapa Fault (see figs. 1.1 and 5.1). Large folds, with wavelengths of 5 km., developed on the islands to the north of the Mainland, such as the Eday syncline, are oriented sub-parallel to the fault trend. Folds with similar wavelengths on Westray and the east Mainland dominantly trend SW or SSW obliquely to the fault. The West Mainland anticline, an open fold with 5-10 km. wavelength, and smaller wavelength (1-3 km.) folds such as the Deerness Syncline on the east Mainland, have an opposite sense of obliquity to the fault, trending N-S to NW-SE. In using these folds as indicators of displacement sense on the East Scapa Fault, Enfield (op.cit.) concludes that they suggest contradictory movement senses, both sinistral and dextral displacements.

Enfield also suggests that small shear bands and folds which show sinistral movement senses are preserved near St. Mary's, and are cross-cut by later faults. The locality which contains these small sinistral movements inicators is not identified in Enfield's thesis, and were not observed in this study. As mentioned in section 5.3.4, the age relationship of the folds developed on Orkney and the age of the faulting is not well-constrained. Definitive evidence which relates the regional-scale folds (with amplitudes of up to 10 km.) to the faults is absent. This thesis will only use very localized fold development adjacent to the East Scapa Fault (folds developed up to 1 km. away from the fault) as possible evidence for movement directions along the fault. However, it is suggested that in this case, even this data should be used with great care, and the possible range of fold orientations developed during faulting events will be discussed below.

The East Scapa Fault is well-exposed at several localities which are described in the following sections. The smaller-scale kinematic indicators observed are presented, together with the detailed analysis of the fault rocks and the related microstructures. These enable an assessment of the displacement history of the fault, and provide insight into the deformation conditions and possible fluid flow events that occurred within the fault zone.

5.5.2 Field and microstructural observations,
The East Scapa Fault at Hemp Stack [HY 443060]

At Hemp Stack [HY 443060], the East Scapa Fault strikes nearly N-S and dips 78° east. Steeply-dipping (75-80° E) East Scapa Sandstone beds in the footwall are observed juxtaposed with relatively shallow-dipping (30-40° E) Rousay beds in the hangingwall (fig. 5.24a). The fault plane is a discrete, planar, surface cutting through the footwall sandstones. Striations (slickensides) are preserved on the fault plane, and are horizontal or gently plunging (up to 35°) to the south.

The fault zone contains discrete fault rock domains trending parallel to the fault plane, each characterised by different fault rock types (fig. 5.25). Deformation in the footwall is localised to the vicinity of the discrete fault plane, and fractures are only rarely observed in the sandstone. Hangingwall deformation is much more intense. At a distance of approximately 3 meters from the fault, the flagstones are brecciated, and a fine-grained fault gouge has developed between more coherent breccia blocks. The blocks of cemented breccia are seen preserved within the incohesive fault gouge, which has a pervasive fabric (fig. 5.24b). This fabric is discussed in the more detailed sections describing the fault rock character in each domain.

Domain A in the footwall is a cohesive, cataclastic sandstone, with a discrete surface of discontinuity with that of domain B. The left margin of domain A has a gradational contact with the parent rock in the footwall. Domain B in the 'footwall' is a 10-20 cm. wide zone containing fine-grained, incohesive, clay fault gouge. The gouge is very similar to the fault rock found in domain D, and is most likely derived from the flagstones in the hangingwall.

Domain C is a 5-15 cm. wide zone of well-cemented cataclastic sandstone, with the smooth fault plane defining its eastern margin. In thin-section, this domain is is observed to contain clasts of cemented sandstone floating in a dark, organic-rich matrix (figs 5.25a and b). The clasts contain angular quartz fragments ranging in size from <20 μm., to >200 μm., in a brown quartz/clay cement. The clast boundaries are either extremely planar (fig. 5.26a), or very irregular and dentate (fig. 5.26b).

Figure 5.24. Photographs of the East Scapa Fault zone at Hemp Stack [HY 443060]. a) View ·looking north showing deformation in Rousay Flagstones (MORS) in hangingwall and Middle Eday Sandstone (?UORS) in the footwall. Fault plane defined by planar, striated (slickensided) surface on cohesive (cemented) sandstone. Note foliated, incohesive gouge in hangingwall. Hammer 32 cm. long. b) Detail of foliated gouge in hangingwall containing cemented blocks of breccia; both showing kinematic indicators indicating extensional (down to the right) movement as labelled. Looking ENE. Compass 10 cm. long.
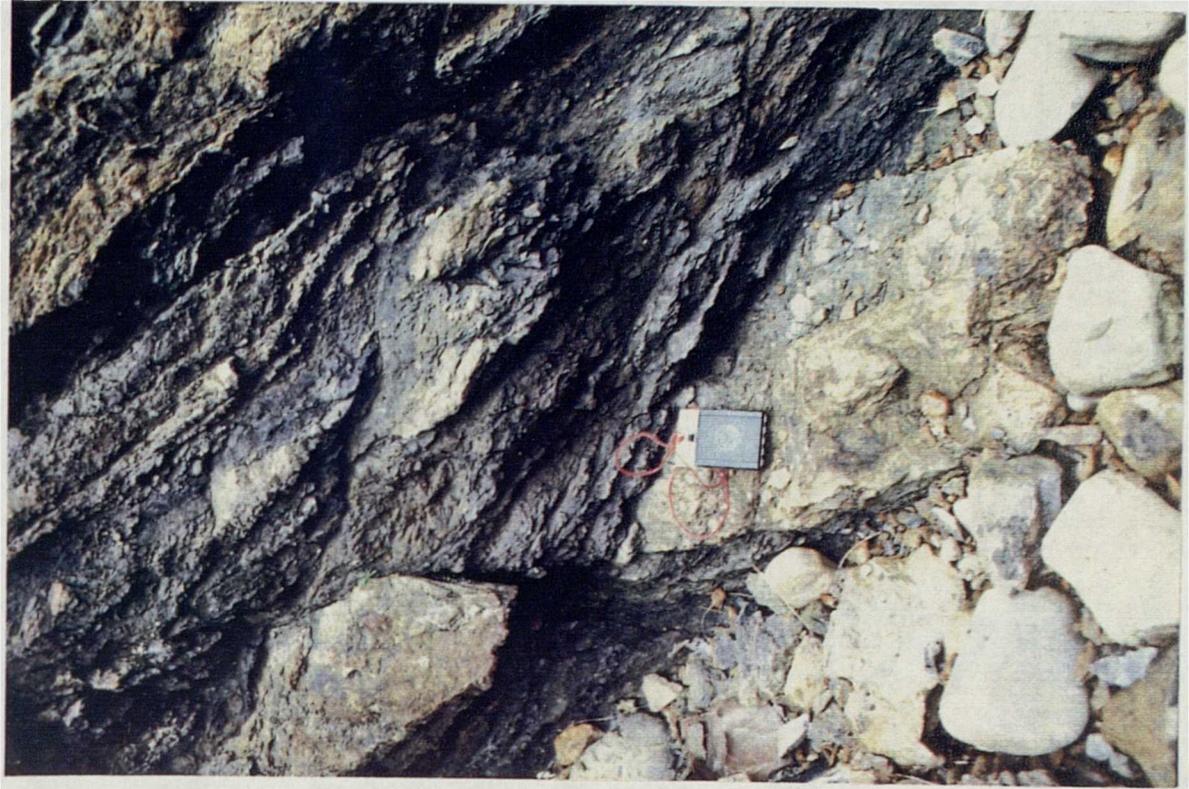
B

A

Figure 5.25.   Photograph and line drawing of fault rock in East Scapa Fault zone at Hemp Stack [HY 443060].   The fault zone is divided into fault-parallel domains A, B, C, and D by nature of the fault rock as labelled and described in the text.   Looking north as in fig. 5.24a.   Hammer 32 cm. long.
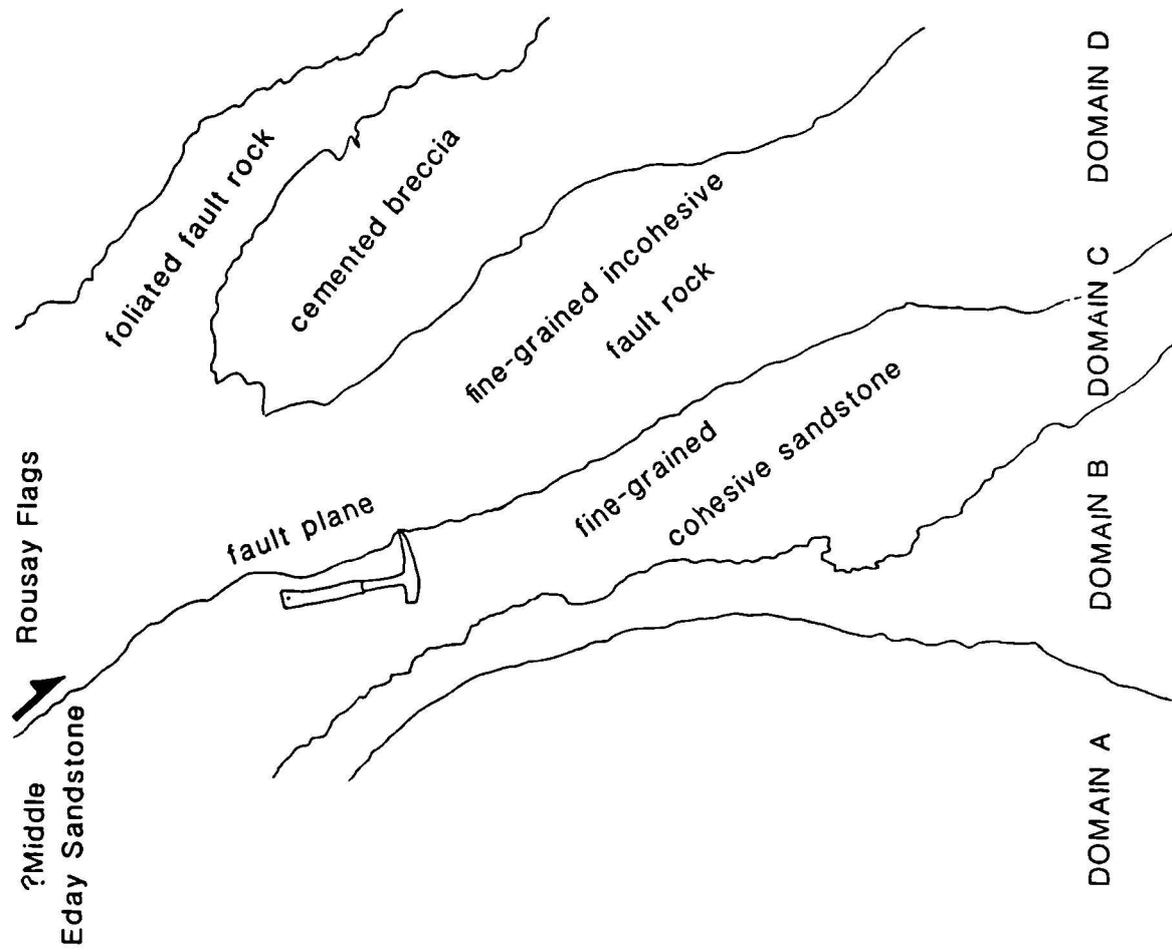
Figure 5.26. Optical micrographs of microstructures in fault rocks described from fault zone domains (fig. 5.25) at Hemp Stack [HY 443060]. a) Sample 50101. Cemented clasts of sandstone or individual grains floating in organic-rich matrix. Note planar boundaries along some clasts, together with irregular, dentate boundaries on others. From domain C (footwall) of fault zone. PPL. Scale bar 0.5 mm. b) Sample 50101. Detail of irregular, dentate boundaries on quartz grains floating in organic-rich matrix in cataclastic sandstone from domain C of fault zone. PPL. Scale bar 0.5 mm. c) Sample 50102. Foliated incohesive gouge from domain D in fault zone. Fault rock from this domain is dominantly derived from the fine-grained hangingwall rocks (Rousay Flagstones). Micrograph shows domains of fine-grained organic-rich zones and coarser-grained quartz-rich zones. PPL. Scale bar 1 mm. d) Sample 50099. Cemented breccia from domain D in fault zone. Clasts of fine-grained organic-rich flagstones floating in a quartz-rich matrix, with cross-cutting carbonate veins. XP, ST. Scale bar 1 mm.
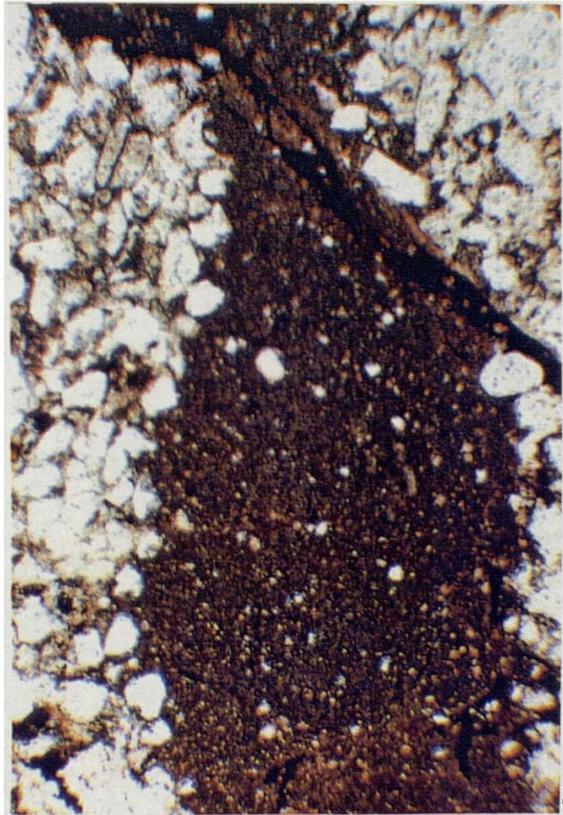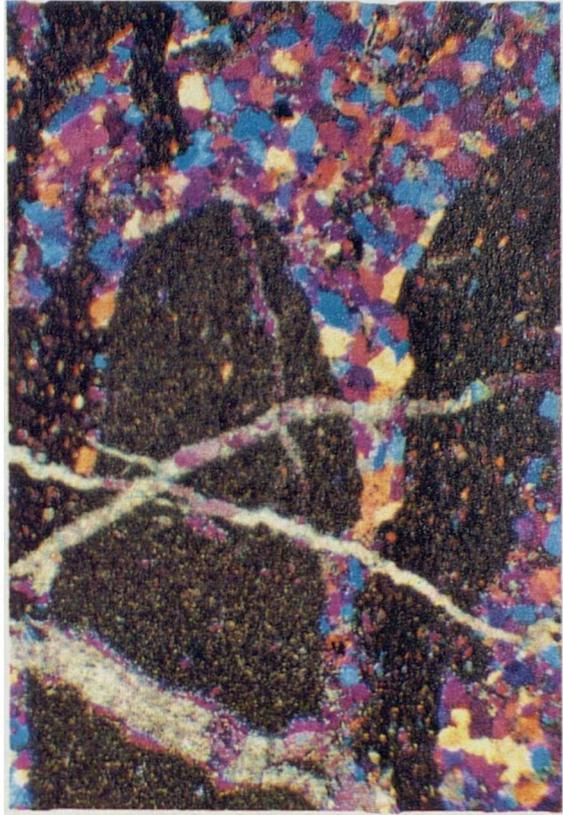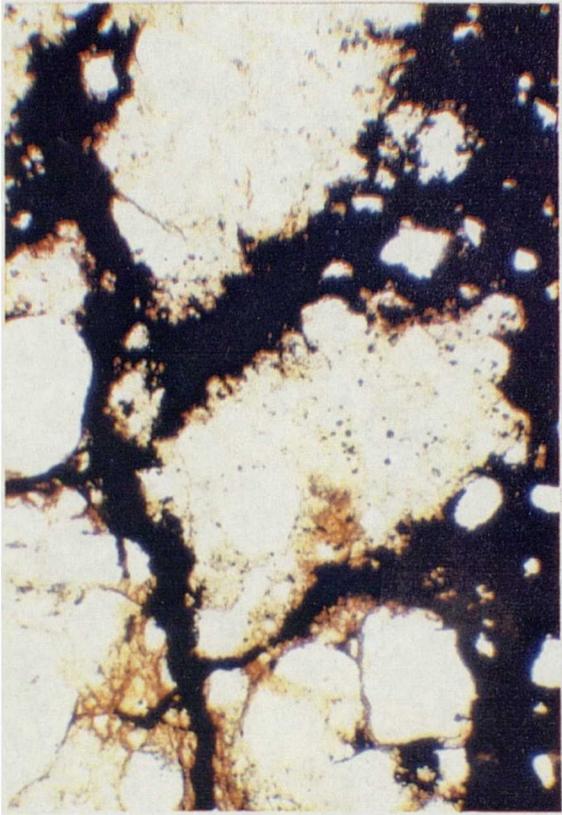
Domain D contains both cemented breccia and incohesive fault rock with a pervasive fabric. The fabric in the fine-grained fault rock is defined by a shallow-dipping foliation (353/59°), and a more steeply dipping set of shear bands which are oriented sub-parallel to the fault plane (001/76°). In thin section, the fine-grained fault rock contains quartz-rich zones rich in organic material, and extremely fine-grained zones dominated by clays (fig. 5.26c). The cemented breccias contain fine-grained clay-rich clasts interspersed in a quartz-rich matrix (fig. 5.26d). The clay-rich clasts are commonly elongate and folded, and the grains within the clasts do not show evidence for fracturing. Carbonate veins cross-cut the clasts within the quartz-rich domains.

5.5.3 Interpretation

Although the large-scale fault geometry at Hemp Stack shows an overall reverse geometry, kinematic indicators in the fault zone suggest that the last phase of movement was dextral and transtensional in nature. For example, in domain D, offsets of blocks of the breccia along the shear bands, and the asymmetry of the composite planar fabric indicate an extensional(down to the east) shear sense in the fault gouge (fig. 5.25b). The slickensides on the fault plane demonstrate a component of strike-slip movement. The magnitude of the reverse and transtensional displacements are unknown due to the lack of offset regional markers.

The fault rocks described above contain microstructures which suggest that at least two phases of faulting occurred. The fault rock from domain A contains clasts of cemented cataclastic sandstone. The clasts consist of a range of sizes of angular quartz fragments cemented together by quartz and clay. This cataclastic rock has then been re-brecciated and the clasts are floating in an organic-rich matrix. The irregular and dentate boundaries preserved on the clasts in the breccia suggests that material has been removed by a fluid present at the time of faulting which corroded the clasts. The presence of the organic material in the breccias suggests that hydrocarbons were also mobile during the latter faulting event.

The earlier faulting event which produced the cemented cataclastic sandstone could be related to the earlier extensional event suggested by Astin (1985, in press), or the sinistral movement suggested by Enfield (1988). If the fault was active during the deposition of the Scapa Sandstone sediments, as with the North Scapa Fault (discussed in section 5.4), the East Scapa Fault is in an orientation which would suggest it acted as an oblique

fault for extension which was occurring on the North Scapa Fault at this time, with the Hoy and Dunnet Head river system flowing to the N-NE (Astin, 1985; fig. 5.27). Extension in an NW-SE direction along the North Scapa Fault would be expressed as a sinistral sense of movement on the East Scapa Fault. The cataclastic microstructures in the sandstone therefore most probably correlate with earlier (?)sinistral movement on the East Scapa Fault.

This event is followed by a later faulting event which occurred when the hydrocarbons were mobile. This is most likely related to the basin inversion event during the Carboniferous, which resulted in the present-day reverse geometry along the East Scapa Fault. Both the cemented cataclasite and the fault rock containing evidence for the migration of hydrocarbons are very similar to the fault rocks formed during the (inferred) contemporaneous movements on the North Scapa Fault.

The hangingwall fault rocks also preserve evidence of a complex fault history. The cemented breccias contain elongate and folded clay-rich clasts which suggests that the fault rocks behaved in a ductile manner during an early deformation event before the Rousay Flagstones were fully lithified. This early deformation most probably correlates with the early syn-depositional (?sinistral) movement discussed above. This event is followed by more brittle faulting which formed the breccias. The evolution of the breccias most probably correlates with the inversion event which resulted in the reverse geometry of the fault.

The breccias were then reworked into the foliated gouge which contains extensional movement indicators. The foliated fault rock from domain D has similar fabric geometries as the brittle fault rocks described from the Punchbowl Fault Zone in California (Chester et al., 1985; Chester and Logan, 1986, 1987), which are inferred to have developed during faulting at 2-4 km. depth (75-125° C and 22-45 MPa). Deformation in the Punchbowl Fault Zone was accomplished by cataclastic mechanisms with minor pressure solution (Chester and Logan, 1987). The development of the fine-grained fault rock from domain D probably formed by cataclasis under similar environmental conditions. The evolution of this fault rock most probably correlates with a later (dextral) transtensional event which will be discussed in more detail in section 5.8.

Upper-MORS/UORS Scapa Fault System

SCALE
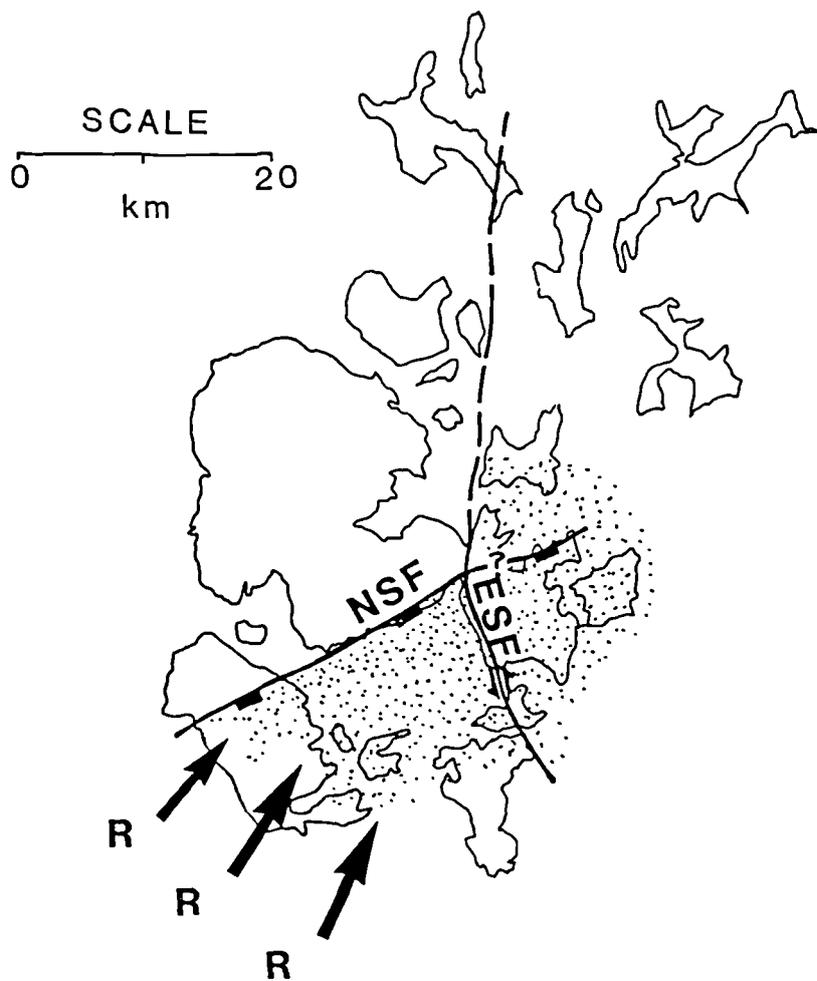
Hoy and Dunnet Head river system

Figure 5.27. Diagram showing probable early displacement history along the Scapa Fault System during the Upper-MORS to UORS. Palaeogeography from Rogers (1987).

5.5.4 The East Scapa Fault south of Long Geo [HY 448048]

South of Long Geo [HY 448048], the East Scapa Fault can be traced for nearly 4 km (fig. 5.23). Although the fault plane is exposed only near St. Mary's at Crow Taing [HY 463011], the fault can be located onshore to within +/- 0.5m. Thus, detailed changes in strike of the fault can be traced, and the relationship of the orientation of structures associated with the fault, (minor folds and faults), can be assessed. In addition, fault rock development along the changing fault geometry can be investigated in detail.

The fault trace south of Long Geo [HY 448048] changes from a NW-SE orientation to a NNE-SSW orientation south of the Bay of Sandoyne [HY 463020] (fig. 5.23). From the Bay of Deepdale [HY 451044] to the Bay of Sandoyne, minor open folds in the Rousay Flagstones have wavelengths of <3m. The axial trace of the folds in the Rousay flags are consistently oriented sub-parallel to the fault trace north of the Bay of Sandoyne (i.e., at [HY 463022] and [HY 461026], as with minor thrusts showing small (<2 m.) reverse displacements to the W-WNW [HY 462022] (fig. 5.23). Minor extensional faults in the hangingwall are oriented slightly oblique, to nearly perpendicular to the fault trace, all showing small downthrows (<3 m.) to the SE-ESE [HY 456033].

The fault rock development at the Bay of Sandoyne, where the fault begins to change strike, is different from that of the other localities described in this section. In the bay, the fault can be traced as a 10-30 cm. wide cataclastic zone separating undeformed flagstones. The cataclastic zone is characterized by a veined breccia with a 'jigsaw puzzle' texture, which contains angular clasts 2-20 cm. in diameter (fig. 5.23). The breccia is very similar to the implosion breccias described by Sibson (1986), which form at dilation jog sites along faults.

South of the Bay of Sandoyne, the fault strikes in a NNE-SSW orientation at Crow Taing [HY 463011] (fig. 5.23). In the hangingwall of the fault at Crow Taing, the East Scapa Fault is associated with a wide deformation zone with varied intensities of folding and fault rock development, as shown on the detailed map of this area (fig. 5.28). At Howequoy Head [HY 465007], chevron folds with vertical or subvertical axial planes occur in the hangingwall of the fault, and verge both east and west. The chevron folds have amplitudes ranging from 0.5 m. to 10 m, and wavelengths of 1 to 20 m. The fold axes are oriented obliquely to the fault (NNW-SSE, 159-180°) (fig. 5.28), and plunge

gently (30-50°) to the south. Nearer to the East Scapa Fault between Clett [HY 464007] and Crow Taing [HY 463011], there are several steeply-dipping minor faults oriented parallel to the fault (fig. 5.28). This has resulted in 10-15 m.-wide domains of relatively coherent 'packets' of strata separated by fault zones in which bedding becomes disrupted nearer to the fault and cataclasis becomes more intense.

The East Scapa Fault exposure at Crow Taing [HY 463011], and the associated minor fault zones contain extensional kinematic indicators, and fault rocks which provide information about the deformation history of the East Scapa Fault. The field and microstructural observations in these fault zones are described in the following sections.

5.5.4.1 Field and microstructural observations, The East Scapa Fault at Crow Taing [HY 463011]

The East Scapa Fault exposed near St. Mary's at Crow Taing [HY 463011] (fig. 5.29) strikes 015°, dips 56° east, and shows the same reverse fault geometry observed at Hemp Stack (see fig. 5.25a). The undeformed East Scapa Sandstone in the footwall is a low porosity (<10%), carbonate-cemented sandstone with quartz grain sizes of 100-150 μm. (fig. 5.30a). The sandstone is relatively undeformed up to 1 meter from the fault: fractures are rare, and the original microstructure is well-preserved. The fault plane is a smooth, planar surface, and a cohesive cataclastic sandstone is observed up to 10 cm. from the fault. The fault plane contains slickensides plunging steeply (70-80°) to the SSW. The cataclastic sandstone contains quartz fragments <<20 μm, cemented by carbonate (fig. 5.30b). In addition, seams of clay and organic-rich material (<0.5 mm thick) are observed in the cataclastic sandstone (fig. 5.30c).

The beds in the hangingwall of the fault are 'disrupted' up to 10 meters from the fault: elongate, cemented blocks of breccia lie in fine-grained gouge which posseses a pervasive fabric (fig. 5.29b). At 2-3 meters from the fault, breccia blocks ranging in size from 5 cm. to 1 m. are completely surrounded by gouge. At 0.5 m. from the fault, the fault zone is exclusively fine-grained gouge. The gouge zone contains quartz grains <50 μm in size cemented by carbonate. Clay and organic-rich seams (<0.5 mm. thick) define the fabric in the hangingwall fault rocks (fig. 5.30d).

Figure 5.29. Photographs of East Scapa Fault zone near St. Mary's at Crow Taing [HY 463011]. a) Relatively undeformed East Scapa Sandstones in footwall separated from foliated incohesive gouge in hangingwall by planar, slickensided fault plane. Kinematic indicators in the fault zone demonstrate extensional movement down to the ESE. b) Detail of deformation in the Rousay Flagstones in the hangingwall of the ESF. Rounded to elongate blocks of cemented breccia in foliated gouge. Compass 10 cm. long.

A

B

Figure 5.30. Optical micrographs of microstructures from the East Scapa Fault zone near St. Mary's at Crow Taing [HY 463011] as shown in fig 5.29. a) Sample 50103. Undeformed East Scapa Sandstone from footwall outside of fault zone. Note low porosity (<<10%) and carbonate cement. XP. Scale bar 0.5 mm. b) Sample 50091. Deformed East Scapa Sandstone directly adjacent fault plane, showing cataclastic grain size reduction zones and seams of organic-rich material. XP. Scale bar 1 mm. c) Fault rock sample as in 5.30b (50091), but under PPL, showing clearly the seams of organic-rich material in zones of localized cataclasis. Scale bar 0.5 mm. d) Sample 50092. Foliated incohesive gouge from hangingwall, showing domains of fine-grained quartz-rich breccias cemented by carbonate, cross-cut by seams of organic-rich material. XP, ST. Scale bar 1 mm.
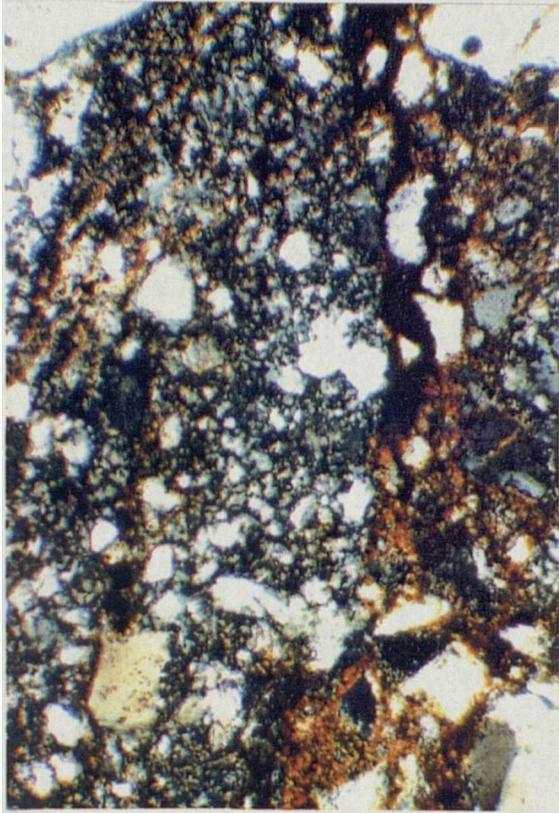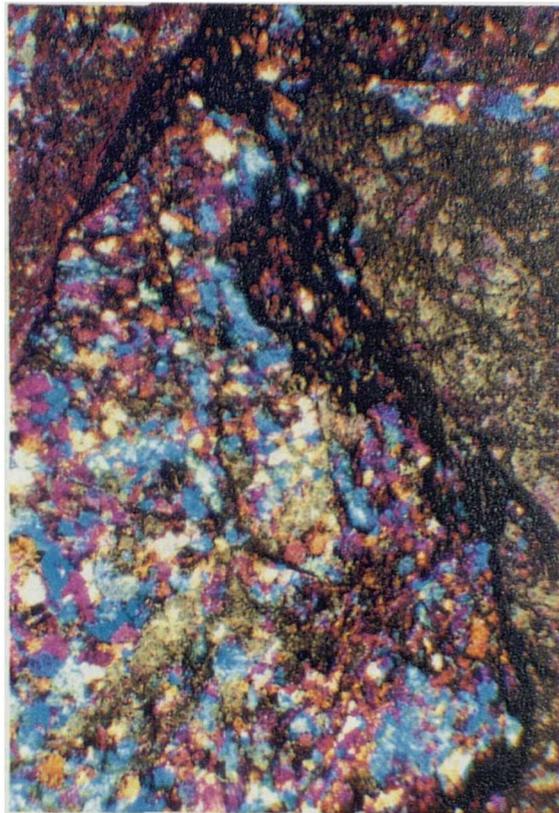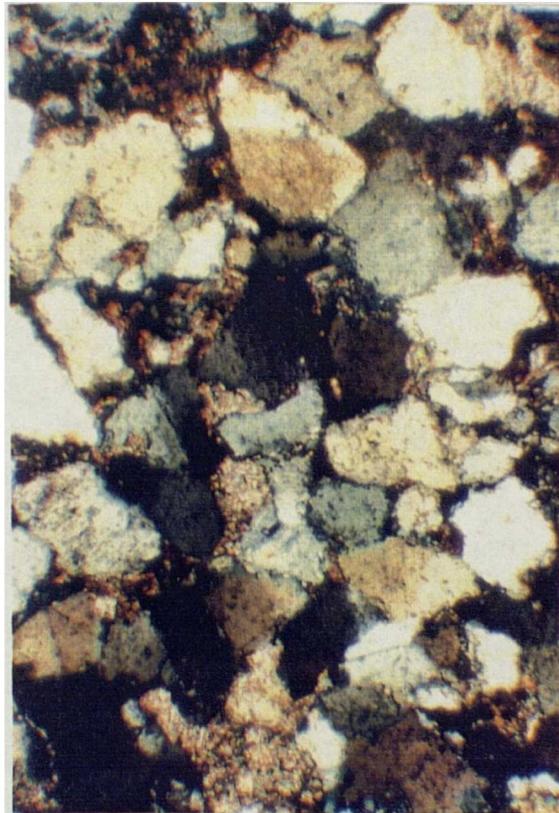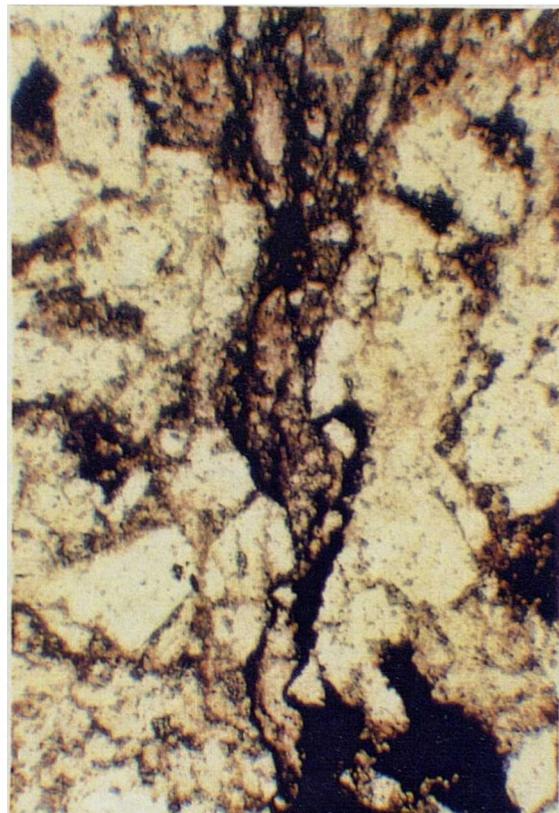
5.5.4.2 Interpretation

The field and microstructural observations of the East Scapa Fault exposed at Crow Taing are similar to those at Hemp Stack. The sandstones appear to be relatively undeformed in the field and contain few fractures. However in thin section, grain size reduction has occurred up to 10 cm. from the fault, resulting in a fine-grained cataclastic sandstone. The flagstones in the hangingwall show intense cataclasis, resulting in the development of a clay-rich, foliated gouge in the fault zone.

The foliation in the hangingwall is defined by clay and organic-rich seams oriented sub-parallel to the fault. The material in the seams most probably represents material which was deposited as a result of the influx of fluids through the anisotropy defined by the foliation. The fabric in the fault zone and the slickensides indicate an extensional movement sense, with a slight oblique (dextral) component. These observations are similar to data from the Hemp Stack locality, but the slickensides at Hemp Stack imply a dominantly strike-slip component of movement. However, the fault orientations are slightly oblique to each other (N-S at Hemp Stack, as opposed to NNE-SSW at St. Mary's), and thus the dextral strike-slip movement sense along the N-S fault would be expressed as dominantly extensional displacement along the NE-obliquely oriented part of the fault or associated faults (fig. 5.31). One of the NE-obliquely oriented faults is described next, which lies 10 m. to the east of the ESF locality just described (see fig. 5.28).

5.5.4.3 Field and microstructural observations, fault zone '1' [HY 464011]

Fault zone '1' [HY 464011] (fig. 5.28 and 5.32a) lies in the hangingwall, 5 m. to the east of the ESF, and contains fault rocks showing a complex history of cataclastic deformation and fluid flow. The fault strikes 016° and dips 33° ESE (i.e. parallel to the East Scapa Fault exposure described above). The footwall is dominated by elongate blocks of cemented breccia varying in size from 50 cm. to 2 m. in length. The elongate blocks are oriented sub-parallel to the fault (fig. 5.32a). Both the fault plane and the fault surfaces along the blocks show slickensides plunging steeply $(70-85^o)$ to the SSW. The blocks of breccia vary from zones containing angular clasts with extensive carbonate veining (fig. 5.32b), to completely disrupted zones with rounded clasts in an extremely fine-grained matrix (fig. 5.32c). An incohesive, clay-rich fault rock surrounds the blocks.
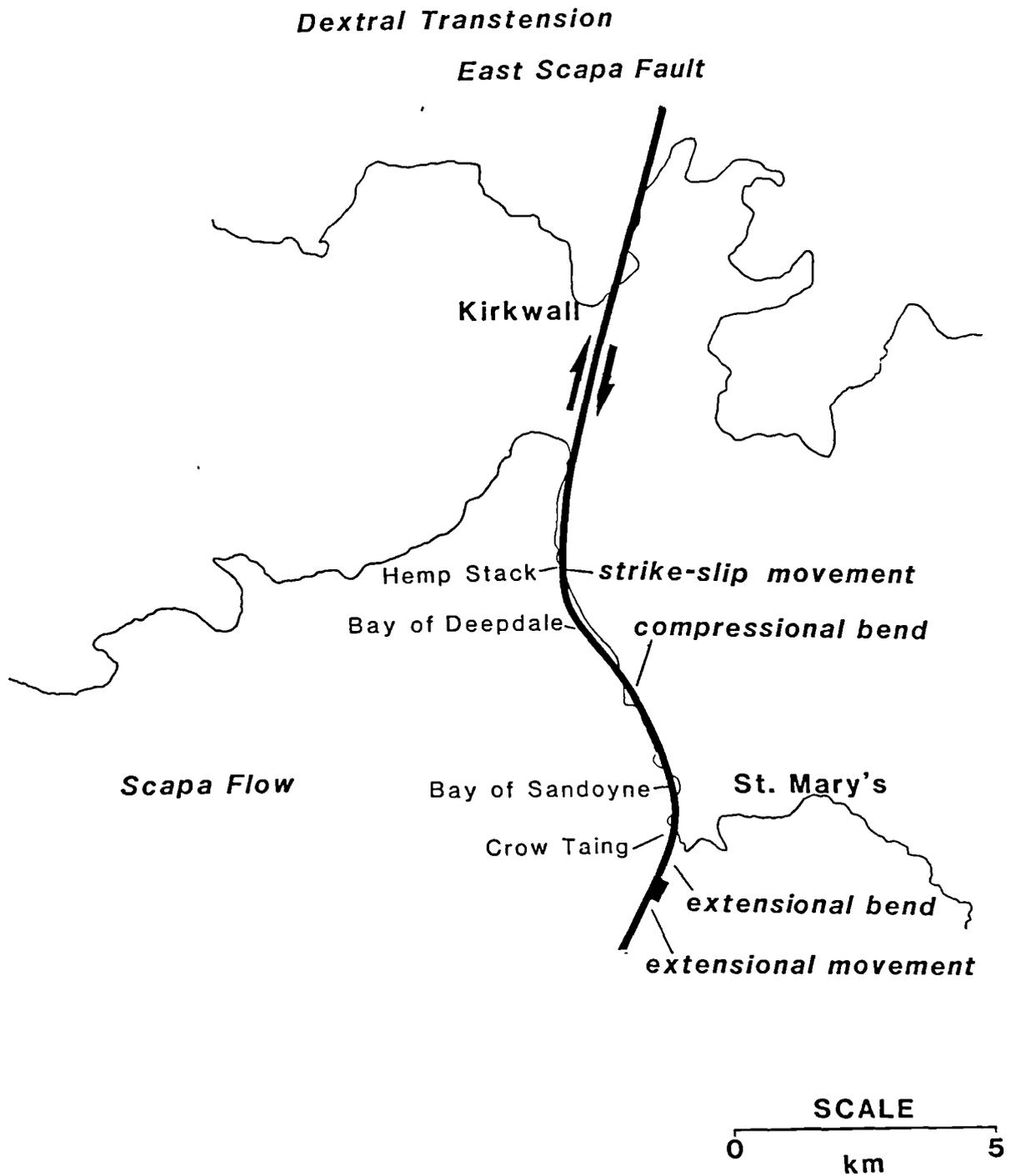
Figure 5.31. Diagram showing movement senses along the East Scapa Fault during dextral transtension.

Figure 5.32. Photographs of fault zone '1' in Rousay Flagstones near St. Mary's at Crow Taing [HY 463011]. a) View looking north at fault zone. Footwall dominated by cemented breccia 'blocks' 50 cm. to 2 m. in length, oriented sub-parallel to fault (arrowed, F). The blocks are surrounded by fine-grained, foliated, fairly incohesive, clay-rich matrix. Features indicating down-dip extensional movement are observed on the planar surfaces on the blocks (slickensides) and the foliated matrix (asymmetry in fabric). Hangingwall is dominated by foliated, cemented and veined fault rock (see fig. 5.33a for details). Footwall and hangingwall blocks separated by 20-30 cm. wide zone of quartz-rich sandstone (see figs. 5.33b, c & d for details). Hammer resting on fault plane 60 cm. long. b) Detail of footwall deformation in Rousay Flagstones, hammer oriented N-S (32 cm. long). Note only slightly disrupted bedding with angular clasts near bottom of picture, and patchy veining. c) Detail of footwall deformation in Rousay Flagtones showing completely disrupted zone containing rounded clasts 'floating' in fine-grained matrix. Compass 10 cm. long. See text for details.
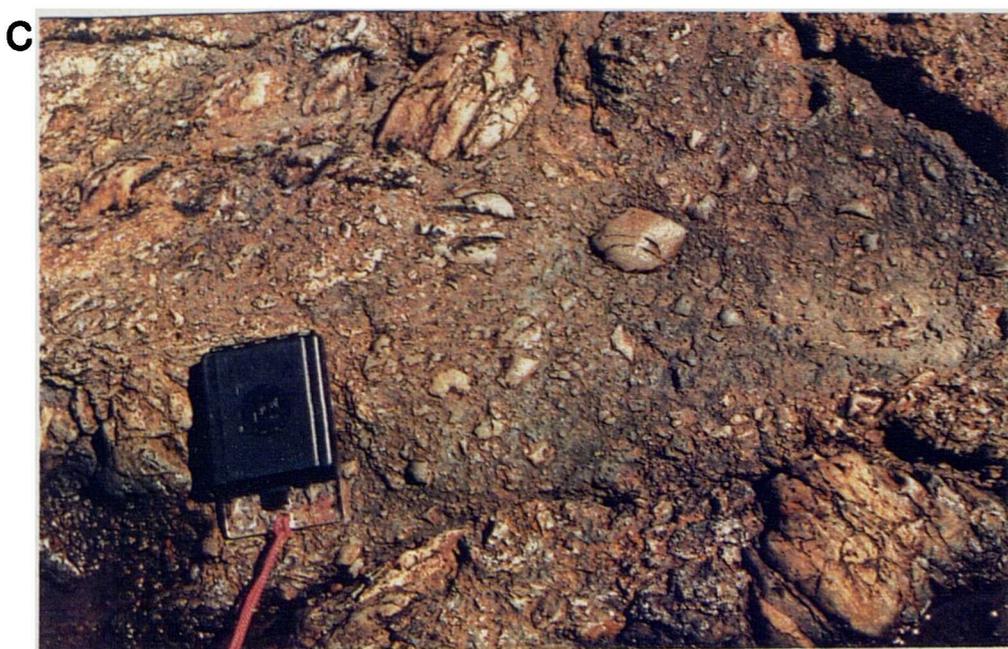
The hangingwall contains cemented fault rock with a pervasive fabric (fig. 5.33a). The fabric is defined by a foliation which is oriented sub-parallel to the fault, and more steeply-dipping shear bands. The hangingwall and footwall are separated by a 10-20 cm. wide zone of white sandstone (fig. 5.33b). Within this zone, rounded clasts of cemented sandstone are contained in a finer-grained incohesive matrix which contains clay and organic-rich zones. In some cases, organic-rich veins are observed within the white sandstone (fig. 5.33c). The organic-rich veins are sometimes deformed (fig. 5.33d), and provide kinematic indicators showing extensional offsets down to the E-ESE.

The microstructures within the fault rocks just described are shown in fig. 5.34. The white sandstone is characterised by quartz clasts 100-200 μm in diameter within an extremely clay-rich, fine-grained matrix cemented by carbonate (fig. 5.34a). The foliated fault rock from the hangingwall contains cemented clasts of quartz in a fine-grained clay-rich matrix. The foliation is again defined by organic-rich seams, which 'flow' around the cemented clasts of quartz grains (fig. 5.34b). The blocks of cemented breccia in the footwall contain clasts of fine-grained organic-rich flagstone, often floating in carbonate cement (fig. 5.34c).

5.5.4.4 Interpretation

The fault zone contains field-scale structures (the fabric in the hangingwall fault rocks, and the offset of the organic-rich veins in the fault zone) which indicate an extensional displacement sense (down to the E-ESE) for the last phase of faulting, with a slight dextral component of movement. This movement sense is consistent with observations of the East Scapa Fault zone locality described in section 5.5.4.1.

The fault rocks in fault zone '1' indicate that the fault was an open pathway for fluids and material several times. The origin of the white sandstone, which is not derived from the footwall or hangingwall rocks, is enigmatic and appears to have come from a non-local source. The delicate nature of the organic-rich vein in the white sandstone suggests that the material in the vein was poorly lithified at the time of influx into the fault zone. The seams of organic matter which define the foliation in the hangingwall fault rocks again most probably represent the deposition of material in microscale fluid pathways which were created during the deformation.

Figure 5.33.   Detailed views looking north into fault zone '1' in the Rousay
Flagstones near St. Mary's at Crow Taing [HY 463011].   a)   Deformation in
hangingwall just above fault plane showing foliated, cemented and veined
fault rock.   Compass 10 cm. long.   b)   Detailed view of white sandstone in
fault zone showing rounded clasts of cemented sandstone in fine-grained
matrix with dark, organic-rich zones.   Compass 10 cm. long.   c)   Organic-rich
vein   in   sandstone   within   fault   zone;   vein   oriented   dominantly
perpendicular to the fault plane. Two pence piece for scale.   d)   Organic-rich
vein within the white sandstone in the fault zone; the vein is deformed and
offset;   kinematic   indicators   on   offsets   demonstrate   extensional   movement
down to the E-ESE.   Fifty pence piece for scale.
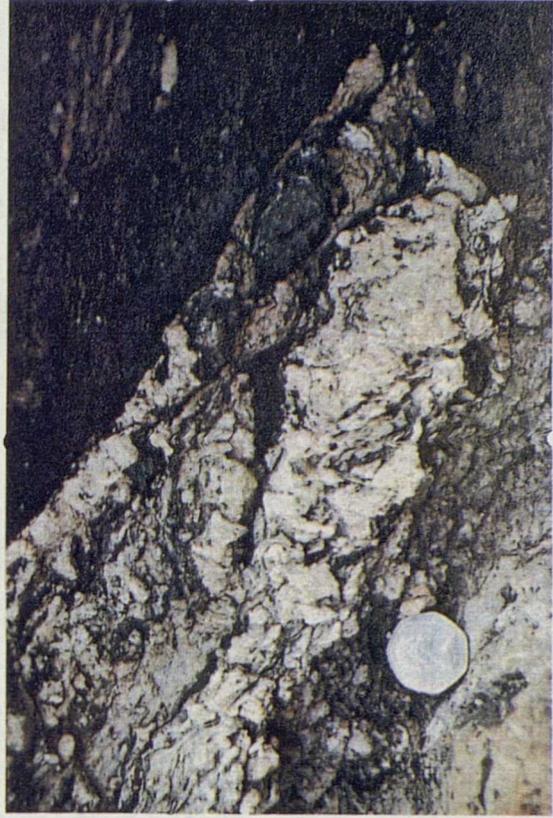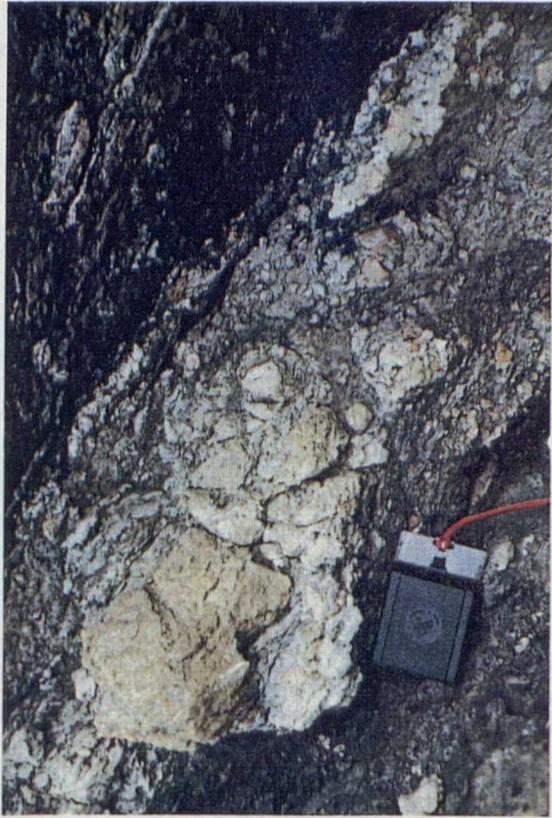
Figure 5.34. Optical micrographs of microstructures from fault rocks in fault zone '1' shown in figs. 5.32 and 5.33. a) Sample 50100. Poorly sorted, 'white' sandstone within fault zone showing large quartz grains in clay-rich matriz (left). XP. Scale bar 0.5 mm. b) Sample 50096. Foliated, cemented flagstones from hangingwall as shown in fig. 5.35a. Note foliation (F) defined by organic-rich seams oriented sub-parallel to the fault and 'flowing' around cemented clast near centre. PPL. Scale bar 0.5 mm. c) Sample 500975. Microstructuresin cemented breccia 'block' from footwall (as shown in fig. 5.32a). Cemented clasts of organic-rich flagstone 'floating' in carbonate cement. XP, ST. Scale bar 0.5mm.
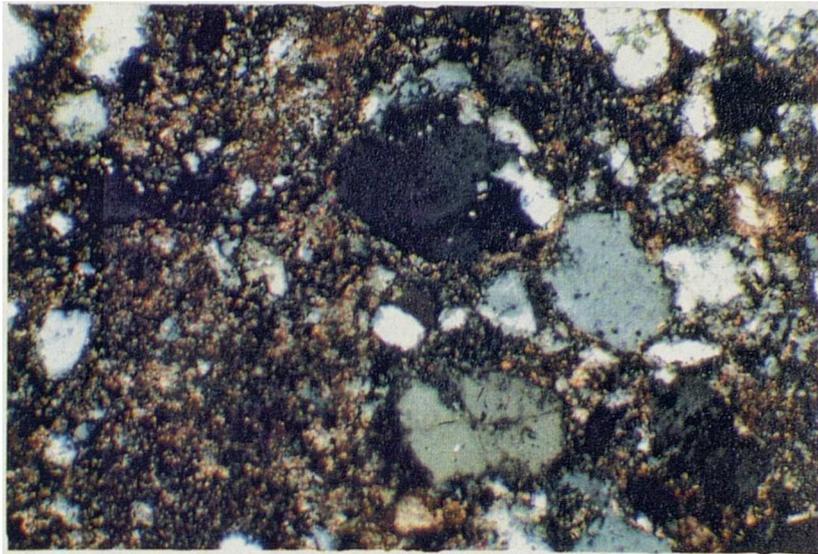
A
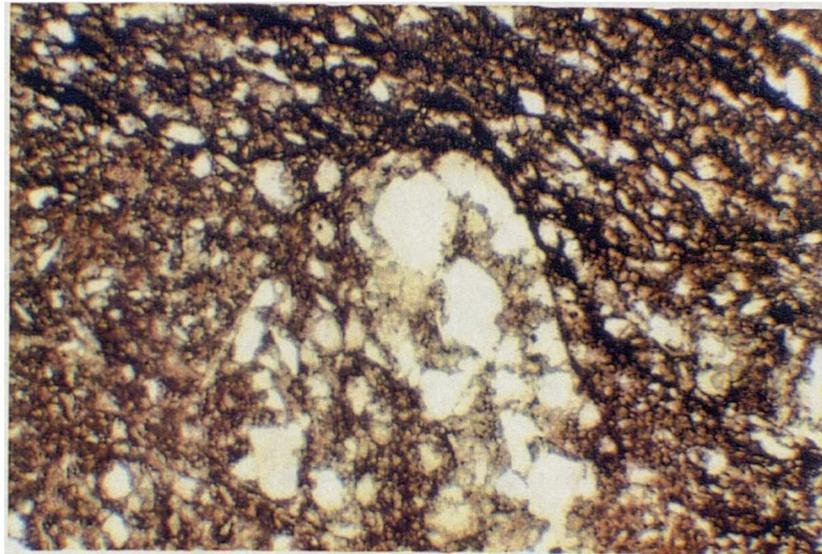
B

C

5.5.5 Discussion: East Scapa Fault history and fluid flow events

Although sedimentological evidence indicates that the East Scapa Fault was active during the deposition of the Scapa Sandstones (Astin, 1985, in press), the fault zone exposures have been modified by later deformation and structural evidence for the earlier faulting event is at the present time obscured. However, microstructurally, clay-rich clasts which have been deformed in a ductile manner are preserved within the cemented fault breccias in the Rousay Flagstones at Hemp Stack. This would suggest an early deformation event took place when the flagstones were less lithified, prior to the later faulting which is responsible for the present-day outcrop of the fault.

Enfield (1988) has suggested that early sinistral movements occurred on the East Scapa Fault. The evidence for early extension on the North Scapa Fault during deposition of the Scapa Sandstone (section 5.4) would correlate with sinistral, extensional movement on the East Scapa Fault, creating a small half-graben which was active during deposition of the Scapa Sandstone in southern Orkney (as discussed in section 5.5.3; see fig. 5.27).

This is compatible with Astin's (1985, in press) sedimentological data, which shows that palaeogeography and thickness variations of the upper MORS strongly suggests control of subsidence by the Scapa Fault System. If the evidence for the earliest movements are valid, the East Scapa Fault has acted as a N-S lineament in the Orkney area since at least the upper MORS. The present-day reverse stratigraphic offset along the fault indicates that at some time in the basin history, the fault was affected by a compressional tectonic event, most probably during uplift of the basin in the Carboniferous. The fault zone localities described at Hemp Stack and Crow Taing each demonstrate evidence for later dextral, extensional movement which overprints the reverse movement implied by the fault geometry. The N-S oriented fault plane at Hemp Stack shows evidence for a dominantly dextral, strike-slip component of movement. The NNE-SSW faults near St. Mary's demonstrate dominantly dip-slip movement. At both localities, the foliated fault gouge in the Rousay Flagstones indicate extensional displacement down to the E-ESE. These observations are compatible with later dextral, transtensional movement along the length of the East Scapa Fault, as this would be expressed as an extensional component of movement on NNE-SSW obliquely-oriented faults (e.g. see fig. 5.31).

As discussed in section 5.3.4, Enfield and Coward (1987) and Coward et al. (1989) suggest that the East Scapa Fault moved dextrally subsequent to the earlier sinistral movement, both during inversion of the basin (related to Variscan deformation), and in a transtensional sense in the Mesozoic. Coward et al. (1989) suggest that both dextral movements along the ESF relate to dextral movements on the Great Glen Fault System. Coward et al. (1989) have inferred that changes in strike, dip, and movement sense on the small-scale faults along the ESF suggests that dextral negative-flower structures were superimposed on earlier dextral positive-flower structures (sensu Wilcox et al., 1973). They suggest that the local change from transpressive to transtensional displacement is related to the change in fault strike from NNW to NNE south of Kirkwall, and the movement of rocks from a compressive bend to an extensional bend between Kirkwall and St. Mary's.

Enfield (1988) used fold obliquity to determine movement directions along the fault, but as discussed in section 5.5.1, the relationship of the regional folds to movements on the East Scapa Fault is not clear. During dextral movement along the East Scapa Fault, folds could form in a limited range of orientations, from NW-SE to NNW-SSE. However, complex overprinting relationships of minor folds and faults could develop due to the presence of bends in the fault strike, as pointed out by Coward et al. (1989).

This thesis has presented detailed data of the folds which have developed locally along the East Scapa Fault. With the exception of the folds at Howequoy Head [HY 465007], minor folds are oriented consistently parallel to sub-parallel to the fault (fig. 5.23). At Howequoy Head (on an extensional bend where the fault has changed strike to a NNE-SSW orientation), the folds are oriented obliquely (NNW-SSE) (fig. 5.28). Thus, one possible alternative to the Coward et al. (1989) model is that the folds with axes trending parallel to the fault formed during the compressional event responsible for the reverse offset along the fault, with compression oriented in an approximately E-W direction. (Further evidence for an E-W oriented compression will be discussed in section 5.6). The NNW-SSE obliquely-oriented folds observed on the extensional bend at Howequoy Head could then be related to the later dextral transtensional movement along the East Scapa Fault, which is most probably compatible with Coward and Enfield's (1987) Mesozoic dextral movements. The development of the regional scale folds could be related to these movements, but appears to be too speculative to confirm their relationship with movement along the East Scapa Fault.

5.5.6   Conclusions

A wide range of fault rocks from the East Scapa Fault zone have been described in this section.   The important conclusions are listed below.

1.   The range of fault rocks observed reflects evolution of the fault zone during a complex movement history.

2.   The extent and distribution of the cataclastic deformation in the footwall and hangingwall rocks adjacent to the fault is heterogeneous, varying from intense cataclasis up to 3 metres from the fault plane in the fine-grained flagstone lithology, to limited cataclasis up to 10 cm. from the fault in the sandstone lithology.

3.   The evolution of different fault rock types along the strike of the fault can be identified.   In some cases, this can be related to changes in fault geometry,   such as the implosion breccia zone which is present at the Bay of Sandoyne, which is the location of an extensional bend on the East Scapa Fault.

4.   Present-day exposure of the fault indicates a net reverse stratigraphic displacement on the fault.   The compressional tectonic event responsible for this displacement might have been oriented in an approximately E-W direction, as indicated by minor folds and faults which trend parallel to the dominantly N-S trending fault.

5.   Slickensides on the N-S oriented East Scapa Fault plane at Hemp Stack indicate a dominant strike-slip component of movement on the fault, while the obliquely-oriented faults show dominantly dip-slip movement at Crow Taing.   The kinematic indicators (fabrics in the fault gouge) within the fault zone exposures at both Hemp Stack and Crow Taing indicate that the later reactivation of the fault was dextral and transtensional in sense.   Minor folds with a NNW-SSE trend developed on an extensional bend near St. Mary's, most probably during the later dextral displacements.

6. The fault rocks preserved at Crow Taing indicate that the fault acted as a pathway for fluids and both locally and non-locally derived material during the transtensional reactivation.

5.6 North Coast Section

5.6.1 Introduction

This section describes an approximately E-W section across the north coast, from the Point of Buckquoy [HY 240284] to Eyenhallow Sound [HY 360274], traversing perpendicular to the N-S structures in the area. This traverse has been selected in order to assess the fault geometries resulting from: 1. initial gravity-driven movement of sediments down tilted half-grabens during burial of the lower MORS fine-grained lacustrine facies rocks, and; 2. the interaction of the earliest developed structures with contractional structures inferred to have developed during subsequent inversion of the basin. The orientation of the late contractional fault geometries might aid in elucidating the possible compression/transpression direction which existed at the time of basin inversion. In addition, the conditions of deformation are investigated through detailed microstructural analysis of the fault rocks.

The structure of the north Mainland, Orkney, is characterised by the broad, open West Mainland Anticline, with the fold axis trending north-south, approximately through Oyce [HY 286297]. Bedding is generally flat-lying or gently-dipping across the north coast, as shown in figs. 5.35 and 5.36. However, several "bedding parallel fault zones" within the MORS lacustrine facies Stromness flagstones are observed, as also noted by Coward and Enfield (1987), and Enfield (1988). Enfield (op.cit.) uses the term "bedding parallel fault zone" in his descriptions of the fault zones. Wilson et. al. (1935) referred to the bedding parallel fault zones as "lines of disturbance", and the structures related to them as "contorted beds".

The bedding parallel fault zones take advantage of the fine-grained 'fish-bed' horizons (sensu stricto, Astin, in press) within the flagstones, and are of regional extent. Astin (in press) has correlated the MORS lacustrine stratigraphy on the island of Rousay and the Mainland, and his sedimentary logging has confirmed the continuous nature of the bedding parallel fault zones. Astin (in press) uses the term "decollement horizon" for the bedding parallel fault zones, as extensional faults are observed to link, or decoll onto the bedding parallel fault zones.

The linked extensional/detachment horizon fault systems are considered to have formed during early extension in the basin (Coward and Enfield, 1987; Enfield and Coward, 1987; Enfield, 1988). These worker suggested that the bedding parallel detachment horizons formed by gravity gliding along sediments that dip due to rollover towards major listric growth faults, with the linked extensional faults accommodating the geometrically necessary extension generated within the rollover in the hangingwall of the fault.

Many thrusts are observed to use the anisotropy of the detachment horizons, follow the horizon for tens of meters before ramping up section, and show displacements to the WNW. The frequency of thrusts or back-thrusts ramping up section from any particular detachment horizon is always observed to increase in the hangingwall toward ORS extensional faults exposed on the north coast, and complex folds and contractional fault geometries observed to be associated with these thrusts are consistently developed adjacent the ORS extensional faults. Coward and Enfield (1987) suggest that the thrusts (which commonly breach and invert the early normal faults) may result from the shortening of beds caused by the partial reversal of displacement on major normal faults during minor tectonic inversion of the basin. However, they state that as the thrusts verge only in a direction perpendicular to major Devonian growth faults, and appear to be confined to individual half grabens, the driving force for their formation would have also been generated by the potential energy created within tilted half-graben sediments during extension and growth of the basin.

A discussion of the origin of the detachment horizons, and the evolution of the complex contractional geometries is presented after the field-scale geometries of these structures are described, and their microstructures assessed.

5.6.2 Description of the detachment horizons

The Stromness Flagstones represent a thick sequence of fine-grained sediments, mainly dark grey, muddy to silty calcareous or dolomitic limestones, and are typically laminated (Astin, in press). The detachment horizons have developed in particularly fine-grained, organic-rich 'fish bed' units in the Stromness Flagstones, and vary in thickness from 10-100 cm. The fish beds have fine sedimentary laminae averaging about 0.5-1 mm. thick, mainly due to alternation between clastic and carbonate laminae, which reflects annual productivity cycles (Rayner, 1963).

Astin (in press) has correlated the fish-beds on the north coast of the Mainland by the nature of individual fish-beds, including their overall thickness, the abundance, size and degree of articulation of fish, and the presence or absence of stromatolites.

The detachment horizons are characterised by shear zone geometries between bedding surfaces along which slip has occurred (fig. 5.37). The complex shear zone geometries contain both contractional and extensional geometries, ranging from tight, overturned folds (fig. 5.37a) to discrete faults forming both contractional and extensional duplexes (fig. 5.37b). Abrasion slickenside lineations are present along the bedding planes upon which slip has occurred. The shear zone geometries and lineations indicate a consistent transport direction to the WNW (approximately 105°) (see lineation readings on figs. 5.35 and 5.36). The transport direction is consistently oriented sub-perpendicular to the extensional faults exposed on the north coast. In most cases it is not possible to assess the amount of slip which has occured along the bedding planes bounding the detachment horizon, nor the contraction or extension which has occurred within the detachment horizon.

5.6.3   Haafs Helia [HY 316304]

A well-exposed section (both vertically and horizontally due to a series of coastal platforms) at Haafs Helia [HY 316304] provides a good example of contractional structures developed in the hangingwall block of an earlier extensional fault.

The major extensional fault at Haafs Helia contains several small displacement (1-2 m.) antithetic and synthetic extensional faults in its hangingwall, all of which link to the upper detachment horizon observed at the top of the cliff (fig. 5.38a). Displacements along the minor extensional faults exposed at the top of the cliff can be assessed by the offset of a 25 cm.-thick coarse-grained quartz-rich horizon within the finer-grained flagstones (fig. 5.38b). Bedding within the coarser-grained horizon is often slightly disrupted from horizontal along these early extensional faults, with localised breccia zones exposed (fig. 5.39a). It is uncertain whether the major extensional fault links to the lower detachment horizon observed along the length of the lower coastal platform to the west of the fault (fig. 5.39a), as the cliffs just near the base of the fault are inaccessible.

Figure 5.37. Photographs of structures in the Upper Stromness Flagstones near Haafs Helia [HY 316304]. a) Bedding-parallel detachment horizon, 10-20 cm. in thickness, showing tight contractional folding and minor faulting. Looking north. Chisel is 18 cm. long. b) Bedding-parallel detachment horizon, 20 cm. in thickness between undisturbed beds. Note the many extensional features (arrowed, 'e'). Looking south. Compass 10 cm. in length. c) Small displacement back-thrust (arrowed) detaching from bedding plane movement horizon, with displacement decreasing into tip-fold above. Looking south; ramps and thrusts along section show movement direction 110° to the east (to the right in picture). 200 m. west of major ORS mormal fault at Haafs Helia. (See fig. 5.35 for location). Tape measure 5 m. in length. d) Complex inversion-related structure at Haafs Helia; looking east at detachment horizon (dh). Anticlinal fold axis (arrowed) parallel to strike of ORS normal fault which has been slightly deformed during later contractional deformation (see fig. 5.38). Normal fault offset 25 m.to east along bedding plane detachment horizon; complex fold and thrust structure also displaced from hangingwall of ORS fault onto footwall block. 1 m. high stick with coat hanging in centre.
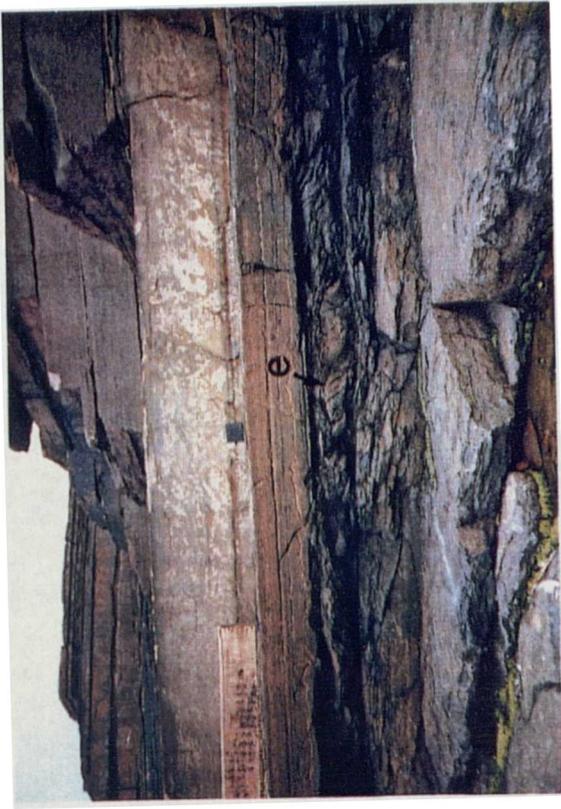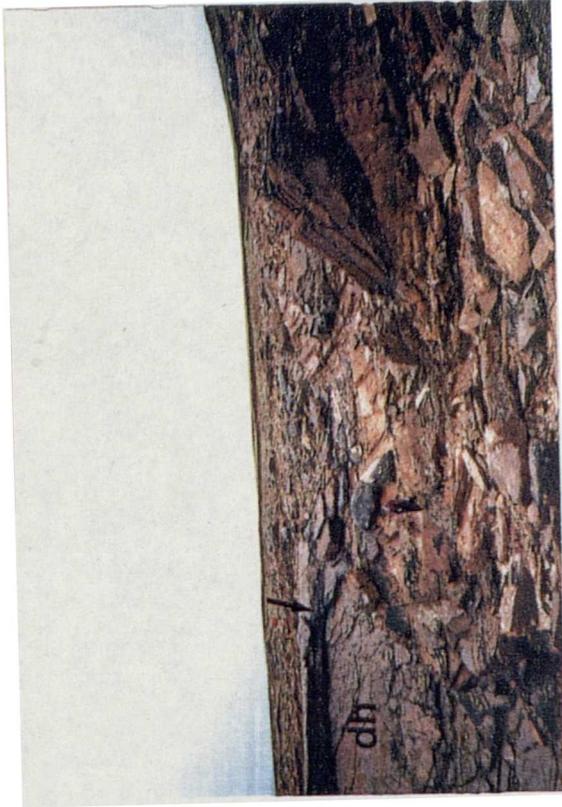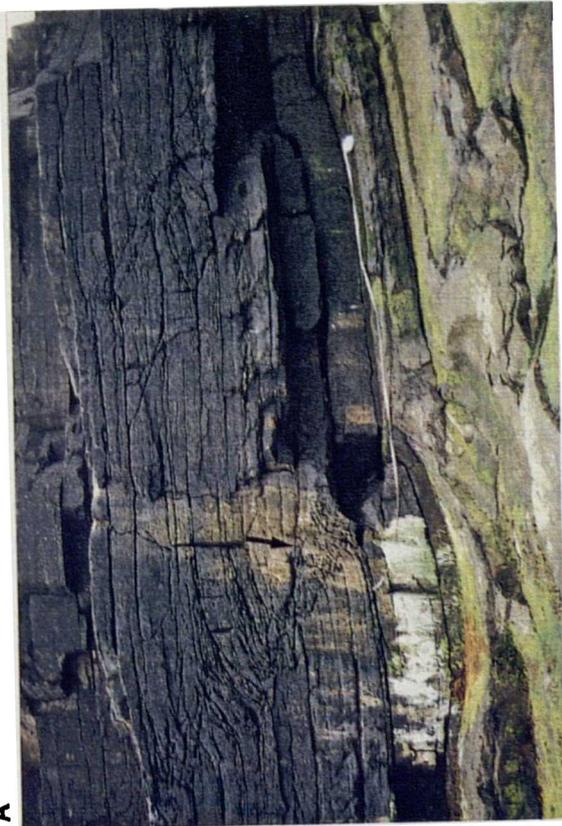
Haafs Helia, North Coast (HY 316304)

Upper Stromness Flags (MORS)
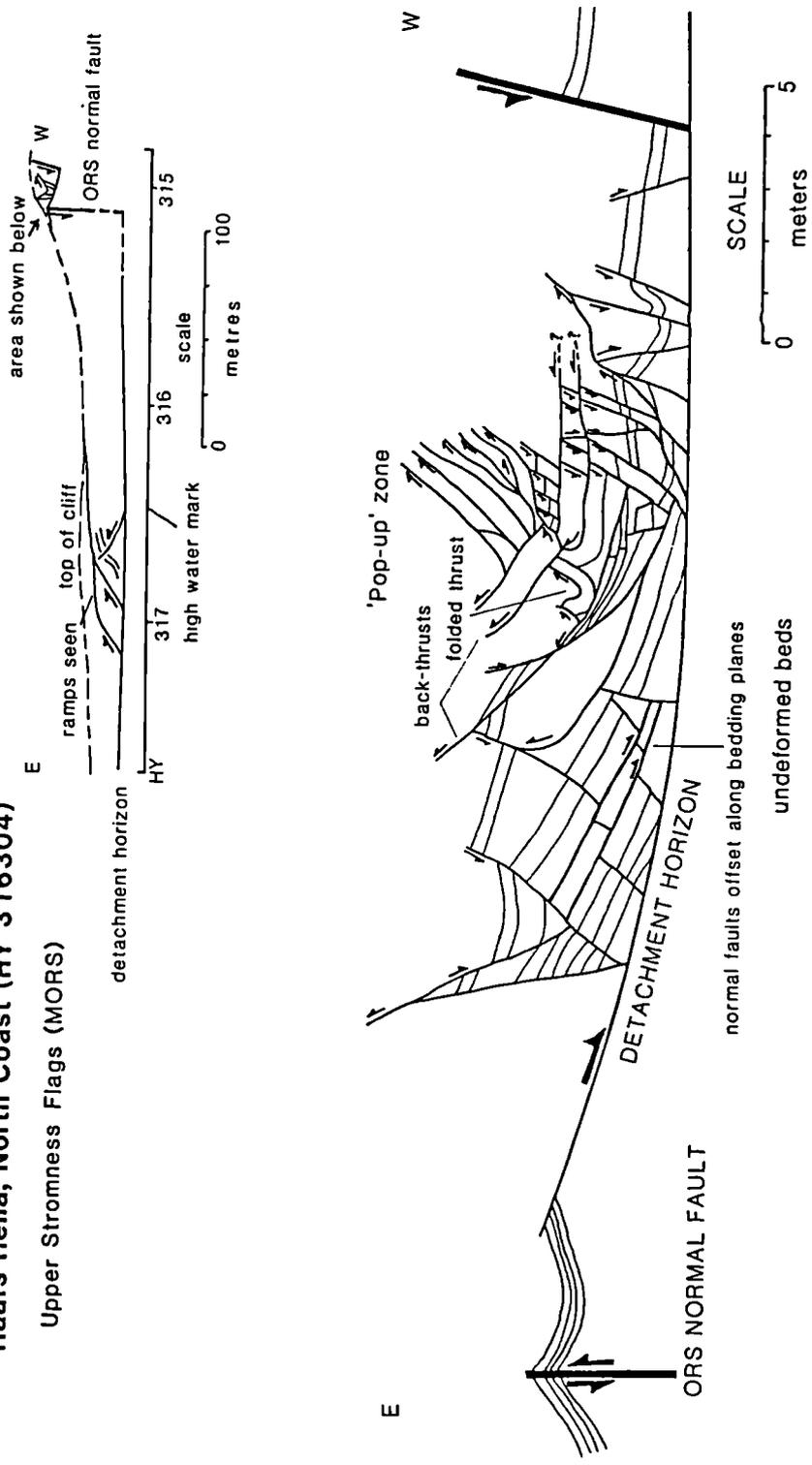
Figure 5.38. Cross sections at Haafs Helia on the north coast, Mainland [HY 316304]. a) Cross section showing structures in the hangingwall of the steeply-dipping ORS normal fault which formed due to later contractional deformation related to inversion of the basin. b) Detailed section of the area shown in fig. 5.38a. Complex fold and thrust structure displaced onto footwall block of the ORS normal fault during inversion of the basin. See text for details.

Figure 5.39. Photographs of detailed structures seen at Haafs Helia [HY 316304]. a) Breccia seen on early (ORS) normal fault plane. Looking west. Fifty pence piece for scale. b) Thrusts cutting through early extensional faults (arrowed). Looking south. Ten pence piece for scale. c) Detail of duplex structure developed between two major thrusts seen in pop-up structure (a) in fig. 5.38b. Looking south. Ten pence piece for scale.
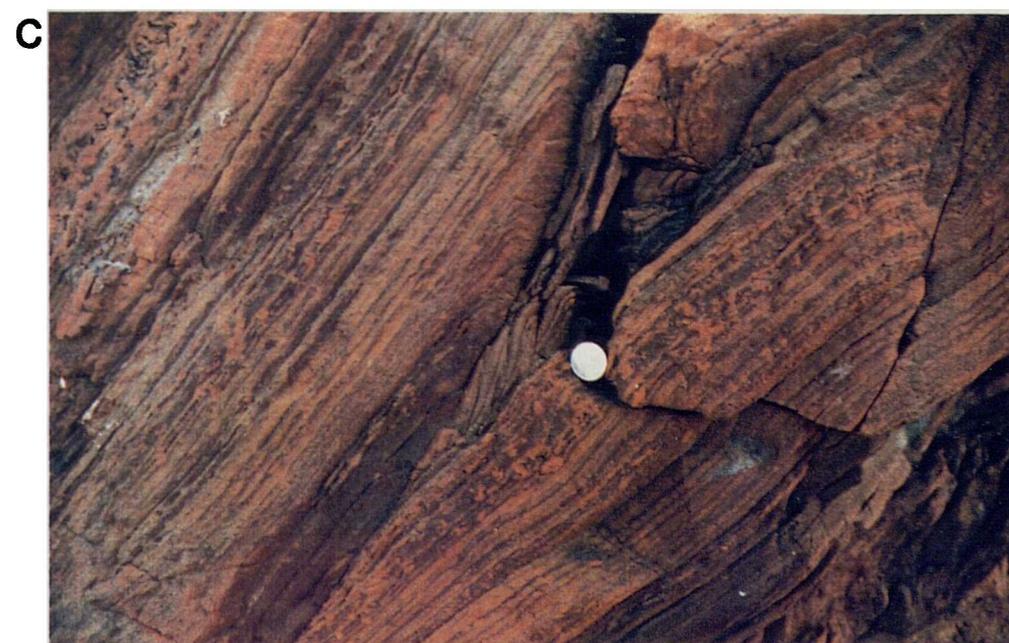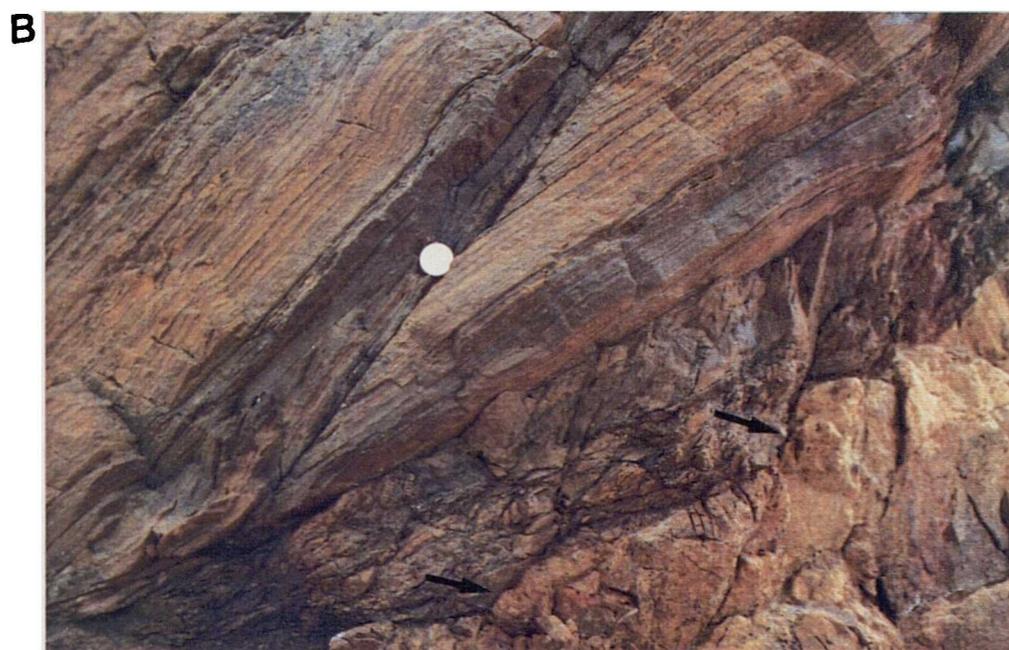
The Geological Survey's map (1932) indicates that the major fault downthrows to the east. The present-day cliff top exposure level shows that the fault strikes NNE-SSW (026°), and dips nearly vertical (figs. 5.35 and 5.38a). The bedding directly adjacent to the fault has been folded such that a minor fold axis trends parallel to the strike of the fault, suggesting that the major fault has been deformed and probably slightly rotated since the extensional deformation (figs. 5.37d and 5.38a). The original extensional displacement is unknown due to the inaccessible cliffs.

Approximately 200 meters east from the extensional fault, on a low coastal platform, a small displacement back-thrust is observed to propagate to the west from the lower detachment horizon, with displacement decreasing into a tip-fold above and below (fig. 5.37c). Two thrusts are also observed to ramp up from the lower detachment horizon, showing displacement to the east (fig. 5.38a). At the top of the cliff, a complex fold and thrust structure is developed above the upper detachment horizon, which now lies in the footwall block of the early extensional fault (figs. 5.37d and 5.38). Fore-thrusts and back-thrusts are observed to offset the N-S trending extensional faults (figs. 5.38b, and 5.39b). In detail, as the thrusts propagate to the west and encounter the early extensional faults, the thrusts ramp up section, and contractional duplexes are developed to accommodate displacement on all scales, resulting in steepening of the thrust planes (fig. 5.39c). Back-thrusts are also often developed to accommodate the displacement, resulting in the 'pop-up' structure above the detachment horizon (fig. 5.38b).

The probable fault sequence is shown in fig. 5.40. After the linked extensional/detachment horizon fault system formed during initial extension in the basin (fig. 5.40a), later contractional deformation resulted in minor fore-thrust and back-thrust development to the west of the fault, and initial folding adjacent to the fault (fig. 5.40b). During further contraction, buttressing adjacent to the fault resulted in development of the fore-thrusts and back-thrusts in the pop-up structure, which cut the minor extensional faults in the hangingwall of the major extensional fault (fig. 5.40c). In addition, the thrusts to the west of the fault ramped up and joined the upper detachment horizon (fig. 5.40c). Subsequently, the major extensional fault at Haafs Helia was cut and offset to the west (25 m.) by the thrust fault which joined and re-used the upper detachment horizon, thus carrying the pop-up structure in its hangingwall, and placing it in the footwall block of the early extensional fault (fig. 5.40d).

A UNDEFORMED HALF GRABEN

ORS NORMAL FAULT

E   W

DETACHMENT HORIZONS

LINKED?

HY   317   316   315

B FORE-THRUST AND BACK-THRUST

DEVELOPMENT

FOLDING

C BUTTRESSING

THRUST JOINS UPPER

DETACHMENT HORIZON   pop-up structure formed

FAULT ROTATED SLIGHTLY ?

D THRUST CUTS ORS NORMAL FAULT

scale

0   100

metres
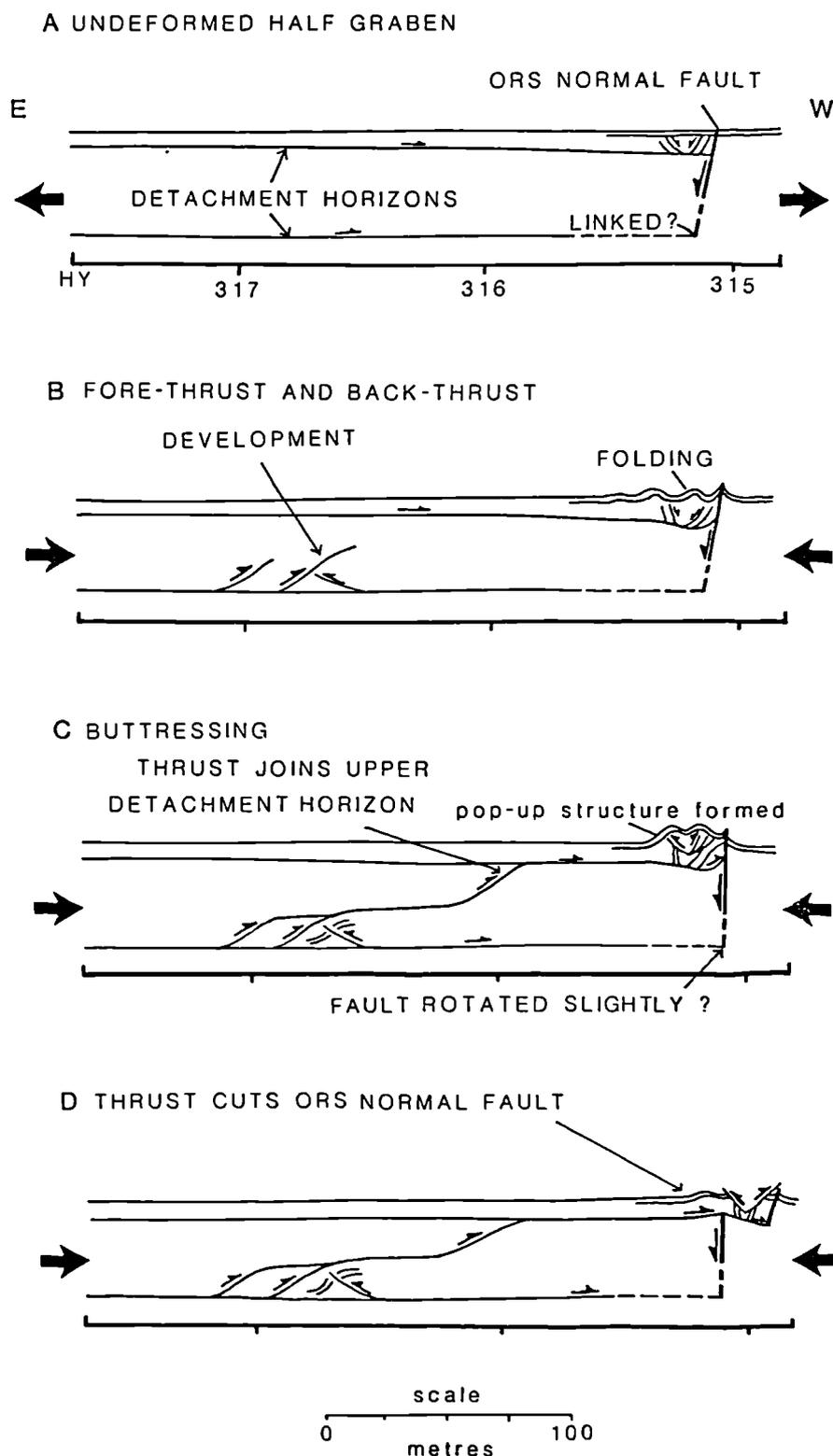
Figure 5.40. Diagram of sequential evolution of structures at Haafs Helia [HY 316304]. a) Undeformed half-graben showing development of linked extensional/detachment horizon system during the lower-MORS. It is uncertain whether the extensional fault links to the lower detachment horizon shown, as the cliffs are inaccessible. b) Shortening due to inversion of the basin; folding adjacent to the fault and minor fore-thrusts and back-thrust detach off of lower detachment horizon. c) Buttressing against east-dipping extensional fault; thrusts ramp up to join upper detachment horizon. d) Early extensional fault cut and displaced to the west by thrust.

In the case of earlier extensional faults dipping in the same direction to an advancing thrust, Welbon (1988) found that thrusts may ramp ahead of the normal fault such that the thrust interacts with the normal fault at a change in angle of ramp, cuts through the fault, or is pinned in the footwall, followed by buttressing above the thrust. Both ramping of thrust faults and intense deformation (buttressing) adjacent to the earlier extensional fault at Haafs Helia is observed. In addition, slight rotation of the earlier extensional fault has occurred (fig. 5.40c). Welbon (1988) suggests that slight rotation of the earlier extensional fault can result in changing stress trajectories during the deformation such that the earlier fault can be cut and displaced by the thrusts (c.f. Wiltschko and Eastman, 1983). The example at Haafs Helia indicates that this has most probably occurred during the later contractional event.

5.6.4 Whitaloo Point [HY 259288]

One hundred metres west of Whitaloo Point, at [HY 259288], an extensional fault system is observed to be modified by later contractional deformation. An east-dipping extensional fault detaches onto a lower bedding parallel detachment horizon at 'b', and a west-dipping extensional fault detaches onto an upper detachment horizon at 'e' (figs. 5.41 and 5.42). Two thrusts have ramped up from the lower detachment horizon: one in the hangingwall to the east of the east-dipping extensional fault at 'a', and one in the footwall of the east-dipping extensional fault, 2 metres west of 'b' (figs. 5.41 and 5.43a). Both thrusts re-use the detachment horizons, and contractional deformation has localised around the early extensional faults at 'c' and 'd' (figs. 5.41 and 5.43b and c). All of these structures are best observed on the headland of Whitaloo Point itself, which juts out slightly north of the coast (see fig. 5.36).

The structural sequence can be assessed by the cross-cutting relationships of the faults. The east-dipping extensional fault dips 68°, and 10-20 cm. of fault rock (cemented gouge) is observed along the fault plane (fig. 5.43c). The thrust which ramps up from the lower detachment horizon in the hangingwall of the east-dipping extensional fault joins the upper detachment horizon at 'c', and offsets the fault rock found on the east-dipping extensional fault, but by just 0.5 metres (figs. 5.41 and 5.43c). The upper detachment horizon has been deformed in a strongly asymmetrical fold at 'd' (figs. 5.41 and 5.43a). The fold is overturned along part of its exposure, and verges to the west.

Whitaloo Point (HY 259288)
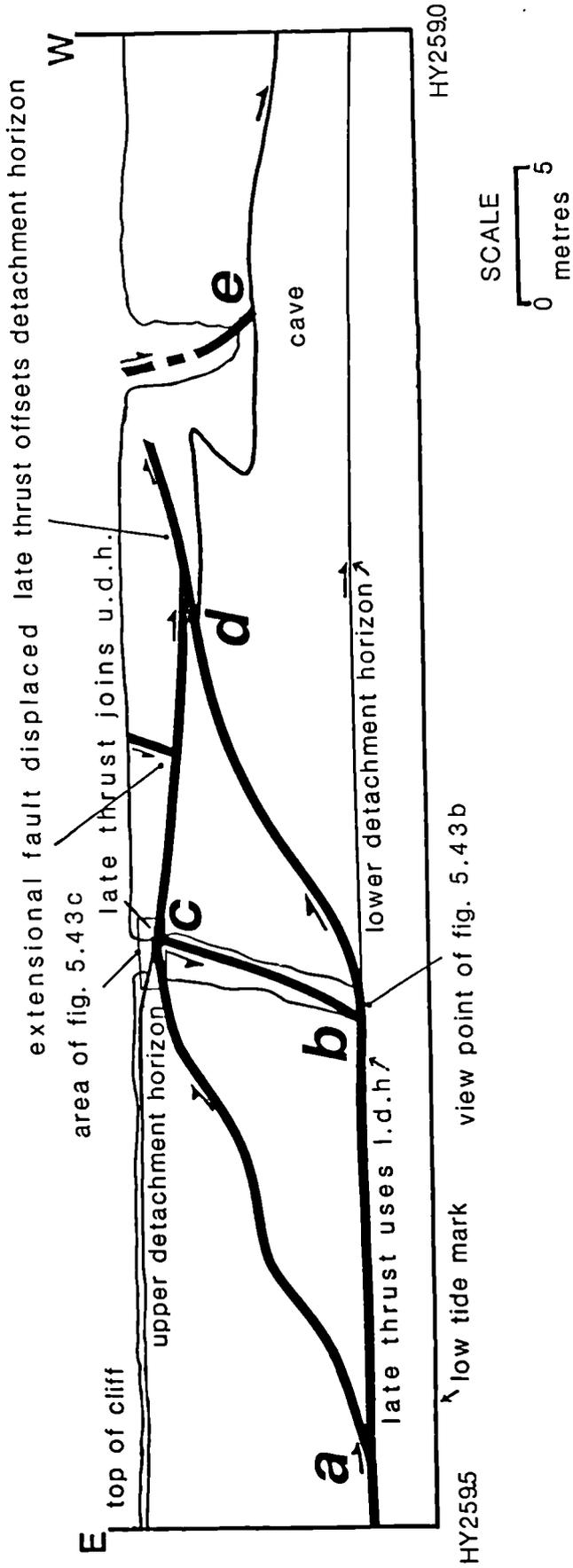
Figure 5.41. Cross section through Whitaloo Point [HY 259288], showing early linked extensional/detachment horizon fault system modified by later contractional deformation. Late thrusts ramp from bedding parallel detachment horizons at 'a' and 2 m. west of 'b'. Extensional fault links to lower detachment horizon at 'b', is cut by late thrust joining upper detachment horizon and offsets upper detachment horizon at 'd'.
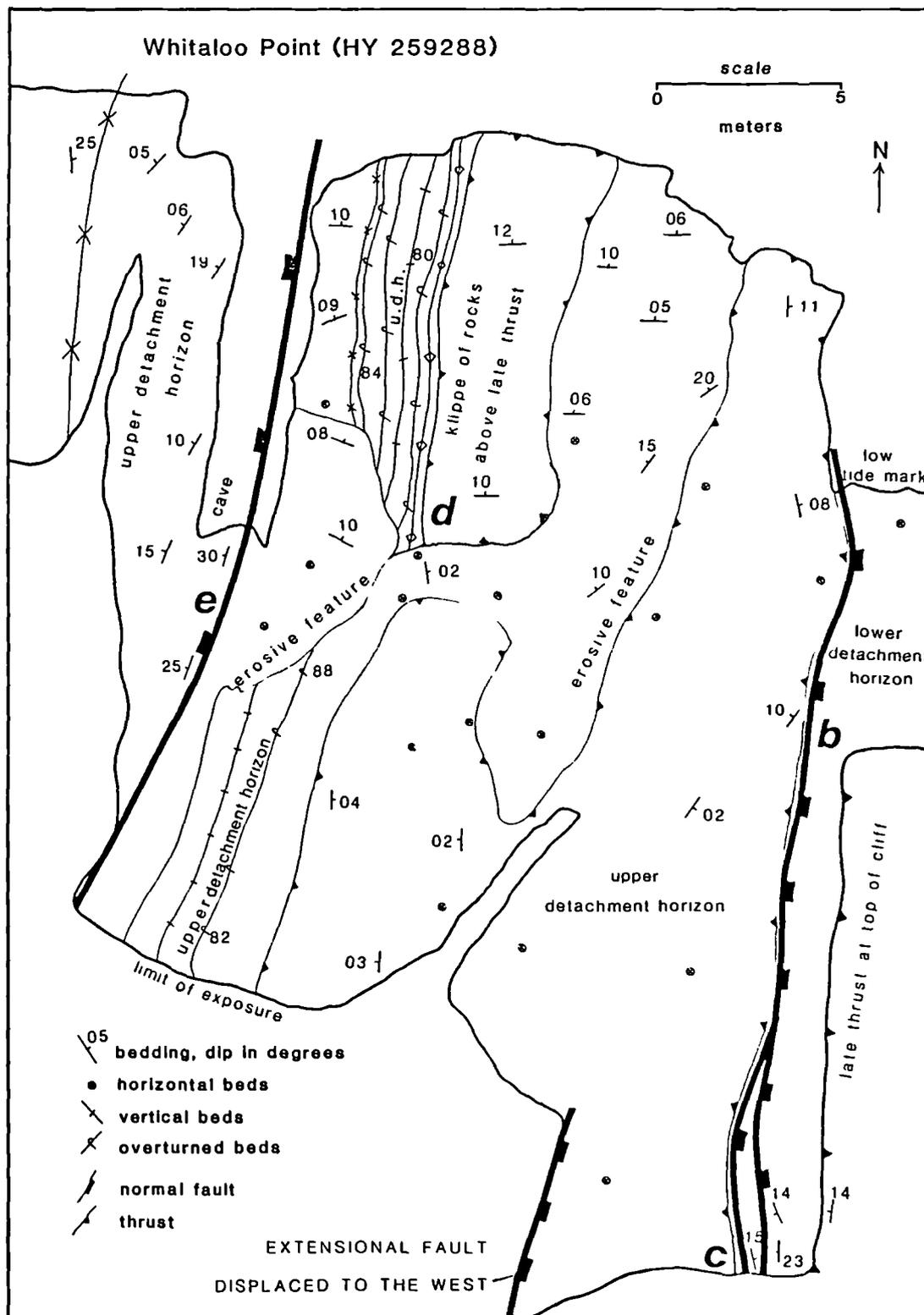
Figure 5.42. Detailed map of structures at Whitaloo Point, North Coast [HY 259288]. Note that upper and lower detachment surfaces represent approximately 5 m. in vertical distance apart. Klippe of rock rides on late thrust which re-uses upper detachment horizon, which displaces early extensional fault (see fig. 5.41). Tight asymmetric fold verging west deforms upper detachment horizon. See text for details.

Figure 5.43. Photographs of structures at Whitaloo Point, North Coast [HY 259288]. a) View looking north at asymmetric, west-verging fold developed in footwall of west-dipping early normal fault (see fig. 5.41). Upper detachment horizon(arrowed, D) is deformed in fold. Note also late thrust (arrowed, t) cuts through top of fold. Hammer 32 cm. long. b) View looking south (located on fig. 5.41) at early extensional fault. Main fault plane dips 68° ESE, but smaller fault splay is observed 2 m. into the footwall, giving 'lensoidal' appearance to fault zone. Bedding plane in forefront is lower detachment horizon onto which the extensional fault links. Note thrust ramping from lower detachment horizon (arrowed, t). Vertical distance from 'b' to 'c' is 5 m. c) View south at detail of top of breached and slightly inverted extensional fault at 'c'. Fault rock associated with earlier extensional faulting (arrowed, FR) displaced by small thrusts below upper detachment horizon (arrowed, UDH) to which part of the contractional displacement is transferred. Note considerable thickening of sediments above upper detachment horizon. The extensional fault at 'c' is displaced nearly 8 m. to the west (not shown); therefore, movement along this thrust clearly. post-dates extension on the normal fault. Tape measure 15 cm. in diameter. See text for details.
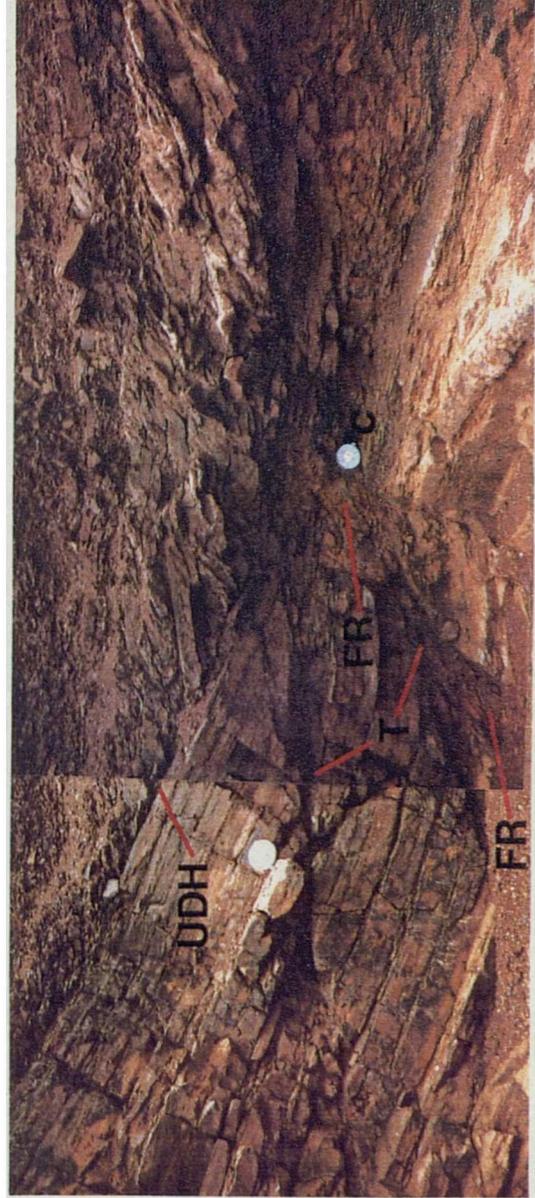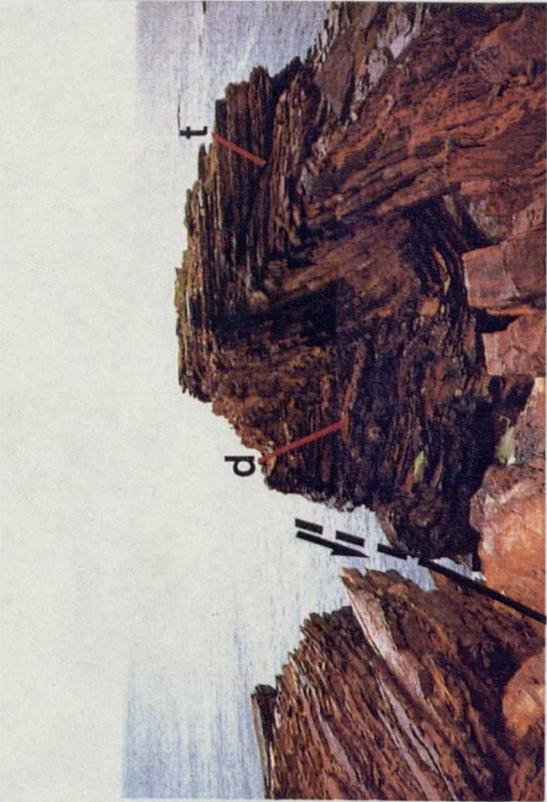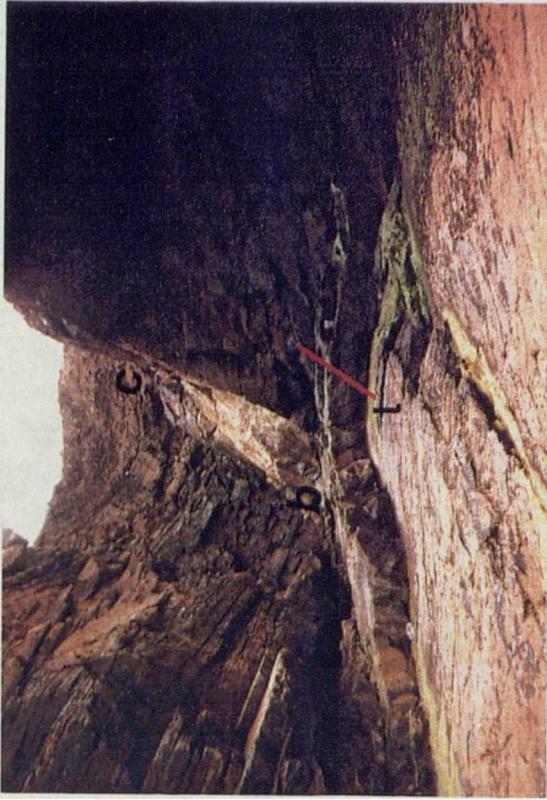
The thrust which ramps up from the lower detachment horizon in the footwall of the east-dipping extensional fault cuts through the upper detachment horizon 2 metres to the east of 'd' , and is observed cutting through the top of the asymmetrical fold (figs. 5.41 and 5.43a). The fold represents localised contraction which has buttressed against the west-dipping extensional fault. Breccias are preserved on the west-dipping extensional fault at 'e', similar to those described at Haafs Helia.

A duplex has developed above the upper detachment horizon, resulting in considerable thickening of the sediments (fig 5.43c). The total displacement on this contractional system is small; the normal fault has been displaced just 7-8 m. to the east along the detachment horizon which has been re-used by the later thrust (figs. 5.41 and 5.43). Shortening displacements have been accommodated by several structures: the thrust faults, duplex structure, and the asymmetrical fold. The development of the thrust and duplex structures would have aided in transferring displacement to an easier slip horizon structurally above which was not affected by the extensional faulting.

The observations at Whitaloo Point indicate that the earlier linked extensional/detachment horizon fault system has been breached by later thrusts showing movement to the W-WNW. The early east-dipping extensional fault has been only slightly reactivated in a reverse sense during the later contractional deformation, as the fault rock which is observed along its surface is displaced less than 0.5 metres. A well-developed vein array is present at this locality, and the related microstructures provide information about fluids which might have played an important role in the development of the contractional structures, and the probable timing of the contractional deformation. This is discussed in section 5.6.6.

5.6.5 Point of Nether Quina, Birsay [HY 250285]

A low-angle thrust fault ramping up from a detachment horizon and displacing early extensional faults to the W-WNW is observed 1 km. to the north of Birsay at the Point of Nether Quina [HY 250285] (figs. 5.36, 5.44, and 5.45).

Figure 5.44. Detailed map of Point of Nether Quina, Birsay [HY 286250]. Early ORS normal faults (red) displaced to west along late thrust (green) which has ramped from earlier-developed bedding-parallel detachment horizon (yellow). The offset portion of the ORS faults (effecting younger parts of stratigraphy) have been eroded away, so are only dashed. Extensional reactivation of ORS faults during the ?Mesozoic only affects portion of fault which has (inferred) deeper detachment. Note that a result of this is that the detachment horizon, which dips fairly steeply (25°) to the west, and the erosional exposure of the late thrust (green) are therefore offset and exposed on erosional highs represented by the Sowa Skerry Rock 'Pop-up' zone to the Skeres Naque 'Pop-up' zone. See text for details.

250

Point of Nether Quina, Birsay (HY 286250)

late thrust displaces ORS faults to WNW

Sowa Skerry Rock
'Pop-up' zone

Doonagua

Sowaskerry Geo

Skeres Naque
'Pop-up' zone

detachment horizon

The Runoos

late thrust

**Late thrust fault offset by
reactivated ORS faults**

displacement along late thrust decreases to the south

late extensional fractures cut dyke

dyke not offset by fault

dyke

285

285

Stromness Flags (MORS)

inaccessible cliffs

Skipi Geo

ORS normal fault
dip-slip movement indicators

?Mesozoic normal fault

ORS normal fault

detachment horizon offset by minor
(?Mesozoic) normal faults
(displacements <1-10 m.)

**Minor (?Mesozoic)
reactivation of ORS normal faults**

dyke

scale

0   100
meters

250

Figure 5.45. Photographs of structures at the Point of Nether Quina, Birsay [HY 286250]. a) View to WNW of erosional exposure of late thrust (arrowed, T) and bedding-parallel detachment horizon (arrowed, DH) on Sowa Skerry Rock (see fig. 5.45 for location). Sample bag in foreground 25 cm. long. b) Photo (looking north) of early ORS normal fault (arrowed, F) cut and displaced to WNW by late thrust on which hammer (32 cm. long) rests. Sowasker Geo is seen to the left. See fig. 5.44 for location. c) View to the east of extensional fractures cutting through dyke (horizontal at bottom of picture) (see fig. 5.44 for location). Hammer 32 cm. long.

A

B

C
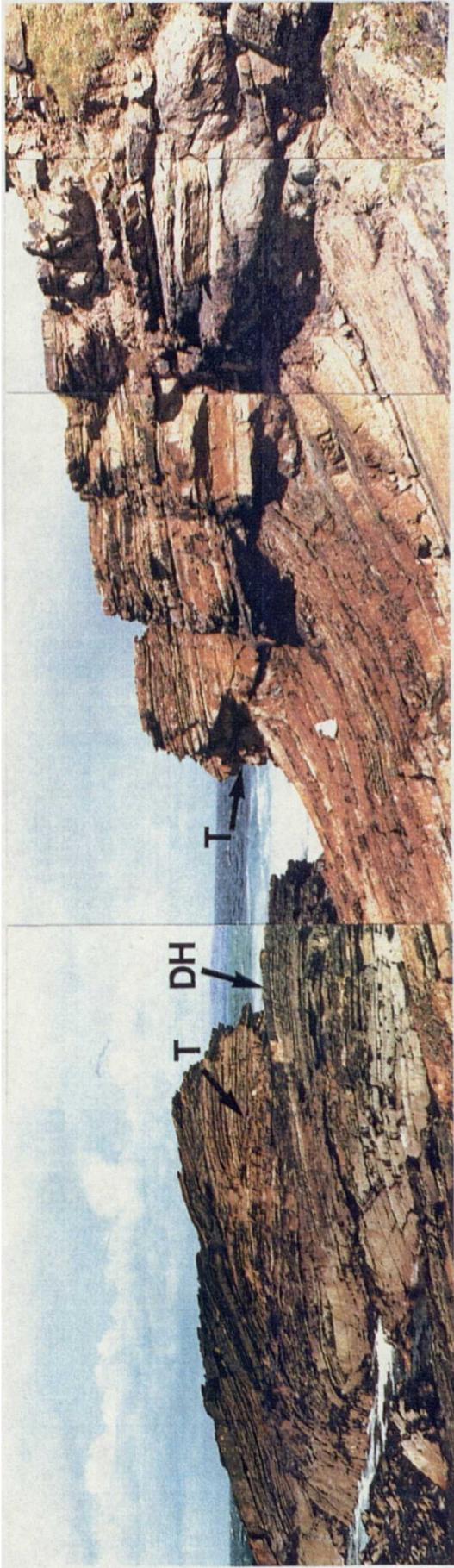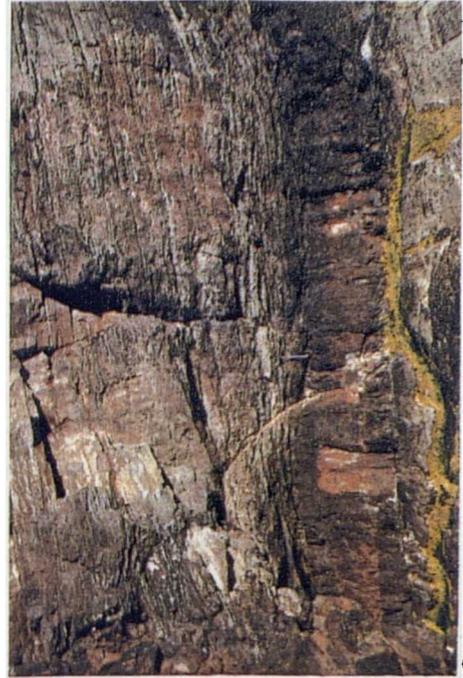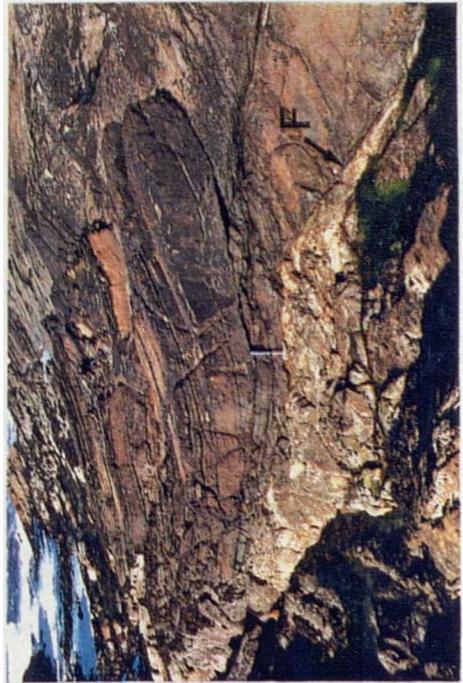
The two early extensional faults at Sowasker Geo and Doonagua trend N-S to NNE-SSW (fig. 5.44). A later thrust which ramps up from the earlier developed detachment horizon (figs. 5.44 and 5.45a) offsets the two early extensional faults at Sowasker Geo and Doonagua, 10 and 50 metres to the W-WNW, respectively (figs. 5.44 and 5.45b). The displacement on the thrust dies to the south. Fore-thrusts and back thrusts form pop-up structures which were developed during the later contractional deformation.

Later extensional faulting showing an E-W extension direction has affected the area and deformed a Permo-Carboniferous dyke exposed only at low tide (fig. 5.45c). The later extensional deformation has resulted in minor reactivation of the two early MORS faults at the Point of Nether Quina, offsetting the horizon containing the pop-up structures approximately 5 meters down to the east. The pop-up zones are now seen both at Sowa Skerry Rock and Skeres Naque (fig. 5.44). Astin's (in press) new sedimentological data suggests that a 250 m. extensional displacement down to the east is associated with a major N-S trending fault at the Point of Buckquoy [HY 247283], (fig. 5.36). This is the only definitive post-Permian extension observed along the north coast section.

5.6.6 Microstructures

This section describes the microstructures associated with the fault geometries mapped along the north coast section. An emphasis has been placed on establishing the role of fluids during deformation, and identifying the possible fluid pathways involved in each deformation event. The dominant deformation mechanisms operating during each deformation event will be discussed. Deformation microstructures will be described which are associated with: 1) the development of breccias along the fault planes of the early normal faults at Haafs Helia and Whitaloo Point; 2) displacement along the detachment horizons; and, 3) the development of the contractional structures, using the Whitaloo Point locality as the example.

5.6.6.1 Extensional fault breccias

The coarser-grained flagstone units at Haafs Helia and Whitaloo Point show the development of 1-3 cm. wide cemented breccias along the fault planes of extensional faults with displacements of 5 cm. to 5 m. (see fig. 5.38a). The breccias contain angular to blocky clasts 0.5-3.0 cm. in diameter, typically showing only slight rotation from the original bedding fabric in the horizon in which they are contained (fig. 5.46a).

Figure 5.46.   Optical micrographs of microstructures in breccia associated with extensional fault in coarser-grained unit of Stromness Flagstones, Haafs Helia, North Coast, Mainland, Orkney (sample 50090).   a)   Detail of relatively discrete planar fault zone (arrowed in centre) separating intact, indeformed rock (right, 'U') from breccia zone (left, 'BR').   Fault zone oriented parallel to the normal fault seen in the field, contained in breccia zone 3 cm. in total width.   Fault zone consists of fine-grained quartz matrix having irregular, dentate boundary with carbonate cement in undeformed rock and breccia zone.   The carbonate cement has many irregular, corrosive boundaries with quartz grains in both the matrix and undeformed rock, indicative of a replacement texture (arrowed).   XP. Scale bar 0.5 mm.   b) Clast ('C') 'floating' in matrix zone in breccia.   Note coarseness of grains in clast (similar to intact, undeformed rock) as compared to the matrix zone.   In PPL, matrix zone shows significantly higher percentage clay content than the undeformed rock and clasts in the breccia.   Note replacement texture of carbonate cement is also seen in the clast (arrowed).   XP. Scale bar 1.0 mm.
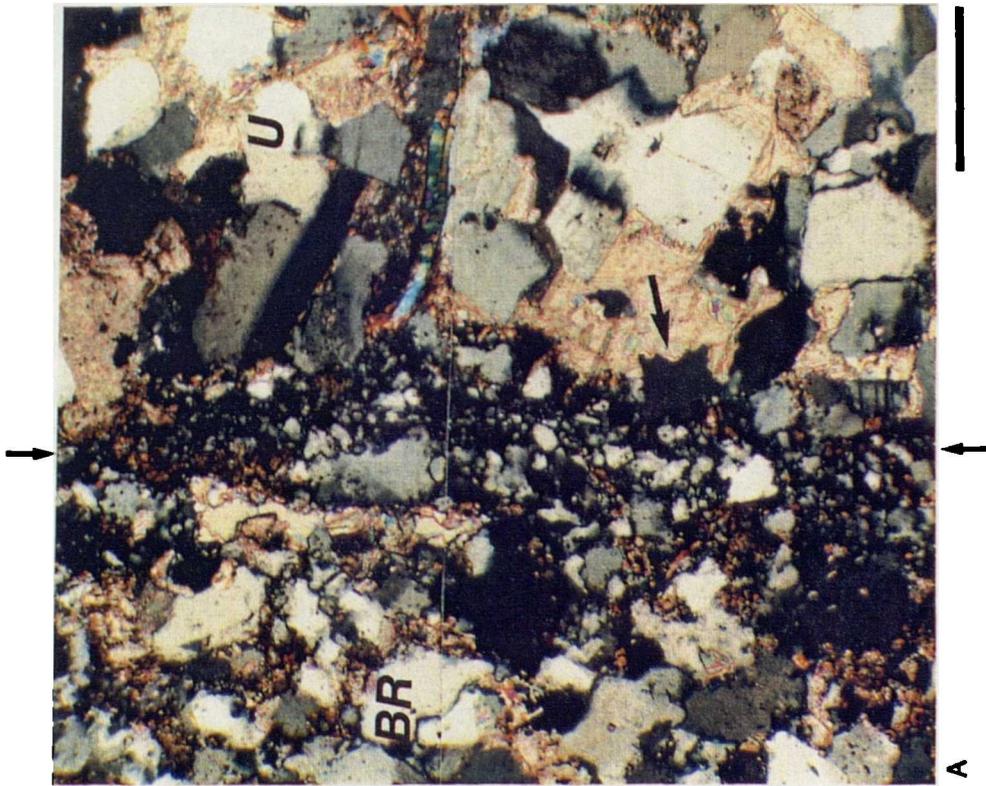
The undeformed coarser-grained units are dominated by 200-450 μm. quartz grains, commonly with sutured grain contacts, and contain negligible (<5%) porosity (fig. 5.46a). A carbonate cement completely fills pores which are frequently as large as the quartz grains. The boundary between the carbonate cement and quartz grains is commonly irregular and dentate. These observations suggest that dissolution and replacement are associated with the production of the carbonate cement.

A thin-section cut perpendicular to the fault shows a ' discrete, 0.5 mm.-wide, fault zone which separates the undeformed sediments from the breccia zone (fig. 5.46a). The fault zone is characterized by fine-grained quartz (20-200 μm.) with only minor amounts of carbonate cement. The margins of the fine-grained zone are irregular and dentate. The breccia zones are characterised by 0.5-2.5 mm. clasts of parent rock floating in a fine-grained matrix (fig. 5.46b). The matrix consists of quartz grains <200 μm. in diameter in a carbonate cement, and contains a significantly higher percentage of clay. The fine-grained clay is not present in the undeformed parent rock. The margin of the clast is defined by an irregular boundary which appears to follow the quartz grain boundaries in the clasts (fig. 5.46b). The grains within the breccia zone do not show any evidence for fracturing or cataclasis.

5.6.6.2 Detachment horizons

The sedimentary laminae in the organic-rich fish bed horizons alternate between quartz-rich domains, with grains <50 μm. in diameter cemented by carbonate, and clay-rich domains in which organic material is contained (fig. 5.47a). The laminae vary in thickness between 0.5 and 1.0 mm. During displacement along the detachment horizons, the laminae are tightly folded and also faulted by discrete low-angle extensional or contractional microfaults with up to 3 cm. offset. The microfaults are now defined by seams of organic material and clays. There is no evidence for fracturing or cataclasis of the grains.

Figure 5.47. Optical micrographs of microstructures in fault rocks from structures in Stromness Flagstones mapped in the field on the North Coast, Mainland, Orkney. a) Sample 49125. Fine-grained detachment horizon showing sedimentary laminae ('L') of relatively finer-grained, organic-rich domain (centre), and coarser, quartz-rich domains (outside), both rich in carbonate cement. Note solution seem (vertical) filled with organic-rich material and clays. XP. Scale bar 1.0 mm. b) Sample 50088a. Late carbonate vein offsetting fine-grained, organic rich domain in detachment horizon. Vein oriented perpendicular to, and links to bedding-parallel fault-flat carbonate vein (not shown). Note also linking vein-perpendicular 'flats', which follow anisotropy in fine-grained domain. See text for details. XP, ST. Scale bar 1.0 mm. c) Sample 50088b. Fault-flat carbonate vein along bedding-parallel fault ('F'). Fault and vein cross-cut the locally steeply-dipping laminae (defined by the fine- and coarse-grained domains) in the detachment horizon. XP. Scale bar 0.5 mm. d) Sample 50088a. Carbonate vein which links, and is oriented perpendicular to, a fault-flat vein below (not shown). Note bitumen filling vuggy pore space in centre. PPL. Scale bar 0.5 mm.
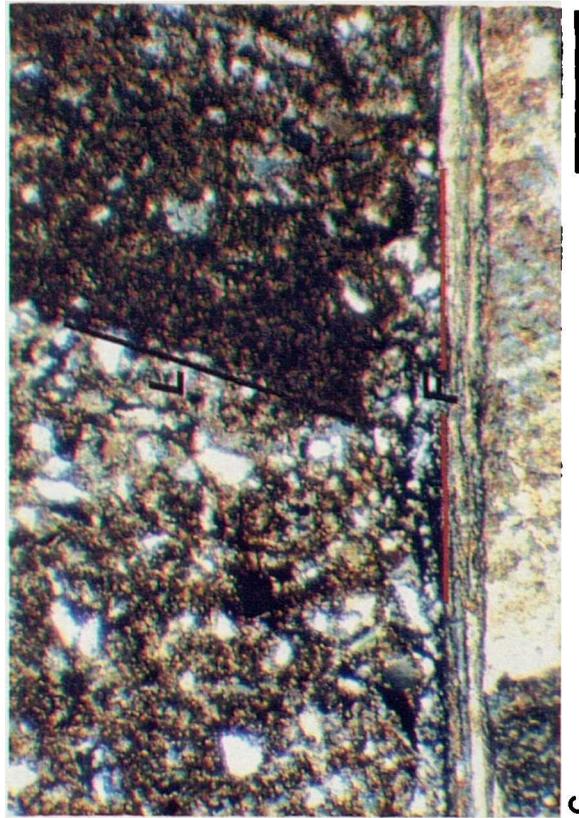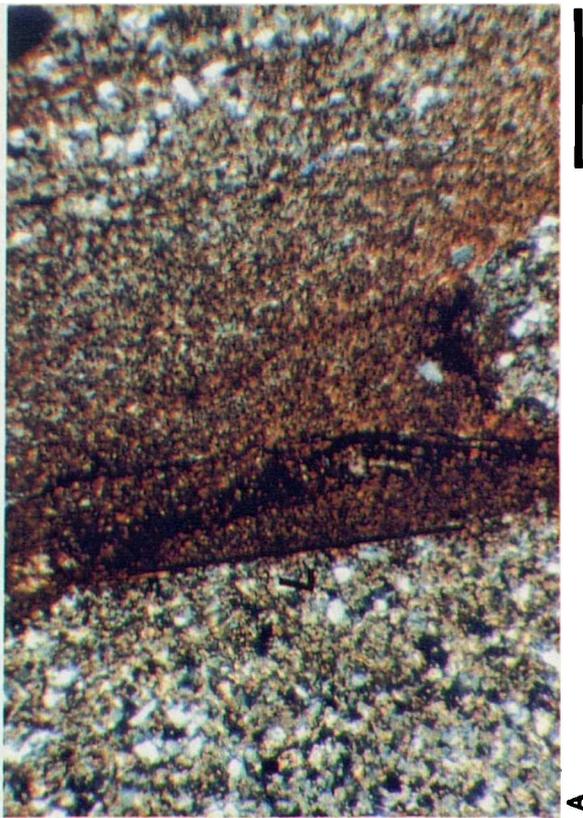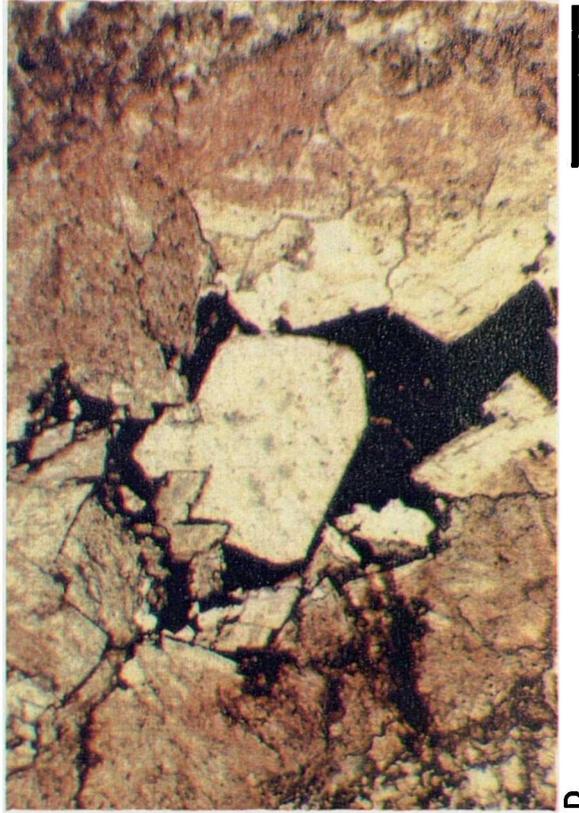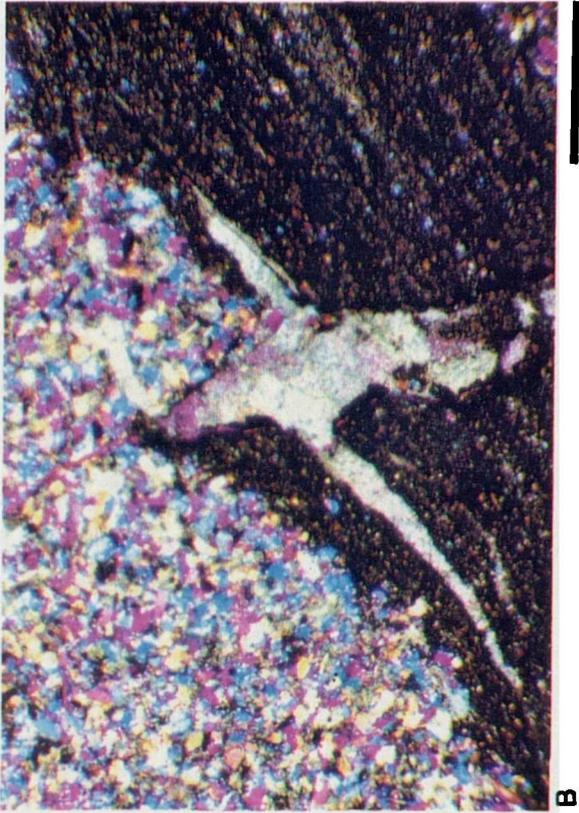
5.6.6.3 Contractional structures: Whitaloo Point as an example

Fig. 5.47b shows a thrust surface which has re-used a detachment horizon at Whitaloo Point; a fault-parallel carbonate vein cross-cuts and trends perpendicular to the sedimentary laminae in the detachment horizon. The fault-parallel veins are observed on both the fault-flats and .the fault ramps. There are also many lenticular carbonate veins which cross-cut and offset the sedimentary laminae (fig. 5.47c). These veins trend sub-perpendicular to, and link onto the fault-flat carbonate veins. Many of the fault-parallel and fault-perpendicular veins (1-4 cm. wide) can be observed on the field-scale at Whitaloo Point associated with the contractional structures. Enfield (1988) has reported similar fault-parallel veins from Scarfsferry in Caithness. In addition, the carbonate veins often contain vugs filled with solidified bitumen (fig. 5.47d). The carbonate veins are not seen along portions of the detachment horizons which are not re-used by the later thrusts.

5.6.7 Discussion of field and microstructural observations

5.6.7.1 Linked extensional/detachment horizon fault system

5.6.7.1a Conditions of deformation

The field work in this thesis confirms that the linked extensional/detachment horizon fault systems are the earliest developed structures observed in the area. This section will assess the conditions under which this gravity gliding could occur using the field and basin-scale information which is available.

Enfield (1988) has suggested that at this time, very large extension values (Beta values up to 2 to 3) in the Orcadian Basin correlate with the deposition of these sediments, some 4-5 km. of lower MORS Stromness and Rousay Flagstones, in a time period of 10 My. The thicknesses of these sediments have just recently been revised to a total of no more than 900 m. in the Orkney area (Astin, in press). However, up to 4 km. of MORS sediments are present in the Caithness area (Mykura, 1983). The large extension values (Enfield, op.cit.) and the thickness of sediments deposited suggests that relatively high subsidence rates were present at this time.

Due to the presence of the late Middle Devonian volcanics (in the Eday Group), and early maturation (at shallow depths) of the sediments, Astin (in press) has suggested that a high geothermal gradient (50° C per km.) existed in the Orkney area. The Stromness Flagstones were mature just prior to basin inversion, at less than 2.5 km. depth (see fig. 5.22). Therefore, active extension within the Stromness Flagstones during the MORS was occurring at depths of less than 2.5 km., and at temperatures of $\leq 125^{\circ}$ C.

5.6.7.1b Fluid flow directions and pore pressures

In a thick sequence of fine-grained sediments such as these, compactional fluids should be expected to be expelled vertically up in the sediment pile (Magara, 1976). However, overpresurring can result from incomplete drainage during compaction of a fine-grained sediment (Crans et al., 1980), or insufficient rates of fluid expulsion (Shi and Wang, 1986). Factors contributing to high pore pressure generation in sedimentary basins are overburden (Dickey, 1975), or aquathermal pressuring (Baker·, 1972; Bradley, 1975) or both (Shi and Wang, 1986). In the Orcadian Basin, both the subsidence rate and geothermal gradient were high at this time, as discussed above (Enfield, 1988; Astin, in press). Thus, overpressure could easily have developed in the Stromness Flagstones. In these conditions, Crans et al. (1980) showed that gravity gliding can occur in thin sediment packets on very gentle slopes ($<3^{\circ}$). Westbrook and Smith (1983) also showed that high pore fluid pressures may be associated with down-slope gravity driven movement. Thus, the conditions of deformation within the Orcadian Basin agree with the model presented by Enfield and Coward (1987) and Coward et al., (1989) for the formation of the linked extensional/detachment horizon fault system.

5.6.7.1c Deformation mechanisms

There is no evidence for fracturing or cataclasis of the grains in the breccias along the extensional faults linked to the detachment horizons. Clasts are observed floating within a fine-grained matrix within the breccia zones, and are internally undeformed. The matrix zones in the breccia contain grain sizes similar to that of the surrounding finer-grained horizons, and a significant amount of clay. The coarser-grained unit appears to have disaggregated during faulting, such that aggregates of the coarser grains were displaced into the fault zone filled with material from the surrounding finer-grained horizons. This is an example where grain-scale 'mixing' of juxtaposed sediments has occurred during faulting.

It is suggested that fracturing along the quartz grain boundaries disaggregated the clasts into the matrix zones in which independent particulate flow operated. Independent particulate flow is favoured in partially lithified sediments, and is facilitated by high pore fluid pressures (Borradaile, 1981). The initial grain boundary fracturing which acted to disaggregate the clasts into the breccia zones also would have been facilitated by high pore fluid pressures thought to have existed at this time.

The microstructures within the detachment horizons indicate that a small component of the displacement was localised along discrete microfaults which disrupted the sedimentary laminae. The lack of intragranular deformation associated with the discrete microfault zones and within the folds suggests that the sediments were weakly lithified at the time of disruption. A combination of disaggregation and independent particulate flow processes are suggested to have operated during displacement in the detachment horizons. Diffusive mass transfer mechanisms then operated to deposit the material within the microfaults. A larger component of displacement is suggested to have been accommodated along the interfaces between the bedding parallel detachment horizons and the undisturbed bedding surfaces above and below, where high pore fluids were most probably localised.

5.6.7.2 Late contractional faults

The cross-cutting field relationships of the thrusts with the linked extensional/detachment horizon fault system, and the microstructures of the fault rocks suggests that the thrusts are later features which formed subsequent to the early extensional/detachment horizon fault system.

The relationship of the late thrusts to the basin inversion event appears to be well-constrained. Astin (in press) has suggested that inversion of the Orcadian Basin occurred sometime in the Carboniferous, just after the Stromness Flagstones reached the oil window (see fig. 5.22). In the presence of mature hydrocarbons, fault systems formed at this time might provide pathways for the migration of the hydrocarbons.

Indeed, the veins related to the later contractional structures are filled with bitumen, indicating the mobility of hydrocarbon-related fluids, and suggesting that the thrusts were active just subsequent to maturation, most probably during basin inversion.

Fault-parallel veins are observed on the fault flats and ramps, cross-cutting, and also linking to fault veins which are sub-perpendicular to the fault flats. The presence of the veins suggests that high pore fluid pressures existed during the contractional deformation. In the Orcadian Basin, fluids expelled from the organic-rich mudrocks as a result of the hydrocarbon maturation could have contributed to creating the high pore fluid pressures. Pressure gradients created by the generation of hydrocarbons (Galloway, 1986), together with the . high geothermal gradients in the basin (Astin, in press) would have contributed to a thermobaric pore water drive during maturation which could have helped to 'feed' the pore fluid system.

The earlier extensional faults are only weakly reactivated in each example discussed along the north coast, and instead cut through and displaced by the thrusts, all of which show displacements to the W-WNW. At Whitaloo Point, the limited reactivation can be explained by the presence of a 10-20 cm.. thickness of fault rock which developed along the east-dipping extensional fault plane during extension (fig. 5.43c). The fault rock consists of well-cemented, fine-grained clays, representing an impermeable zone which would not easily provide a conduit for fluids during the later deformation. Thus the pore fluids released during maturation were channelled along the horizontal anisotropy of the detachment horizons, and displacement was most easily accommodated by thrusts moving along the surfaces with the high pore fluid pressures.

5.6.8 Conclusions

Section 5.6 focused on the structures and microstructures formed during early extension and gravity-driven movement of sediments along detachment horizons, and the subsequent inversion of the Orcadian Basin. The following points can be re-emphasized:

1. During early extension in the basin, the formation of detachment horizons showing shear to the WNW resulted from gravity-driven movement of sediments in the tilted hangingwalls of half-graben structures.

2. The detachment horizons represent localised slip horizons along which high pore fluid pressures existed. The high pore fluid pressures most likely resulted from insufficient rates of fluid expulsion in a thick sediment pile undergoing rapid subsidence at higher than usual geothermal gradients.

3. A combination of disaggregation and independent particulate flow processes operated in the detachment horizons, which appear to have been weakly lithified at the time of deformation.

4. Extensional faults which link onto the detachment horizons are associated with the development of 1-3 cm. wide breccia zones in the coarser-grained units of the flagstones. The breccias also show evidence that deformation took place in weakly lithified sediments, in which grain boundary fracture acted to disaggregate the sediments into the fault zone. Independent particulate flow mechanisms operated during mixing of aggregates of the coarser-grained sediment with the surrounding clay-dominated sediments.

5. Thrusts which re-use the earlier developed detachment horizons displace the early extensional faults. The contractional structures are most likely related to later tectonic inversion of the basin, most probably during the Carboniferous, just after hydrocarbon maturation was reached in the basin. The thrusts show displacements to the W-WNW.

6. During the later tectonic inversion, high pore fluid pressures were present along the thrust fault surfaces. In this case, evidence for the mobility of carbonate and hydrocarbon fluids is observed in the field and in thin section. Fluids released as a result of hydrocarbon maturation are suggested to have contributed to creating the high pore fluid pressures.

7. Post-Permian extensional structures are seen at Birsay, deforming a Permian dyke. The later extension (?Mesozoic) occurred in an approximately NE-SW direction, but resulted in only minor reactivation of the MORS extensional faults.

5.7   Synthesis

This section will synthesize the data and conclusions presented in each of the last three sections into the context of the tectonic evolution of the Orcadian Basin, together with the available data from other sources.   Fig. 5.48 is a summary diagram which shows the history of fault activity on the Mainland, Orkney.

5.7.1 Tectonic evolution and timing of development of the basin

As discussed in section 5.3, Rogers (1987) has discounted any evidence for the influence of strike-slip tectonics in the Orcadian Basin, as proposed by Ziegler (1985), Glennie (1984), Hamilton and Trewin (1985) and Trewin (1985).   Rogers (1987) showed quite convincingly that the Orcadian Basin sediments and palaeogeography do not show the pattern of small deep basins with contrasting stratigraphies and subsidence histories and localized inversion events which would be expected in a strike-slip setting (c.f. Ballance and Reading, 1980).   Roger's sedimentological data shows evidence for a pattern of syndepositional faulting most readily explained by NW-SE crustal stretching, and he strongly suggests the data reflects a common style of interaction of drainage and tectonism throughout Orcadian times.   Indeed, the control of the Caledonide structures on NW-SE extension in the Orcadian Basin has been demonstrated by Coward and Enfield (1987), Enfield and Coward (1987) and Coward et al. (1989).   In western Norway, previous ideas of strike-slip control for Devonian basins by Steel (1976) and Steel and Gloppen (1980) have been discounted by Hossack (1984) and Norton (1986), who found the basins were controlled by E-W extension.   The low angle boundary fault of these basins is an extensionally reactivated Caledonian thrust.   McClay et al. (1986) also document a number of Devonian extensional structures in the southern Scandinavian Caledonides.

A cause for the post-Caledonian Devonian extension in western Norway has been attributed to gravity-driven collapse of extremely thickened crust by Norton (1986).   The c. 80 km.-thick crust produced by the collision of Laurentia and Baltica in the middle Silurian was extended in the early-Middle Devonian in Norway (Norton, 1986).   The time gap between the shortening and extensional events is suggested to reflect the time necessary for decay of the strength of the thickened lithosphere.   McClay et al. (1986) and Beach (1985) have suggested that the orogen collapse model can be applied to the whole of the ORS extensional region.

A. lower MORS
Stromness Flagstone times

development of linked
extensional/detachment horizon
fault system

B. upper MORS to UORS
Scapa Sandstone times

NW-SE extension
on the NSF

sinistral transtension on the ESF

C. ?Carboniferous basin inversion
syn- to post- hydrocarbon
maturity

late thrusts and reverse
movement on the
North Coast faults

sinistral/oblique
slip on the NSF

N-S folds formed?

reverse movement on the ESF

D. ?Mesozoic transtension
post Permo-Carb. dyke
intrusion

extensional reactivation
on ORS faults at
Birsay

NNE-SSW folds
formed?

dextral transtension
on the ESF

SCALE

0   20
km

Figure 5.48. Summary diagram showing fault activity during Orcadian Basin evolution, and during subsequent uplift and strike-slip deformation of the basin. a) Lower MORS NW-SE extension; b) Upper MORS-?UORS extension/growth faulting; c) Post-UORS/Pre-Permo-Carboniferous uplift (?E-W compression); d) Post-Permo-Carboniferous dextral transtensional deformation.

Indeed, west of Orkney, Cheadle et al. (1987) have used BIRPS seismic data to calculate a pre-extension crustal thickness of c. 42-56 km., and the (probable) Devonian half grabens in the West Orkney Basin can be explained by gravitational collapse. However, as it is unknown how much displacement occurred on the thick mylonites which form the Moine Thrust, the thickness of the crust prior to the formation of the basins which are responsible for the ORS sediments observed onshore in NE Scotland is more speculative. Only a minimum estimate of displacement on the Moine Thrust Zone in northern Scotland can be made. The minimum displacement estimates are on the order of 50-70 km. (Elliott and Johnson, 1980; Butler and Coward, 1984). At least 50 km. of this displacement occurred after the intrusion of the Loch Borrolan igneous complex (Coward, 1985; Halliday et al., 1977), which is dated at 430 ± 4 Ma (van Breeman et al., 1979). Coward et al. (1989) suggest that if a displacement rate of 0.5 mm. per year is assumed, then Moine thrust activity would have continued until about 420 Ma. The earliest age assigned to the Lower ORS sediments is 394 Ma. Thus, a time span of approximately 25+ My occurred before deposition of the earliest preserved post-orogenic sediments (Coward et al., 1989). An even shorter time lag is possible when the positive topography present during initial extension on the over-thickened crust is considered (Coward et al., 1989). Sub-aerial basins which form at this time and remain elevated are subject to erosion, and thus sediments which represent early extensional phases of basin formation might not have been preserved. Uplift and erosion of the Caledonian belt might of occurred during this time. Watson (1985) has shown with geochronometric, P-T and stratigraphic data that most of the presently exposed Moine and Dalradian was metamorphosed at c. 30 km. and up to 40 km. depth, and that most of the 30 km. had been removed by erosion before the start of the Orcadian deposition.

Enfield (1988) notes that the time lag observed in the Orcadian Basin area appears to be considerably shorter than the time lags for the Southern Basin and Range Province (Wernicke, 1985) and the Himalayas (Coward et al., 1988). Both of these areas have very large magnitudes (up to 80 km.) of present day crustal thicknesses. Enfield suggests that the timing of extension of the Scottish Devonian basins might have been controlled by the post-Caledonian thermal evolution of the crust. Enfield follows the model of Kusznir and Park (1987), which explains how "whole lithosphere failure" can occur for given stress conditions. After crustal thickening the crust is weaker and is thus more prone to failure at lower stresses. When the Moho reaches 750° C, the strength of the lithosphere decreases to a critical point where the continental crust will fail in extension and begin to spread under

its own mass (Sonder et al., 1987). A time lag occurs after crustal thickening during which the lithosphere thermally equilibrates and the Moho reaches 750° C. The length of the time lag is dependent upon the magnitude of crustal thickening and the crust's initial thermal structure (Sonder et al., 1987). Thus, under certain conditions, the model can explain the "gravitational collapse" model invoked in other basins.

The relatively short time lag in the Orcadian Basin can thus be explained by suggesting that the thermal evolution of the Caledonides was different or possessed a different initial thermal structure (Enfield, 1988; Coward et al. 1989). The basins extended soon after thickening possibly due to a greater heat flux, indicated by the presence of late Caledonian granites beneath the Devonian basins and the limited Devonian volcanics seen on Shetland and Orkney (Halliday et al., 1987). Astin's (in press) burial history for the Orkney area also suggests a high heat flow was present during basin development, as discussed in section 5.3.

The early, dominantly NW-SE extension in the basin is reflected in the minor extensional faults seen in the lower MORS lacustrine facies sediments on the north coast of the Mainland (fig. 5.48a; see also section 5.6). The thick MORS sediment pile was undergoing rapid subsidence (Enfield, 1988), such that compactional fluids were expelled at insuffucient rates. This resulted in the development of high pore fluid pressures, which contributed to the gravitationally-driven movement of sediments in the tilted hangingwalls of the extensional half-grabens. The high heat flow which was inferred from the burial history of the sediments (Astin, in press) also contributed to the generation of the high pore-fluid pressures. This agrees with the high heat flux which was suggested to have existed during development of the basin, as inferred from the large-scale tectonics (Enfield, 1988').

Subsequent extension on the Scapa Fault System during the upper MORS to UORS occurred during deposition of the alluvial Scapa Sandstone (Astin, 1985, in press; Rogers, 1987) (fig. 5.48b). Early extension on the NSF is evidenced by the presence of fault rock directly adjacent to the fault which acted as a seal prior to hydrocarbon migration. Fluid pathways were influenced by the early extension and the fault seal records the precipitation of a pervasive illite cement. Kinematic indicators for early movements on the ESF are overprinted by later deformation. However, if the NSF was active in an extensional sense at this time, movement on the ESF in a sinistral sense is probable. This might correlate with the early sinistral movements suggested by Enfield (1987).

5.7.2 Evidence for basin inversion events

Coward et al. (1989) suggests that a "Middle Devonian basin inversion" may be due to the end effects of the Caledonian compression such that initial extension may have strengthened the crust sufficiently for the transmission of compressive deformation from the latest phases of the Caledonian orogeny. However, they prefer a mechanism involving inversion due to strike-slip movements, possibly on an early equivalent of the Great Glen Fault.

Rogers (1987) has shown that although the offshore data discussed by Enfield and Coward (1987) and Coward et al. (1989) may suggest a Middle Devonian inversion event (discussed in section 5.3.2), the onshore data shows no evidence for this. The problem with the interpretation of the offshore data is dating the fills within the basins. Shallow drilling by the British Geological Survey shows that the oldest sediments reached are of Permo-Triassic age. Enfield and Coward (1987) suggest that the basins contain predominantly ORS fills and therefore correlate inversion events within ORS sedimentation. Both Brewer and Smythe (1984) and Cheadle et al. (1987) suggest the basins are filled with a thicker Permo-Triassic sequence, and argue that Torridonian sediments are present in the basins to the west (Minches and Outer Isles). The only confirmed unconformity observed onshore is the MORS-UORS unconformity seen on Hoy (Rogers, 1987). The unconformity is very limited in extent, and may only be related to uplift of a footwall block during extension (Rogers, 1987). Rogers suggests that the active extension occurring on the Scapa Fault System (discussed above) during deposition of the Scapa Sandstones is in fact coincident with the time gap represented by the local unconformity seen on Hoy. Thus, he concludes that the ORS sediments in the Orcadian Basin represent a single, continuous, extensionally-controlled episode of subsidence which lasted from Siegennian/Emsian to Frasnian times. Astin's (pers. comm.) recent correlation of the Scapa Sandstones with the Hoy Sandstone confirms that the unconformity is probably only very localized.

In addition, as discussed before, there is no evidence for strike-slip movement on the Great Glen fault system at any time during deposition of the ORS sediments in the Orcadian Basin (Rogers, 1987). Thus, inversion events within the Middle Devonian, controlled by strike-slip movements on the Great Glen or not, are unlikely. Evidence for a Middle Devonian inversion event was not observed during the course of this study.

Evidence for a probable E-W oriented compressional event was observed (fig. 5.48c). Section 5.6 described thrust and fold structures striking sub-parallel to the early extensional faults on the north coast of the Mainland, in all cases offsetting the earlier faults. The thrusts show displacements to the W-WNW. Veins arrays associated with the contractional faults contain carbonate and bitumen, and it was suggested that the compressional event occurred just after hydrocarbon maturity was reached in the basin. As the Permo-Carboniferous dykes (Brown, 1975; Rock, 1983; Baxter and Mitchell, 1984) are not deformed as a result of the compression, the timing of the compressional event would thus best correspond to the subsequent inversion of the ORS basin in post-ORS to Carboniferous times, as discussed in section 5.6 (Astin, in press).

In addition, hydrocarbon migration pathways have been controlled by movement on the North Scapa Fault which post-dates initial extension on the fault (section 5.4, and discussed above). Sedimentological data suggests that the fault was initially active in upper MORS to UORS times (Astin, 1985, in press; Rogers 1987). Thus, the faulting event which influenced the migration pathways adjacent to the North Scapa Fault (inferred to be sinistral and oblique-slip in sense from the kinematic indicators), can also be related to the basin inversion event (fig. 5.48c).

The present-day reverse stratigraphic offset along the East Scapa Fault post-dates the probable upper MORS to UORS extension described by Astin, (1985, in press) and Rogers (1987), and pre-dates later dextral/transtensional movement on the fault (Enfield, 1988; see also section 5.5). Evidence for contemporaneous movement of hydrocarbons during the reverse movement on the fault is observed in the cataclastic fault rocks in the footwall of the East Scapa Fault. The minor folds and reverse faults in the hangingwall of the fault suggest compression was oriented in an approximately E-W direction. Thus, the reverse movement on the East Scapa Fault probably corresponds with the uplift event, just proceeding hydrocarbon maturity, and agrees with the dominantly E-W compressional structures observed on the north coast of the mainland (fig. 5.48c).

Coward et al. (1989) have suggested that Variscan deformation is associated with the post-ORS/Carboniferous inversion event discussed above. As mentioned in section 5.3.2, Coward et al. (1989) state that the orientation of folds on Shetland and Orkney, and the juxtaposition of the ORS basins of Shetland were a result of dextral strike-slip deformation along the Walls Boundary-Great Glen Fault systems during the Variscan. This corresponds

well with Roger's (1987) assessment of the timing of the 17 km. of dextral displacement along the Great Glen during the latest Devonian to early Permian. However, the structures mapped in this study suggest that the inversion was expressed dominantly as E-W compression along the N-S oriented faults, and that the N-S oriented folds most probably formed at this time. The NNW-SSE obliquely oriented folds adjacent to the NE-SW trending East Scapa Fault near St. Mary's represent folds which most probably formed during the later dextral strike-slip deformation described below.

5.7.3 Post-Permian strike-slip deformation in the basin

As discussed in sections 5.5.4 and 5.5.5, the reverse stratigraphic offset on the East Scapa Fault has been overprinted by extensional deformation, with a component of dextral strike-slip movement observed on the N-S trending portions of the fault (fig. 5.48d). This transtensional deformation post-dates intrusion of late Permian dykes (Brown, 1975; Rock, 1983; Baxter and Mitchell, 1984), and correlates with Coward and Enfield's (1987) later transtensional deformation event in the Orcadian Basin, most likely related to Mesozoic basin development in the Moray Firth. These events would also fit well with Roger's (1987) assessement that a further 8 km. of dextral displacement occurred on the Great Glen Fault system during the Mesozoic. The NNW-SSE orientated folds which are locally developed near St. Mary's are probably a result of the transtensional deformation. Slight extensional reactivation of the lower MORS faults near Birsay also occurred at this time.

5.8 Fault rock development along major faults on the Mainland

This section aims to summarize fault rock development along the major faults on the Mainland of Orkney mapped in this study, and to outline some of the more important influences on fault rock development in sedimentary basins. A summary fault rock map of the Mainland (fig. 5.49) is presented in order to provide a reference to the range and distribution of fault rock types. General microstructural observations of the fault rocks will be included in the discussion below in order to provide details about the fluid flow history in the fault zones.

The first point is that the fault rocks evolved at different times in the basin history, and this is important in terms of the mechanisms involved in their development. For example, independent particulate flow processes dominated the development of the fault rocks on the north coast of the Mainland, which were only weakly lithified at the time of deformation.
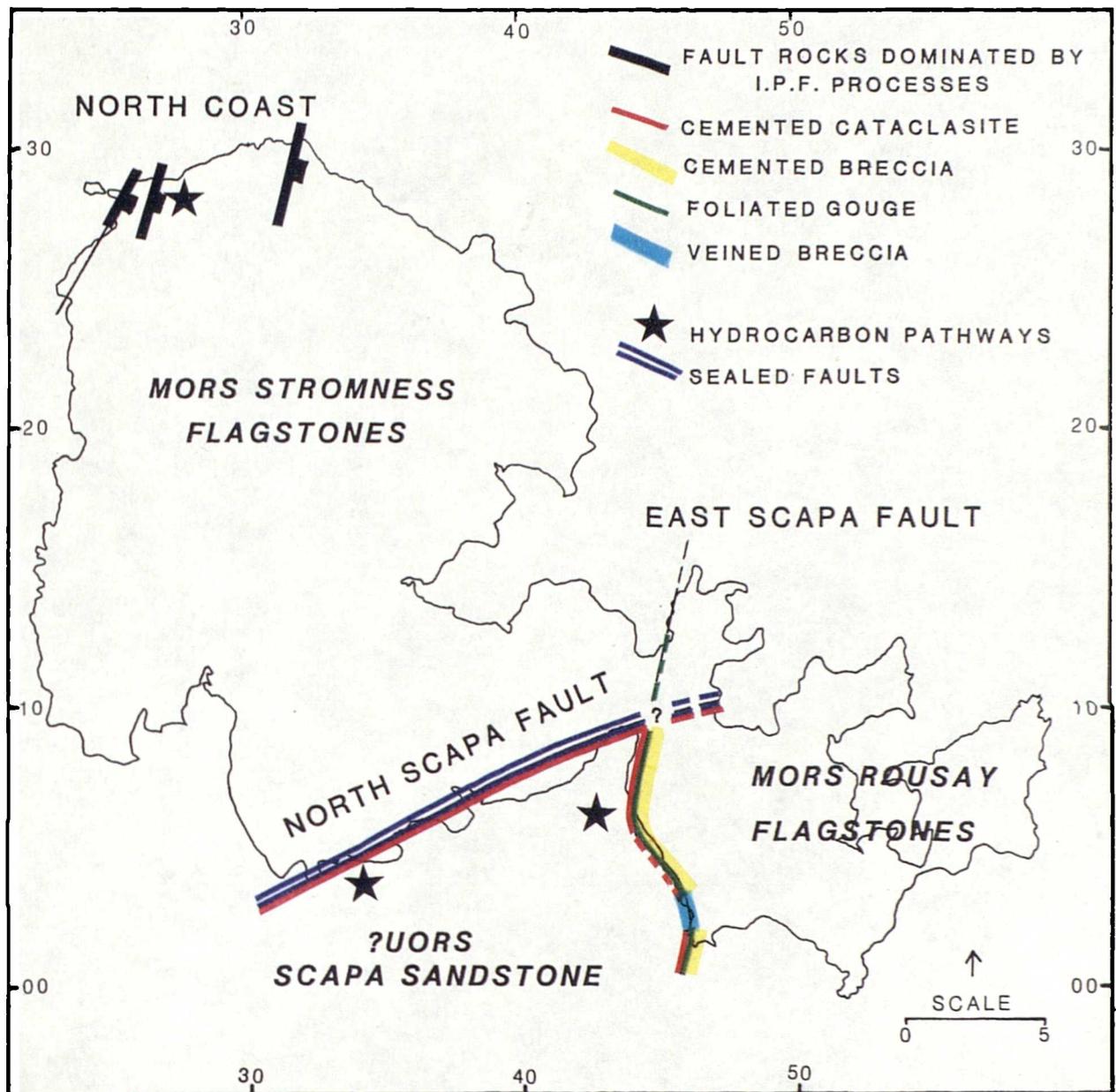
Figure 5.49. Summary diagram showing fault rock development on the major faults of the Mainland, Orkney.

In the case of the extensional fault breccias associated with displacement along the linked extensional/detachment horizon fault systems exposed on the north coast, disaggregation and limited mixing of coarser-grained horizons with the finer clay-dominated horizons occurred by independent particulate flow processes operating within the fault zone. The presence of clay would act to reduce the permeability and porosity in the fault zone. The sediments in the detachment horizons also formed by independent particulate flow mechanisms, which disrupted the sedimentary laminae within these localised displacement horizons. Diffusive mass transfer mechanisms then operated to deposit material within discrete microfaults within the detachment horizons. In both examples, the presence of high pore fluid pressures aided the independent particulate flow processes. Thus, while at the time of deformation these fault zones acted as fluid pathways, both presently contain material (clays and organic matter) which would inhibit later fluid flow into these zones.

In contrast, the fault rocks derived from the relatively porous sandstones adjacent to the North Scapa and East Scapa Faults during faulting relatively early in the diagenetic history of the sediments show evidence for intense cataclasis. The cataclastic sandstone adjacent to the North Scapa Fault contains pervasive illite cementation, which records evidence for enhanced fluid flow through the sandstones. The cataclasis, coupled with the post-faulting cementation, has resulted in a fault rock which acted as a seal to the migration of fluids later in the basin history (fig. 5.49). This example also has indicated that strain hardened zones can preserve fault seals during later reactivation of the fault. However, the example also shows that later cataclastic deformation can still affect the fault zone directly outside the sealed domain, and provide pathways for fluids where fracture permeabilities are high.

Cataclastic fault rock development in lithologies with very different starting microstructures than the porous sandstones discussed above can be contrasted by examination of the fault rocks derived from the fine-grained Rousay Flagstones adjacent to the East Scapa Fault (fig. 5.49). The fault rocks derived from the flagstones during faulting late in the basin history (i.e., during inversion and later deformation events along the East Scapa Fault), are fine-grained, incohesive gouges with a pervasive fabric oriented sub-parallel to the fault. Microscopically, the foliated fault gouges show evidence for fluid flow in the form of seams and microfaults filled with clays and organic material. The material represents the migration of fluids through the anisotropy created by the foliation.

Cemented fault breccias have been reworked into the foliated fault gouges along the East Scapa Fault (fig. 5.49). Blocks of the breccia are often oriented sub-parallel to the fault. Their pervasive cementation suggests that they preserve evidence of fluid flow associated with an earlier faulting event. The orientation of the cemented blocks represents a permeability barrier within the foliated fault gouge such that fluids in the fault zone are likely to flow parallel, rather than perpendicular, to the fault plane, as evidenced by the material now deposited sub-parallel to the foliation.

The East Scapa Fault provides an example of the heterogeneous nature of fault rock development along major faults (fig. 5.49). In this case, the fault geometry and movement sense during transtensional reactivation of the fault appears to have influenced the fault rock evolution. A veined breccia, most probably representing an implosion breccia, has developed at the site of an extensional bend along the fault. Locations of dominantly extensional movement sense contain material in the fault zone which indicates significant dilatancy accompanied the deformation at this time, as some of the material is derived from a non-local source. A zone of dominantly dip-slip to oblique-slip movement along the fault is characterised by fault zones with discrete fault rocks domains oriented sub-parallel to the fault (fig. 5.49). Each fault rock domain preserves evidence for a long movement history, demonstrating that microstructural analysis can aid in elucidating fault histories within basins.

In summary, these examples show that fault geometry and kinematics, lithology, and the timing of the deformation within the basin history (and thus the mechanisms which operate in the fault zone) are important factors in the evolution of fault rocks along major intrabasinal structures. Detailed microstructural analysis of the fault rocks has also provided information about fluid flow within these fault zones.

Chapter 6. The Durness Fault Array

6.1 Introduction and Aims

In the NW Sutherland region, a NW-SE/NE-SW trending extensional fault array affects Lewisian basement rocks and Cambro-Ordovician sequence rocks (fig. 1.1). In Sango Bay, Durness, [NS 415675], the extensional faults cut through thrusts developed during the Caledonian Orogeny, 430-408 Ma. (Johnson et al., 1985), (fig. 6.1). Offsets of the Caledonian thrust sheets in the bay can be used to estimate displacements along the extensional faults cutting through the area. This chapter focuses upon extensional fault rock evolution within a mylonitic quartzite thrust sheet approximately five meters in thickness in Sango Bay, which lies in the hangingwall block of the NE-SW trending Sangomore Fault (figs. 6.1 and 6.2). The fracturing and cataclasis involved in the development of the extensional fault rocks studied in Sango Bay suggests that the fault rocks deformed at depths less than 10 km. (Sibson, 1977). At normal geothermal gradients of $\sim 25^{\circ}$C/km., this corresponds to temperatures of $<250^{\circ}$ C.

The aims of this chapter are to: 1. outline the range of cataclastic deformation features observed in the field associated with the extensional faulting; 2. describe in detail the cataclastic microstructures in the quartz mylonite affected by the extensional faulting; 3. identify the mechanisms and processes involved in the development of the cataclastic fault rocks; 4. assess the influence of the initial mylonite microstructure on the fracture processes, and; 5. place the data from Sango Bay into context of the regional fault array.

First, section 6.2 provides a regional background of the study area. Section 6.3 reviews the previous work on the extensional fault array in the region. Section 6.4 presents background field observations from Sango Bay. Section 6.5 focuses in detail on the cataclastic fault rocks and the related microstructures developed from the quartz mylonite. Section 6.6 discusses the deformation mechanisms involved in the development of the quartz cataclastic fault rocks. Section 6.7 discusses the influence of initial microstructure on the evolution of the fault rocks, and the data from Sango Bay in context of the regional fault array. Section 6.8 outlines the conclusions to this chapter.
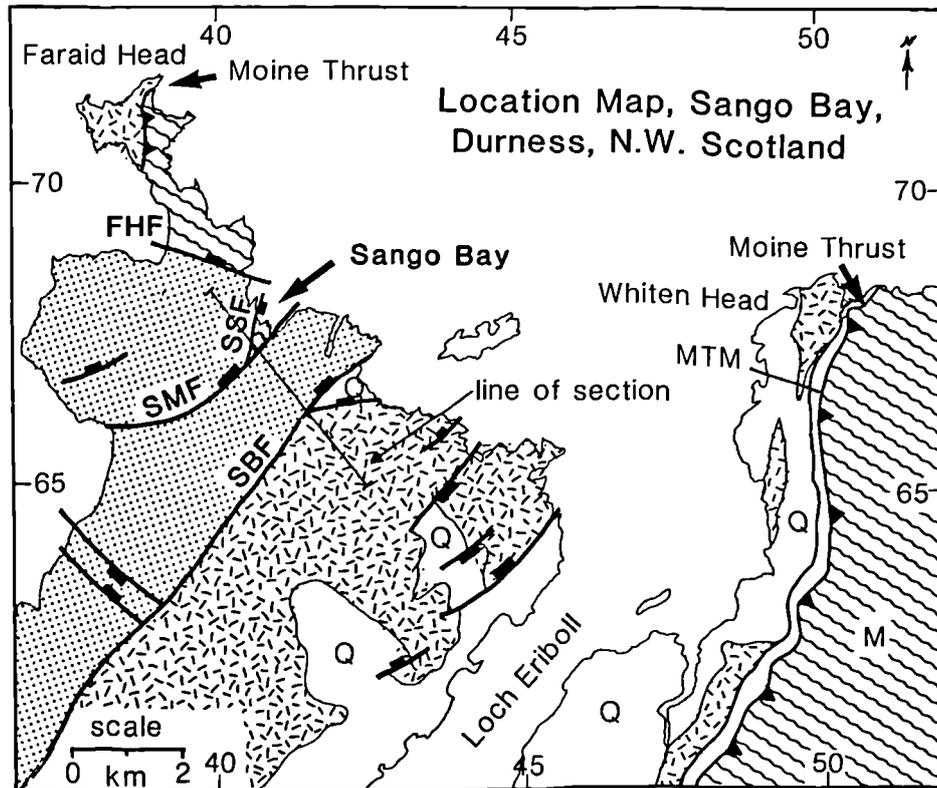
Figure 6.1. Location map for Sango Bay, Durness, N.W. Scotland. FHF, Faraid Head Fault; SSF, Sango Sands Fault; SMF, Sangomore Fault; SBF, Sangobeg Fault; Q, Cambrian quartzite; Lst, Durness Limestone Sequence (dot ornament); MTM, Moine Thrust mylonites; Lewisian (dashed line ornament); Moines (wavy line ornament). Line of section shown in fig. 6.2.
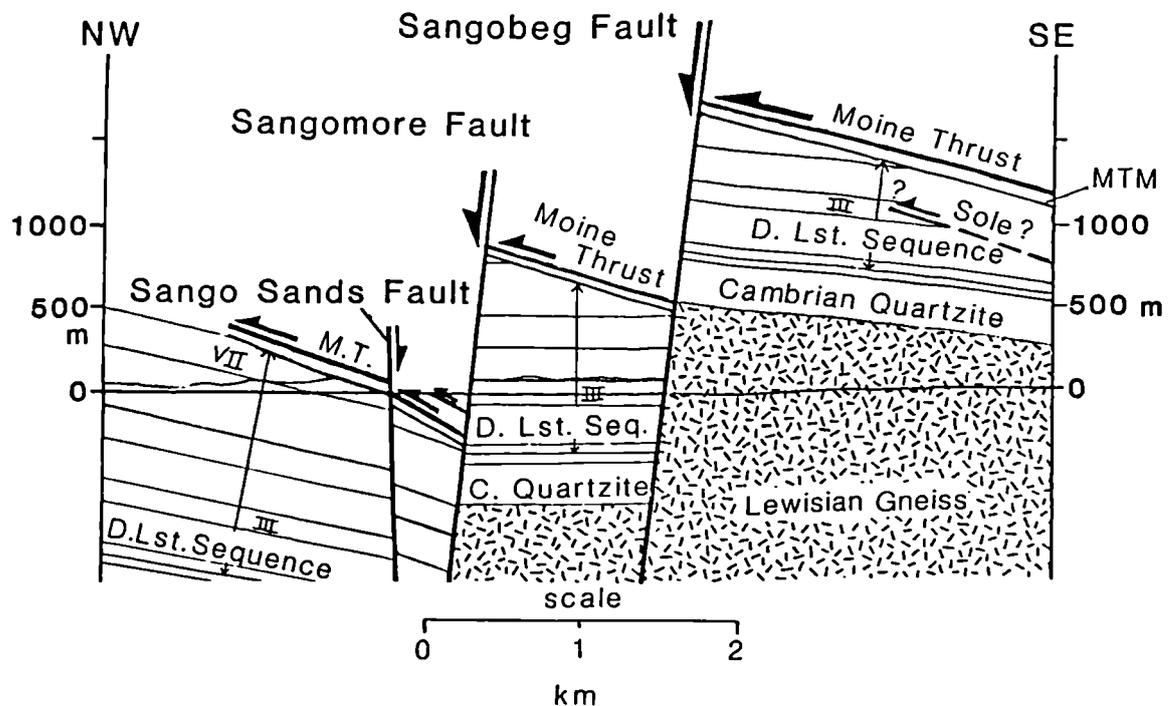
Figure 6.2. Cross section through the Durness area showing Moine Thrust plane (projected from thrust zone to the east of Loch Eriboll) carrying Moine rocks to the WNW over Lewisian basement, Cambrian quartzite and Durness Limestone Sequence, and displaced vertically by steeply-dipping normal faults near Durness. III is Sailmhor Member of Durness Limestone Sequnce, VII is Durine Member. Thrust carrying Moine Thrust mylonites shown just below Moine Thrust. Moine Thrust faulted down in Sango Bay (to the east of the SSF) carries Oystershell mylonite in hangingwall; thrust carrying Lewisian mylonite in hangingwall shown structurally above (see fig. 6.3). Sole? is Sole Thrust Plane. Location of section shown in fig. 6.1.

6.2 Regional background

In the north west Highland Region, WNW-directed thrusting of intensely deformed Moine (Proterozoic) sediments over a foreland sequence of Lewisian (Archean to lower Proterozoic) basement, Torridonian (upper Proterozoic) arkosic sandstones, grits and conglomerates, and Cambro-Ordovician shelf sediments (e.g. Peach et al., 1907; McClay and Coward, 1981) occurred during the Caledonian Orogeny, 430-408 Ma (Johnson et al., 1985). The resulting mylonitic rocks, in particular the Cambrian quartzites, have been the focus of many studies on ductile deformation related to the emplacement of the deeper level thrust sheets to the higher structural levels in the Moine Thrust Zone (e.g. Weathers et al., 1979; White, 1979; Law et al., 1984, 1986; Ord and Christie, 1984; Knipe and Law, 1987; Law and Potts, 1987; Law, 1987). Cataclastic deformation related to movement on shallow level thrusts, now the structurally lowest thrust sheets in the Moine Thrust Zone, has been studied by Blenkinsop and Rutter (1986) and Bowler (1987, 1989). Knipe (1989b) investigated deformation processes involved in fault rock evolution on all the major faults in a traverse across the Moine Thrust Zone at Assynt.

6.3 Previous work on the extensional fault array in N.W. Scotland

The steeply-dipping, NE-SW trending extensional faults in the Durness region are of opposing dip (to the north west) to those seen in the MOIST profile, and also to faults in the West Orkney Basin, some of which link to onshore structures in north east Scotland, which contain Old Red Sandstone fills in their hangingwalls (Enfield and Coward, 1987) (fig. 1.1). Laubach and Marshak (1987) studied the NE-SW/NW-SE trending fault array onshore in north west Sutherland, and concluded that the fault orientation has been controlled by basement-fabric geometry and that the principal extension direction was NW-SE. Kirton and Hitchen (1987) observed two opposing structural styles in seismic data to the north west of Scotland. The area to the north of the Solan Bank High, a NE-SW trending horst just north west of the West Orkney Basin (fig. 1.1), is dominated by listric, transfer, and domino type faults, all downthrowing to the north west, as in the Durness area. To the south east of the Solan Bank High, the area is dominated by faults downthrowing to the south east, including those of the West Orkney Basin.

Kirton and Hitchen (1987) concluded that extensional tectonism north of the Scottish mainland occurred in two distinct locations and times: the north west-dipping faults to the north of the Solan Bank High, initiating extension during the middle Jurrasic, and the extensional reactivation of the former Caledonian thrusts to the south east of the Solan Bank High occurred in the Permo-Triassic. Duindam and van Hoorn (1987) also conclude that the northerly Sula Sgeir and West Shetland half-graben basins (fig. 1.1), with west-dipping bounding faults, cannot be explained as reactivated Caledonian thrust planes. They suggest that it is possible that these west-dipping faults form a large-scale antithetic set belonging to a major east-dipping fault further west.

NW-SE trending structures are also present in the north west Sutherland region, most notably the Faraid Head Fault, which displaces the Moine Thrust (senso stricto) vertically several kilometers (fig. 6.1). The NW-SE trending structures have been put into context by Laubach and Marshak (1987), who also studied the style of faulting and associated fault block rotation in north west Sutherland. The large displacement (>1 km.), NE-SW trending extensional faults in the region show decreasing displacements inland (toward the south west) (Laubach and Marshak, 1987). Movement on the NW-SE trending faults is interpreted as reflecting the accommodation of differential extension of the hangingwall along the large NE-SW trending faults (Laubach and Marshak, op.cit.). The NW-SE trending faults are also thought to divide the hangingwall into blocks which moved independently.

Therefore, Laubach and Marshak (op.cit.) suggest the decrease in displacement along the NE-SW trending faults occurred in "abrupt jumps", though the regional expression of these jumps resulted in a scissors geometry. They found that slip lineations on the NE-SW trending faults in the region are down-dip and coaxial, and complex and non-coaxial on the NW-SE trending faults. From these observations, they suggest two models for the evolution of the extensional faults in the NE-SW orientation (fig. 6.3). In both models, the NW-SE trending faults are considered to be confined to the hangingwall blocks of the NE-trending faults. The first model is one in which the NE-SW trending faults are planar (fig. 6.3a). In this case, the slip lineations on the NW-SE trending faults would be oblique but parallel to the dip-slip lineations on the NE-SW trending faults. In the second model, the NE-SW trending faults are modelled to be listric, or to have rotated around a horizontal axis during progressive extension (fig. 6.3b).
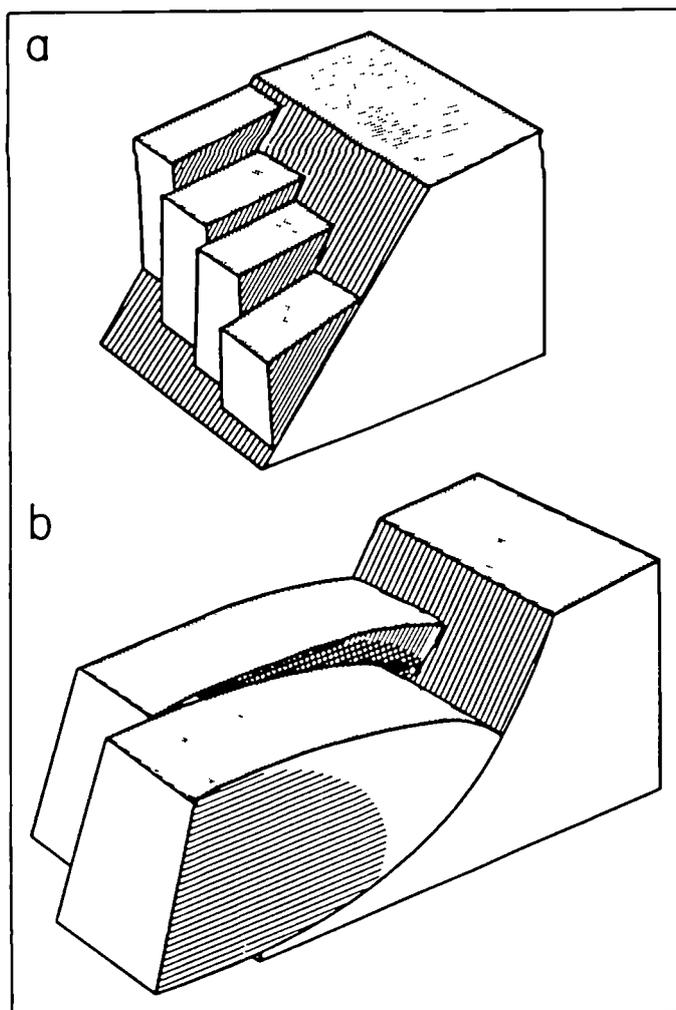
Figure 6.3. Block diagrams of planar and listric normal faults and the predicted pattern of slip indicators on master and cross-faults. a) Geometry of hangingwall fautl blocks on a planar fault. b) Geometry of hangingwall fault blocks above a listric fault. Note crossing sets of slip lineations. (from Laubach and Marshak, 1987).

In this situation, the hangingwall blocks would rotate, and the increments of movement on NW-trending faults would be non-coaxial (c.f. Jackson and McKenzie, 1983). They conclude that the slip lineation observations favour the last model.

Major structures with similar NW-SE trends have been suggested to exist just offshore. For example, to accommodate for differences in Caledonian structures onshore and offshore in northern Scotland, Coward (1986) has suggested a Caledonian tear fault or lateral ramp along the north coast of Scotland separates the thickened crust in the north from the thin-skinned thrust zone in Sutherland. Duindam and vanHoorn (1987) have suggested a transfer fault zone, the Coastal Transfer Zone, formed just offshore from the north coast during the Devonian extensional event. Laubach and Marshak's (1987) onshore . data of fault displacements and fault movement directions suggests that the NW-SE faults represent the transfer set to the NE-SW faults.

Nevertheless, the age of the north-west dipping fault system is still unresolved. Coward and Enfield (1987) suggest these faults appear to be confined to the eastern margin of the Minch Basin (fig. 1.1). This is a large half graben to the west of the mainland which is considered to have been initiated in the Mesozoic (Steel and Wilson, 1975) or earlier, in the Torridonian (Kilenyi and Standley, 1985) or Devonian (Enfield and Coward, 1987). Coward and Enfield (1987) state that the north west-dipping faults cannot be seen on the seismic reflection profiles offshore to the north, and that they most probably represent antithetic faults associated with extension in the Minches.

6.4 General field observations from Sango Bay

6.4.1 Introduction

In Sango Bay, mylonites deformed during the Caledonian Orogeny and derived from Cambrian quartzite and Lewisian gneiss are thrust over the youngest member of the Cambro-Ordovician Durness Limestone Sequence, the Durine Member (fig. 6.1). The thicknesses of the members in the Durness Limestone Sequence derived by Swett (1965) have been used in the construction of the cross section shown in fig. 6.2, in which the Moine Thrust has been projected from the east side of Loch Eriboll (fig. 6.1). The Sangomore Fault has juxtaposed the Durine Member rocks and overlying thrusts in the hangingwall against the Sailmhor Member of the Durness

Limestone Sequence in the footwall (figs. 6.1 and 6.2). The thicknesses of the Durness Limestone Sequence members indicate that a minimum of 1064 metres offset down to the NW has occurred along the Sangomore Fault (fig. 6.2). A further minimum of 1118 metres offset down to the NW has occurred along the Sangobeg Fault (fig. 6.2). Thus, just over two kilometers of vertical offset down to the NW has occurred along NE-SW trending extensional faults near Durness.

Fig. 6.4 shows the dominant NE-SW orientation of the steep extensional faults in Sango Bay which lie in the hangingwall of the Sangomore Fault. Fig. 6.4 also shows the range of displacements on these faults and their spacing. These minor faults within the hangingwall block commonly show dip-slip movement indicators (slickensides) and their displacements range from one to seven meters. The area has been divided into four sub-areas for structural analysis, each with boundaries defined by major faults. Each sub-area is described below.

6.4.2 Description of sub-areas

Sub-area 1 in Sango Bay (see fig. 6.4) contains Lewisian mylonites thrust over Moine "oystershell" rock. The Moine Thrust system is considered to have evolved in a piggy-back fashion, such that younger thrusts developed at progressively deeper levels, carrying the older thrusts structurally above (Elliott and Johnson, 1980; Butler, 1984). The structurally highest thrust carrying Moine rocks over Caledonian foreland rocks has been defined historically as the Moine Thrust (sensu stricto) by earlier workers (Peach et al., 1907; Christie, 1960, 1963; Weathers et al., 1979; Coward, 1983), and more recently by Law et al. (1986). The Moine Thrust (sensu stricto) is considered to be the oldest thrust (Elliott and Johnson, 1980). The thrust in sub-area 1 therefore represents a late breach in the Moine Thrust. This structural association occurs in several other places along the Moine Thrust in the North West Highlands (Butler, 1982; and Law, pers. comm. 1989). Butler (1982, 1987) has shown that the Moine Thrust has been breached at Creag Shomhairle [NS 385510], (south of Loch Eriboll) and Glendhu, near Assynt [NS 280350]. Law has shown that the Moine Thrust is breached at Straith Kanaird [NS 150020], 10 km. north of Ullapool. The implications of this are not the focus of this study, and therefore will not be considered any further here.

Sub-area 1 is separated from sub-area 2 by the Sango Sands Fault (SSF; fig. 6.2). Knipe (unpublished data) has outlined a 'stratigraphy' for the Moine mylonites exposed at Kempie Bay (east of Loch Eriboll), and correlates the Moine rocks exposed in Sango Bay with mylonites from Kempie Bay which lie 25 m. above the Moine Thrust (sensu stricto) (Knipe, pers. comm., 1989). Therefore, a minimum displacement of 25 m. has been placed on the SSF.

Lewisian mylonite is thrust directly over Cambrian quartz mylonite in sub-area 2. Minimum displacements of the faults in sub-area 2 are assessed by offset of this Lewisian/Cambrian thrust contact. The minor fractures and faults in sub-area 2 show dominantly dip-slip movement indicators (slickensides) on their surfaces, but occasionally slightly oblique slickenside movement indicators are observed on the minor faults and fractures (approximately 25% of the slickensides observed) (for details see section 6.5.2 below).

The fault separating sub-area 2 from sub-area 3 displaces the Lewisian/Cambrian thrust contact a minimum of 6 m. (fig. 6.4). This normal fault is defined by a steeply-dipping, planar outcrop face of Durness Limestone (see section 6.4.3 below). Sub-area 3 is juxtaposed with sub-area 4 by a fault with a minimum displacement of 2 m. The fault is also defined by a steeply-dipping planar outcrop face of Durness Limestone. Due to weathering (sand-blasting) of the limestone, movement indicators (slickensides) have not been preserved on the outcrop surface. Outcrops of cataclastic fault rocks are rare in sub-area 4, and therefore cataclastic deformation in this sub-area will not be considered in any further detail.

6.4.3 Cataclastic rocks in the Durness Limestone

The extensional fault separating sub-area 2 from sub-area 3 is defined by the limestone outcrop face contains abundant carbonate veining (fig. 6.5a). The fault zone contains 'sheets' of brecciated limestone, and weathering of the fault plane has provided an exposure of a fault-perpendicular section through one of these sheets, 30 cm. in width (fig. 6.5b). The fault breccia is completely cemented, and contains clasts ranging in size from <0.5 cm. to 3 cm. in diameter (fig. 6.5b). The clast shape ranges from angular to sub-rounded (fig. 6.5c). The matrix material in the breccia is either red, iron-rich, or white, carbonate-rich cement, and defines 'bands' trending sub-parallel to the fault (figs. 6.5b and c).

Figure 6.5. *Photographs of cataclastic deformation* in Durness Limestone, Sango Bay, Durness. a) Breccia 'sheet' in fault zone defined by steep outcrop face of Durness Limestone. Minimum displacement on fault 6 m. b) Detail of 30 cm. wide breccia sheet shown in fig. 6.5a. Note gray limestone clasts 'floating' in red, iron-rich matrix. Five pence piece for scale. c) Close-up of clasts in breccia shown in fig. 6.5b. Note clasts of 'reworked' breccia (red) floating in carbonate cement (arrowed).
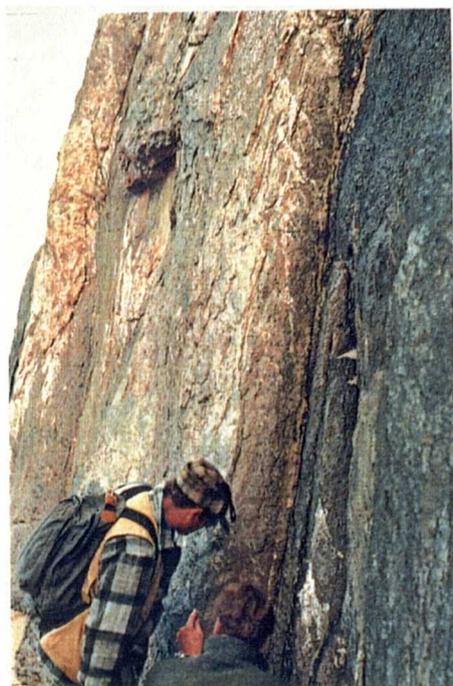
A

B

C

Occasionally, clasts of previously-brecciated and cemented material are observed floating in the breccia (fig. 6.5c, arrowed). Thus, the breccia zone records evidence for syn-kinematic fluid flow and cementation.

The 'sheets' of breccia are observed along the length of the fault outcrop face. Although 'pockets' of cataclastic quartzite are found cemented to the limestone fault surfaces, it is very rare to observe clasts (<20 cm.) of quartzite intermixed with the limestone fault breccias. Fig. 6.5 shows the homogeneous composition of the carbonate fault rocks. Similarly, limestone clasts are rarely found within the quartz cataclastic fault rocks. Thus, although displacements greater than the thickness of the quartz thrust sheet exist, such that the lithologies are completely juxtaposed with each other, 'mixing' of the cataclasites on the scale of clasts has not occurred.

6.4.4 Mineral lineation data: implications for fault block rotation

Mineral lineations associated with transport of the mylonitic rocks to the WNW during the Caledonian Orogeny (Soper, 1971; Elliott and Johnson, 1980; Butler, 1984) have been recorded from all the mylonitic lithologies in Sango Bay (the Moine, Lewisian, and Cambrian quartzites). Here the lineation readings have been displayed on separate stereoplots for each sub-area in order to assess the presence of any rotation (within the foliation plane containing the mineral lineation) of the fault blocks during displacement along the NE-SW trending faults which bound the sub-areas (assuming no rotation has occurred prior to the extensional faulting). The mineral lineation data from Sango Bay (fig. 6.4), is consistent with observations from elsewhere along the Moine Thrust system in the North West Highlands (Elliott and Johnson, 1980; Butler, 1984). Slight deviations from this WNW-transport direction are observed within the quartz mylonite thrust sheet in Sango Bay. However, this is observed only within this lithology, and the range in readings is most probably related to the intense cataclasis which is dominantly contained within the quartz thrust sheet. Therefore, no significant bulk rotation of the fault blocks (within the plane containing the mineral lineation) is thought to have occurred in Sango Bay.

6.5 Field and microstructural observations of the quartz
    fault rocks

### 6.5.1 Initial quartz mylonites

The quartz mylonites unaffected by the extensional faulting in Sango Bay contain microstructures associated with the evolution of the Caledonian Moine Thrust system, and are similar to those described by Weathers et al. (1979), White (1979a,b), Ord and Christie (1984), and Knipe and Law (1987). The quartzite contains domains of elongate ribbon-like grains 100-1000 μm in width and up to 3 mm. in length, and totally recrystallized zones (fig. 6.6a). On the thin section scale, the recrystallised domains occur in 10-30 mm. zones. Transmission electron microscopy (TEM) of the elongate grains has identified a well-developed sub-grain structure (fig. 6.6b).

The recrystallized grain sizes ranging from 6.0 to 35.0 μm, with a mean of 16.1 + 4.1/- 4.0 μm (fig. 6.7a). Measurements of 375 subgrains has revealed that the sub-grain size within the elongate grains ranges from 0.6 to 8.5 μm, with a mean of 2.6 + 1.2/- 1.0 μm. (fig. 6.7b). The methods and assumptions used in the calulation of the mean grain sizes, and the problems related to the calculations of grain sizes from two-dimensional sections are discussed in Appendix 5. Dislocation densities in the undeformed samples range from 1.7 - 5.0 x 10^8 /cm^3. Appendix 6 discusses the methods used in the calculation of the dislocation densities, and contains a listing of the dislocation density data.

6.5.2 Quartz cataclastic fault rocks

There is a range of fractures and cataclastic fault rocks observed in the quartz mylonite thrust sheet in terms of the width of the deformation zone (the cross-sectional dimension perpendicular to the strike and dip of the zone), the clast size and shape, the clast sorting, the clast/matrix proportion, and the estimated displacement associated with each zone. The width of the deformation zone will be used as the main criteria to distinguish the types of cataclastic zones present in Sango Bay: i.e., a) fractures not associated with gouge or breccia development; b) fractures associated with cataclastic zones <1 cm in width; c) narrow cataclastic zones 1-10 cm wide, and; d) broad breccia/cataclastic zones 10-100 cm wide. The fractures (a and b), and the narrow cataclastic zones (c) each show systematic orientations and are described first.

Figure 6.6. a) Optical micrograph of quartz mylonite from Sango Bay not affected by later extensional faulting, showing domains of elongate grains and recrystallised grains. XP. Sample 48444A. Scale bar 0.5 mm.   b) TEM micrograph of subgrain structure from elongate grain in quartz mylonite not affected by later extensional faulting in Sango Bay.   Sample 48444A. Scale bar 1 μm.
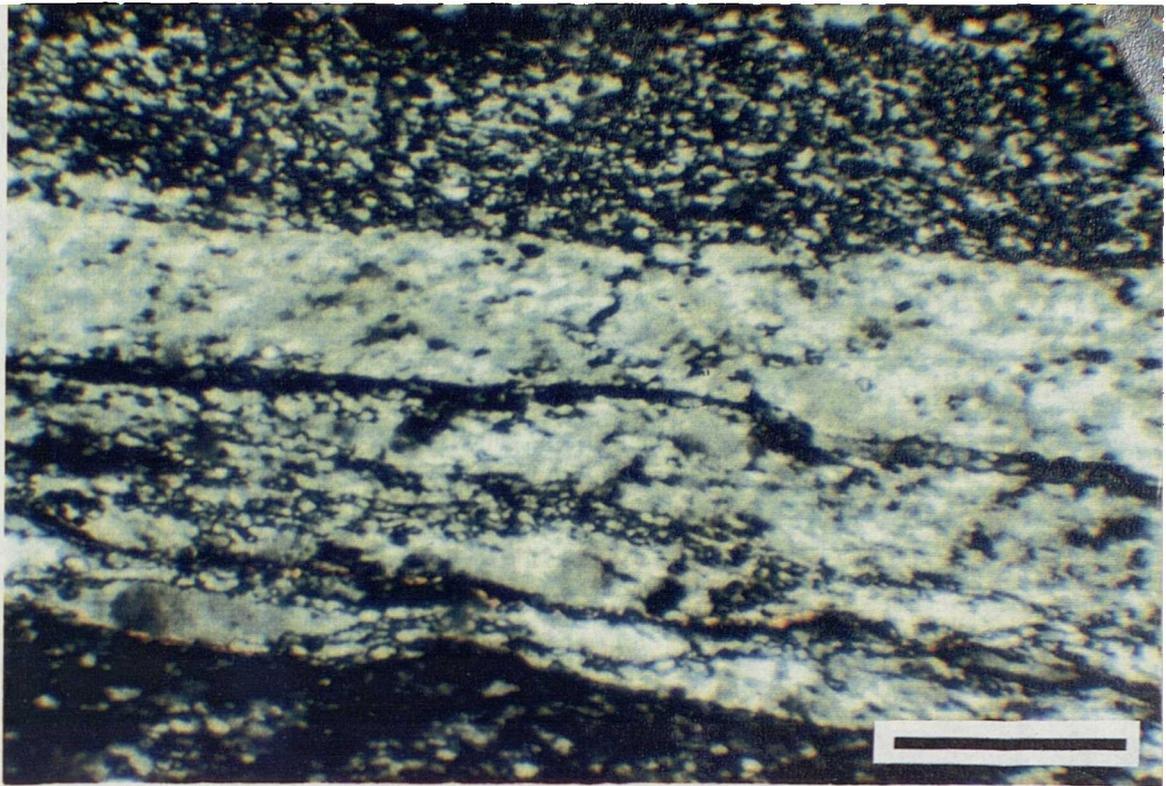
A

B

A   recrystallised grain size, d (μm)
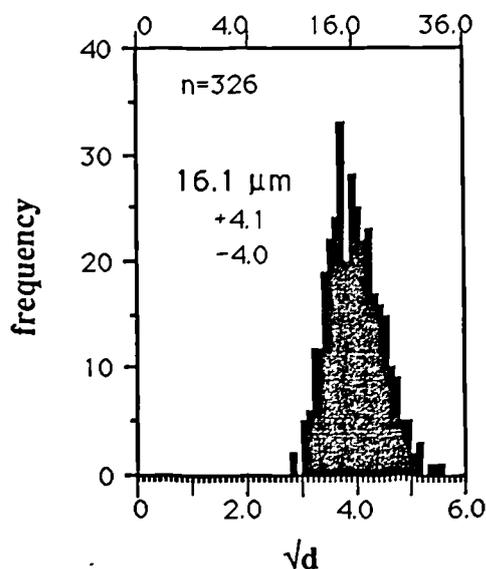
B   subgrain size, d (μm)
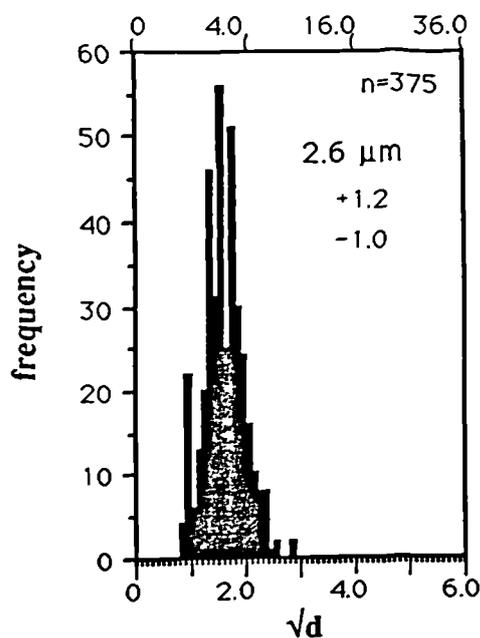
Figure 6.7. a) Frequency distribution for the roots of recrystallised grain size (d) calculated from the grain area from optical micrographs (sample 48444A). Mean grain size and standard deviation (shown inside of graph) calculated assuming a normal distribution of √d. Number of grains measured, n=326. b) Frequency distribution for the roots of subgrain size (d) calculated from the grain area from TEM micrographs. Samples 49519A and 48444A. Mean subgrain size and standard deviation calculated as in fig. 6.7a. Number of grains measured, n=375.

a)   This type of fracture extends 10-50 cm. in length and is not associated with any gouge or breccia development on its surface.   Mesoscopically, no appreciable shear displacement (<<0.5 cm.) of the mylonitic foliation in the quartzites is observed. Only an opening displacement perpendicular to the fracture surface is observed in the field.   The fractures are frequently (approximately 60% of those observed) filled with carbonate or quartz cement.   The fractures are planar and steeply dipping (70-90°), and are consistently cross-cut by other cataclastic deformation features, such as low-angle, high-density localized fracture zones (fig. 6.8a).   The majority of the steeply-dipping fractures are oriented sub-parallel to the minor and major extensional faults in the area (fig. 6.9a).   The fractures are spaced 1 to 10 cm. apart (see also fig. 6.8e).

b) The first type of fracture in this group is less commonly observed, and trends parallel to the fractures in a).   The fractures are observed to have striated, slickensided surfaces (fig. 6.8b), and extend 10-100 cm. in length. The slickensides indicate dominantly dip-slip movement, but occasionally (less than 25% of those observed) indicate oblique movement (fig. 6.10). Red, iron-rich material is commonly cemented to the fracture surface (fig. 6.8b).   These fractures are associated with up to 1 cm. of cataclastic fault gouge, which is cemented and cohesive.   The fractures show 10-50 cm. displacements, and are spaced 50-100 cm. apart.

The second type of fracture in this group is also associated with less than 1 cm. of cataclastic fault gouge, but is curvilinear in section, up to 50 cm. in length, and consistently shows a smooth, polished surface (fig. 6.8c).   These fractures strike consistently perpendicular to the minor and major fault orientations in the area, the discrete fractures described above, and also the narrow cataclastic zones described below (fig. 6.9b).   Displacements associated with these fractures are on the order of 10-50 cm. as indicated from offsets of the mylonitic foliation in the quartzite.   However, due to the polished nature of these fractures, movement indicators, such as slickensides are not observed. The polished fractures do not show a systematic spacing.   They consistently cross-cut the fractures described in a),   but show mutual cross-cutting relationships with the first fracture type in this section (b), described above.

Figure 6.8. Photographs of cataclastic deformation in quartz mylonite thrust sheet, Sango Bay, Durness. a) View looking south at steeply-dipping fractures slightly sheared and cross-cut at high-angles by shallow-dipping high-density localized fracture zones (arrowed). Two pence piece for scale. b) Steeply-dipping fracture showing striated, slickensided surface with red, iron-rich material cemented to fracture surface. Camera lenscap 5 cm. in diameter. c) View looking west at 'polished' fracture with curvlinear surface (arrowed), oriented perpendicular to fractures in figs. 6.7a & b. Camera lenscap 5 cm. in diameter. d) View looking south at narrow cataclastic zone. Field notebook 17 cm. long. e) Broad breccia zone with angular-blocky clasts ranging in size from <2 cm. to 20 cm., cemented by <25% fine-grained matrix. Two pence piece for scale.
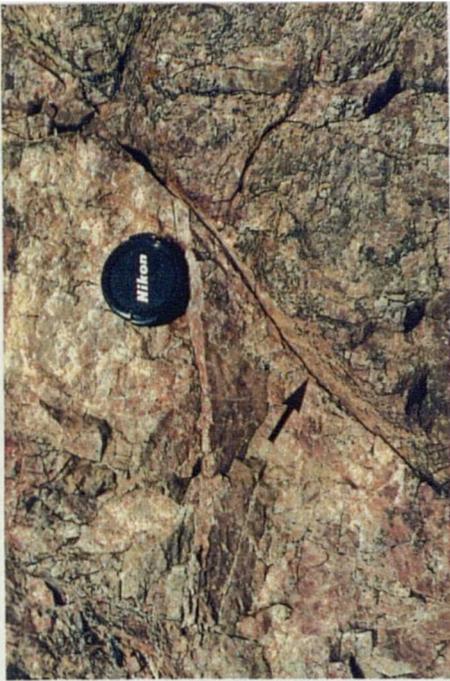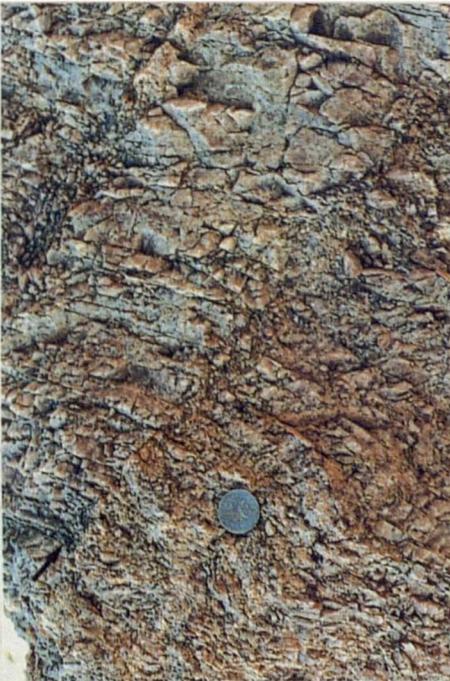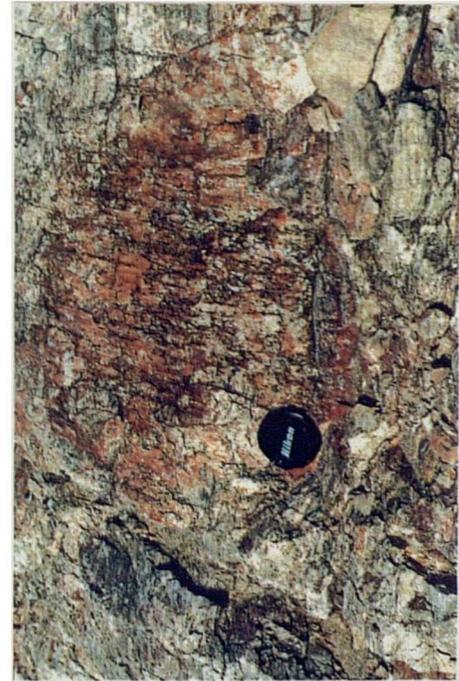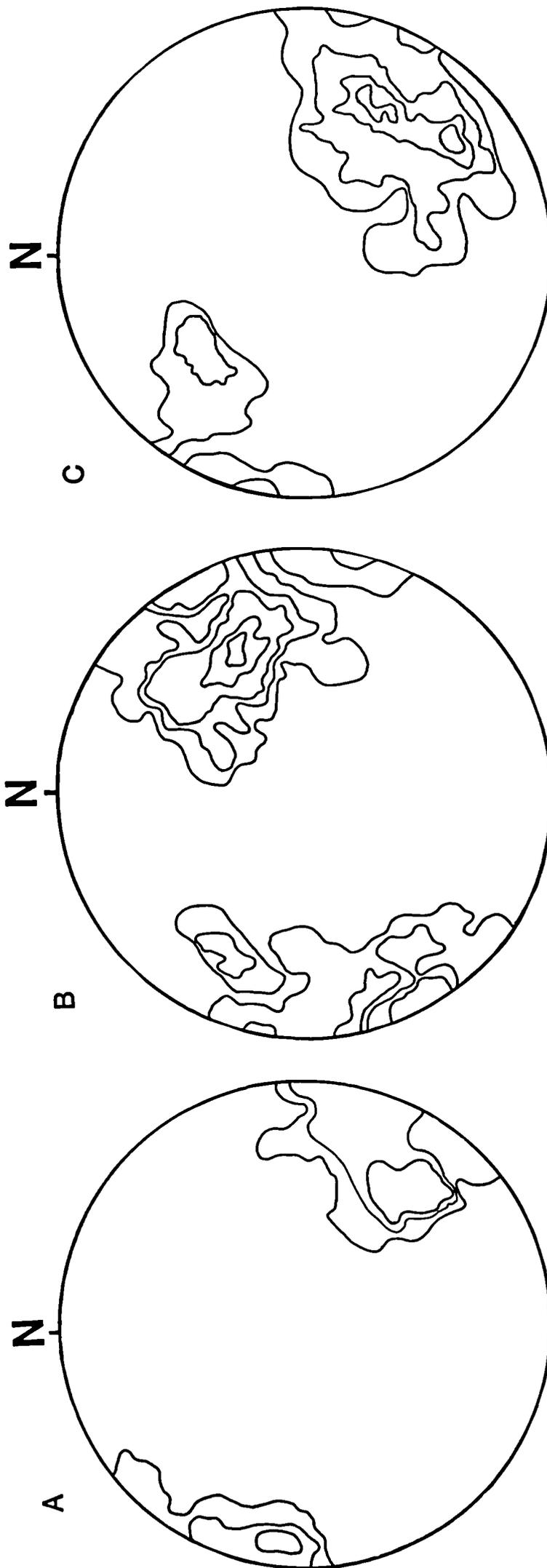
Figure 6.9. Lower-hemisphere, equal-area, contoured stereoplots of poles to fractures and cataclastic zones with quartz mylonite thrust sheet, Sango Bay, Durness. a) Steeply-dipping fractures; contours 22, 10, and 1% per % area, n=109. b) 'Polished' fractures with curvlinear surface; contours 17, 11, 5,2 and 1% per 1% area, n=52. c) Narrow cataclastic zone, contours 14, 10, 4 and 1% per 1% area, n=67.

● POLES TO FRACTURE PLANES

■ SLICKENSIDE LINEATIONS
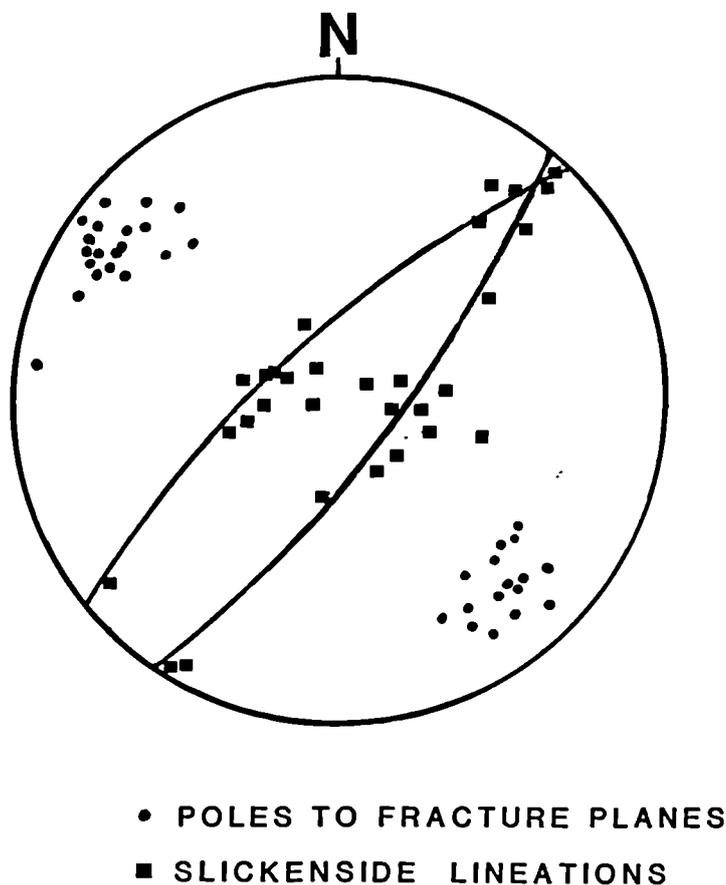
Figure 6.10. Lower-hemisphere, equal-area stereoplot of poles to steeply-dipping shear fractures which are oriented parallel to the minor NE-SW trending faults in Sango Bay (shown in fig. 6.8b). Average great circle of the poles to fracture planes and slickenside lineation plunge data shown. n=35.

c) The narrow (1-10 cm. wide) cataclastic zones are spaced 1 to 5 meters apart, are 1 to 5 meters in length, and show displacements of several cm. up to 1 meter (fig. 6.8c). These zones form a 3D network where one set is sub-parallel to the major fault orientation (fig. 6.9c). The narrow cataclastic zones are most common in sub-area 3 (see fig. 6.4). The displacement on each of the cataclastic zones is not simply related to the amount of grain size reduction within the zone, nor the finite width of the zone. For example, the amount of matrix ranges from 25% to 75% and the clast size ranges from <1cm to >20mm in zones with identical displacements (fig. 6.11). In addition, the matrix ranges from extremely incohesive ('powdery') to fully cohesive (cemented). These zones are similar in character to the attrition breccias described by Sibson (1986), in that they are related to progressive frictional wear along slip surfaces.

d) The broad breccia/cataclastic zones (10-100 cm. wide) contain angular to blocky clasts ranging from <1 to 20 cm. in length, in which matrix accounts for <25% of the zone volume (fig. 6.8d). The matrix in these zones is often incohesive. These broad zones are often discontinuous in that they occur in patches along faults or within the fractured quartz mylonite. Displacments in these zones are very low (<< 10 cm.). They are very similar to the implosion breccias described by Sibson (1986), which form in by the linking of extension fracture systems during rapid dilation events. Implosion breccias are therefore commonly found in dilational jog sites (void spaces) along faults (Sibson, 1986).

6.5.3 Interpretation of the cataclastic fault rocks

The first type of fracture described in section 6.5.2a is steeply-dipping and oriented sub-parallel to the minor faults. On the mesoscopic scale, the fractures show opening displacements but no appreciable shear displacement (<<0.5 cm.). These fractures are interpreted as extension fractures (Griggs and Handin, 1966). The extension fractures are cross-cut by all of the other cataclastic features described, suggesting that they formed relatively early in the fault displacement history. The filled extension fractures acted as fluid pathways during the extensional faulting.

NARROW CATACLASTIC ZONES

scale

0   10

cm

fine-grained matrix

clasts of quartz mylonite

clasts of cemented cataclasite
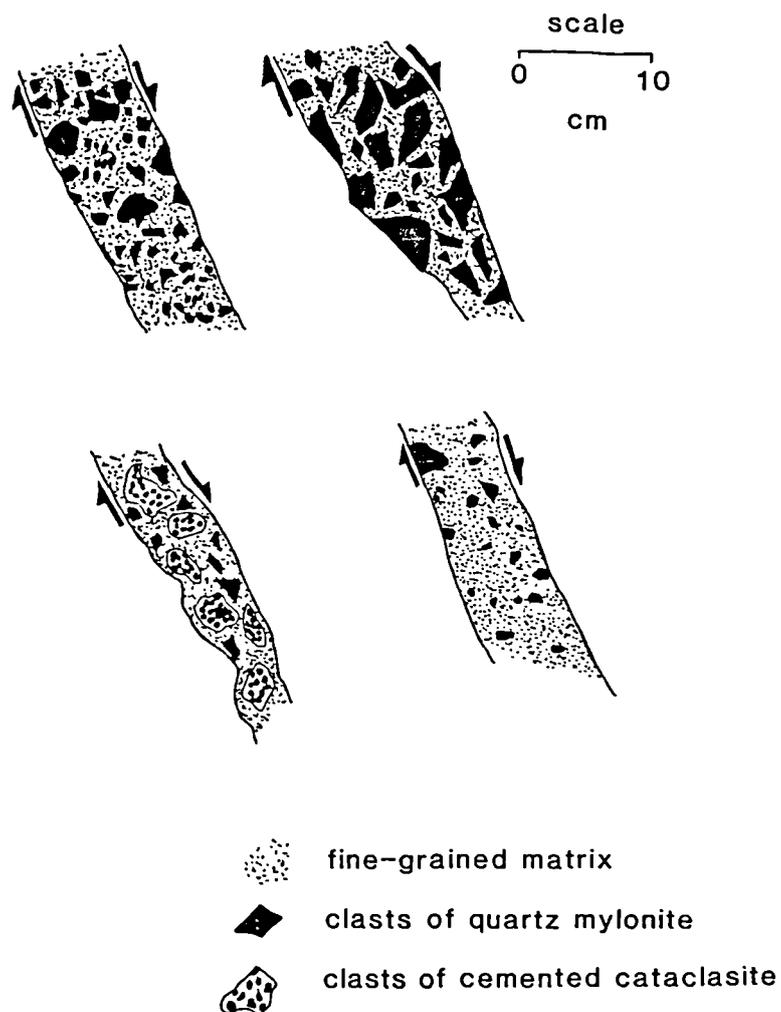
Figure 6.11.   Line drawing showing cross-sections through hand-sample slabs of narrow cataclastic zones in the quartz mylonite thrust sheet, Sango Bay.   A range of clast sizes, shapes and clast/matrix proportions are present in zones which show identical displacements, in this case 2.0 m.

Figure 6.12. Optical micrographs of cataclastic microstructures in quartz mylonite. a) Sample 48453B. Discrete, planar microfractures associated with late extensional faulting, offsetting foliation in quartz mylonite. Displacements 20 to 100 µm.; individual fractures have effective fracture widths of <10 µm. XP. Scale bar 1.0 mm. b) Sample 48453A. Semi-planar microfractures offsetting foliation in quartz mylonite. Displacements >500 µm; individual fractures have effective fracure width of 10-50 µm. XP. Scale bar 0.5 mm. c) Sample 49119A. Microbreccia zone with grain sizes <25 µm. between larger clasts (>1000 µm.) XP. ST. Scale bar 0.5 mm. d) Sample 49290A. Ultracataclasite consisting of approximately 75% fine-grained matrix (<25µm.) with sub-rounded to rounded clasts <1000 µm. in diameter. XP. ST. Scale bar 1.0 mm.
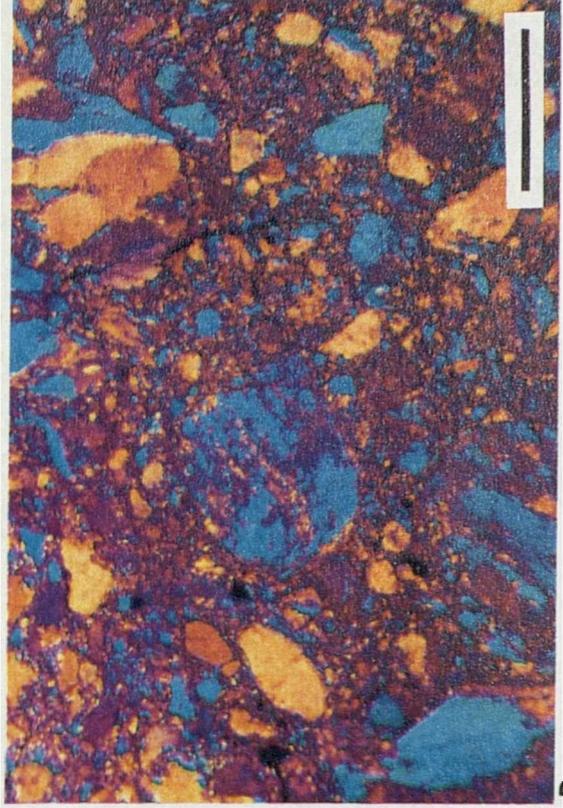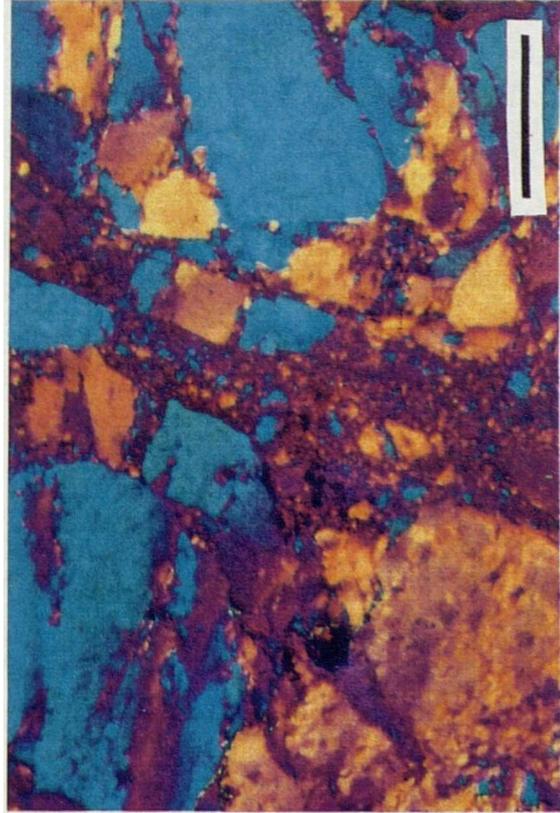
TEM shows that the greater displacement microfractures define boundaries between unfractured quartzite, and narrow zones (approximately 10-30 μm wide) containing angular (fig. 6.13a) to sub-rounded (fig. 6.13b) clasts <1-5 μm in diameter. The fracture boundary between the unfractured quartzite and the narrow zone of cataclastic deformation is often not discrete, but irregular at the scale of the fragments in the fracture zone (fig. 6.13a).

b) Deformation zones (>50 μm wide) include microbreccias, in which fine-grained (<25 μm.) matrix accounts for <10% of the cataclasite on the optical thin section scale (fig. 6.12c), to ultracataclasites, which contain >75% fine-grained matrix (fig. 6.12d).

The clast sizes and shapes in the deformation zones are quite varied on the thin-section scale. In addition, the clast edges in the microbreccias exhibit a range in morphology. Many clasts present in the fault rocks contain features characteristic of the more intact quartzite. For example, some edges are similar to the microfractures described above and are semi-planar (fig. 6.14a). However, a large number of the clast edges are dentate. The irregular dentate boundaries appear to be following the subgrain or recrystallised boundaries in the clasts (fig. 6.14b). In the ultracataclasite zones, there is a predominance of sub-rounded to rounded clasts, (fig. 6.14c), but the clast size can vary, such that large clasts, >2 mm. are observed (fig. 6.14d). Note that even the largest clasts incorporated into the matrix zones have sub-rounded to rounded shapes (e.g., fig. 6.14d).

TEM analysis of the dislocation densities within the clasts <2 mm. in size reveals that they are higher than that of the background range in the 'undeformed' quartzite, ranging from 4.1×10^8 to 1.2×10^9 /cm^3, compared to $< 5.0 \times 10^8$ /cm^3 (see Appendix 6 for the methods used in the calculation of the dislocation densities, and for a listing of the dislocation density data).

The increase in dislocation densities within the clasts suggests that low temperature crystal plasticity contributed to the deformation of the clasts during the cataclastic deformation. In addition, the TEM has shown that there is a significant increase in the development of voids along subgrain and grain boundaries in clasts within the cataclastic zones (fig. 6.15a). The significance of both these features is discussed below.

Figure 6.13.   TEM micrographs of cataclastic microstructures associated with semi-planar microfracture zones in quartz mylonite (i.e., from fig. 6.11b). Sample 48453A.   a)   Microfracture ('F') separating large clast from 1-5 μm. angular microclasts.   Scale bar 1 μm.   b).   Microfracture ('F') separating unfractured quartzite from sub-rounded to rounded microclasts, 1-5 μm. in diameter. Scale bar 1 μm.
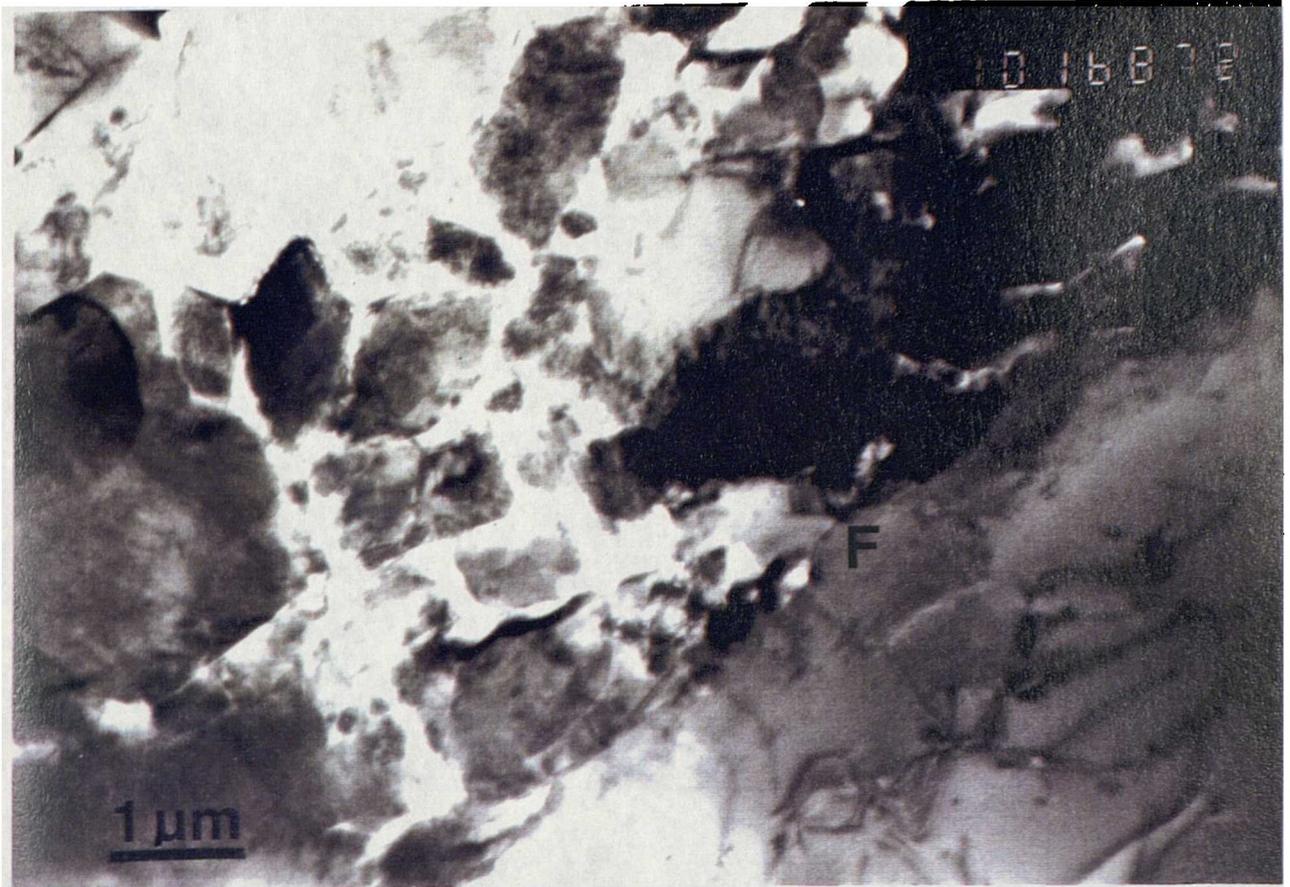
A
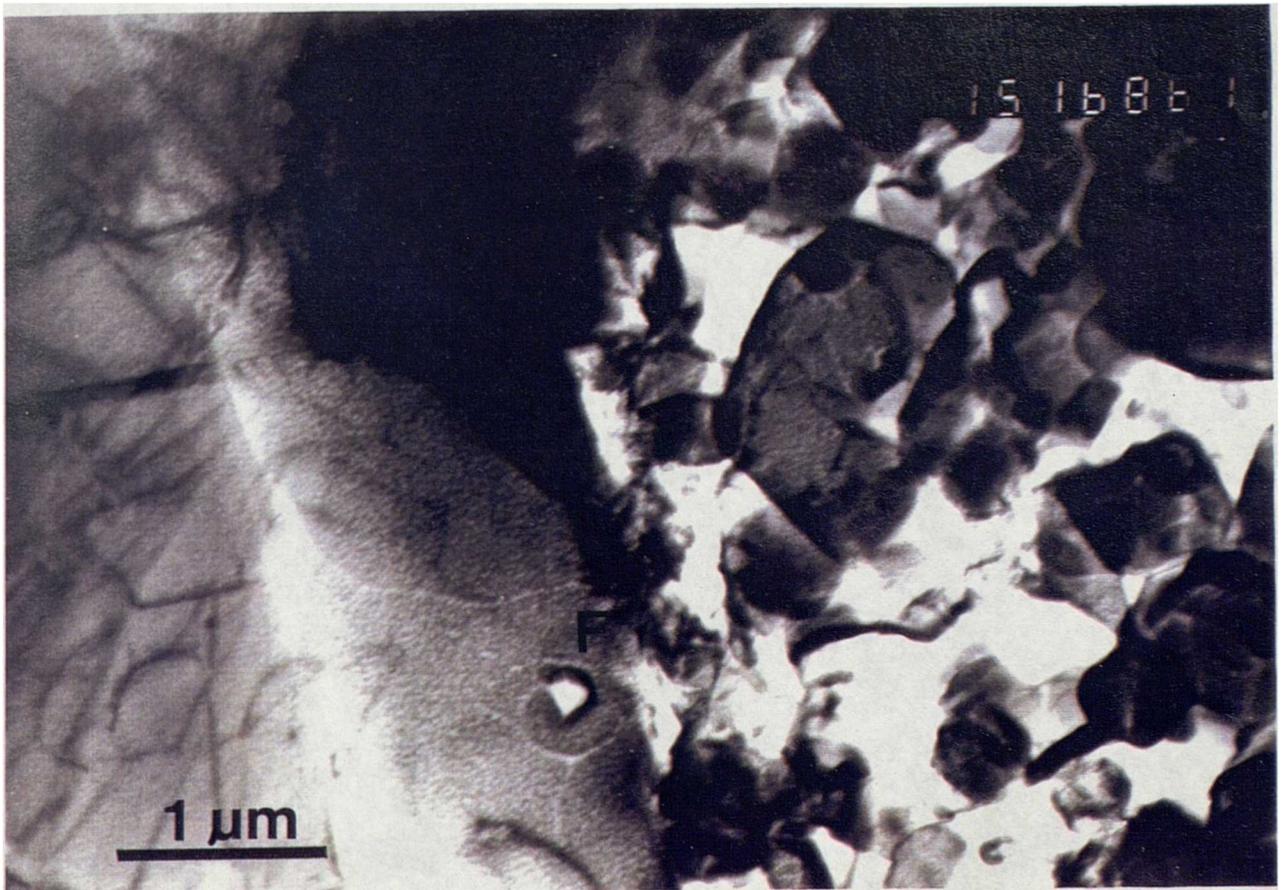
B

Figure 6.14.   Optical micrographs of cataclastic microstructures in quartz
mylonite. a)   Sample 48453B.   Microbreccia zone with grain sizes <25 μm.
between larger clasts (<1000 μm) with semi-planar boundaries.   XP, ST.   Scale
bar 1 mm. b) Sample 49119A.   Ultracataclasite zone with grain sizes <25 μm.
adjacent a larger clast (<1000 μm) with irregular, dentate boundary.   XP.
Scale bar 0.5 mm.   c)   Sample 49290A.   Cataclastic zone containing clasts ≤ 2.0
mm. in size 'floating' in fine-grained ultracataclasite matrix with clasts ≤ 25
μm. in diameter. XP. Scale bar 0.5 mm.   d)   Sample 49119B.   Ultraclasite zone
containing >75% matrix of grains <25 μm., adjacent rounded clast 2-3 mm. in
diameter. XP, ST. Scale bar 1 mm.
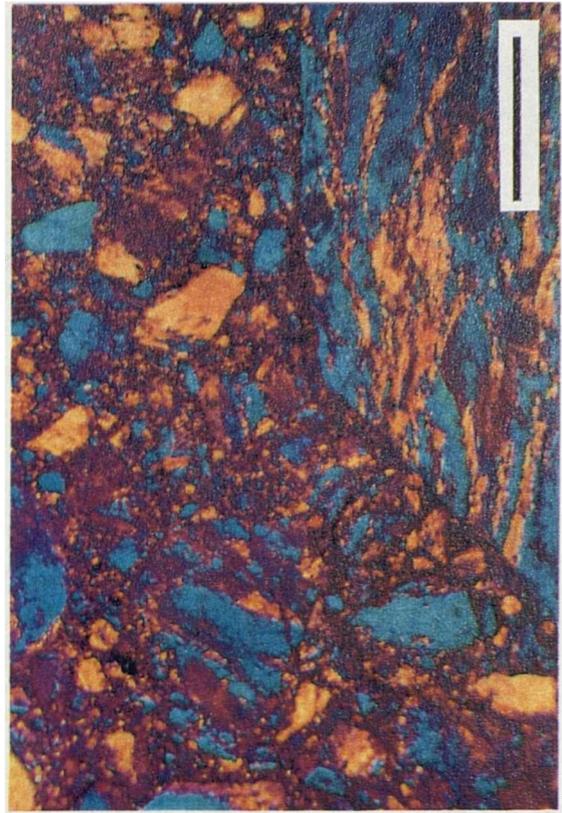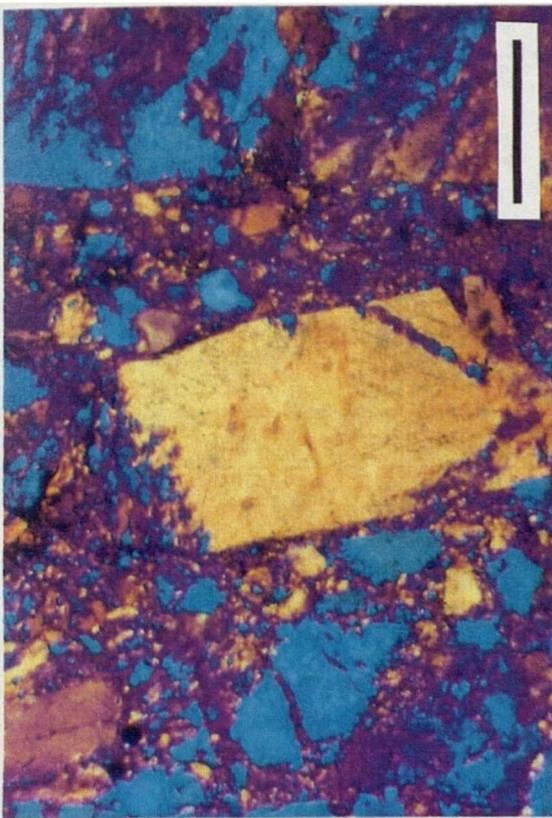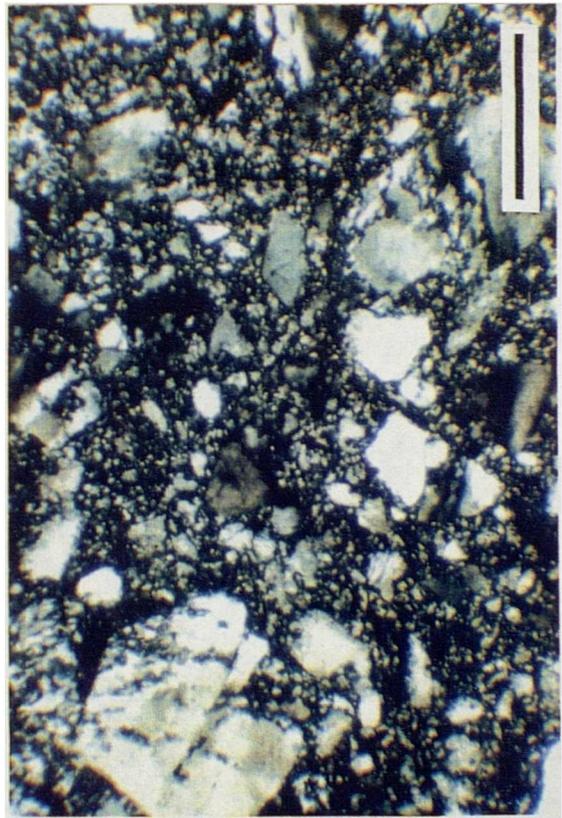
Figure 6.15. a) TEM micrograph of voids along subgrain boundaries adjacent growth feature (fracture fill?) in clast within a cataclastic zone. Sample 49286A. Scale bar 1 μm. b) TEM micrograph of fine-grained ultracataclasite zone showing point contacts between grains. Sample 49119A. Scale bar 1 μm. c) TEM micrograph of 1 μm. microclast adjacent larger grains in microbreccia zone. Note straight boundaries and 120° junctions on the microclast. Sample 49290A. Scale bar 0.5 μm. d) TEM micrograph of matrix grains in microbreccia zone showing straight boundaries on microclasts and preserved porosity. Scale bar 2 μm. Sample 49119A.
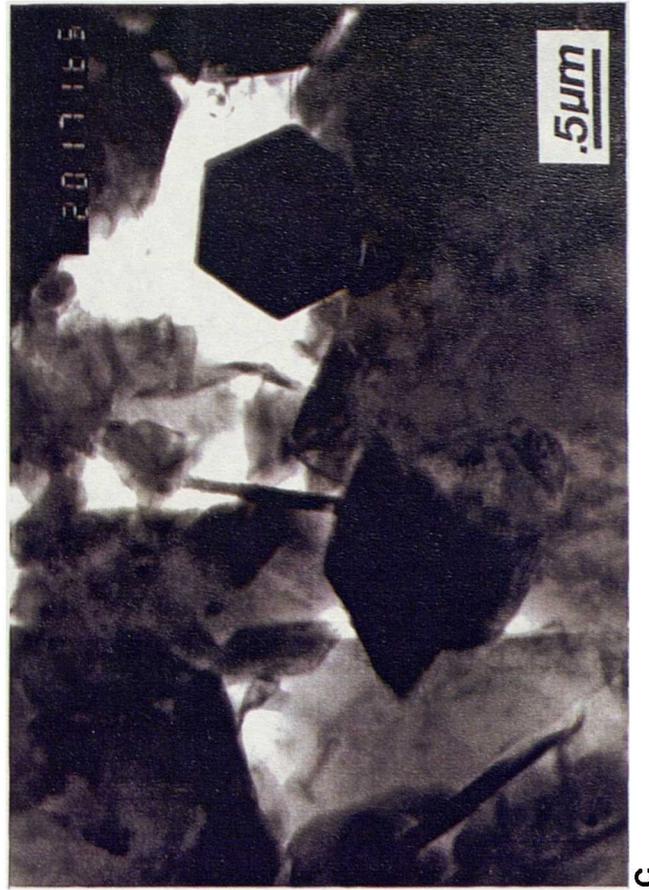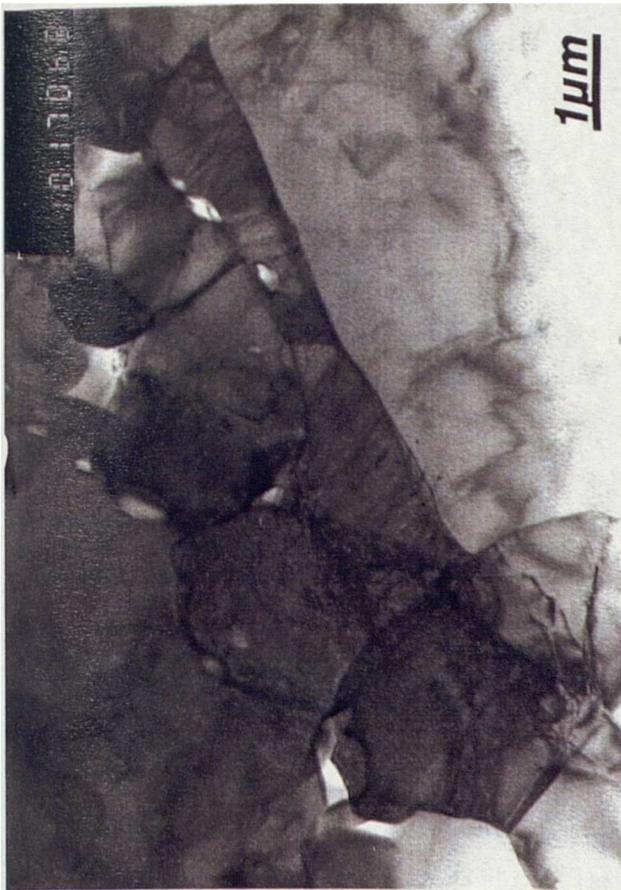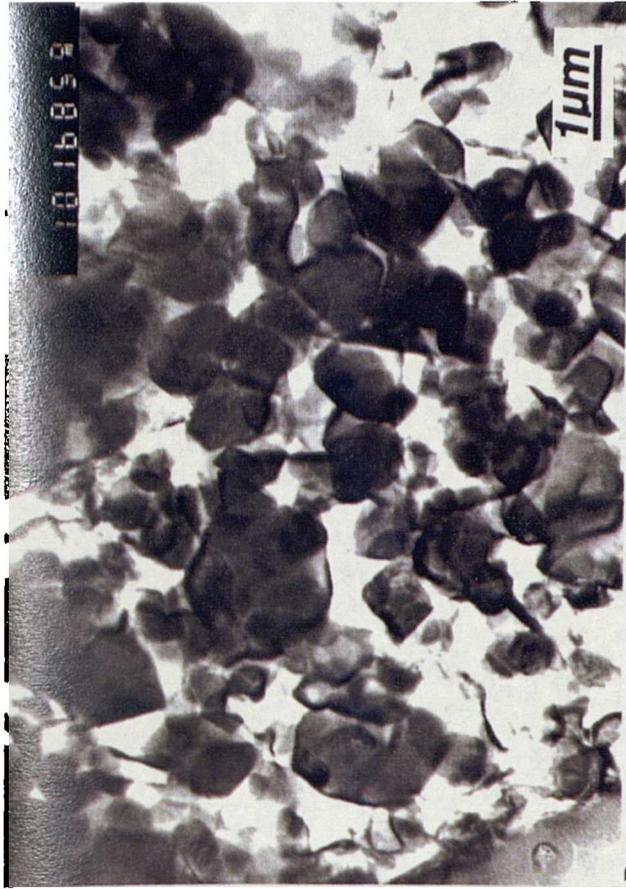
The fine-grained matrix zones in the microbreccias and ultracataclasites is usually composed of an aggregate of angular to rounded fragments (fig. 6.12c and d, 6.14a-d). The grain size ranges from 3.1 to 25.5 μm in the matrix zones in the microbreccias, with a mean of 6.8 + 2.3/- 2.4 μm (fig. 6.16a). In the ultracataclasites, the grain size ranges from 0.1 to 8.0 μm, with a mean matrix grain size of 1.0 + 0.9/- 0.7 μm. (based on TEM measurements of 461 microclasts) (fig. 6.16b).

TEM shows the angular nature of the clasts in the matrix zones of the ultracataclasite, and the grain-to-grain relationships (fig. 6.15b). Patches of matrix are characterised by *straight boundaries, often with 120° junctions* (figs. 6.15b,c and d). The 120° junctions represent overgrowths of quartz on the fine clasts, and emphasize the growth of cement from fluids which were present within the fault zone. The cement does not completely fill the pore space between quartz grains and some porosity (5%-10%) is preserved within these patches. (figs. 6.15c and d). Occasionally a carbonate cement occurs and probably represents fluid infiltration from the underlying limestones, the only source of the fluids now preserved.

6.6 Deformation mechanisms involved in the development of the cataclastic rocks

This section outlines the deformation mechanisms contributing to the cataclastic grain size reduction by reviewing and interpreting the important microstructural observations presented above. The role each mechanism plays in contributing to the grain size evolution in the fault zones studied is discussed.

In the relatively intact quartzite the microfractures present are dominated by planar/semi-planar morphologies and represent transgranular fractures (e.g., figs. 6.12a and b). These microfractures are important to the initial fracturing of the quartz mylonite and the presence of clast margins which are planar suggests that these are used during the isolation of clasts which accompanies the fault rock evolution (fig. 6.17a).

A

microbreccia matrix grain size, d (μm)

0   4.0   16.0   36.0

50

n=305

40   6.8 μm

            +2.3

30   -2.4

frequency

20

10

0

0   2.0   4.0   6.0

√d

B

ultracataclasite grain size, d (μm)

0   4.0   16.0   36.0

80

            n=461

            1.0

60   +0.9

            -0.7

frequency

40

20

0

0   2.0   4.0   6.0

√d
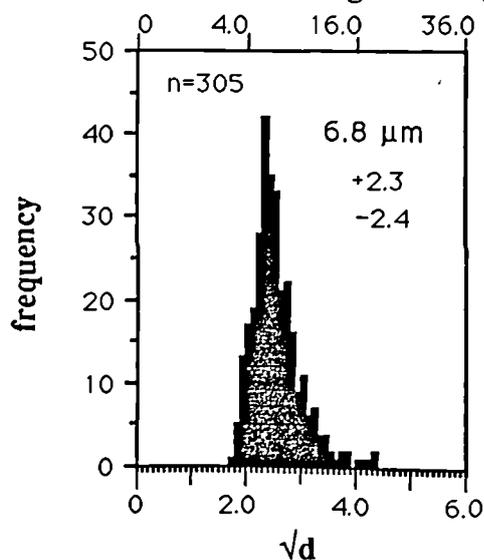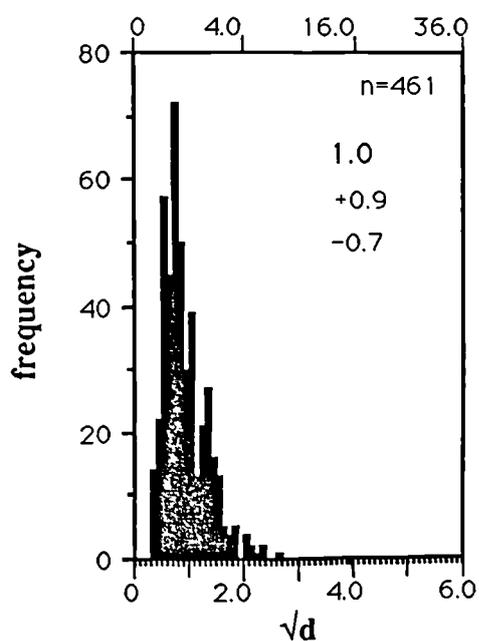
Figure 6.16. a) Frequency distribution for the roots of grain size (d) in microbreccia matrix zone, calculated from the grain area from optical micrographs. Sample 49119A. Mean grain size and standard deviation calculated as in fig. 6.7. Number of grains measured, n=305. b) Frequency distribution for the roots of grain size (d) in ultracataclasite, calculated from the grain area from TEM micrographs. Samples 49119A, 49290A, and 49286A. Mean grain size and standard deviation calculated as in fig. 6.7. Number of grains measured, n=461.

INITIAL MYLONITE

recrystallised domains

SCALE

0   100

μm

elongate grains
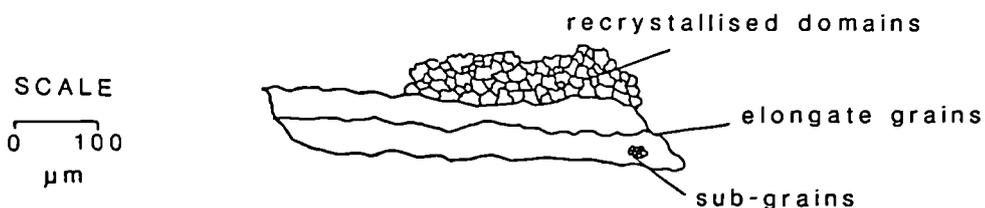
sub-grains

A   transgranular fracture
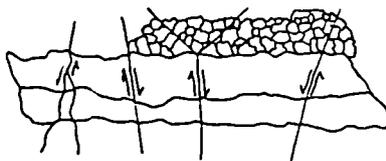
B   grain/sub-grain fracture

void development

grain boundaries

work hardening

sub-grain boundaries

ULTRACATACLASITE

C   transgranular fracture

SCALE

0   10

μm

point contacts
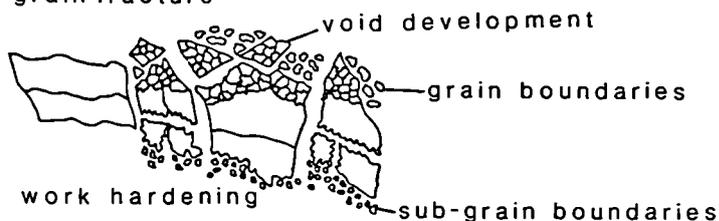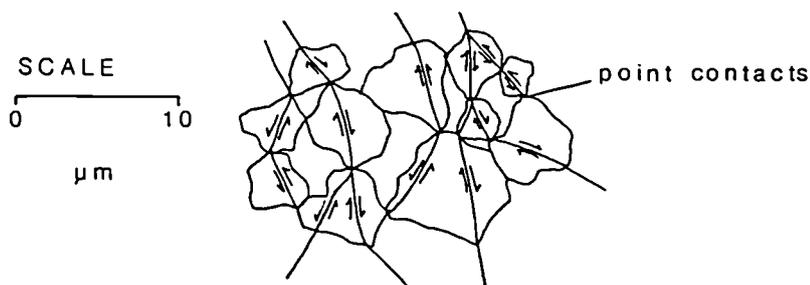
Figure 6.17. Summary diagram showing fracture mechanisms and deformation processes contributing to the microstructural evolution of a cataclasite from the quartz mylonite in Sango Bay, Durness. a.)Transgranular fractures cross-cutting grains in initial mylonite; b.)Fracture located along grain and sub-grain boundaries in the initial mylonite, accompanied by void development and dislocation activity in the cataclasite; c.) Transgranular fracture in the matrix zones of the ultracataclasite resulting from the location of stresses at point contacts.

The increased dislocation density and the number of voids along boundaries within the clasts of the microbreccias and ultracataclasites suggests that crystal plastic deformation processes, possibly accommodated by grain boundary sliding, operated during the faulting. Both these features represent damage which has accummulated in the clasts after their initial formation and isolation from the intact rock. It is likely that they developed during the rotation and straining which occurred as neighbouring clasts interfered with each other during the accommodation of displacement associated with faulting events. This is also evidenced by the rounded edges of many of the clasts within the microbreccias, which suggests wearing of the clasts during deformation (e.g., fig. 6.14d).

The development of the voids along the sub-grain and grain boundaries within the clasts (e.g., fig. 6.15a) has important implications for the progressive grain size reduction and fracturing of the clasts during continued deformation. Voids represent isolated flaws that act as stress concentrators which can promote fracture. Fracture occurs by the coalesence of the flaws during their nucleation and growth, resulting in rapid instantaneous crack propagation (Atkinson and Meridith, 1987). Therefore, although the initial formation of the clast may have been dominated by the generation and linking of planar transgranular microfractures, the void growth during the later straining of the clast may cause a change in the fracturing process to one focussed along sub-grain boundaries or grain boundaries (fig. 6.17b). Lloyd and Knipe (submitted) have also noted the role of sub-grain boundaries and recystallised grain boundaries in localising fracturing.

The clast size of the ultracataclasites is significantly smaller than in the microbreccias indicating that continued fracturing of the disaggregated mylonite takes place during their development. Point contacts between clasts in the ultracataclastites are common (e.g., fig. 6.15b) and the continued grain size reduction may arise from fractures initiated by the stress concentrations developed at these contacts in the manner described by Gallagher (1974), (fig. 6.17c).

The precipitation of cements in the fault zones also has implications for the evolution of the fault rocks. The presence of a cement in the pore space between clasts results in the transfer of stress concentrations at point contacts to a stress which is distributed along the length of the boundaries between the clasts and the cement. The reduced number of point contacts

between clasts may inhibit further fracture in these zones and promote preservation of the early stages of the fault rock evolution as clasts. In addition, the distribution of such cements may also influence the the location of subsequent fracture events by generating stronger domains. Therefore, displacement along existing slip surfaces may continue while stronger domains in a fault zone are not fractured .(i.e., localisation).

The above observations suggest that as the fault rocks evolve, several fracture mechanisms contribute to the grain size reduction process. Initially, transgranular microfracturing dominates the deformation. The generation of the cataclasites appears to be controlled by fracture along existing sub-grain boundaries or grain boundaries weakened by the growth of voids. The production of the ultracataclasites involves further grain size reduction by transgranular fracture processes which appear to be controlled by stress concentrations at point contacts. Work hardening of grains by dislocation activity may also contribute to the fracturing during the development of both the microbreccias and the ultracataclasites. Fig. 6.17 summarizes the possible fracture mechanisms and processes contributing to the grain size reduction during the evolution of the cataclasites from the pre-existing mylonite.

6.7 Discussion

6.7.1 The influence of initial microstructure
on the evolution of the cataclastic fault rocks

The previous sections have outlined the fracture processes which contributed to the grain size reduction during cataclastic faulting in the quartz mylonite. The data has shown that the changing microstructure has influenced the processes which have operated during the faulting. The initial mylonite represents a relatively homogeneous microstructure in which pore space is limited, if not absent. Thus, this microstructure is similar to the type I microstructures outlined by Hadizadeh (1980), which are described as well-cemented, interlocking, low-porosity . microstructures. The stress distribution is initially homogeneous in such rocks during faulting (Hadizadeh, 1980). The development of the semi-planar/planar transgranular fractures in the quartz mylonite from Sango Bay during initial faulting indicates that the stress distribution was initally homogeneous.

However, after the mylonite was 'disaggregated' by these fractures, the rotation and straining of the clasts in the cataclastic zones resulted in void development along grain and sub-grain boundaries. The voids acted as stress concentrators which then promoted fracture along the grain and sub-grain boundaries. The TEM has shown that the resulting microstructure in the cataclasite is similar to the type II microstructure described by Hadizadeh (1980). Type II microstructures are characterised as poorly-cemented, high-porosity rocks, in which the stress distribution is very inhomogeneous, and impingement-induced microstructures are favoured (Hadizadeh, 1980). The cataclasites observed in this study showed evidence for partial cementation and the preservation of a microporosity in even the finest-grained matrix zones in the ultracataclasites. The stress distribution within these zones would thus be very inhomogeneous. Point contacts between the clasts in the matrix zones are also common, and the stress concentrations developed at these contact points favoured impingement-induced microstructures, in this case, the transgranular fractures which operated to further reduce the grain size in the ultracataclasites. Thus, the initial microstructure not only influences the fracture processes, but the changing microstructure during deformation is important in controlling the sequence of mechanisms and microfracture type during evolution of the fault rocks.

6.7.2 Sango Bay in context of the regional fault array

The dominant extension direction in Sango Bay is NW-SE, which corresponds with data from the regional fault array (Laubach and Marshak, 1987). No major NW-SE faults are observed in Sango Bay, and due to limited exposure, it is unknown if differential extension occurs along the north east trending faults, as observed on the larger scale by Laubach and Marshak (op.cit.). However, the slip lineation data from the minor faults and fractures in Sango Bay correlates with that of the regional fault array, i.e., the north east faults show dominantly dip-slip and occasionally oblique-slip movement, and the north west trending fractures are inferred to represent the transfer component of movement. Thus, the cataclastic deformation in Sango Bay reflects the regional extensional fault kinematics and the accommodation of strain during localized displacement along the Sangomore Fault near Durness.

6.8 Conclusions

This chapter has focused on cataclastic deformation in a quartz mylonite thrust sheet resulting from extensional faulting. This section will re-emphasize the important conclusions of this chapter.

In the field, several fracture arrays were identified. Extension fractures oriented parallel to the faults in Sango Bay acted as fluid pathways during the extensional faulting. The extension fractures are also inferred to have been the precursor to discrete fractures along which shear displacement was able to localise. Fractures trending perpendicular to these shear fractures are inferred to represent a transfer component of movement. The clast/matrix sizes and proportions observed in the field show that the evolution of the fault rocks in not simply a function of the displacement magnitude.

In thin section, the cataclastic fault rocks vary from clast dominated microbreccias to matrix dominated ultracataclasites. Several fracture mechanisms contributed to their development. Initially, transgranular fracture mechanisms operated to disaggregate the mylonite. The optical and TEM work suggests that the recrystallised grain size and the sub-grain size in the original mylonite then controlled the development of the matrix in the microbreccias and cataclasites by focusing fracture along sub-grain and grain boundaries. The generation of the ultracataclasite and finer-grained domains in the microbreccia matrix involves further grain size reduction which is dominated by transgranular fracture mechanisms.

The host rock clasts present in the fault zones show a significant increase in dislocation density indicating that a component of low temperature crystal plasticity is associated with the faulting. In addition, the fault rocks show evidence of partial cementation by the growth of quartz and carbonate cements, signifying the important contribution of fluids during the healing of the fault zone.

The fault and fracture data in Sango Bay correlate with the extension directions of the regional fault array in north west Sutherland. The NE-SW trending faults and fractures show dominantly dip-slip, and occasionally oblique-slip movement indicators, with the NW-SE fractures in Sango Bay acting as the transfer component of movement in the array.

Chapter 7. Conclusions

7.1 Introduction

This thesis has outlined the evolution of fault rocks in extensional basin settings, and has identified fluid flow events related to specific fault histories. The approach adopted has been to integrate detailed structural mapping with microstructural analysis of the fault rocks collected from basin structures with different kinematics and geometries. The results suggests that this type of integrated approach can be successful in outlining fault histories and understanding how faults can influence fluid movements at different times in the history of a basin.

Structural mapping has allowed a sequence of deformation to be deduced in which the timing of fault movement and fluid flow can be placed, and microstructural analysis has identified the dominant deformation mechanisms involved in the evolution of the fault rocks. The main conclusions which have been established from these lines of research are outlined below.

7.2 The Orcadian Basin

1. A linked extensional/detachment horizon fault system developed in the lower MORS Stromness Flagstones during burial of the sediments due to gravity-driven displacement of the sediments down the tilted hangingwalls of west-dipping half-grabens.

2. The detachment horizons show both extensional and contractional structures indicating displacement to the W-WNW.

3. Displacement along the detachment horizons was accomplished by localized slip along the bounding surfaces of the detachment horizons, and independent particulate flow processes within the horizons.

4. Slip along the detachment horizons was facilitated by high pore fluid pressures in the compacting sediment pile, which were generated by rapid subsidence of the basin during this time.

5.   Fault breccias along extensional faults which link to the detachment horizons contain microstructures which indicate that initial disaggregation of the sediment took place by grain boundary fracture.

6.   The extensional fault breccias also show evidence for the mixing of sediments which have been juxtaposed.   The matrix zones in the fault breccias contain a significant amount of clay, most probably derived from the surrounding finer-grained horizons.

7.   Microstructural evidence shows evidence for early movements on the Scapa Fault System, which was active during deposition of the upper MORS to UORS fluvial sediments flowing across Caithness and southern Orkney.

8.   The East Scapa Fault acted as an oblique fault to NW-SE extension on the North Scapa Fault during the upper MORS to UORS times, and probably moved in a sinistral sense.

9.   Intense cataclasis directly adjacent to the North Scapa Fault during the early extensional faulting resulted in a cataclasite with extremely variable fragment sizes.   The matrix zones consist of quartz grains 2-4 μm. in diameter, surrounded by pervasive pore-bridging illite.

10.   The cataclastic grain size reduction during initial faulting along the North Scapa Fault occurred by a combination of grain boundary fracture and transgranular fracture.   The presence of corrosive fluids during the faulting is indicated by very irregular and dentate fracture boundaries.

11.   It is suggested that fluids migrating adjacent to the North Scapa Fault during the initial extensional faulting led to the preferential precipitation of the fine-grained illite cement.

12.   The intense cataclasis, together with the illite cementation, resulted in sealing of the fault early in the diagenetic history of the Scapa Sandstone.

13.   During inversion of the basin, existing fault systems were reactivated and acted as pathways for mature hydrocarbons which were migrating from the MORS organic-rich flagstones.

14. The inversion event occurred in post-ORS to Carboniferous times, prior to the intrusion of Permo-Carboniferous dykes.

15. During inversion, thrust and fold structures developed adjacent to the lower-MORS extensional faults on the north coast as a result of buttressing against the earlier faults. In each example discussed in this thesis, the early extensional faults are cut and displaced to the W-WNW by the thrusts.

16. A vein array developed along the thrust flats and ramps observed on the north coast, indicating that high pore fluid pressures existed at the time of the contractional faulting.

17. The veins along the late thrust faults on the north coast contain carbonate cement and bitumen, attesting to the mobility of hydrocarbons at the time of faulting.

18. Existing high heat flow in the basin, coupled with fluids which were released during hydrocarbon maturation, acted to 'feed' the high pore fluid pressures which are inferred to have existed during the inversion event.

19. The early extensional faults on the north coast were only weakly reactivated. It is suggested that the presence of a fine-grained cemented fault rock in the earlier extensional fault zones on the north coast prohibited fluid migration along the earlier-developed fault zones,while displacement was localized on the thrusts, along which fluids were channelled.

20. The Scapa Fault system was reactivated during the basin inversion and also acted as a pathway for the migrating hydrocarbons. Reverse displacement on the East Scapa Fault is suggested to be the consequence of buttressing of compression oriented in an approximately E-W direction.

21. The North Scapa Fault was reactivated in a sinistral, oblique-slip sense during basin inversion, and several fracture sets developed in the fault zone at this time.

22. Fractures directly adjacent to the North Scapa Fault (in domain 4) are oriented sub-parallel to the fault, and resulted in the development of shear lenses.

23. Fractures outside of the sealed domain (4) of the North Scapa Fault zone have developed into three sets. The presence of bedding is suggested to have influenced the fracture array development.

24. Hydrocarbons were channelled parallel to the North Scapa Fault, outside the sealed domain (4), during the later reactivation event.

25. Microstructural observations show that the hydrocarbon pathways are coincident with cataclastic zones in the North Scapa Sandstone.

26. Later dextral transtension deformed Permo-Carboniferous dykes on Orkney and reactivated the East Scapa Fault.

27. Reactivation of the East Scapa Fault overprinted the earlier deformation features in the fault zone. The fault rocks show evidence for dilation during the transtensional faulting, evidenced by the presence of a non-locally derived fine-grained white sandstone and veins of organic-rich material.

28. Incohesive, foliated fault rocks developed in the Rousay Flagstones adjacent to the East Scapa Fault during the later transtensional deformation.

29. NNW-SSE obliquely-oriented folds adjacent to the East Scapa Fault on Howequoy Head at St. Mary's most probably formed during the later transtensional deformation.

30. Slight extensional reactivation of the lower MORS faults in the Stromness Flagstones is observed on the north coast of the Mainland, offsetting earlier fold and thrust systems which are associated with the basin inversion event.

31. Fault rock development in the East Scapa Fault zone is complex and heterogenous depending on fault geometry and kinematics along the fault.

7.3 The Durness Extensional Fault Array

1. Minor faults (with displacements of 1-7 metres) in the hangingwall of the Sangomore Fault near Durness trend in a NE-SW orientation, and offset Caledonian thrust sheets in Sango Bay.

2. Several fracture arrays were identified in the quartz mylonite thrust sheet in Sango Bay. Extension fractures oriented parallel to the minor faults acted as fluid pathways during the extensional faulting, as evidenced by the carbonate cement in the fractures.

3. The extension fractures are inferred to have been the precursor to discrete fractures along which shear displacement was localized.

4. The NE-SW trending shear fractures show dominantly dip-slip, and occasionally (<25%) show oblique-slip movement indicators.

5. NW-SE trending polished, curvilinear fractures are oriented perpendicular to the shear fractures, and are inferred to represent the transfer component of movement to the shear fractures.

6. The faults and fracture data in Sango Bay correlate with the extension directions of the regional fault array in north west Sutherland.

7. The clast/matrix sizes and proportions observed in the field show that the evolution of the fault rocks is not simply a function of the displacement magnitude.

8. Optical microscopy reveals the cataclastic fault rocks contain a range of clast sizes and clast/matrix proportions. The fault rocks range from clast dominated microbreccias (with <10% matrix), to matrix dominated (>75% matrix) ultracataclasites.

9. The microstructures indicate that several fracture mechanisms contributed to the evolution of the cataclastic fault rocks.

10. Initially, transgranular fractures, with planar to semi-planar morphologies, operated to disaggregate the quartz mylonite.

11. The recrystallized grain size and sub-grain size, determined by optical and transmission electron microscopy, controlled the development of the grain size evolution in the fine-grained matrix zones in the microbreccias and cataclasites.

12. The development of voids along grain and sub-grain boundaries contributed to the focusing of fracture along the grain and sub-grain boundaries.

13. Further grain size reduction which generated the ultracataclasites and the finer-grained domains in the microbreccias involved transgranular fracture mechanisms.

14. The clasts (<2 mm. in diameter) in the cataclasites show a significant increase in dislocation density, indicating that a component of low temperature crystal plasticity is associated with the faulting.

15. Transmission electron microscopy indicates that the fault rocks show evidence of partial cementation by the growth of quartz and carbonate cements. This signifies the important contribution of fluids during healing of the fault zone.

16. TEM also reveals that approximately 5% porosity is preserved within the cataclasites, despite the growth of new cements in the fault zones.

7.4 Directions for future work

A number of interesting topics have been unearthed during this work which could be the focus of future research.

1. The detailed microstructural approach should be used in further studies of cataclastic rocks in which fault displacements are tightly constrained. The fault growth and displacement models of Walsh and Watterson (1987, 1988) could be integrated and tested with microstructural analysis of the fault rocks from the well-constrained faults, in order to better understand the temporal changes in fault rock development during the finite displacement history.

2. The type of approach just outlined could then also be used to test the fractal models of gouge development by Sammis et al. (1986, 1987). The fracture mechanisms and deformation processes involved in the development of the self-similar cataclastic fault rocks should be identified microstructurally. The parameters which are responsible for the break-down of the self-similar process of cataclastic deformation might then be identified.

3. Although the fault rocks exposed in extensional neotectonics regimes represent near-surface faulting conditions, these areas provide some of the better constrained models of basin evolution, and microstructural studies of the fault rocks could be tested with the fault zone development models and basin histories presented from Greece and Turkey.

4. The fracture mechanics approach has proved extremely invaluable to the microstructural studies of fault rocks in this study. Further work in this direction should involve not only optical and TEM study, but should be combined with detailed SEM work. In particular, the back-scattered, orientation contrast, and channelling modes on the SEM would facilitate the study of fracture morphology and development in cataclastic fault rocks from varying lithologies and tectonic regimes.

5. Geochemical modelling of the interaction of fluids with cataclastic fault rocks in fault zones should be integrated with detailed microstructural work in order to better contrain rates of mineral growth in fault zones. Thus, the way in which porosity and permeability develop in fault zones could then be better understood in terms of the changing capillary pressure in fault rocks over time.

6. Much scope remains for the assessment of the types of fault seals which are responsible for trapping hydrocarbon accummulations in which the total column height trapped is known. The contribution of each fault sealing process, such as cataclasis, mineral alteration, growth, and cementation in and adjacent to the fault zone, should then be assessed in context of the column height data.

References

Adams, M., and Sines, G. 1978. Crack extension from flaws in a brittle material subjected to compression. Tectonophysics. 49, 97-118.

Agar, S.M. in press. The interaction of fluid processes and progressive deformation during shallow level accretion: Examples from the Shimanto belt of SW Japan. Jnl. Geophys. Res.

Agar, S.M., Prior, D.J., and Behrmann, J.H. in press. Backscattered electron imagery of the tectonic fabrics of some fine-grained sediments: Implications for fabric nomenclature and deformation processes. Geology.

Aki, K., and Richards, P.G. 1980. Quantitative seismology, theory and methods. Vols. I and II. W.H. Freeman, San Francisco.

Allen, P.A., and Marshall, J.E.A. 1981. Depositional environments and palynology of the Devonian SE Shetland Basin. Scott. Jnl. Geol. 17, 257-273.

Anderson, R.E. 1971. Thin skin distension in Tertiary rocks of south eastern Nevada. Bull. Geol. Soc. Am. 82, 43-58.

Anderton, R., Bridges, P.H., Leeder, M.R., and Selwood, B.W. 1979. A dynamic stratigraphy of the British Isles - a study in crustal evolution. George, Allen and Unwin. 301 pp.

Ashby, M.F., Ghandi, C., and Taplin, D.M.R. 1979. Fracture- mechanism maps and their construction for FCC metals and alloys. Acta. Metall. 27, 699-729.

Astin, T.R. 1985. The palaeogeography of the Middle Devonian Lower Eday Sandstone, Orkney. Scott. Jnl. Geol. 21, 353-376.

Astin, T.R. in press. A revised stratigraphy of Devonian Lacustrine sediments of Orkney, Scotland; implications for climate cyclicity, basin structure and maturation history. Jnl. Geol. Soc. Lond.

Atkinson, B.K. 1984. Subcritical crack growth in geological materials. Jnl. Geophys. Res., 89, 4298-4312.

Atkinson, B.K. 1987. Fracture mechanics of rock. Academic Press, London. 534 pp.

Atkinson, B.K. 1987. Introduction to fracture mechanics and its geophysical applications. In: Atkinson, B.K. (ed.). Fracture mechanics of rock. Academic Press, London, 1-26.

Atkinson, B.K., and Avdis, V. 1980. Fracture mechanics parameters of some rock-forming minerals determined using an indentation technique. Int. Jnl. Rock Mechanics and Mining Science, 17, 383-386.

Atkinson, B.K., and Meredith, P.G. 1987. The theory of subcritical crack growth with applications to minerals and rocks. In: Atkinson, B.K. (ed.), Fracture mechanics of rock. Academic Press, London, 111-166.

Aydin, A. 1978. Small faults as deformation bands in sandstone. Pure and Applied Geophys. 116, 913-930.

Aydin, A., and Johnson, A.M. 1978. Development of faults as zones of deformtion bands and as subsurfaces in sandstone. Pure and Applied Geophys. 116, 931-942.

Aydin, A., and Johnson, A.M. 1983. Analysis of faulting in porous sandstones. Jnl. Struct. Geol. 5, 19-35.

Badley, M.E., Egeberg, T., and Nipen, O. 1984. Development of rift basins. Block 30/6 offshore Norway. Jnl. Geol. Soc. Lond. 141, 4, p.639.

Baker, E.G. 1959. Origin and migration of oil. Science, 129, 871-874.

Baker, E.G. 1960. A hypothesis concerning the accumulation of sediment hydrocarbons to form crude oil. Geochim. et Cosmochim. Acta, 19, 309-317.

Baker, E.G. 1962. Distribution of hydrocarbons in petroleum migration and accumulation. In: Fundamental aspects of petroleum geochemistry. New York, Elsevier, 299-329.

Ballance, P. J. and Reading, H.G. 1980. (eds.) Sedimentation in oblique-slip mobile zones. Spec. Publ. Int. Assoc. Sedimentologists, 4.

Bally, A.W., Bernoulli, D., Davis, G.A., and Montadert, L. 1981. Listric normal faults. Oceanologica Acta, 87-101.

Barnett, J.A.M., Mortimer, J., Rippon, J.H., Walsh, J.J., and Watterson, J. 1987. Displacement geometry in the volume containing a singe normal fault. Bull. Am. Assoc. Pet. Geol., 71, 925-937.

Barr, D. 1985. Palinspastic restoration of normal faults in the Inner Moray Firth; implications for extensional basin development. Earth and Planetary Sci. Letters 75, 191-203.

Barr, D. 1987. Lithospheric stretching, detached normal faulting and footwall uplift. In: Coward, M.P., Dewey, J.F., and Hancock, P.L. (eds.) Continental extensional tectonics. Geol. Soc. Spec. Pub. 28, 75-94.

Barton. P., and Wood, R. 1984. Tectonic evolution of the North Sea Basin: crustal stretching and subsidence. Geophys. Jnl. R. Astro. Soc. 79, 987-1022.

Baxter, A.N., and Mitchell, J.G. 1984. Camptonite-monchiquite dyke swarms of Northern Scotland; age relationships and their implications. Scott. Jnl. Geol. 20, 297-308.

Beach, A. 1985. Some comments on sedimentary basin development in the Northern North Sea. Scott. Jnl. Geol., 21, 493-512.

Beard, D.C., and Weyl, P.K. 1973. The influence of texture on porosity and permeability of unconsolidated sand. Bull. Am. Assoc. Pet. Geol. 57, 349-369.

Beaumont, C. 1978. The evolution of sedimentary basins on a visco-elastic lithosphere: theory and examples. Geophys. Jnl. R. Astron. Soc. 55, 471-497.

Berg, R.R. 1975. Capillary pressures in stratigraphic traps. Bull. Am. Assoc. Pet. Geol. 59, 939-956.

Blenkinsop, T.G. and Rutter, E.H. 1986. Cataclastic deformation of quartzite in the Moine Thrust zone. Jnl. Struct. Geol. 8, 669-682.

Blenkinsop, T.G. 1987. Mechanisms and conditions of deformation in quartzites from the Cantabrian and West Austurian-Leonese zones, North Spain. Unpublished PhD thesis, Univ. of Keele.

Blundell, D.J., Hurich, C.A., and Smithson, S.B. 1985. A model for the MOIST seismic reflection profile, N. Scotland. Jnl. Geol. Soc. Lond. 142, 245-58.

Bogomolov, Y.G., Kudelsky, A.V., and Lapshin, N.N. 1978. Hydrology of large sedimentary basins. In: Hydrology of great sedimentary basins. Pub. Int. Assoc. Scientific Hydrology, 120, 117-122.

Borradaile, G.J. 1981. Particulate flow and the generation of cleavage. Tectonophysics, 72, 306-321.

Borradaile, G.J., Bayly, M.B., and Powell, C. M. A. 1982. Atlas of deformation and metamorphic rock fabrics. Springer-Verlag, New York, 551 pp.

Bowler, S. 1987. Deformation processes and strain in thrust systems. Unpublished PhD thesis, Univ. of Leeds.

Bowler, S. 1989. Shape fabric formation by cataclasis in a quartzite from the Moine thrust zone, northwest Scotland. Geology, 17, 353-356.

Brace, W.E., and Bombalakis, E.G. 1963. A note on brittle crack growth in compression. Jnl. Geophys. Res. 68, 3709-13.

Bradley, J.S. 1975. Abnormal formation pressure. Bull. Am. Assoc. Pet. Geol. 59, 957-973.

Brewer, J.A., and Smythe, D.K.J. 1984. MOIST and the continuity of crustal reflector geometry along the Caledonian-Appalachian Orogen. Jnl. Geol. Soc. Lond. 141, 105-120.

Brewer, J.A., and Smythe, D.K.J. 1986. Deep structure of the foreland to the Caledonian Orogen, NW Scotland: Results of the BIRPS WINCH profile. Tectonics, 5, 171-194.

Briggs, R.C., and Troxell, H.C. 1952. Effects of the Arvin-Tehachipi earthquake on spring and stream flows. In: Oakeshoff, G.B. (ed.) Earthquakes in Kern county, during 1952. Calif. Div. Mines and Geol. Bull. 171, 81-97.

Brock, W.G., and Engelder, T. 1977. Deformation associated with the movement of the Muddy Mountain overthrust in the Buffington window, southeastern Nevada. Bull. Geol. Soc. Am. 88, 1667-1677,

Brown, J.F. 1975. Potassium-argon evidence of a Permian Age for the Camptonite Dykes, Orkney. Scott. Jnl. Geol. 11, 259-262.

Bruhn, R.L., and Paulis, T.L. 1981. Late Cenozoic deformation in the forearc region: Matanuska Valley, Alaska: three-dimensional strain in a forearc region. Bull. Geol. Soc. Am. 92, 282-293.

Burley, S.D., Mullis, J., and Matter, A. 1989. Timing diagenesis in the Tartan Reservoir (UK North Sea): constraints from combined cathodoluminescence microscopy and fluid inclusion studies. Marine and Pet. Geol., 6, 98-120.

Butler, R.W.H. 1982. A structural analysis of the Moine Thrust Zone between Loch Eriboll and Foinaven, NW Scotland. Jnl. Struct. Geol. 4, 19-29.

Butler, R.W.H. 1984. Structural evolution of the Moine Thrust Belt between Loch More and Glendhu, Sutherland. Scott. Jnl. Geol. 20, 161-79.

Butler, R.W.H. 1987. Thrust sequences. Jnl. Geol. Soc. Lond. 144, 619-634.

Butler, R.W.H., and Coward, M.P. 1984. Geological constraints, structural evolution and deep geology of the northwest Scottish Caledonides. Tectonics, 3, 347-365.

Cheadle, M.J., McGeary, S., and Warner, M.R. 1987. Extensional structures on the western UK continental shelf: A review of evidence from deep seismic profiling: In, Coward, M.P., Dewey, J.F., and Hancock, P.L., (eds.), Continental Extensional Tectonics. Spec. Pub. Geol. Soc. Lond., 445-65.

Chester, F.M., Friedman, M., and Logan, J.M. 1985. Foliated cataclasites. Tectonophysics 111, 139-146.

Chester, F.M. and Logan, J.M. 1986. Implications for mechanical properties of brittle faults from observations of the Punchbowl Fault Zone, California. Pure and Applied Geophys. 124, 79-106.

Christie, J.M. 1960. Mylonitic rocks of the Moine Thrust Zone in the Assynt region, N.W. Scotland. Trans Edin. Geol. Soc., 18, 93-99.

Christie, J.M. 1963. The Moine Thrust Zone in the Assynt region, northwest Scotland. Univ. California Publ. Geol. Sci. 40, 345-440.

Christie, P.A.F., and Sclater, J.G. 1980. An extensional origin for the Buchan and Witchground Graben in the North Sea. Nature, 283, 729-732.

Collier, R.E.LL. 1988. Sedimentary facies evolution in continental fault-bounded basins formed by crustal extension. The Corinth Basin, Greece. Unpublished PhD thesis, Univ. of Leeds.

Cordell, R.J. 1972. Depths of oil origin and primary migration: a review and critique. Bull. Am. Assoc. Pet. Geol., 56, 2029-2067.

Coward, M.P. 1982. Surge zones in the Moine Thrust Zone of N.W. Scotland. Jnl. Struct. Geol. 4, 247-256.

Coward, M.P. 1983. The thrust and shear zones of the Moine Thrust Zone and NW Scottish Caledonides. Jnl. Geol. Soc. London, 140, 795-811.

Coward, M.P. 1985. The thrust structures of southern Assynt, Moine Thrust Zone. Geol. Mag., 122, 595-607.

Coward, M.P. 1986. Heterogeneous stretching, simple shear and basin development. Earth Planet. Sci. Lett., 80, 325-336.

Coward, M.P., and Enfield, M.A. 1987. The structure of the West Orkney and adjacent basins: In: Brooks, J. and Glennie, K. (eds.). Petroleum Geology of North West Europe, 687-96.

Coward, M.P., Butler, R.W.H., Chambers, A.F., Graham, R.H., Izatt, C.N., Khan, M.A., Knipe, R.J., Prior, D.J., Treloar, P.J., and Williams, M.P. 1988. Folding and imbrication of the Indian crust during Himalayan collision. Phil. Trans. R. Soc. Lond. A326, 89-116.

Coward, M.P., Enfield, M.A., and Fischer, M.W. 1989. Devonian basins of northern Scotland: extension and inversion related to late Caledonian-Variscan tectonics. In: Cooper, M.A., and Williams, G.D. (eds.) Inversion Tectonics. Geol. Soc. Spec. Publ., 44, 275-308.

Crans, W., Mandl, G., and Haremboure, J. 1980. On the theory of growth faulting: a geomechanical delta model based on gravity sliding. Jnl. Petroleum Geology, 2, 265-307.

Dayan, H. 1981. Deformation studies of the folded Mylonites of the Moine Thrust, Eriboll district, N.W. Scotland. Unpublished PhD thesis, Univ. of Leeds.

Davis, R.W. 1987. Analysis of hydrodynamic factors in petroleum migration and entrapment. Bull. Am. Assoc. Pet. Geol. 71, 643-649.

Dennis, P.F., and Atkinson, B.K. 1981. Deformation mechanism maps for flow and fracture of quartz. Geophys. Jnl. Royal Astron. Soc., 65, 278.

Dickey, P.A. 1975. Possible primary migration of oil from source rock in oil phase. Bull. Am. Assoc. Pet. Geol. 59, 337-345.

Duindam, P., & Van Hoorn, B. 1987. Structural evolution of the West Shetland continental margin. In: Brooks, J. and Glennie, K. (eds.). Petroleum Geology of North West Europe, 765- 774.

Dunn, D.E., La Fountain, L.J., and Jackson, R.E. 1973. Porosity dependence and mechanism of brittle fracture in sandstone. Jnl. Geophys. Res. 78, 2403-2417.

Elliott, D., and Johnson, M.R.W. 1980. Structural evolution in the northern part of the Moine Thurst Belt, N.W Scotland. Trans. R. Soc. Edinb. Earth Sci. 71, 69-96.

Ellis, P.G., and McClay, K.R. 1988. Listric extensional fault systems-results of analogue model experiments. Basin Res., 1, 55-70.

Enfield, M.E. 1988. The geometry of normal fault systems and basin development: Northern Scotland and Southern France. Unpublished Ph.D. thesis, Imperial College, London.

Enfield, M.E., and Coward, M.P. 1987. The structure of the West Orkney Basin, northern Scotland. Jnl. Geol. Soc. Lond., 144, 871-84.

Engelder, J.T. 1974. Cataclasis and the generation of fault gouge. Bull. Geol. Soc. Am., 85, 1515-1522.

England, P.C., and Jackson, J.A. 1987. Migration of the seismic- aseismic transition during uniform and non-uniform extension of the continental lithosphere. Geology, 15, 29-294.

Etheridge, M.A., and Wilkie, J.C. 1981. An assessment of dynamically recrystallized grainsize as a palaeopiezometer in quartz-bearing mylonite zones. Tectonophysics, 78, 475-508.

Etheridge, M.A., Wall, V.J., and Vernon, R.H. 1983. The role of the fluid phase during regional deformation and metamorphism. Jnl. Metam. Geol. 1, 205-226.

Etheridge, M.A., Wall, V.J., Cox, S.F., and Vernon, R.H. 1984. High fluid pressures during regional metamorphism and deformation. Implications for mass transport and deformation mechanisms. Jnl. Geophys. Res. 89, 4344-4358.

Exner, M. E. 1972. Analysis of grain and particle size distribution in metallic materials. Int. metallurgical reviews. 17, 25-42.

Eyidogon, H., and Jackson, J.A. 1985. A seismological study of normal faulting in the Demirci, Alaseher and Gediz earthquakes of 1969-1970 in western Turkey: implications for the nature and geometry of deformation in the continental crust. Geophys. Jnl. R. Astro. Soc. 81, 569-607.

Fannin, N.G.T. 1970. The sedimentary environment of the old red sandstone of western Orkney. Unpublished PhD thesis, Univ. of Reading.

Ferguson, C.C., LLoyd, G.E., and Knipe, R.J. 1987. Fracture mechanics and deformation processes in natural quartz: a combined Vickers Indentation SEM and TEM study. Can. Jnl. Earth Sci. 24, 544-555.

Flourney, L.A., and Ferrell, R.E. 1980. Geopressure and diagenetic modifications of porosity in the Lirette field area, Terrebonne parish, Louisiana. Gulf Coast. Assoc. Geol. Soc. Trans. 30, 341-345.

Friedman, M., and Logan, J.M. 1970. Microscopic feather fractures. Bull. Geol. Soc. Am. 81, 3417-3420.

Gallagher, J.J., Friedman, M., Handin, J. and Sowers, G.M. 1974. Experimental studies relating to microfracture in sandstone. Tectonophysics 21, 203-247.

Galloway, W.E. 1986. Hydrogeological regimes of sandstone diagenesis. In: McDonald, D.A., and Surdam, R.C. (eds.). Sandstone Diagenesis. Am. Assoc. Pet. Geol. Memoir 37, 3-13.

Galloway, W.E., Hobday, D.K., and Magara, K. 1982. Frio Formation of Texas Gulf coastal plain: depositional systems, structural framework, and hydrocarbon distribution. Bull. Am. Assoc. Pet. Geol. 66, 649-688.

Gans, P.B. 1987. An open-system, two-layer crustal stretching model for the Eastern Great Basin. Tectonics 6, 1-12.

Ghandi, C., and Ashby, M.F. 1979. Fracture mechanism maps for materials which cleave FCC, BCC and HCP metals and ceramics. Acta. Metall. 27, 1565-1602.

Gibbs, A.D. 1983. Balanced cross-section contruction from seismic sections in areas of extensional tectonics. Jnl. Stuct. Geol. 5, 153-160.

Gibbs, A.D. 1984a. Structural evolution of extensional basin margins. Jnl. Geol. Soc. Lond. 141, 609-620.

Gibbs, A.D. 1984b. Clyde field growth fault secondary detachment above basement faults in North Sea. Bull. Am. Assoc. Pet. Geol. 68, 1029-1039.

Giles, M.R. 1987. Mass transfer and problems of secondary porosity creation in deeply buried hydrocarbon reservoirs. Marine and Petroleum Geology, 4, 188-204.

Gillcrist, R., Coward, M., and Mugnier, J.L. 1987. Structural inversion and its controls: examples from the Alpine foreland and the French Alps. Geodynamica Acta, 1, 5-34.

Glennie, K.W. 1984. The structural framework and pre-Permian history of the North Sea area. In: Glennie, K.W. (ed.) Introduction to the petroleum geology of the North Sea. Blackwell, Oxford. 17-39.

Grant, N.T. 1989. Deformation and fluid processes in thrust sheets from the Central Pyrenees. Unpublished PhD thesis, Univ. of Leeds.

Grant, N.T., Banks, D.A., McCaig, A.M., and Yardley, B.W.D. in press. The chemistry, source and behaviour of fluids involved in Alpine thrusting of the Central Pyrenees. Jnl. Geophys. Res.

Gratier, J.P., and Guiguet, R. 1986. Experimental pressure solution deposition on quartz grains. The crucial effect of the nature of the fluid. Jnl. Struct. Geol. 8, 845-856.

Griffith, A.A. 1920. The phenomena of rupture and flow in solids. Philos. Trans. R. Soc. Lond. A221, 163-178.

Griggs, D., and Handin, J. 1966. Observations on fracture and a hypothesis of earthquakes. In: Rock Deformation, Griggs, D., and Handin, J., (eds.) Geol. Soc. Am. Mem. 79, 347-364.

Groshong, R.H.Jr. 1972. Strain calculated from twinning in calcite. Bull. Geol. Soc. Am. 83, 2025-2038.

Gross, W.W., and Hillmeyer, F.L. 1982. Geometric analysis of upper-plate fault patterns in the Whipple-Buckskin detachment terrane, California and Arizona. In: Frost, E.G. and Martin, D.L (eds). Mesozoic-Cenozoic tectonic evolution of the Colorado River region. 256-265.

Guidish, T.M., Kendall, C.G., Lerche, I., Toth, D.J., and Yarzab, R.F. 1985. Basin evolution using burial history calculations: an overview. Bull. Am. Assoc. Pet. Geol. 69, 92-105.

Hadizadeh, J. 1980. An experimental study of cataclastic deformation in a quartzite. Unpublished PhD thesis, Imperial College, Univ. of London.

Halliday, A.N., McAlpine, A., and Mitchell, J.G. 1977. The age of the Hoy lavas, Orkney. Scott. Jnl. Geol. 13, 43-52.

Hamilton, R.F.M., and Trewin, N.H. 1985. excursion guide to the devonian of Caithness. Pet. Expl. Soc. G.B., Aberdeen Branch, 35 pp.

Handy, M.R. 1986. The structure and rheological evolution of the Polgallo Fault Zone, a deep crustal dislocation in the Southern Alps of Northwestern Italy. Unpublished Ph.D. thesis, Basel.

Harding, T.P. 1983. Structural inversion at Ramputan oil field. In: Seismic expression of structural styles - a picture and work atlas. AAPG studies in Geology 15. 3, 3.3-13 to 3.3-18.

Harding, T.P. 1985. Seismic characteristics and identification of negative flower structures, positive flower structures, and positive structural inversion. Bull. Am. Assoc. Pet. Geol., 69, 582-600.

Harding, T.P. and Lowell, J.D. 1979. Structural styles, their plate tectonic habitats and hydro-carbon traps in petroleum provinces. Bull. Am. Assoc. Pet. Geol., 63, 1016.

Harding, T.P., and Tuminas, A.C. 1988. Interpretation of footwall (lowside) fault traps sealed by reverse faults and convergent wrench faults. Bull. Am. Assoc. Pet. Geol. 72, 738-757.

Harms, J.C. 1966. Stratigraphic traps in a valley fill, western Nebraska. Bull. Am. Assoc. Pet. Geol. 50, 2119-2149.

Heald, M.T., and Larese, R.E. 1974. Influence of coatings on quartz-cementation. Jnl. Sed. Petrol. 44, 1269-1274.

Hillier, S.J., and Marshall, J.E.A. 1988. Hydrocarbon source rocks, thermal maturity and burial history of the Orcadian Basin, Scotland. In: Fleet, A.J., Kelts, K., and Talbot, M.R., (eds), Lacustrine petroleum source rocks, Geol. Soc. Lond. Spec. Pub. 40, 203.

Hobbs, B.E. 1968. Recrystallization of single crystals of quartz. Tectonophysics, 6, 353-401.

Hobbs, B.E., McClaren, A.C., and Paterson, M.S. 1972. Plasticity of single crystals of synthetic quartz. In: Heard, H.C., Borg, I.Y., Carter, N.I., and Raleigh, C.B. (eds.). Flow and fracture of rocks. Monograph Am. Geophys. Un., 16, 29-53.

Horii, H., and Nemat-Nasser, S. 1986. Brittle failure in compression: splitting faulting and brittle-ductile transition. Philos. Trans. R. Soc. Lond. A319, 337-374.

Hossack, J. 1984. The geometry of listric growth faults in the Devonian Basins of Sunnfjord, W. Norway. Jnl. Geol. Soc. Lond. 141, 629-37.

House, W.M. and Gray, D.R. 1982. Cataclasites along the Saltville Thrust, U.S.A. and their implications for thrust sheet emplacement. Jnl. Struct. Geol. 4, 257-270.

Houseknecht, D.W. 1988. Intergranular pressure solution in four quartzose sandstones. Jnl. Sed. Petrol. 58, 228-246.

Hubbert, M.K. 1953. Entrapment of petroleum under hydrodynamic conditions. Bull. Am. Assoc. Pet. Geol. 37, 1954-2026.

Hubbert, M.K., and Rubey, W.W. 1959. Role of fluid pressure in mechanics of overthrust faulting. Bull. Geol. Soc. Am. 70, 115-166.

Hunt, J.M. 1975. Is there a geochemical depth limit for hydrocarbons? Petroleum Eng. March, 112-124.

Jackson, J.A. 1987. Active normal faulting and lithospheric extension. In: Coward, M.P., Dewey, J.F., and Hancock, P. (eds). Continental Extensional Tectonics. Spec. Publ. Geol. Soc. Lond. 28, 3-18.

Jackson, J., and McKenzie, D. 1983. The geometrical evolution of normal fault systems. Jnl. Struct. Geol. 5, 471-482.

Jackson, J.A., and White, N.J. 1989. Normal faulting in the upper continental crust: observations from regions of active extension. Jnl. Struct. Geol. 11, 15-36.

Jackson, J.A., White, N.J., Garfunkel, Z., and Anderson, H. et al. 1988. Relations between normal fault geometry, tilting and vertical motions in extensional terrains: an example from the Southern Gulf of Suez. Jnl. Struct. Geol. 10, 155-170.

Jamison, W.R., and Stearns, D.W. 1982. Tectonic deformation of Wingate sandstone, Colorado National Monument. Bull. Am. Assoc. Pet. Geol. 66, 2584-2608.

Jarvis, G.T., and McKenzie, D.P. 1980. Sedimentary basin formation with finite extension rates. Earth Planetary Science Letters. 48, 42-52.

Johnson, M.R.W., Kelley, S.P., Oliver, G.J.H., and Winter, D.A. 1985. Thermal effects and timing of thrusting in the Moine Thrust Zone. Jnl. Geol. Soc. Lond. 142, 863-874.

Jones, M.E., and Preston, R.M.F. 1987. Introduction to Deformation of sediments and sedimentary rocks. In: Jones, M.E., and Preston, R.M.F., (eds.). Deformation of Sediments and Sedimentary Rocks. Geol. Soc. Spec. Pub. 29, 1-8.

Jourdan, A., Thomas, M., Brevart, O., Robson, P., Sommer, F., and Sullivan, M., 1987. Diagenesis as the control of Brent sandstone reservoir properties in the Greater Alwyn area, E. Shetland Basin. In: Brooks, J., and Glennie, K. (eds.). Petroleum Geology of North-West Europe. 951-961.

Kerrich, R. 1978. An historical review and synthesis of research on pressure solution. Zentbl. Miner. Geol. Palaont., 5, 572-550.

Kilenyi, T., and Stanley, R. 1985. Petroleum prospects in the northwestern seaboard of Scotland. Oil and Gas Jnl. 7-10, 100-108.

Kirton, S.R., and Hitchen, K. 1987. Timing and style of crustal extension north of the Scottish mainland. In: Coward, M.P., Dewey, J.F., and Hancock, P.L. (eds.), Continental extensional tectonics. Spec. Publ. Geol. Soc. Lond., 28, 501-510.

Knipe, R.J. 1986a. Faulting mechanisms in slope sediments: examples from cores. In: Moore, J. C. (ed.) Structural fabrics in DSDP cores from forearcs. Geol. Soc. Am. Mem. 166, 45-54.

Knipe, R.J. 1986b. Microstructural evolution of vein arrays preserved in DSDP cores from Japan trench leg 57. In: Moore, J.C. (ed) Structural fabrics in DSDP cores from forearcs. Geol. Soc. Am. Mem. 166, 75-88.

Knipe, R.J. 1986c. Deformation mechanism path diagrams for sediments undergoing lithification. In: Moore, J. C. (ed.) Structural fabrics in DSDP cores from forearcs. Geol. Soc. Am. Mem. 166, 151-160.

Knipe, R.J. 1989a. Deformation mechanisms - recognition from natural tectonites. Jnl. Struct. Geol. 11, 127-146.

Knipe, R.J. 1989b. Microstructural analysis and tectonic evolution in thrust systems. In: Barber, D.J., and Meridith, P. (eds.). Deformation of Materials.

Knipe, R.J. and Law, R.D. 1987. The influence of crystallographic orientation and grain boundary migration in microstructural and textural evolution in an S.C. mylonite. Tectonophysics 135, 153-169.

Kohlstedt, D.L., Cooper, R.F., Weathers, M.S., and Bird, J.M. 1979. Palaeostress analysis of deformation induced microstructures: Moine Thrust Zone and Iquertoq Shear Zone. Analysis of actual fault zones in bedrock. U.S.G.S. Open File Report, 79-1239, 394-425.

Kranz, R.L. 1983. Microcracks in rocks: a review. Tectonophysics 100, 449-480.

Kusznir, N.J., and Park, R.G. 1987. The extensional strength of the continental lithosphere: its dependence on geothermal gradient, and crustal composition and thickness. In: Coward, M.P., Dewey, J.F., and Hancock, P.L., (eds.). Continental extensional tectonics. Spec. Publ. Geol. Soc. Lond., 28, 35-52.

Laubach, S.E., and Marshak, S. 1987. Fault patterns generated during extensional deformation of crystalline basement, NW Scotland. In: Coward, M.P., Dewey, J.F., and Hancock, P.L., (eds.). Continental extensional tectonics. Spec. Pub. Geol. Soc. Lond., 28, 495-99.

Law, R.D. 1987. Heterogenous deformation and quartz crystallographic fabric transitions: natural examples from the Moine Thrust Zone at the Stack of Glencock, northern Assynt. Jnl. Struct. Geol. 9, 819-333.

Law, R.D., Casey, M. and Knipe, R.J. 1986. Kinematic and tectonic significance of microstructures and crystallographic fabrics within quartz mylonites from Assynt and Eriboll regions of the Moine Thrust Zone. Trans. R. Soc. Edinb. Earth Sci. 77, 99-125.

Law, R.D., Knipe, R.J., and Dayan, H. 1984. Strain path partitioning within thrust sheets: microstructral and petrofabric evidence from the Moine Thrust Zone at Loch Eriboll, N.W. Scotland. Jnl. Struct. Geol. 6, 477-497.

Law, R.D., and Potts, G.J. 1987. The Tarskavaig Nappe of Skye, northwest Scotland: a re-examination of the fabrics and their kinematic significance. Geol. Mag. 124, 231-248.

Lawn, B.R. 1983. The physics of fracture. Jnl. Amer. Ceram. Soc. 66, 83-91.

Lawn, B.R. and Wilshaw, T.R. 1975. Fracture of Brittle Solids. Cambridge Univ. Press. London.

LePichon, X., and Sibouet, J-C. 1981. Passive margins: a model of formation. Jnl. Geophys. Res. 86, 3708-3720.

LePichon, X., Angellier, J., and Sibouet, J-C. 1982. Plate boundaries and extensional tectonics. Tectonophysics. 81, 239-256.

Lee, M., Aronson, J.L., and Savin, S.M. 1989. Timing and Conditions of Permian Rotiegende Sandstone Diagenesis, Southern North Sea: K/Ar and Oxygen Isotopic Data. Bull. Am. Assoc. Pet. Geol., 73, 195-215.

Leeder, M.R., and Gawthorpe, R. 1987. Sedimentary models for extensional tilt-block/half-Graben basins. In: Coward, M.P., Dewey, J.F., and Hancock, P.L. (eds.). Continental extensional tectonics. Geol. Soc. Spec. Pub., 28, 139-152.

Leverett, M.C. 1941. Capillary behavior in porous solids. Amer. Int. M. E. Trans., 142, 152-169.

Lindquist, P.A., Lai, A.H., and Alm, O. 1984. Indentation fracture development in rock continuosly observed with a scanning electron microscope. Int. Jnl. Rock. Mech. Min. Sci. and Geomech. Abstr. 21, 165-184.

Lloyd, G.E. and Knipe, R.J. Submitted. Deformation mechanisms accommodating faulting of quartzite under upper crustal conditions. Jnl. Struct. Geol.

Logan, J.M., Higgs, N.G., and Friedman, M. 1981. Laboratory studies on natural gouge from the US Geological Survey Dry Lake Valley N.1 well, San Andreas fault zone. Geophys. Monogr. 24, Amer. Geophys. Union, 121-134.

Magara, K. 1976. Water expulsion from clastic sediments during compaction, directions and volumes. Bull. Am. Assoc. Pet. Geol. 60, 543-553.

Magara, K. 1987. Fluid flow due to sediment loading - an application to the Arabian Gulf Region. In: Goff, J.C., and Williams, B.P.J., (eds.). Fluid flow in Sedimentary Basins and Auquifers. Geol. Soc. Spec. Publ. 34, 19-28.

Maltman, A. 1984. On the term 'soft sediment' deformation. Jnl. Struct. Geol. 6, 589-592.

Marshall, J.E.A. 1988. Devonian miospores from Papa Stour, Shetland. Trans. R. Soc. Edinb. Earth Sci. 79, 13-18.

Marshall, J.E.A. 1989. Devonian miospores from the Walls Group, Shetland. Scott. Jnl. Geol.

Marshall, J.E.A., and Allen, K.C. 1982. Devonian miospore assemblages from Fair Isle, Shetland. Palaeontology 25, 277-312.

McAlpine, A. 1978. The upper old red sandstone of Orkney, Caithness and neighbouring areas. Unpublished PhD thesis, Univ. of Newcastle-upon-Tyne.

McAuliffe, C.D. 1979. Oil and gas migration-chemical and physical constraints. Bull. Am. Assoc. Pet. Geol. 63, 761-781.

McClay, K.R., and Coward, M.P. 1981. The Moine Thrust Zone: an overview. In: McClay, K.R., and Price, N.J. (eds.). Thrust and nappe tectonics Spec. Publ. Geol. Soc. Lond., 9, 241-260.

McClay, K.R., and Ellis, P.G. 1987a. Analogue models of extensional fault geometries. In: Coward, M.P., Dewey, J.F., and Hancock, P.L.(eds.) Continental extensional tectonics. Spec. Publ. Geol. Soc. Lond., 28, 109-125.

McClay, K.R., and Ellis, P.G. 1987b. Geometries of extensional fault systems developed in model experiments. Geology 15, 341-344.

McClay, K.R., Ellis, P.G., and Knipe, R.J. 1987. Model studies of inversion structures. In: Inversion tectonics, (abstracts), Tectonics Studies Group.

McClay, K.R., Norton, M.G., Coney, P., and Davis, G.H. 1986. Collapse of the Caledonian Orogen and the Old Red Sandstone. Nature, 323, 147-149.

McKenzie, D.P. 1978. Some remarks on the development of sedimentary basins. Earth Planet. Sci. Lett., 40, 25-32.

Mitra, S. 1988. Effects of deformation mechanisms on reservoir potential in Central Appalachian Overthrust Belt. Bull. Am. Assoc. Pet. Geol. 72, 536-554.

Moore, J. C., Roeske, S., Lundberg, N., Schoonmaker, J., Cowan, D.S., Gonzales, E., and Lucas, S.E. 1986. Scaly Fabrics from Deep Sea Drilling Project cores from forearcs. In: Moore, J.C., (ed.) Structural fabrics in DSDP cores from forearcs. Geol. Soc. Am. Mem. 166., 55-73.

Morrow, C.A., Shi, L.Q., and Byerlee, J.D. 1982. Strain hardening and strength of clay-rich fault gouges. Jnl. Geophys. Res., 87, 6771-6780.

Murchison, R.I. 1859a. On the succession of the older rocks in the northernmost counties of Scotland. Quart. Jnl. Geol. Soc. Lond. 17, 145-151.

Murchison, R.I. 1859b. On the succession of the older rocks in the northernmost counties of Scotland; with some observations on the Orkney and Shetland Isles. Quart. Jnl. Geol. Soc. Lond. 18, 353-418.

Mykura, W. 1976. British regional geology: Orkney and Shetland. H.M.S.O.

Mykura, W. 1983. Old Red Sandstone. In: Craig, G.Y. (ed.) Geology of Scotland. Academic Press, London, 205-221.

Naylor, M.A., Mandl, G., and Sijpestein, C.H.K. 1986. Fault geometries in basement-induced wrench faulting under different initial stress states. Jnl. Struct. Geol. 7, 737-752.

Nicolas, A., and Poirier, J.P. 1976. Crystalline plasticity and solid state flow in metamorphic rocks. Wiley, London. 444pp.

Norton, M.G. 1982. The kinematics and microstructural development of some shear zones. Unpublished Phd. thesis, University of London.

Norton, M.G. 1986. Late Caledonide extension in western Norway: a response to extreme crustal thickening. Tectonics 5, 195-204.

Olgaard, D.L., and Brace, W.F. 1983. The microstructures of gouge from a mining-induced seismic shear zone. Int. Jnl. Rock Mech. Min. Sci. and Geomech. Abstr. 20, 11-19.

Ord, A. and Christie, J.M. 1984. Flow stresses from microstructures in mylonitic quartzites from the Moine Thrust Zone, Assynt area, Scotland. Jnl. Struct. Geol. 6, 639-654

Ord, D.M., Clemmey, H., and Leeder, M.R. 1988. Interaction between faulting and sedimentation during Dinantian extension of the Solway Basin, S.W. Scotland. Jnl. Geol. Soc. Lond., 145.

Parnell, J.T. 1983. The distribution of hydrocarbon minerals in the Orcadian Basin. Scott. Jnl. Geol. 19, p.205-210.

Parnell, J.T. 1985. Hydrocarbon source rocks, reservoir rocks and migration in the Orcadian Basin. Scott. Jnl. Geol. 21, 321-336.

Peach, B.N., Horne, J., Gunn, W., Clough, C.T., and Hinxman, L.W. 1907. The Geological structure of the Northwest Highlands of Scotland. Mem. Geol. Survey. GB.

Philippi, G.T. 1965. On the depth, time and mechanism of petroleum generation: Geochim. et Cosmochim. Acta., 29, 1021-1049.

Pickering, F.B. 1976. The basis of quantitative metallography. Inst. of metallurgical techniques monograph. 1, 1-55.

Pickering, K.T. 1984. The upper Jurassic 'Boulder bed' and related deposits: a fault-controlled submarine slope, N.E. Scotland. Jnl. Geol. Soc. Lond., 141, 357-374.

Pittman, E.D. 1981. Effect of fault-related granulation on porosity and permeability of quartz sandstones, Simpson Group (Ordovician), Oklahoma. Bull. Am. Assoc. Petrol. Geol. 65, 2381-2387.

Poirier, J.P. 1985. Creep of crystals: high temperature deformation processes in metals, ceramics and minerals. Cambridge Univ. Press, Cambridge, 240pp.

Poirier, J.P., and Guillope, M. 1979. Deformation induced recrystallization of minerals. Bull. Mineral, 102, 67-74.

Poirier, J.P., and Nicolas, A. 1975. Deformation induced recrystallization due to progressive misorientation of subgrains, with special reference to mantle peridotites. Jnl. Geol. Soc. 83, 707-720.

Pollard, D.D., and Segall, P. 1987. Theoretical displacements and stresses near fractures in rock: with applications to faults, joints, veins, dikes and solution surfaces. In: Atkinson, B.K., (ed.) Fracture mechanics of rock. Academic Press, London, 277-349.

Porter, K.W., and Weimer, R.J. 1982. Diagenetic sequence related to structural history and petroleum accumulation: Spindle Field, Colorado. Bull. Am. Assoc. Pet. Geol. 66, 2543-2560.

Price, L.C. 1976. Aqueous solubility of petroleum as applied to its origin and primary migration. Bull. Am. Assoc. Pet. Geol. 60, 213-244.

Prior, D.J. 1988. Deformation processes in the Alpine Fault Mylonites, South Island, New Zealand. Unpublished PhD thesis, Univ. of Leeds.

Prior, D.J., and Behrmann, J.H. In press a. Backscatter imagery of fine-grained sediments from hole 671B, ODP leg 110: preliminary results. Proceedings of the ODP, V.110, Part B. U.S. Gov. Printing Office, Washington.

Prior, D.J., and Behrmann, J.H. In press b. Thrust related mudstone fabrics from the Barbados Forearc: a backscattered SEM study. Jnl. Geophys. Res.

Proffett, J.M. 1977. Cenozoic geology of the Yerington District, Nevada, and implications for the nature and origin of Basin and range faulting. Bull. Geol. Soc. Am. 88, 247-266.

Rayner, D.H. 1963. The Achanarras limestone of the middle old age sandstone, Caithness, Scotland. Proc. Yorks. Geol. Soc. 18, 5-20.

Reches, Z. 1978. Analysis of faulting in three-dimensional strain field. Tectonophysics, 47, 109-29.

Reches, Z. 1983. Faulting of rocks in three-dimensional strain fields II. Theoretical analysis. Tectonophysics, 95, 133-156.

Ridgeway, J.M. 1974. Sedimentology of the Eday Group, Middle Old Red Sandstone, Orkney. Unpublished PhD thesis, Univ. of London.

Robinson, M.A. 1985. Palaeomagnetism of volcanics and sediments of the Eday Group, southern Orkney. Scott. Jnl. Geol. 21, 285-300.

Robinson, M.A. 1986. Palaeomagnetism of old red sandstones and related rocks of the Orcadian Basin, including mineralogical studies of the Remanence carriers. Unpublished PhD thesis, Univ. of Leeds.

Rock, N.M.S. 1983. The Permo-Carboniferous camptonite-monchiquite dyke suite of the Scottish highlands and islands: distribution, field, and petrological aspects. Report Inst. of Geol. Sciences, E82/14.

Rogers, D.A. 1987. Devonian correlations, environments and tectonics across the Great Glen Fault. Unpublished PhD thesis, Univ. of Cambridge.

Rogers, D.A. Marshall, J.E.A., and Astin, T.R. 1989. Devonian and later movements on the Great Glen Fault System, Scotland. Jnl. Geol. Soc. London, 146, 369-72.

Rogers, J.J. and Head, W.B. 1961. Relationship between porosity median size, and sorting coefficients of synthetic sands. Jnl. Sed. Pet., 31, 467-470.

Rossel, N.C. 1982. Clay mineral diagenesis in Rotliegend aeolian sandstones of the southern North Sea. Clay Minerals, 17, 69-77.

Royden, L., and Keen, C.E. 1980. Rifting process and thermal evolution of the continental margin of Eastern Canada determined from subsidence curves. Earth. Planet. Sci. Lett. 51, 343-61.

Rudnicki, J.W. 1980. Fracture mechanics applied to the Earth's crust. Ann. Rev. Earth Planet. Sci. Lett. 8, 489-525.

Rutter, E.H., and Mainprice, D.H. 1978. The effect of water on stress relaxation of faulted and unfaulted sandstone. Pure and Applied Geophys. 116, 634-654.

Rutter, E.H., Maddock, R.H., Hall, S.H. and White, S.H. 1986. Comparative microstructures of natural and experimentally produced clay bearing fault gouges. Pure and Applied Geophys. 124, 3-30.

Rutter, E.H., and White, S.H. 1979a. The effects of water, temperature, and time on the microstructural and mechanical properties of experimentally produced fault gouge. Bull. Mineral. 102, 93-101.

Rutter, E.H., and White, S.H. 1979b. The microstructures and rheology of fault gouges produced experimentally under wet and dry conditions at temperatures up to 400° C. Bull. Mineral. 102, 101-109.

Sammis, C.G., Osborne, R.H., Anderson, J.L., Banerdt, M., and White, P. 1986. Self similar cataclasis in the formation of fault gouge. Pure and Applied Geophys. 124, 53-78.

Sammis, C., King, G., and Biegel, R. 1987. The kinematics of gouge deformation. Pure and Applied Geophys. 125, 777-812.

Schmid, S.M. 1982. Microfabric studies as conditions of deformation mechanisms and flow laws operative in mountain building. In: Hsu, K.J. (ed.). Mountain Building Processes. Academic Press, London, 95-110.

Scholz, C.H. 1982. Scaling laws for large earthquakes; consequences for physical models. Bull. Seism. Soc. Am. 72, 1-14.

Scholz, C.H. 1989. Mechanics of faulting. Ann. Rev. Earth. Planet. Sci.. Lett. 17, 309-34.

Schowalter, T.T. 1979. Mechanics of secondary hydrocarbon migration and entrapment. Bull. Amer. Assoc. Pet. Geol. 63, 723-760.

Sclater, J.G., and Christie, P.A.F. 1980. Continental stretching: an explanation of the post-mid-Cretaceous subsidence of the Central North Sea Basin. Jnl. Geophys. Res. 85, 3711-3739.

Seeburger, D.A. 1981. Studies of natural fractures, fault zone permeability, and a pore space-permeability model. Unpublished. PhD thesis, Stanford Univ.

Seranne, M., and Seguret, M. 1987. The Devonian Basins of western Norway, tectonic and kinematics of an extending crust. In: Coward, M.P., Dewey, J.F., and Hancock, P. (eds). Continental extensional tectonics. Spec. Pub. Geol. Soc. Lond. 28, 537-48.

Shelton, J.W. 1984. Listric normal faults: an illustrated summary. Bull. Am. Assoc. Petrol. Geol. 68, 801-815.

Shi, Y., and Wang, C.Y. 1986. Pore pressure generation in sedimentary basins: overloading versus aquathermal. Jnl. Geophys. Res. 91, 2153-2162.

Sibson, R.H. 1977. Fault rocks and fault mechanisms. Jnl. Geol. Soc. Lond. 133, 191-213.

Sibson, R.H. 1981. Controls on low-stress hydro-fracture dilatancy in thrust, wrench and normal fault terrains. Nature 289, 665-667.

Sibson, R.H. 1983. Continental fault structure and the shallow earthquake source. Jnl. Geol. Soc. Lond. 140, 741-767.

Sibson, R.H. 1986. Brecciation processes in fault zones. Inferences from earthquake rupturing. Pure and Applied. Geophys. 124, 159-175.

Sibson, R.H. 1987. Earthquake rupturing as a mineralizing agent in hydrothermal systems. Geology, 15, 701-704.

Sibson, R.H., Robert, F., and Poulson, K.H. 1988. High-angle reverse faults, fluid-pressure cycling, and mesothermal gold-quartz deposits. Geology, 16, 551-555.

Sibson, R.H. 1989. Earthquake faulting as a structural process. Jnl. Struct. Geol. 11, 1-14.

Sibson, R.H., Francois, R., and Poulsen, K. 1988. High-angle reverse faults, fluid pressure cycling, and mesothermal gold-quartz deposits. Geology 16, 551-555.

Sibson, R.H., McMoore, J., and Rankin, A.H. 1975. Seismic pumping - a hydrothermal fluid transport mechanism. Jnl. Geol. Soc. Lond., 131, 653-659.

Smith, D.A. 1966. Theoretical consideration of sealing and non-sealing faults. Bull. Am. Assoc. Pet. Geol. 50, 363-374.

Smith, D.A. 1980. Sealing and non-sealing faults in Louisiana Gulf Coast Salt Basin. Bull. Am. Assoc. Pet. Geol. 64, 145-172.

Smith, D.I. 1977. The Great Glen Fault. In: Gill, G. (ed.) The Moray Firth Area Geological Studies, Inverness Field Club.

Smythe, D.K., Dobinson, A., McQuillin R., Brewer, J.A., Matthews, D.H., Blundell, D.J., and Kelk, B. 1982. Deep structure of the Scottish Caledonides revealed by the MOIST reflection profile. Nature, 299, 338-40.

Sommer, F. 1978. Diagenesis of Jurassic sandstones in the Viking Graben. Jnl. Geol. Soc. Lond., 135, 63-67.

Sonder, L.J., England, P.C., Wernicke, B.P., and Christiansen, R.L. 1987. A physical model for Cenozoic extension of western North America. In: Coward, M.P., Dewey, J.F., and Hancock, P.L. (eds.). Continental extensional tectonics. Spec. Publ. Geol. Soc. Lond., 28, 187-201.

Soper, N.J. 1971. The earliest Caledonian structures in the Moine Thrust belt. Scott. Jnl. Geol. 7, 241-247.

Spencer, J.E., and Chase, C.G. 1989. Role of crustal flexure in initiation of low-angle normal faults and implications for structural evolution of the basin and range province. Jnl. Geophys. Res., 94, 1765-1775.

Steel, R.J. 1976. Devonian basins of western Norway: sedimentary response to tectonism and to varying tectonic context. Tectonophys., 36, 207-224.

Steel, R.J., and Gloppen, T.G. 1980. Late Caledonian (Devonian) basin formation, western Norway: signs of strike-slip tectonics during infilling. In: Ballance, P.J. and Reading, H.G. (eds.). Sedimentation in oblique-slip mobile zones. Spec. Publ. Int. Assoc. Sedimentologists. 4, 79-103.

Steel, R.J., and Wilson, A. C. 1975. Sedimentation and tectonism (?Permo-Triassic) on the margin of the North Minch Basin, Lewis, Jnl. Geol. Soc. Lond. 131, 183-202.

Summers, R., and Byerlee, J. 1977. A note on the effect of fault gouge compostion on the stability of frictional sliding. Int. Jnl. Rock Mech. Min. Sci. and Geomech. Abstr. 14, 155-160.

Sunderland, J. 1972. Deep sedimentary basins in the Moray Firth. Nature 236, 24-25.

Swain, M.V., and Atkinson, B.K. 1978. Fracture surface energy of olivine. Pure and Applied Geophys. 116, 886-872.

Swain, M.V., and Lawn, B.R. 1976. Indentation fracture of brittle rocks and glasses. International Jnl. of Rock Mechancis and Mining Science, 13, 311-319.

Swensen, F.A. 1964. Groundwater phenomena associated with the Hebgen Lake earthquake. USGS Prof. Paper 435, 159-165.

Swett, K. 1965. Petrology of the Cambro-Ordovician succession of the North West Highlands of Scotland. Unpublished Ph.D. thesis, Univ. of Edinburgh.

Tanner, C.B., and Jackson, M.L. 1948. Nomographs of sedimentation times for soil particles under gravity or centrifugal acceleration. Soil Science Soc. Am. Proc. 12, 60-65.

Teuffel, L.W. 1981. Pore volume changes during frictional sliding of simulated faults. In: Carter, N.L., Friedman, M., Logan, J.M., and Stearns, D.W. (eds.). Mechanical behaviour of crustal rocks Am. Geophys. Un. Monogr. 24, 135-145.

Thompson, G.A., and Burke, D.B. 1974. Regional geophysics of the Basin and Range Province. Annual Rev. Earth Planet. Science Letters, 2, 213-238.

Tissot, B., Califet-Debyser, Y., Deroo, G., and Oudin, J.L. 1971. Origin and evolution of hydrocarbons in Earl Toarcian shales, Paris Basin, France. Bull. Am. Assoc. Pet. Geol. 55, 2177-2193.

Trewin, N.H. 1976. Correlation of the Achanarras and Sandwick Fishbeds, middle old red sandstone, Scotland. Scott. Jnl. Geol. 12, 205-208.

Trewin, N.H. 1985. Orcadian Basin Issue. Editorial Introduction. Scott. Jnl. Geol. 21, 225-226.

Tullis, T.E. 1986. Friction and Faulting. Spec. Issue, Pure and Appl. Geophys. 124, 375-608.

Twiss, R.J. 1977. Theory and applicability of recrystallised grain size palaeopiezometer. Pure and Applied Geophys., 115, 227-244.

Underwood, E.E. 1970. Quantitative stereology. Addison Wesley. 244 pp.

Urai, J.L., Means, W.D., and Lister, G.S. 1986. Dynamic recrystallization of minerals. In: Hobbs, B.E., Heard, H.C. (eds.). Mineral and Rock Deformation, Laboratory studies. 161-199.

van Breeman, O., Aftalion, M., and Johnson, M.R.W. 1979. Age of the Loch Borralon complex, Assynt and late movement of the Moine Thrust. Jnl. Geol. Soc. Lond., 136, 489-496.

Vandervoo, R., and Scotese, C. 1981. Paleomagnetic evidence for a large (2000 km) sinistral offset along the Great Glen Fault during Carboniferous time. Geology, 9, 583-589.

Walsh, J.J., and Watterson, J. 1987. Distribution of cumulative displacement and of seismic slip on a single normal fault surface. Jnl. Struct. Geol. 9, 1039-1046.

Walsh, J.J., and Watterson, J. 1988. Analysis of the relationship between displacements and dimensions of faults. Jnl. Struct. Geol. 10, 239-248.

Wang, C.H. 1986. Internal Structures of Fault Zones. Spec. Issue, Pure and Appl. Geophys. 124, 373 pp.

Watts, N.L. 1987. Theoretical aspects of cap-rock and fault seals for single and two-phase hydrocarbon columns. Marine and Petroleum Geology, 4, 274-307.

Watson, J.V. 1985. Northern Scotland as an Atlantic - North Sea divide. Jnl. Geol. Soc. Lond. 142, 221-243.

Watterson, J. 1986. Fault dimensions, displacement and growth. Pure and Applied Geophys. 124, 365-373.

Weathers, M.S., Bird, J.M., Cooper, R.F., and Kohlstedt, D.C. 1979. Differential stress determined from deformation induced microfractures of the Moine Thrust Zone. Jnl. Geophys. Res. 84, 7495-7509.

Weber, K.J. 1980. Influence on fluid flow of common sedimentary structures in sand bodies. Soc. of Pet. Eng., 9247, 1-12.

Weber, K.J., and Daukoru, E. 1975. Petroleum geology of the Niger Delta: 9th World Petroleum Congress Transactions, 2, 209-221.

Weber, K.J., and Mandl, G. 1978. The role of faults in hydrocarbon migration and trapping in Nigerian growth fault structures. Proc. 10th Annual Offshore Tech. Conf. Houston, Texas, 4, 2643-2653.

Weber, K.J., and Pilaar, W.F., Lehner, F., and Precious, R.G. 1978. The role of faults in hydrocarbon migration and trapping in Nigerian growth fault structures. Offshore Technology Conference, Paper 3356, 2643-2652.

Welbon, A. 1988. The influence of intrabasinal faults on the development of a linked thrust system. Geolog. Rundschau, 77, 11-24.

Wernicke, B. 1981. Low-angle normal faults in the Basin and Range Province. Nappe Tectonics in an expanding Orogen. Nature, 291, 645-693.

Wernicke, B. 1985. Uniform-sense normal simple shear of the continental lithosphere. Can. Jnl. Earth Sci., 22, 108-125.

Wernicke, B., and Burchfiel, B.C. 1982. Modes of extensional tectonics. Jnl. Struct. Geol. 4, 105-115.

Westbrook, G.K., and Smith, M.J. 1983. Long decollements and mud volcanoes; evidence from the Barbados Ridge Complex for the role of high pore-fluid pressure in the development of an accretionary complex. Geology, 11, 279-283.

Westoll, T.S. 1979. Devonian fish biostratigraphy. In: House, M.R., Scrutton, C.T., and Bassett, M.G. (eds.), The Devonian System. Spec. Pap. Palaeontol. 23, 341-353.

Wheeler, J. 1987. Variable-heave models of deformation above listric normal faults: the importance of area conservation. Jnl. Struct. Geol., 9, 1047-1049.

White, N.J. 1989. Nature of lithospheric extension in the North Sea. Geology, 17, 111-114.

White, N.J., Jackson, J.A., and McKenzie, D.P. 1986. The relationship between the geometry of normal faults and that of the sedimentary layers in their hangingwalls. Jnl. Struct. Geol., 8, 897-909.

White, S.H. 1973a. The dislocation structures responsible for the optical effects in some naturally deformed quartzites. Jnl. Material Sci., 8, 490-499.

White, S.H. 1973b. Syntectonic recrystallisation and texture development in quartz. Nature Phys. Sci. 244, 276-278.

White, S.H. 1976. Effects of strain on the microstructures fabrics and deformation mechanisms in quartzites. Phil. Trans. R. Soc. London, A283, 69-86.

White, S.H. 1977. Geological significance of recovery and recrystallization processes in quartz. Tectonophysics 39, 143-170.

White, S.H. 1979a. Difficulties associated with palaeostress estimates. Bull. Mineral. 102, 210-215.

White, S.H. 1979b. Grain and sub-grain size variations across a mylonite zone. Contr. Miner. Petrol. 70, 193-202.

White, S.H., Evans, D.J., and Zhong, D.-L. 1982. Fault rocks of the Moine Thrust Zone: microstructures and textures of selected mylonites. Textures and Microstructures, 5, 33-61.

Wilcox, R.E., Harding, T.P. and Seely, D.R. 1973. Basic wrench tectonics. Bull. Am. Assoc. Pet. Geol., 57, 57-96.

Williams, G., and Vann, I. 1987. The geometry of listric normal faults and deformation in their hanging wall. Jnl. Struct. Geol., 9, 789-796.

Wilson, G.V., Edwards, W., Knox, J., Jones, R.C.B., and Stevens, J.V. 1935. The geology of the Orkneys. Mem. Geol. Surv. G.B.

Wilson, H.H. 1975. Time of hydrocarbon expulsion, paradox for geologists and geochemists. Bull. Am. Assoc. Pet. Geol. 59, 69-84.

Wiltschko, D.V., and Eastman, D.B. 1983. Role of basement warps and faults in localising thrust fault ramps. Geol. Soc. Am. Mem. 158, 177-190.

Wood, R., and Barton, P. 1983. Crustal thinning and subsidence in the North Sea. Nature, 302, 134-136.

Wood, J.R., and Hewett, T.A. 1982. Fluid convection and mass transef in porous sandstones - a theoretical model. Geochim. et. Cosmochim. Acta 46, 1707-1713.

Wood, S.H., Wurts, C., Lane, T., Ballenger, N., Shalleen, M., Totorica, D., and Waag, C. 1985. Increased groundwater discharge caused by the 1983 Idaho (USA) earthquake. In: Proc. 17th Int. Congress Assoc. of Hydrologists. Hydrology of rocks of low permeability, 741-751.

Ziegler, P.A. 1983. Inverted basins in the Alpine Foreland. In: Seismic expression of structural styles - a picture and work atlas. AAPG studies in Geology 15. 3, 3.3-3 to 3.3-12.

Ziegler, P.A. 1985. Late Caledonian framework of western and central Europe. In: Gee, D.G., and Sturt, B.A. (eds.). The Caledonian Orogen - Scandinavia and related areas. Wiley & Sons, Lond., 3-17.

Appendix 1

Microstructural techniques/TEM specimen preparation

The microstructural work described in this thesis is based on the study of oriented hand specimens collected in the field. Due to their incohesiveness, many of the fault rocks were impregnated with resin before slabbing. Oriented thin sections prepared at the University of Leeds were cut from these rocks for optical microscopy study. Polished thin sections were prepared from some samples in which the fine grain size and/or fine scale microstructures neccessitated high resolution optical study.

The oriented sections were cut as near as possible to perpendicular from the movement plane and parallel to the movement direction in the quartz mylonites from Sango Bay. In all specimens of sandstone used for data collection adjacent the North Scapa Fault on Orkney, two oriented sections were cut: one perpendicular to the fault plane and parallel to the movement direction, and one parallel to the fault plane and to the movement direction.

Uncovered lakeside thin sections were prepared from specimens chosen for transmission electron microscopy (TEM) work. In this case, nickel or aluminum slot foils (1 x 2 mm.) were glued to the lakeside section with epoxy and allowed to dry for 24 hours. The section was then immersed in ethanol for several hours or overnight until the rock slice 'floated' off the glass section. The rock slice was then carefully placed on special tissue paper and allowed to dry. Foils chosen for TEM work were then carefully extracted from the rock slice with tweezers, and ion beam thinned for 8 to 20 hours. The thinning time was dependent on: rock type and composition; and ion current (kV), specimen current, and thinning angle in the ion beam thinner. Records of rock type and the thinning parameters listed above for samples used in this thesis can be found in the Structural Laboratory, Department of Earth Sciences, University of Leeds.

The instruments used in the study were as follows:

1. Iontech ion beam thinner in the Department of Earth Sciences, and Gatan ion beam thinner in the Department of Metallurgy, both at the University of Leeds. Use of the Gatan thinner courtesy of Mark Rainforth and Dr. Ron Stevens of the Department of Metallurgy.

2. TEM work on the JEOL-200 CX 220KV scanning transmission electron microscope in the Electron Optics Centre, Department of Metallurgy, University of Leeds. Qualitative microanalyses were carried out on this instrument using a Link System 860, Series 2 Energy Dispersive microanalyser.

Appendix 2

Methods of fracture orientation and spacing measurement, and calculations of fracture density

Measurements of fracture orientation, spacing, and density have been made in porous sandstone adjacent the North Scapa Fault on Orkney. Many methods have been used to measure the orientation and spacing of fractures in the field by other workers, as reviewed by Blenkinsop (1986). In this case, an outcrop face approximately perpendicular to the fault was the only section available to take the measurements. A tape measure was stretched across the surface, and every fracture encountered, regardless of length, was recorded. The number of fractures per 0.5 m. interval (fracture spacing) was then calculated. The fracture densities were calculated from tracings of photographs taken of the same outcrop face along the exact direction and intervals. The precision associated with this method of data collection is described here. Also, the errors involved in the calculation of fracture density are discussed.

Fracture Orientation

Blenkinsop (1986) used two methods to measure fracture orientations: the first involved measuring the first 50 or 100 fracture orientations observed at a locality and classifying them as they were recorded; and, in the second method, a fixed number of fractures were recorded. The first method, similar to the one employed in this thesis, has the advantage of complete objectivity. The precision of the measurement is based on the maximum precision of a Silva compass, which is 1° in both dip and strike.

Fracture Spacing

Fracture spacing measurements which are not taken in a direction perpendicular to the fracture surface will be apparent values, not true values. However, in this study, the objective was to measure the relative increase or decrease of fracture spacing in regard to distance from the fault, not to measure the spacing of a specific fracture set. Therefore, a direction approximately perpendicular to the fault was chosen on the only available outcrop face. Jamison and Stearns (1982) and Dumpleton (pers. comm. in Blenkinsop, 1986) used a similar approach. Jamison and Stearns measured the number of intercepts on a 200 mm length in two directions on either bedding surfaces or cross-sectional surfaces. In Dumpleton's study, he averaged the frequency of all fractures in two perpendicular directions. Dumpleton used a counting frame consisting of two perpendicular metre long rules placed flat on a longwall coal face, from which frequency per metre in both directions was counted directly. These methods, as the one used in this study, suffer from the fact that only one surface is used. The measured frequency is thus clearly dependent on the orientation of the fractures relative to that surface.

To overcome this problem, Blenkinsop (1986) used two other methods. In the first, fracture frequencies for each set were measured at each locality by counting the number of fractures of that set alone, along a 500mm or 250 mm line perpendicular to the fracture surface. Several measurements were made on parallel lines and averaged, and the final density taken as the sum of the averages. Blenkinsop then compared this method with the Dumpleton method, which gave very similar values.

Blenkinsop also used the "fracture log" method at some of his localities, similar to the method used in this study. In his study, a tape measure was stretched across a flat surface, perpendicular to the apparent strike of the most frequent fracture set, and the distance from the origin of every fracture intersecting the tape was recorded. The measuring surface was chosen wherever possible to be perpendicular to the fracture set such that the fracture frequencies are approximately equal to the sum of the true fracture frequencies of the most frequent set and the apparent frequencies of all other sets.

Sources of error for the continuous fracture logs are parallax between the fracture and the tape where the taut tape is not in contact with the uneven measuring surface, and the omission of a fracture, or the inclusion of features which may not be fractures. In Blenkinsop's study, the errors were analysed by repeating the fracture log. He found that the error due to parallax was negligible (+/- 0.586 mm for 99 fractures). Of more significance was the omission of 13 fractures and the inclusion of 10 others in the repeated measurements. The omissions and inclusions were distributed randomly throughout the log and produced a net imbalance of only 3 fractures.

To test the precision of the measurements in this study, the 15 m. long log was not repeated as it was rendered too time consuming. Another method was employed which was similar to that used by Dumpleton, and the data obtained from this method was compared with that of data from the fracture log method. A 0.5 m^2 frame was placed as near as possible to flat on the outcrop face, and photographs were taken of each frame up to 15 meters from the fault. The fractures in the photographs were then traced. The tracing of the area within the frame was then used in a fracture density calculation, using the following method. Each fracture observed on the tracing was measured in length on a digitizing table linked to a computer. A computer program (written by D.J. Prior) then calculated the fracture density (m/m^2) from the fractures measured within the two-dimensional area. This area density was then converted to a volume density assuming a volume equivalent to a cube with each side equal to the measured area. The error involved in calculating a three-dimensional density from two-dimensional data is a factor of two (D.J. Prior, pers.comm., 1989). The densities calculated and amount of error for each interval are shown on fig. 5.12b.

The methods used to measure the fracture spacing in this study remained biased due to the orientation problem. However, as noted above, the aim was to obtain information about the relative increase or decrease of the fracture spacing away from the fault. When the data from each method is compared, the results show that a fracture spacing increase corresponds with a fracture density decrease. Therefore, the fracture spacing and densities quoted in this study are a reliable indicator of the variation in intensity of fractures adjacent to the North Scapa Fault.

Appendix 3

X-ray diffraction specimen preparation and data

X-ray diffraction was carried out on specimens adjacent the North Scapa Fault with a Siemens X-ray diffraction instrument in the Department of Earth Sciences, University of Leeds. The rock samples were first reduced to approximately 1 cm. diameter pieces using a jaw crusher and sample splitter. Approximately 60-100 gms. of this material was then placed in a tungsten carbide barrel in the TEMA rock grinding instrument and crushed for 45-55 seconds to obtain a sample which passed through a 100 mesh nylon sieve.

The grain size fractions were obtained using the sedimentation method of Tanner et al. (1948), as follows. The TEMA sample was mixed in a 5-liter beaker with distilled and deionized water and allowed to settle for 15 hours and 50 minutes. At this time, the top 20 cm. of solution was cyphonated and poured through a modified Buckner funnel with a cellulose nitrate filter (pore size 0.2 μm). The clays collected from the filter were mixed with water and allowed to settle on a glass slide suspended in a small beaker, supplying the <2 μm. grain size fraction.

The same procedure of mixing and filtering was repeated until a clear solution was obtained, usually 2-3 times. This clear solution was allowed to settle for one hour and 43 minutes at which time the top 20 cm. were again cyphonated into a small beaker. A glass slide was suspended in the small beaker and the clays were allowed to settle on the slide to obtain the 2-6 μm grain size fraction.

Both the 2-6 and <2 μm fractions were analyzed, then each was treated with ethol glycol to observe if peaks changed, signifying the presence of expandable clays. The glycolated samples were then heat treated at 200° C for 1 hour and run again to look for peak changes. 2Θ peaks were picked with a program written by A.Gray. The following data set represents this process executed on one sample each collected from domains 1, 3 and 4 adjacent the North Scapa Fault. g= glycolated, h=heat treated.

a. Sample 49519.	Domain 4; 2-6 μm	
b.	Domain 4; 2-6 μm; g	
c.	Domain 4; 2-6 μm; g,h	
d.	Domain 4; <2 μm;	
e.	Domain 4; <2 μm; g	
f.	Domain 4; <2 μm; g,h	
g. Sample 49520.	Domain 3; 2-6 μm	
h.	Domain 3; 2-6 μm; g	
i.	Domain 3; 2-6 μm; g,h	
j.	Domain 3; <2 μm	
k.	Domain 3; <2 μm; g	
l.	Domain 3; <2 μm; g,h	
m. Sample 49517.	Domain 1; 2-6 μm	
n.	Domain 1; 2-6 μm; g	
o.	Domain 1; 2-6 μm; g,h	

A

B

C

G

H

I
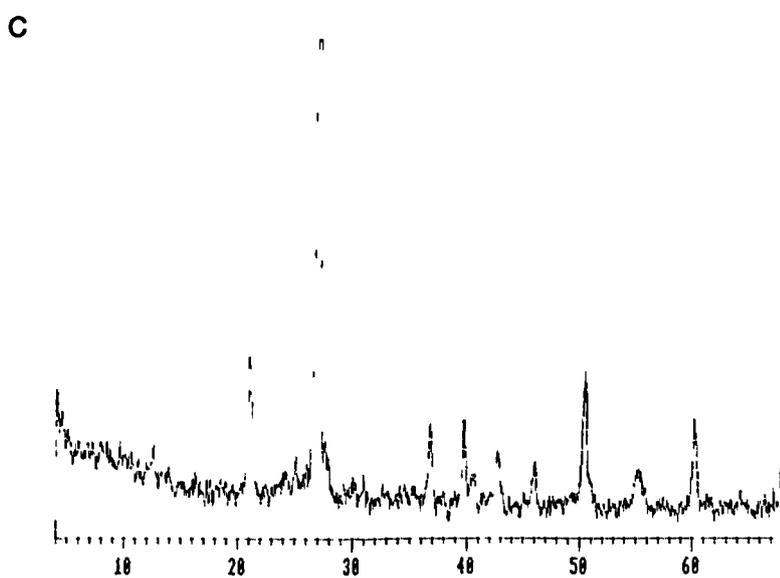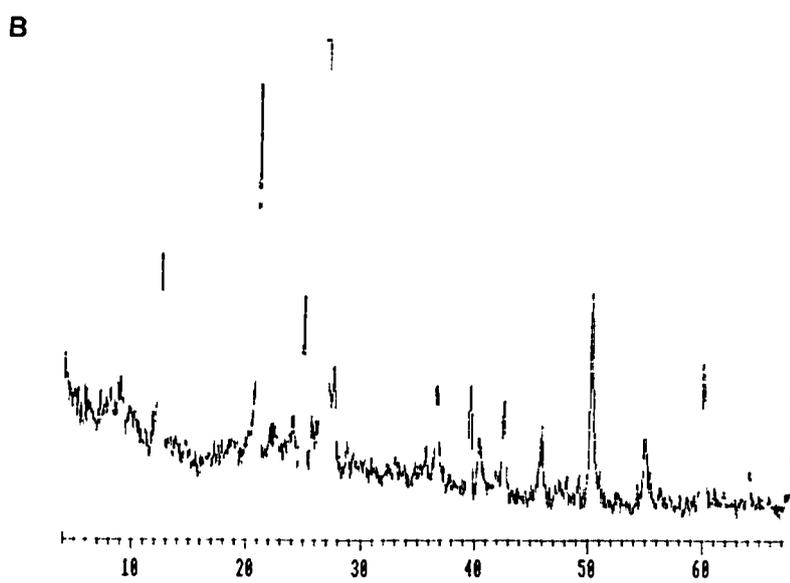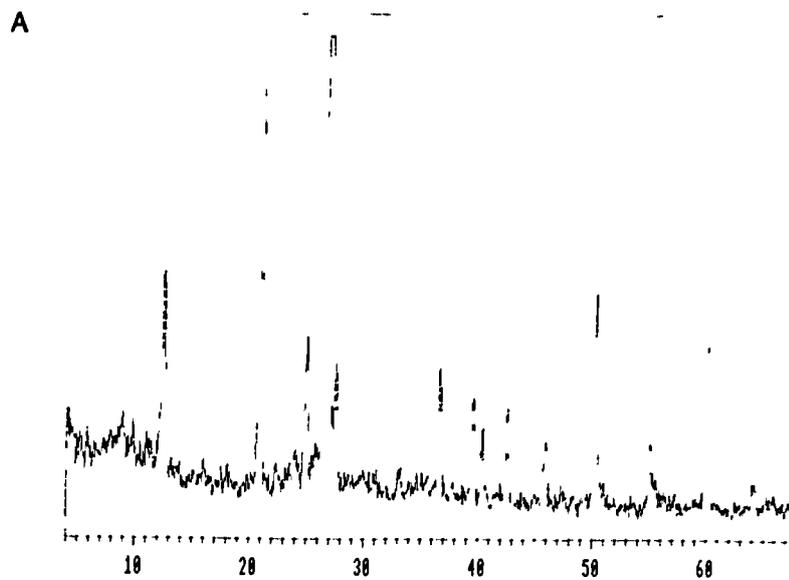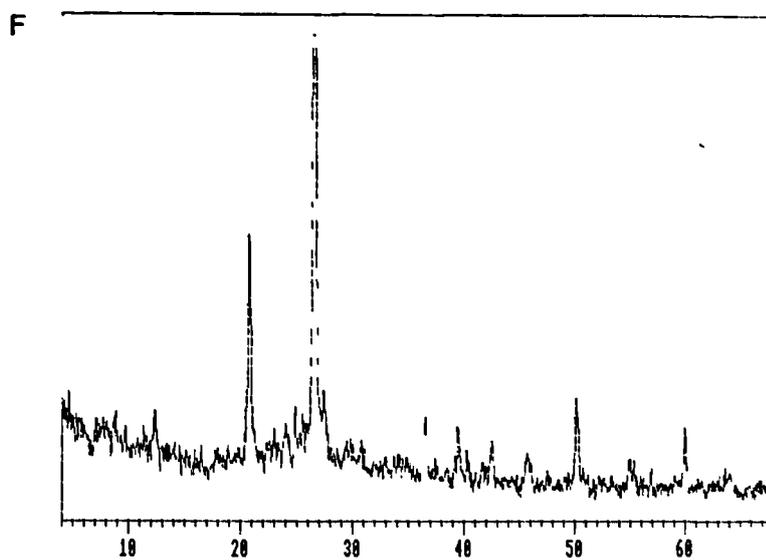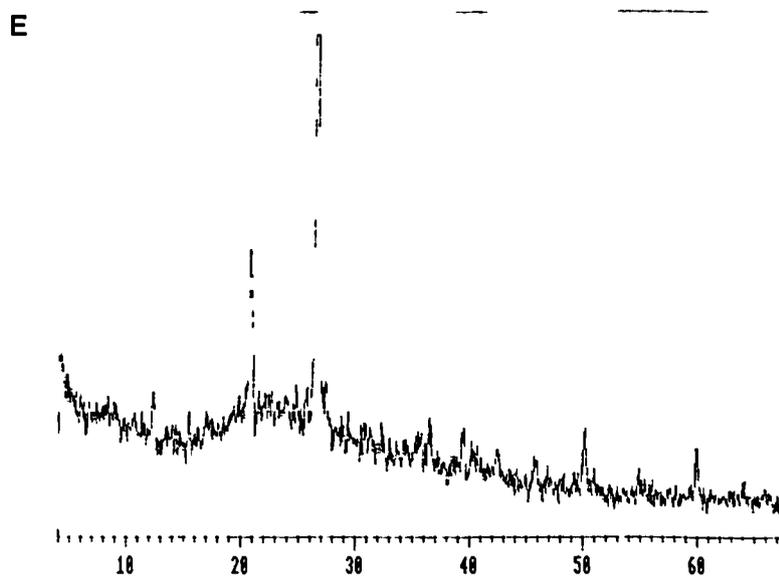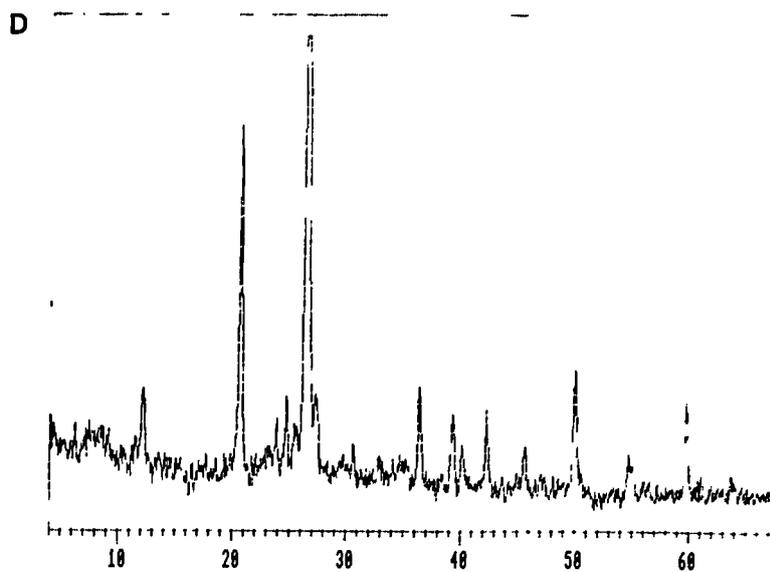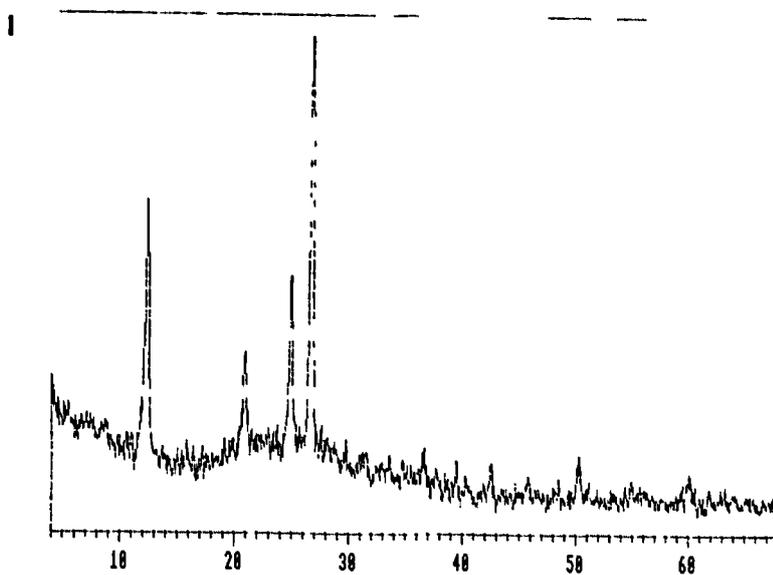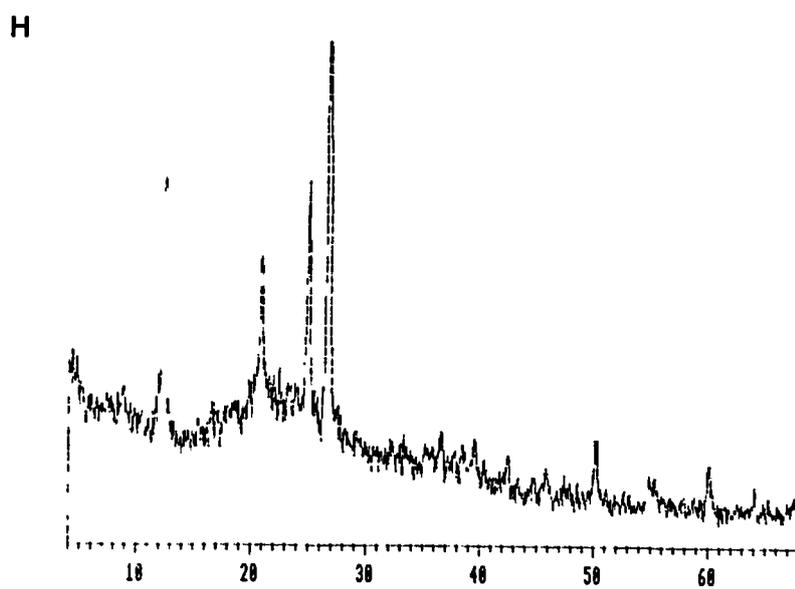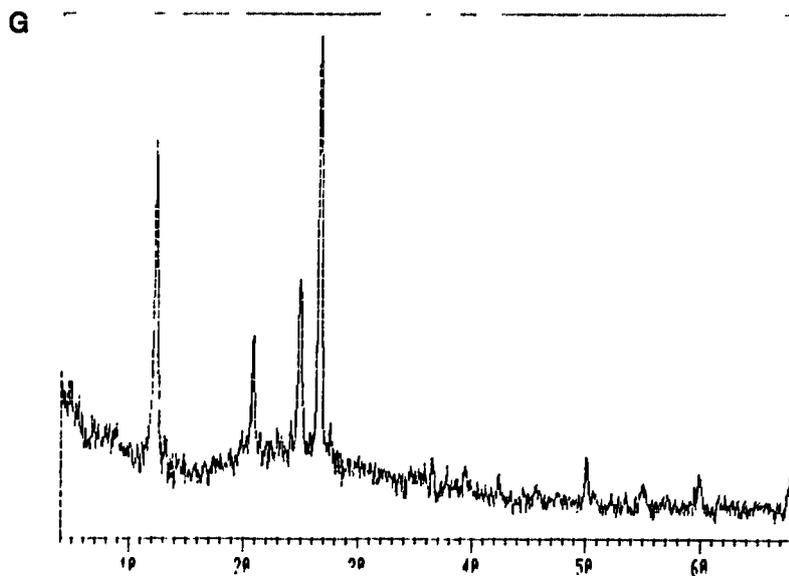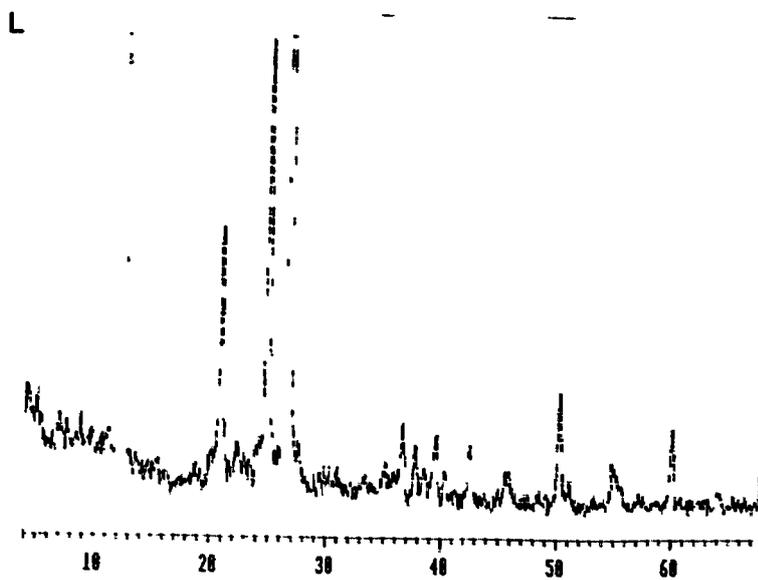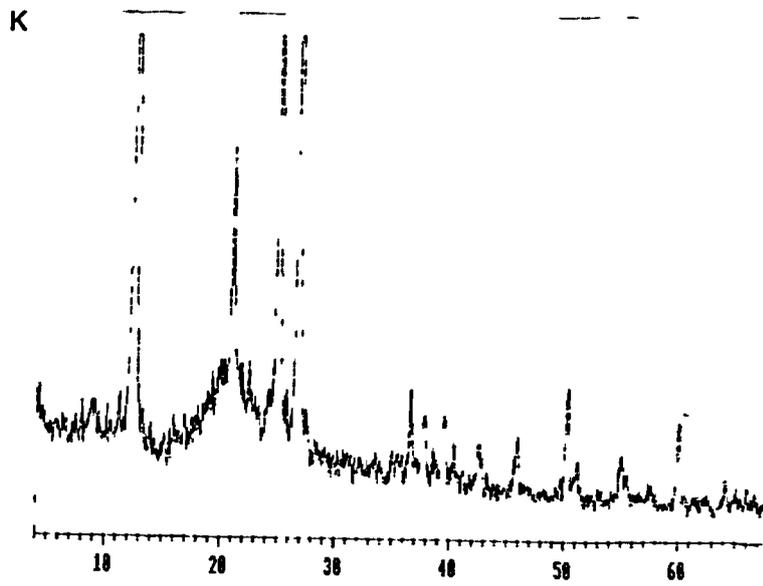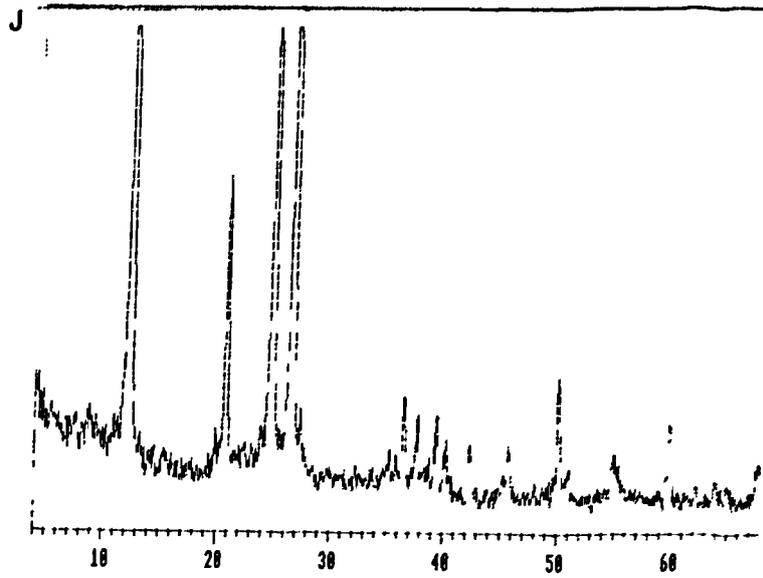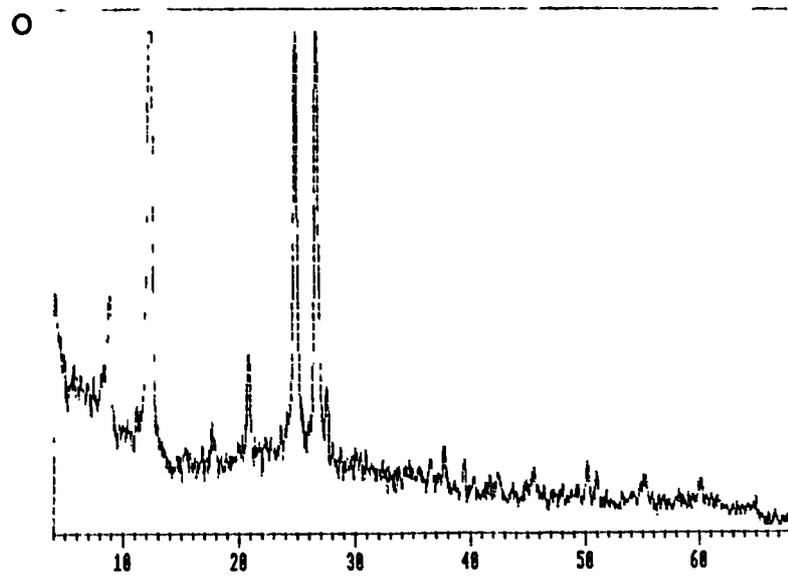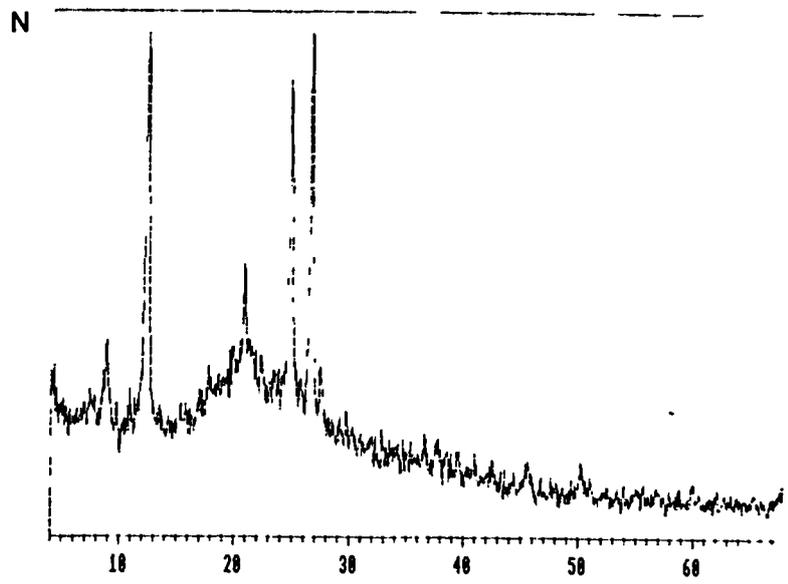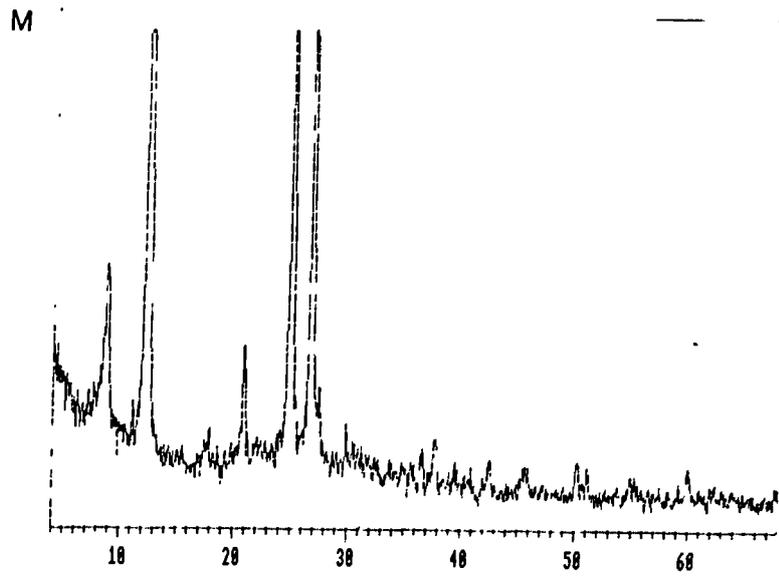
Appendix 4

Gas chromatography specimen preparation

Samples used for gas chromatography analyses were taken from the same TEMA crushed samples which were used for the X-ray diffraction analyses described above. The instrument used is a Carlo Erba Strumentazione Elemental Analyzer Model 1106, in the Department of Earth Sciences, University of Leeds. The principles of operation, as layed out by the company, are as follows.

The samples are held in a lightweight tin container and dropped at preset intervals of time into a vertical quartz tube maintained at 1030° C, through which a constant flow of helium is run. When the samples are introduced, the helium stream is temporarily enriched with pure oxygen. Flash combustion takes place, primed by the oxidation of the container. Quantitative combustion is then achieved by passing the mixture of gases over Cr_2O_3. The mixture of combustion gases is then passed over copper at 650° C to remove the excess of oxygen and reduce oxides of nitrogen to nitrogen. The gas then passes through a chromatographic column of Porapak QS heated to approximately 100° C. The individual components are then separated and eluted as N_2-CO_2-H_2O. They are measured by a thermal conductivity detector, whose signal feeds a potentiometric recorder and in parallel an integrator with digital printout. The instrument is calibrated by combustion of standard compounds.

Two more analyses were then run on each sample after first being acid washed, and then acid washed and run through a cellulose nitrate filter to remove any non-organic carbon. The data is shown in Table 5.1.

Appendix 5

Grain size measurements: problems, assumptions, calculations, and methods

Grain size measurements were made from samples of North Scapa sandstone adjacent the North Scapa Fault, Orkney, and from quartz mylonites collected from Sango Bay, Durness. The assumptions, calculations and problems associated with the grain size measurements are discussed before the methods used are described.

The problems of grain size measurements are reviewed by Dayan (1981), Norton (1982), Handy (1986), and Prior (1988). First, because the measurements are made in two dimensional sections, stereological problems arise, as true grain geometry is three dimensional. Use of solid geometry and grain size measurements in metallurgy as reviewed by Underwood (1970), Exner (1972) and Pickering (1976) show that if grains are assumed to be spheres, then the diameter of any grain in a two dimensional section is likely to be an underestimate of its three dimensional diameter. It was also shown that small grains are less likely to be included in a two dimensional section than large grains and therefore will be under-represented in grain size statistics. The grain size corrections depend on section orientation and grain shape fabric (if present), further complicating the two and three dimensional grain size relationships. In the case of tectonites, grain shapes are unlikely to represent spheres, but Dayan (1981) has shown that the mathematics required for the stereological correction of a realistic tectonite fabric is complex and the extra measurements and time required were not justified for the margin of error reduction which would result. Tectonite grain size measurements by Dayan (1981), Norton (1982), Kohlstedt et al. (1979) and Ord and Christie (1984), for example, have used stereological corrections which assume spherical or cubic grain shapes. For two dimensional grain size measurements, as in this study, assuming spherical grains, the true grain size (D) is related to the mean two dimensional grain diameter (d) by the relation:

$$D = \frac{4d}{pi} \qquad \text{[Exner (1972)]}.$$

Additional problems arise, as measurements from optical thin sections can result in grain overlap, which becomes more acute as the grain size becomes less than the section thickness, in this case 25-30 μm. In addition, problems relating to scale arise, as smaller grains are resolved if observations are made at higher magnifications. In a statistical analysis, Dayan (1981) demonstrated that the precision of grain size estimates is a function of the time available for measurements. Dayan showed that after the measurement of 100 grains for a particular sample, the precision gained from any more measurements drops off significantly for the additional time used.

In this study, the grain sizes measured from the Scapa sandstone were made from line drawings of the grain boundaries from the thin sections on a shadowmaster. Each grain was measured individually from this line drawing with a digitizer linked to a computer. 100 grains were measured from each thin section. Two thin sections were analysed for each sample as described in Appendix 1. In the case of the quartz mylonites from Sango Bay, photomicrographs of thin sections were used for measurement of both the recrystallised grain size and the microbreccia grain size. TEM micrographs ranging in magnification from 5,000x to 20,000 were used for measurements of the sub-grain size and ultracataclasite grain size. Over 300

grains were measured for each data set from the quartz mylonites. In the measurement of the recrystallized grain size in the quartz mylonite, grains were measured down to the scale such that no internal deformation features which can further subdivide the grain were observed. The same policy was used in the measurements of the subgrains from the TEM micrographs.

The program PALPIEZ or SHAPES written by D.J. Prior at the University of Leeds was then used to calculate the mean grain size from each data set. In these programs, the diameter of each grain measured is estimated as the diameter (d) of a circle of equivalent area to the measured area of the grain (A), shown by the relation:

$$d = 2(A/pi)^{1/2}$$

Next, the measured grain sizes were plotted on histograms by using the program HISTOGRA, written by D.J. Prior. The data set for each sample was distributed for each of the functions (f(d)) of (d)0.5, (d)0.33, (d)0.25 and ln(d) to find the function which gave an approximately normal distribution frequency distribution histogram. It was found that the nearest approximation to a normal distribution for the undeformed samples was the (d)0.5 function. Therefore, the mean grain size and standard deviation quoted was calculated assuming a normal distribution of (d)0.5, ($\sqrt{d}$). Due to resolution problems on the optical microscope in the deformed samples with grains less than 25 μm. in diameter, the grain size measurements in the deformed samples did not plot in a normal distribution. Thus, the means quoted are biased indications of the true grain size means in the deformed samples. Therefore, the approximate limit of resolution is marked on the graphs, and observations from the TEM were used as an indication of the grain size range in the cataclasites.

In summary, with regard to the assumptions, methods and calculations used in the measurement of grain sizes, Dayan (1981) points out that the most serious errors involved are the stereological corrections, possibly as much as $\pm$ 30 %. The error estimates quoted in this study are variations from the mean for the measured grain size distributions. The grain size data from both the Scapa Sandstone and the quartz mylonites from Sango Bay are not being used as palaeopiezometers. Therefore, although the errors could be as much as $\pm$ 30 %, the grain size data provides an adequate assessment of the relative amount of grain size reduction adjacent to the fault.

Appendix 6

Methods and calculations used in dislocation density measurements

Dislocations density measurements in the quartz mylonite from Sango Bay were calculated using the following methods. First, to obtain a range of representative measurements, 2 to 6 foils were thinned from each sample for TEM observation. At a range of magnifications (5,000x-37,000x), the specimens were tilted until the maximum amount of dislocations were observed in a given area. At least three micrographs of representative areas from each sample were then taken, and individual dislocation lengths within these areas were measured by using a digitizer linked to a computer. The program used to calculate the density measurement was written by D.J. Prior (University of Leeds). The program calculates a density based on the length per cross-sectional area measured on the micrograph. Thus, if the dislocations are measured within a 1 μm^2 area, the dislocation density quoted assumes a volume of 1 μm^3. As a result, the dislocation density value is an underestimate if the thickness of the specimen is less than 1 μm thick, and an overestimate if the specimen is over 1 μm thick. The range of thickness in several samples was therefore measured, in the following way. A micrograph was taken of a feature which cuts through the thickness of the sample. The sample was tilted, and another micrograph was taken. The thickness of the sample was calculated from the increase in line length of the feature parallel to the direction of the tilt between the two micrographs. The resulting calculated thicknesses were found to vary consistently between 0.5 and 1.5 μm. Therefore the dislocation density for each sample was calculated for thicknesses of 0.5, 1.0, and 1.5 μm, and is shown in Table A1 below. At least three density measurements are shown from each sample, totalling 9 measurements for the inital quartz mylonite microstructure, and 16 for the cataclastic rock. Means were then calculated from the dislocation densities for each thickness. Ranges of these means are: 1.7 x 10^8 to 5.0 x 10^8 cm/cm^3 in the 'unaffected' mylonite, and 4.1 x 10^8 to 1.2 x 10^9 cm/cm^3 in the cataclastic fault rock. The ranges of the means are those quoted in the text.

Table A.1
Dislocation Density Data: Quartz mylonites and cataclasites
(all data $x10^8$ cm/cm³)

	Sample Thickness		
	0.5 μm	1.0 μm	1.5 μm
Mylonites Sample No.			
48453A	1.6	3.2	4.8
	2.1	4.2	6.3
	3.0	6.0	9.0
49519A	0.6	1.1	1.7
	1.3	2.6	3.9
	1.2	2.3	3.5
48444A	1.4	2.8	4.2
	1.5	2.9	4.4
	2.3	4.6	6.9
MEAN	**1.7**	**3.3**	**5.0**
Cataclasites Sample No.			
48453B	2.6	5.1	7.7
	3.3	6.6	9.9
	3.4	6.8	10.2
48449B	3.8	7.6	11.4
	4.8	9.5	14.3
	3.9	7.8	11.7
49286A	3.1	6.2	9.3
	4.6	9.1	13.7
	3.6	7.2	10.8
49290A	3.8	7.6	11.4
	4.4	8.8	13.2
	5.0	10.0	15.0
	3.9	7.8	11.7
49119A	3.2	6.4	9.6
	6.0	12.0	18.0
	5.5	11.0	16.5
MEAN	**4.1**	**8.1**	**12.2**

Key to Orcadian Basin maps in this thesis

28 $\diagdown$ orientation of bedding, dip in degrees

$\otimes$ horizontal bedding

$\times$ vertical bedding

$\diagup$ normal fault, block on downthrown side

$\diagup$ reverse fault, teeth on upthrown side

115/52   orientation of normal fault, dip in degrees

$\times$ axial trace of syncline

$\diamondsuit$ axial trace of anticline
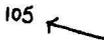
105 $\leftarrow$ direction of abrasive slickenside lineations on detachment horizons on the North Coast

Limit of exposure (shaded)
Scapa Sandstone/Eday Group (?UORS)

Rousay Flagstones (MORS)

Stromness Flagstones (MORS)

high water mark

low water mark

[HY 295425]   Grid references/numbers; quoted according to British National grid reference system.

STRUCTURAL MAP of NORTHERN SCOTLAND and adjacent off-shore areas

Scale 1:250,000

KEY

SEDIMENTARY ROCKS
- Undivided
- NEOGENE–PALAEOGENE
- Upper / Lower — CRETACEOUS
- Undivided / Upper / Middle / Lower — JURASSIC
- Undivided — TRIASSIC
- PERMO-TRIASSIC
- Undivided — PERMIAN
- Undivided / Upper / Middle / Lower — DEVONIAN
- Undivided — CAMBRO-ORDOVICIAN

METAMORPHIC ROCKS
- Moine
- Torridon, affinities uncertain
- Lewisian
- Tawisian, affinities uncertain

SYMBOLS
- Geological boundary
- Fault at surface, tick on downthrown side
- Fault not at surface, tick on downthrown side
- Periods of fault activity:
  - A. Post-Lower Cretaceous
  - B. Post-Middle Jurassic–pre-Lower Cretaceous
  - C. Post-base Lower Jurassic–pre-Upper Jurassic
- Axial trace of anticline
- Axial trace of syncline
- DEPTH TO TOP OF BASEMENT (TWT)
- CUT-OUT ZONE FOR TOP OF BASEMENT
- BASEMENT AT SURFACE

Study area (see fig. 5.1)

Study area (see fig. 6.1)

ATLANTIC OCEAN

NORTH SEA

THE MINCH

ORKNEY-SHETLAND PLATFORM

PAPA BANK HIGH

SOLAN BANK HIGH

WEST SHETLAND FAULT

PAPA BASIN

NOUP BASIN

NORTH SHOAL

BASIN COMPLEX

WEST ORKNEY

STACK SKERRY BASIN

STORM BANK

STORM BANK BASIN

STORMY BANK

HUM ROCK

SULE SKERRY

HULDA

EDAY SYNCLINE

WESTRAY

ROUSAY

EDAY

MAINLAND

WEST MAINLAND ANTICLINE

SANDAY

STRONSAY

SHAPINSAY

ORKNEY ISLANDS

DEERNESS SYNCLINE

HOY

SOUTH RONALDSAY

WEST FAIR ISLE BASIN

CAITHNESS RIDGE

BRIMS-RISA FAULT

DUNNET HEAD

STRATHY POINT

BIRSTHY POINT

TONGUE

MOINE THRUST LINE

CAPE WRATH

Durness

Scourie

WICK FAULT

HELMSDALE FAULT

GREAT GLEN FAULT

AXIS OF MAIN BASIN

SOUTH EAST BASIN

CENTRAL RIDGE

MORAY FIRTH

DORNOCH FIRTH

Nairn

Elgin

kilometres

statute miles

nautical miles (latitude minutes)

St. Mary's / Howequoy Head (HY 008465)

STRUCTURAL MAP OF SANGO BAY
DURNESS, N.W. SCOTLAND

SANGOMORE FAULT

R. Holdsworth 1988

FARAID HEAD FAULT

SUB-AREA 1

SUB-AREA 2

SUB-AREA 3

SUB-AREA 4

Durness

Sango Sands Oasis

A838

Access road

Fence line

Stereonets

Poles to minor normal faults
n = 22

Sub-area 4:
lineations in quartz mylonite
n=15, contours 6,20 & 36%

Sub-area 3:
lineations in quartz mylonite
n=38, contours 2.5,13,24 & 34%

Sub-area 3:
lineations in Lewisian mylonite
n=4, contours 7,21, & 55%

Sub-area 2:
lineations in quartz mylonite
n=52, contours 1.5,21 & 32%

Sub-area 3:
lineations in Lewisian mylonite
n=24, contours 4,13,25 & 35%

Sub-area 2:
lineations in Oystershell mylonite
n=22, contours 4,9,18 & 31%

Sub-area 1:
lineations in Oystershell mylonite
n=26, contours 3,7,18 & 34%

Sub-area:
poles to foliation in Lewisian mylonite
n=52, contours 3,9,15 & 25%

Legend

LEWISIAN MYLONITE

MOINE MYLONITE: "Oystershell rock"

QUARTZ MYLONITE (Cambrian)

DURNESS LIMESTONE (Cambro-Ordovician sequence)

DYKE

OUTCROP EXTENT

CONTACT (FAULTED)
known
inferred

NORMAL FAULT (block on downthrown side)
known
inferred

029/83   Fault orientation

d = 1.0   Fault displacement estimate (meters)

26   MYLONITIC FOLIATION (dip in degrees)

20   BEDDING (dip in degrees)

Scale

SCALE
0   50   100
meters

SCALE

0   250   500

metres

N
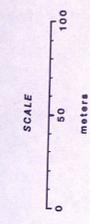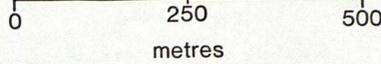
325   330   335   340   345

045   045

040   040

035   035

325   330   335   340   345
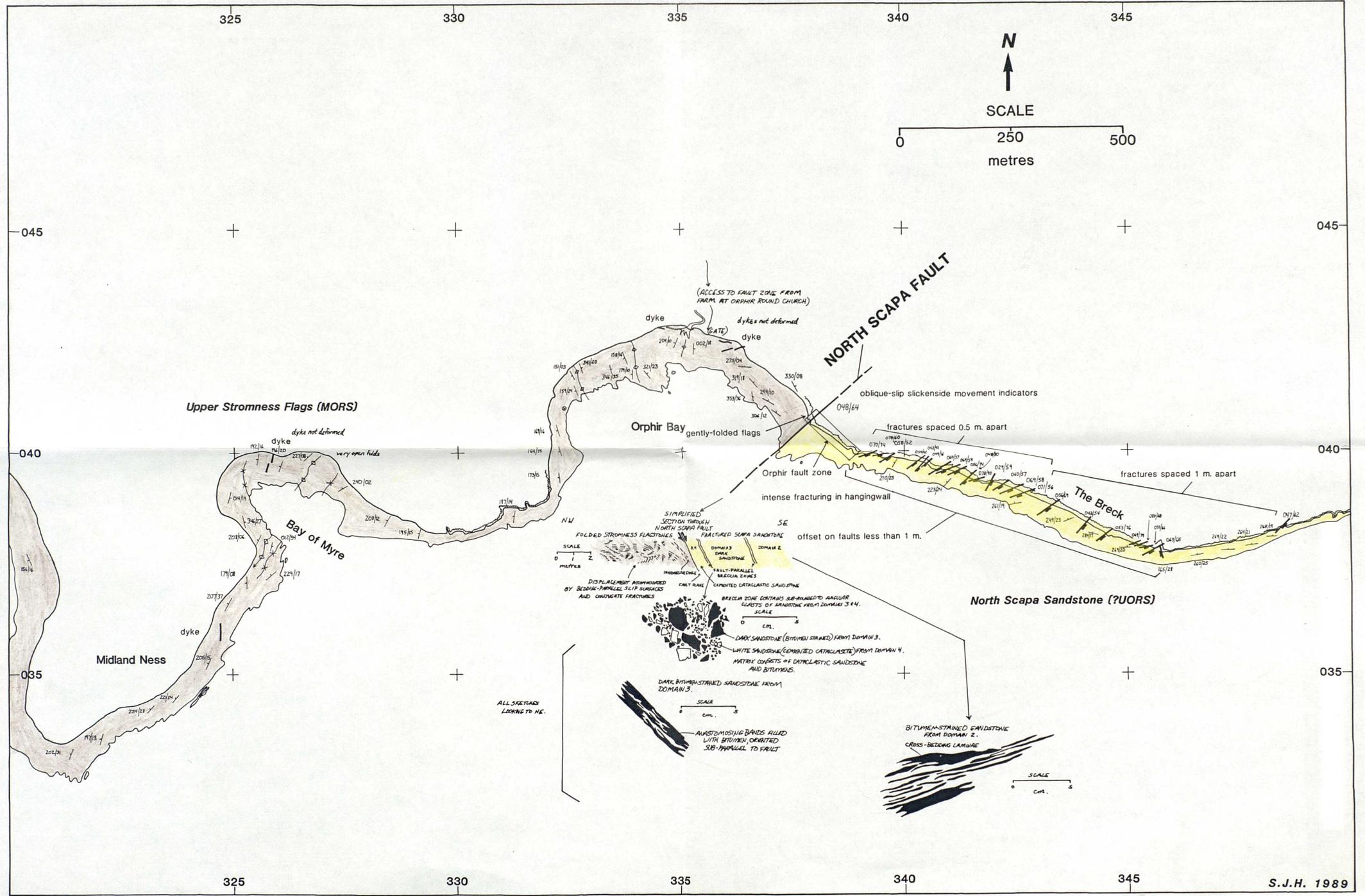
NORTH SCAPA FAULT

(ACCESS TO FAULT ZONE FROM FARM AT ORPHIR ROUND CHURCH)

dyke

(GATE)

dykes not deformed

dyke

Upper Stromness Flags (MORS)

dyke not deformed

dyke

very open folds

Orphir Bay

gently-folded flags

oblique-slip slickenside movement indicators

fractures spaced 0.5 m. apart

fractures spaced 1 m. apart

Orphir fault zone

intense fracturing in hangingwall

The Breck

Bay of Myre

NW

SE

SIMPLIFIED
SECTION THROUGH
NORTH SCAPA FAULT

FOLDED STROMNESS FLAGSTONES   FRACTURED SCAPA SANDSTONE

SCALE

0   1   2

metres

DOMAIN 3
DARK
SANDSTONE

DOMAIN 2

FAULT-PARALLEL
BRECCIA ZONES

CEMENTED CATACLASTIC SANDSTONE

FAULT PLANE

offset on faults less than 1 m.

Midland Ness

DISPLACEMENT ACCOMMODATED
BY BEDDING-PARALLEL SLIP SURFACES
AND CONJUGATE FRACTURES

North Scapa Sandstone (?UORS)

BRECCIA ZONE CONTAINS SUB-ROUNDED TO ANGULAR
CLASTS OF SANDSTONE FROM DOMAINS 3 & 4.

SCALE

0   5

cm.

DARK SANDSTONE (BITUMEN STAINED) FROM DOMAIN 3.

WHITE SANDSTONE (CEMENTED CATACLASTE) FROM DOMAIN 4.

MATRIX CONSISTS OF CATACLASTIC SANDSTONE
AND BITUMENS.

DARK BITUMEN-STAINED SANDSTONE FROM
DOMAIN 3.

SCALE

0   5

cm.

ALL SKETCHES
LOOKING TO NE.

ANASTOMOSING BANDS FILLED
WITH BITUMEN, ORIENTED
SUB-PARALLEL TO FAULT

BITUMEN-STAINED SANDSTONE
FROM DOMAIN 2.

CROSS-BEDDING LAMINAE

SCALE

0   5

cm.

S.J.H. 1989